Selective autophagy in host defense against mycobacterial infection

Rui Zhang

PhD thesis with summary in Dutch

Cover (front): Confocal micrograph showing co-localization of the GFP-Lc3 autophagy marker (Green) with clusters of *Mycobacterium marinum* bacteria (Red) in infected zebrafish larvae at 3 days post infection (dpi).

Cover (back): Principle of CRISPR/Cas9 mutagenesis: The guide RNA forms a complex with Cas9 and directs this enzyme to cut the genomic DNA at the target site complementary to the guide RNA.

Cover design: Rui Zhang

Printed by: IPSKAMP printing, The Netherlands

ISBN:

Selective autophagy in host defense against mycobacterial infection

Proefschrift

ter verkrijging van

de graad van Doctor aan de Universiteit Leiden,

op gezag van Rector Magnificus prof.mr. C.J.J.M. Stolker,

volgens besluit van het College voor Promoties

te verdedigen op donderdag 8 november 2018

klokke 16.15 uur

door

Rui Zhang

geboren te Inner Mongolia, China

op 7 Juni 1987

Promotor:	Prof. dr. Annemarie H. Meijer	
Co-promotores:	Dr. Michiel van der Vaart and Dr. Monica Varela	
Promotiecommissie:	Prof. dr. Herman P. Spaink	
	Prof. dr. B. Ewa Snaar-Jagalska	
	Prof. dr. Tom H.M. Ottenhoff	(Leiden University Medical Center)
	Dr. Philip M. Elks	(University of Sheffield)

To my lovely parents, my brother and my wife! For always being there!

Despite the 7681 and 8652 km

Table of contents

Chapter 1

Introduction and outline of thesis

1. General introduction to Tuberculosis

1.1 Tuberculosis remains a global health threat

Tuberculosis (TB) has affected humans since ancient times and remains a dangerous infectious disease today. It usually affects the lungs, although it can also invade other organs of the body, such as the brain, the intestine, the kidneys, or the spine [1]. *Mycobacterium tuberculosis* (Mtb) is the causative agent of TB. There are two general types of TB infection based on the clinical symptoms: latent and active TB. TB spreads when people who have active TB cough, spit, speak, or sneeze in the vicinity of uninfected individuals, who then inhale the aerosols containing the bacteria [2]. Patients with latent TB do not manifest visible clinical symptoms, as bacteria can maintain a dormant state inside the host for a long period of time. However, latent TB can progress to clinically active TB because of various factors that can compromise the immune system of the host, such as malnutrition, diabetes, smoking, alcohol addiction, or reinfection. Overall, there is a chance of around 10% that latent TB becomes active [3]. The clinical signs of active TB include chronic coughing, pain in the chest, weakness or fatigue, weight loss, fever, and night-sweats. Evidence of TB infections in Europe can be tracked centuries back. Based on historic records, around 25% of the population died due to a TB epidemic in the 19th century, frequently referred to as 'consumption' due to the associated weight loss [1]. In modern times, TB remains a leading cause of morbidity and mortality in worldwide, with 10.4 million new cases and 1.7 million deaths in 2015 [4]. Moreover, TB infection often coincides with human immunodeficiency virus (HIV) infection, or immunocompromising chronic diseases such as diabetes mellitus. The resulting comorbidity and the increased occurrence of drug resistant Mtb strains have contributed to an increase in TB manifestations and associated mortality [5, 6]. According to the World Health Organisation (WHO), TB is a pandemic disease that represents a significant health burden for developing Countries. WHO estimated that more than one-third of the world's population is currently infected with Mtb and about 10-15% of this large number of carriers will progress to active TB. Furthermore, drug-resistant TB is a serious health threat for both developing and developed countries, as these strains are (becoming) resistant to the most frequently used first- and second-line anti-TB drugs [4].

1.2. Pathogenesis of tuberculosis

Mtb is a bacterial pathogen that can parasitize host immune cells. It was first described in 1882 by Robert Koch. In most cases, TB patients are infected by Mtb, but other strains of the Mtb complex can also cause TB, such as *M. bovis*, *M. africanum*, *M. canetti*, and *M. microti*. However, cases of TB caused by these other mycobacterial species have not been documented worldwide and are generally limited to regions with poor public health [7].

TB infections start when the mycobacteria-enclosed aerosols reach the pulmonary alveoli. Invading mycobacteria can be recognized by alveolar macrophages through several pattern recognition receptors (PRRs), including toll-like receptor (TLR) 1, TLR2, TLR4, and TLR9 [8-10]. Macrophages attempt to eliminate the bacteria from the infected tissue through phagocytosis [11]. During this process, Mtb is engulfed (phagocytosed) and temporarily resides in a membrane-bound vesicle, called a phagosome. Bacteria-containing phagosomes normally fuse with lysosomes to form phagolysosomes. Phagolysosome fusion presents a major anti-bacterial strategy by exposing engulfed bacteria to lysosomal acidic hydrolases [3]. The critical survival strategy of Mtb inside macrophages is to prevent the fusion between phagosomes and lysosomes. Furthermore, Mtb can also resist the acidic environment of lysosomes [12, 13] and initiate various countermeasures to protect itself against other host defense mechanisms, such as generation of reactive oxygen species (ROS) and nitrogen species (RNS) [14]. Thus, Mtb is able to survive and replicate inside macrophages and will eventually overgrow and kill the immune cells [12, 15]. To achieve this, Mtb not only resists the phagolysosomal pathway, but can also escape from phagosomes into the cytosol. Once inside the cytosol, the bacteria have access to sufficient nutrients, which improves its replication rate inside of macrophages [16]. This process requires the type VII secretion system ESX-1 (6-kDa early secretory antigenic target (ESAT-6) secretion system 1) [17]. This secretion system allows Mtb to resist host immune responses by exporting several effector proteins [18, 19]. A recent study showed that the ESX-1 secretion system directly affects the acidification of Mtb-containing phagosomes [20]. Furthermore, the ESX-1 secretion system has multiple other functions that contribute to the ability of Mtb to survive and replicate inside macrophages and to promote its cell-to-cell spreading [21].

Mtb infected macrophages produce inflammatory cytokines and chemokines to recruit other immune cells to form a compact and organized structure called a granuloma – the clinical hallmark of TB [22]. The recruitment of macrophages in the early stage of infection depends on the local production of ligands (CCL2/MCP-1, CCL12, and CCL13) that bind to the chemokine receptor CCR2 [23]. Adaptive immune cells, like T cells and B cells, are also recruited to the forming granuloma during later stages of the infection. Maintaining the structure of the granuloma requires the production of TNF-α by infected macrophages and T cells [24].

The granuloma is situated at the core of TB pathogenesis. This inflammatory structure functions to restrict mycobacteria in a limited area and provides a local environment where cells of the immune system can interact with the bacteria [22, 23]. However, recent studies have found that mycobacteria also utilize the granulomas to avoid killing by the host's immune response [24-26]. For example, macrophages in the granulomas have been shown to undergo an epithelioid transition that is characterized by downregulation of immune-related genes and upregulation of epithelial markers, a process which is induced by bacterial virulence factors [22, 24, 25, 27]. Formation of tight junctions between neighboring epithelioid macrophages further limits access to the granuloma core by newly recruited immune cells and prevents bacterial clearance [22, 24, 28]. Thus, macrophages and dendritic cells (DCs) inside of the granulomas are unable to delivery antigens to lymphocytes, effectively repressing the adaptive immune response [29, 30]. Mtb inside the granuloma can become metabolically dormant and persist for decades before reactivation occurs [22].

1.3. Prevention and control of tuberculosis

The “End TB strategy” was launched in 2014 by the WHO and achieved much progress in reducing new TB cases by improving treatment regimens and public health awareness [31]. TB prevention principally depends on the immunization of infants. Currently, Bacillus Calmette-Guérin (BCG) is the only TB vaccine used worldwide [32]. The BCG vaccine was generated as an attenuated live vaccine derived from a virulent strain of the *M. bovis* species by more than 200 times of consecutive passage [33]. The BCG vaccine effectively prevents forms of TB during childhood. However, BCG vaccination provides a highly variable level of protection against TB in

different populations and regions [34].

Both latent and active TB can be diagnosed and cured. Diagnostic tools for latent and active TB are readily available. Latent TB is efficiently detected by the Mantoux tuberculin skin test (TST) and the Interferon-gamma release assay (IGRA). The Mantoux test is based on a subcutaneous injection of tuberculin purified protein derivative (PPD), followed by a measurement of the resulting induration (palpable, raised, hardened area or swelling) as a read out of the level of immune recognition of tuberculin peptides. The interferon-gamma release assay is based on the quantification of Interferon-gamma production in response to the presence of TB antigens in the whole blood [35]. For active TB, chest radiography and bacterial cultures are efficient and rapid diagnostic methods [36].

Preventive therapy is necessary to lower the risk of disease progression from latent to active TB. The standard treatment of latent TB recommended by the WHO is an oral antibiotic regimen (e.g. isoniazid and/or rifampicin) for 6 to 9 months [35, 37]. However, the use of a single antibiotic frequently leads to development of drug resistance in active TB cases. Thus, treatment of active TB usually consists of a combination of antibiotics to kill the bacteria and lower the chance of Mtb developing drug resistance. Eradication of Mtb from the body by drug treatment is hard and time consuming, due to the special structure and chemical composition of the mycobacterial cell wall, which strongly inhibits the penetration of drugs and makes many antibiotics ineffective [38]. If TB patients do not receive sufficient treatment, it leads to a growing incidence of drug resistant strains: Multidrug-resistant (MDR), Extensively drug-resistant (XDR) and Totally drug-resistant (TDR) strains. This further reduces the treatment options and increases the incidence of death [39, 40]. In summary, there is a large variability in levels of protection provided by the current vaccine and Mtb is becoming increasingly resistant to many anti-TB drugs, which both stress the need for new therapeutics and more effective anti-TB treatments.

1.4. Zebrafish as a model to study mycobacterial pathogenesis

Researchers have frequently used – and are still using – *in vitro* Mtb cultures or Mtb infected macrophages to investigate the mechanisms of Mtb infection. However, results obtained from *in vitro* studies may be difficult to translate into human therapies, as two-dimensional cell cultures lack the TB granuloma characteristic of this disease [41]. Recently, successful attempts have been made to culture granulomas in three dimensions, using media that resemble the extracellular environment found in tissues [42]. In addition, reliable animal models are essential to improve our understanding of the mechanisms of TB pathogenesis. Artificially infected animal models are an indispensable approach to investigate the host and bacterial factors involved in TB pathology, and to select new candidates for drugs and vaccines [43].

Currently, several animal species are being used to study Mtb infections, which include mice, guinea pigs, rabbits and non-human primates. In murine infection models, it has been difficult to replicate human TB pathologies as the commonly used mouse strains do not develop the highly organized granuloma structures observed in humans and in non-human primates [22]. However, alternative mouse strain, such as C3HeB/FeJ, DBA/2 and CBA/J, can develop necrotic granulomas in the lungs following infection with Mtb [44-46]. These models were generated by selecting for mouse strains with increased susceptibility to Mtb, which resulted in the identification of genetic loci that prevent the formation of necrotic granulomas [46, 47]. These new TB models have been used to screen for anti-TB drugs and to test new vaccine candidates [45, 48]. Other mammalian models (such as guinea pigs and rabbits) have been developed that mimic human TB pathology, including the formation of necrotic granulomas [43]. However, both the guinea pig and rabbit models lack of immunological reagents available for mice and are difficult in genetic manipulation [49]. The primate infection models present similar clinical signs as human TB and form classical TB granuloma structures. However, the costs and ethical considerations arising from the use of these models imply that they can only be used sparsely. Thus, additional animal models are necessary to study TB pathogenesis.

During the last 10 years, the zebrafish has become a widely used alternative animal model to study mycobacterial pathogenesis [50-52]. Adult zebrafish have fully functional innate and adaptive

immunity, which is highly similar to the mammalian immune system [53]. Furthermore, zebrafish are naturally susceptible to *Mycobacterium marinum* (Mm), the causative agent of TB in ectotherms. As a close relative of Mtb, Mm shares many of its virulence factors [54, 55]. The zebrafish-Mm model presents additional advantages that are distinct from those of other TB models [56]. Zebrafish embryos and larvae are transparent, which allows intravital imaging of host-pathogen interactions following microinjection of Mm [57]. At 1 day post fertilization or at later stages, zebrafish larvae can form organized and compact Mm granulomas, which have high similarity to the early stages of granulomas generated by Mtb in primates [58]. Zebrafish transgenesis methods have been well established, and the recent breakthroughs in gene editing with CRISPR/Cas9 have facilitated the generation of knock-out and knock-in zebrafish [59]. On the bacterial side, Mm presents advantages over working with Mtb, including lower biosafety restrictions (BSL2 instead of BSL3) and a considerably shorter replication time [58]. In recent years, the insights from the Mm-zebrafish embryo infection model have contributed significantly to our understanding of TB pathogenesis [27, 59-62].

2. Autophagy: an important immune defense mechanism against Mtb

2.1 The basic function of autophagy

Autophagy is an evolutionary conserved lysosomal degradation pathway in eukaryotic cells that can degrade cytoplasmic materials and organelles. By removing unwanted cellular contents, autophagy functions in maintaining cellular homeostasis. This physiological phenomenon was first discovered by Christian De Duve around 55 years ago [63]. The process is genetically well-defined and many of the factors involved are conserved in eukaryotes from yeast to humans [64]. Autophagy is recognized as a survival mechanism in response to different types of stress, including nutrient deficiency, growth factor deficiency, and hypoxia [65]. The autophagic degradation of cytoplasmic material recycles amino acids and other nutrients, e.g. to fuel metabolic pathways in nutrient-deficient conditions. Autophagy can also be stimulated by other stress factors that include diseases and infections [66]. Activation of autophagy in these contexts generally follows upon an increased transcriptional activation and/or post translational protein modification of autophagy-related factors and regulators by the host cells [67].

Three main categories of autophagy are identified in mammalian cells, based on the mechanisms used to capture cytosolic cargo. These include macroautophagy, microautophagy, and chaperone-mediated autophagy. All of them rely on proteolytic degradation of cytosolic materials in lysosomes [68]. Macroautophagy is characterized by capturing cargo in a double membrane-bound structure. During this process, the isolation membrane (or autophagophore) undergoes expansion and elongation to form a double membrane vesicle, known as an autophagosome, which eventually fuses with a lysosome to generate an autophagolysosome [69] . The term "autophagic flux" is used to describe the whole process from autophagosome formation to the degradation of the cytoplasmic cargo by hydrolases [70]. Microautophagy is a non-selective degradation process during which cytosolic components are directly engulfed by lysosomes [71]. Finally, chaperone-mediated autophagy (CMA) was identified in 1981 and is quite different from macro- and microautophagy in terms of its selectivity and mechanism of cargo degradation [72]. CMA only eliminates targeted proteins and delivers them to the lysosomes via a process assisted by chaperone proteins/heat shock cognate proteins, such as Hsc-70. Hsc-70 can be recognized by the lysosomal membrane receptor lysosomal-associated membrane protein 2A (LAMP-2A), which leads to degradation of the Hsc-70 protein complex [73]. Of the three types of autophagy, macroautophagy is the most abundant process and is therefore also the most extensively studied form of autophagy.

Macroautophagy (hereafter referred to solely as autophagy) is historically regarded as a non-specific pathway. However, it has become clear that this process can also be used to selectively remove material from the cytoplasm. In that case, so called selective autophagy receptors (SLRs) identify and capture targets for autophagosomal degradation based on a molecular tag, such as ubiquitin [74]. Ubiquitination is a highly regulated process that is conserved in all eukaryotes. Ubiquitination can delivery covalently tagged substrates to (1) the proteasome, (2) the lysosome or, (3) the autophagosome [75]. The crosstalk between ubiquitination and autophagy relies on SLRs, which act like a bridge by simultaneously binding to ubiquitinated cargos and the forming autophagophore [76]. The selective autophagic degradation of misfolded proteins is called aggrephagy, that of mitochondria is called mitophagy, while the selective elimination of invading microbes is called xenophagy [77].

Xenophagy (also known as bacterial or anti-microbial autophagy) is considered a cell-autonomous defense mechanism against invading pathogens [77]. Deficiency of intracellular nutrients due to competition from invading pathogens is one of the signals sensed by eukaryotic cells to identify microbial invading and to diminish invading pathogens via autophagy [66]. Anti-microbial autophagy was first described in response to *Streptococcus pyogenes* (group A Streptococcus) infection [78]. The bacteria are sequestered into autophagosomes and fuse with lysosomes to form autophagolysosomes. This process results in elimination of most of the bacteria [78]. Around the same time, another study confirmed that stimulating autophagy can inhibit Mtb survival in infected macrophages [79]. This study has shown that either physiological or pharmacological induction of autophagy decreased the viability of Mtb, while induction of autophagy was beneficial for the maturation of Mtb-containing phagosomes [79]. Until now, autophagy has been shown to be able to directly target a diverse spectrum of pathogens, including various bacteria, viruses, and intracellular parasites [80].

2.2 The components of the autophagy machinery

Autophagy is a dynamic process which requires a series of distinct steps to complete. Autophagy is activated with the formation of a structure called the isolation membrane, also known as a phagophore. This lipid bilayer is thought to originate from the endoplasmic reticulum (ER) and/or the trans-Golgi network and endosomes [81]. The phagophore then elongates and expands around the cargo, sequestering the cytoplasmic material into a double membrane structure. This double membrane structure defines the autophagosome. The autophagosome eventually matures and undergoes fusion with lysosomes, which promotes the degradation of the autophagosomal contents by lysosomal acid proteases [68] (Fig1). This process is driven by autophagy-related proteins, which are controlled by a number of signaling pathways in response to cellular stress factors, such as the mammalian target of rapamycin (mTOR) signaling pathway for nutrient sensing and pattern recognition receptor (PRR)-signaling for invading microbes [66, 82]. The importance of autophagy is well established in mammals and other vertebrates, but the underlying molecular mechanisms have been uncovered using genetic analysis of yeast. Currently, more than 41 different ATGs have been revealed and identified in yeast by genetic

screening, followed by identification of homologs in higher eukaryotes [83].

Starvation, a classical inducer of autophagy, can result in low nutrient and amino acid levels, which induces autophagy by inhibiting the function of mTOR [84]. In turn, mTOR then relieves its inhibition of unc-51-like kinases 1/2 (ULK1 and ULK2) [84, 85], which are recruited to the phagophore to bind with the autophagy related gene 13 (ATG13) and FAK family kinase-interacting protein of 200kDa (FIP200) [85]. ULK1 and ULK2 have significant homology both in the C terminal and N-terminal regions. The C-terminal regions of ULK1 and ULK2 are required for interactions with ATG13 and FIP200, and for the translocation of ULK1 to nascent phagophores [84]. Assembly of this complex is essential for autophagy, because it allows the attraction of other ATG proteins to the phagophore assembly site (PAS) and activates several downstream targets through phosphorylation [67, 86]. The activation of the ULK1/2 complex results in binding with Beclin1 (ATG6 in yeast) and ATG14L, which attracts additional proteins to the PAS for initiation of phagophore formation [68]. This process requires the class III phosphatidylinositol-3 kinase (PI3KC3), resulting in the generation of phosphatidylinositol 3-phosphate (PI3P) by vesicular protein sorting 34 (Vps34) and recruitment of other effectors of the autophagy pathway [87]. PI3P is strictly required for elongation of phagophore and attracts other ATG proteins to the phagophore [88, 89].

The subsequent elongation and closure of the phagophore requires the recruitment of two ubiquitin-like proteins, ATG8/LC3 and ATG12 [90]. ATG8/LC3 (Microtubule-associated protein 1 light chain 3; hereafter referred to as LC3) can occur in two forms: LC3-I, which resides freely in the cytoplasm; and LC3-II, which is the membrane bound form of LC3. LC3-II is formed when LC3-I is conjugated to the lipid phosphatidylethanolamine (PE). Upon activation of autophagy, ATG12 is conjugated to the crucial autophagy factor ATG5. The ATG12-ATG5 conjugate forms a complex with ATG16L1, which lipidates LC3 to direct its localization in the membrane of the forming autophagosome. To date, at least 6 selective autophagy receptors (SLRs) have been identified, namely Sequestosome 1 (SQSTM1/p62), Neighbor of BRCA1 gene1 (NBR1), Nuclear dot protein 52 kDa (NDP52), Optineurin (OPTN), BCL2-interacting protein 3 like (BNIP3L), and NDP52-like receptor TAX1-binding protein (TAX1BP1) [76, 91, 92]. The common feature of these

receptors is that they contain an LC3 interaction region (LIR) motif and a ubiquitin binding domain (UBD). The LIR enables the targeting of selective receptors to LC3 (or other homologs of the LC3 family) attached to the membrane of a forming autophagosome [93]. The UBDs (diverse ubiquitin binding domains in each receptor) can recognize and bind ubiquitin [94]. UBDs ensure that selective receptors bind to ubiquitinated cargos to target them for autophagy [95].

Eventually, during the maturation of autophagosomes into autophagolysosomes, the tail-anchored SNARE syntaxin 17 recruited to the membrane of autophagosome allows fusion with lysosomes [96]. This process also requires lysosomal membrane proteins LAMP1 and LAMP2 [97]. The result of autophagolysosomal fusion is the degradation of sequestered cargo by lysosomal hydrolases (Fig1)

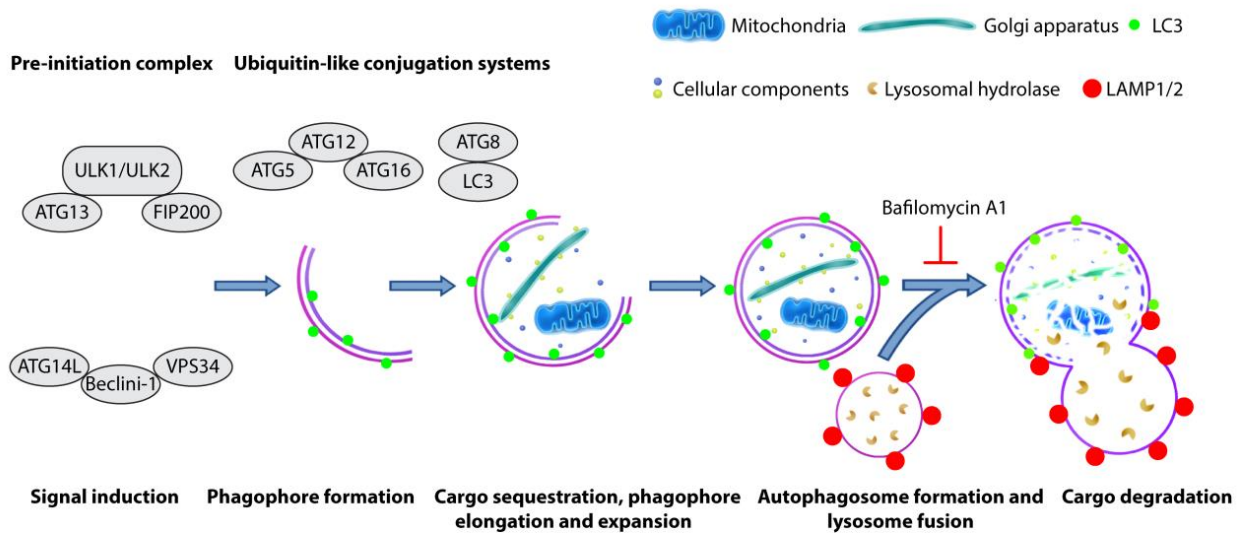

Figure 1: Schematic representation of the autophagy pathway

The basal level of autophagy activity is low under healthy conditions. To maintain homeostasis, autophagy is activated upon sensing cellular stress signals, such as nutrient deprivation or intracellular infections. Autophagy is induced through the activation of the ULK1/ULK2 complex which also contains ATG13 and FIP200. This complex subsequently interacts with the VPS34-Beclin1-Atg14L complex, contributing to the initiation of the isolation membranes (phagophores) from endomembrane sources such as endoplasmic reticulum (ER), Golgi apparatus, the mitochondria and the plasma membrane-derived endocytic organelles. Phagophores can sequester cargo via selective or autonomous recognition. The elongation and expansion of phagophores containing cargo requires the

involvement of the ATG5-ATG12-ATG16 and ATG8-LC3 ubiquitin-like conjugation complexes to form double-membraned autophagosomes. The maturation of autophagosomes involves fusion with lysosomes to form autophagolysosomes. This event requires the lysosomal membrane proteins LAMP1/2. After fusion, the sequestered cargo is degraded into amino acids and other small molecules by lysosomal and acidic hydrolases. The degraded material can be recycled and utilized as a source of energy for maintenance of cellular functions under the various stresses. LC3 is widely used as a general marker for autophagic activity and is involved in the entire process of autophagy.

2.3 Role of autophagy in immunity

Recent studies have demonstrated that defects in autophagy are associated with many diseases, including neuro-degenerative diseases, diabetes, cancer, and infectious diseases [98]. In this thesis, we focus on the function of autophagy in immunity, and in particular on its role in defense against the intracellular mycobacterial pathogens that cause TB. The main functions of autophagy in innate and adaptive immunity can be classified as follows: elimination of invading pathogens; control of pro-inflammatory signaling; antigen presentation to activate the adaptive immune system; and secretion of immune mediators [66].

Autophagy is a prominent innate immune mechanism by which an infected cell eliminates intracellular pathogens [66]. Invading microbes are recognized by pattern recognition receptors (PRRs), such as toll like receptors (TLRs) and NOD like receptor (NLRs). These receptors can recognize pathogen-associated molecular patterns (PAMPs), which are derived from microbes. PAMPs consist, for instance, of nucleic acids (e.g. bacterial DNA, double and single stranded RNA), or other molecules that are specific for invading pathogens (e.g. flagellin) [99]. For instance, recognition of lipopolysaccharide (LPS) – the outer membrane constituent of Gram-negative bacteria – by TLR4 leads to activation of autophagy [100]. Furthermore, LPS-induced autophagy enhanced the colocalization between mycobacteria and autophagosomes in cultured macrophages [100]. The function of autophagy in host defense against infection is well established for a number of invading microbes, including Mtb, Salmonella *Typhimurium*, *Shigella flexneri*, *Listeria monocytogenes* and *Streptococcus pyogenes* [101].

There is also increasing evidence that the process of autophagy participates in reduction and

modulation of inflammatory responses [102]. For instance, single nucleotide polymorphisms (SNPs) in genes central to the autophagy machinery significantly increase the susceptibility for Crohn's disease, which is characterized by uncontrolled inflammation in the gastrointestinal tract [103]. These results implicate that autophagy can affect the outcome of inflammatory disorders like Crohn's disease. One explanation for this is derived from the fact that autophagy controls the homeostasis and development of immune cells, such as macrophages, neutrophils and lymphocytes. These cells are all necessary for host immune and inflammatory responses and secrete cytokines and chemokines. Thus, defects in autophagy could indirectly result in poorly controlled inflammatory responses [66, 104].

However, a direct effect of autophagy on inflammatory processes has also been uncovered. Saitoh et al. (2008) first described that the loss of a central component in the autophagy machinery (ATG16L1) increased the production of pro-inflammatory cytokines when macrophages were stimulated with the endotoxin LPS. Their results demonstrated that autophagy directly controls the activity of the inflammasome, a multiprotein structure that promotes the maturation of interleukin 1 beta (IL1b) and interleukin 18 (IL18) and pyroptosis, an inflammation-associated type of programmed cell death [102]. Other studies expanded on these important findings, and it is now clear that autophagy controls the activity of inflammatory cytokines at the transcriptional level [105]; at the inflammasome-dependent processing step [102]; and during the excretion of mature cytokines [106]. This immune function of autophagy is highly relevant to TB pathogenesis, since nonresolving inflammation during mycobacterial infection fuels the generation of TB granulomas [107].

Several studies have demonstrated that autophagy is also involved in adaptive immune responses, including the regulation of antigen processing and presentation [66]. Inside antigen-presenting cells (APCs), autophagy can deliver cytoplasmic and nuclear antigens to lysosomes, which can then be presented to cells of the adaptive immune system ($CD4^+$ T cells) through the major histocompatibility complex class II (MHC-II) molecules [108]. This function of autophagy is also relevant to TB prevention, as it has been shown that stimulating autophagy-mediated antigen presentation increases the efficacy of BCG vaccination [109].

2.4 Autophagy as defense mechanism against Mtb infections

Susceptibility to active TB is partially genetically determined and variations in genes involved in the autophagic pathway have been identified that might disturb the host response to Mtb infection. A genome-wide association study has revealed a link between certain polymorphisms in ATGs and predispositions to TB in human patients. Three autophagy-related genes were identified from this screen, namely ATG16L1, IRGM, and VDR [110]. Multiple other studies have experimentally demonstrated the involvement of autophagy factors in controlling Mtb infections in cultured cells [79, 111, 112], including the demonstration of an important role for IRGM in the elimination of intracellular mycobacteria [113].

During Mtb infection, bacteria prevent phagosome maturation and are able to permeabilize the phagosomal membrane using region of difference 1 (RD1)-dependent virulence factors, which are secreted through the bacterial ESX-1 system [114]. This enables the pathogen to escape into the cytoplasm, which activates selective autophagy following recognition of the bacteria by PRRs. Even when Mtb remains inside a permeabilized and immature phagosome, its extracellular bacterial DNA can still leak from the phagosome and be recognized by the cytosolic DNA sensor STING (stimulator of interferon genes) [115]. Recognition by STING results in the labeling of bacteria with ubiquitin, which requires the ubiquitin ligases PARK2 (Parkin) and SMURF1 [116, 117]. This subsequently targets Mtb, or Mtb-containing immature phagosomes, for autophagolysosomal degradation via the ubiquitin-binding selective autophagy receptors p62 and NDP52 [115] (Fig2).

Besides directly targeting intracellular bacteria for xenophagy, p62 also contributes to defense against mycobacteria by delivering ubiquitinated cytosolic proteins to autophagolysosomes, where they are proteolytically converted into products capable of eliminating Mtb [118]. Thus, selective autophagy via the ubiquitin-binding receptor p62 presents an effective defense mechanism against intracellular mycobacterial infections via at least two mechanisms of action.

Despite the strong evidence – mostly from *in vitro* studies – demonstrating a role for autophagy in host defense against mycobacteria, the *in vivo* relevance of these mechanisms has recently

been questioned [119]. In a seminal study, Watson et al. (2012) previously found that mice with a monocyte/macrophage-specific deficiency in ATG5 were highly sensitive to Mtb infection and displayed elevated lung tissue damage. ATG5 is required for the early stage of autophagosome formation and ATG5 deficiency therefore affects the basal levels of autophagy [120, 121]. The study by Kimmey et al. (2015) recently showed that macrophage-specific ATG5 depletion indeed resulted in increased Mtb infection, but this was mostly due to an overstimulated inflammatory response, rather than to impaired autophagy. Furthermore, macrophage-specific depletion of other autophagy factors – including ULK1, ULK2, ATG4B, and p62 – did not affect the outcome of Mtb infection in mice. Instead, the authors of this paper suggest that autophagy-associated proteins may function independent of xenophagy to influence bacterial pathogenesis [119].

The discrepancies between *in vitro* and *in vivo* studies illustrate the need for further investigations into the role of autophagic defense against mycobacteria in animal models for TB. In this light, work using the zebrafish TB model can help to bridge the gap between mechanistic findings in cell culture models and their implications for disease outcome [52, 54, 58]. For instance, a study from our laboratory that combined *in vitro* and *in vivo* experiments, demonstrated the relevance of a novel signaling pathway controlling autophagic defense against mycobacterial infections [62]. In this study, analysis in Mtb infected human macrophages and the zebrafish model for TB revealed that the DNA damage-regulated autophagy modulator 1 (DRAM1) is activated downstream of pathogen recognition by TLRs. Signaling via the TLR-MYD88-NFκB innate immune sensing pathway activated DRAM1 and promoted selective autophagy against the bacteria. Transient knockdown of *dram1* in the zebrafish TB model leads to increased mycobacterial infection, whereas transient overexpression of Dram1 reduces infection by activation of autophagy. Finally, DRAM1-mediated selective autophagic defenses required the cytosolic DNA sensor STING and the selective autophagy receptor p62 [62].

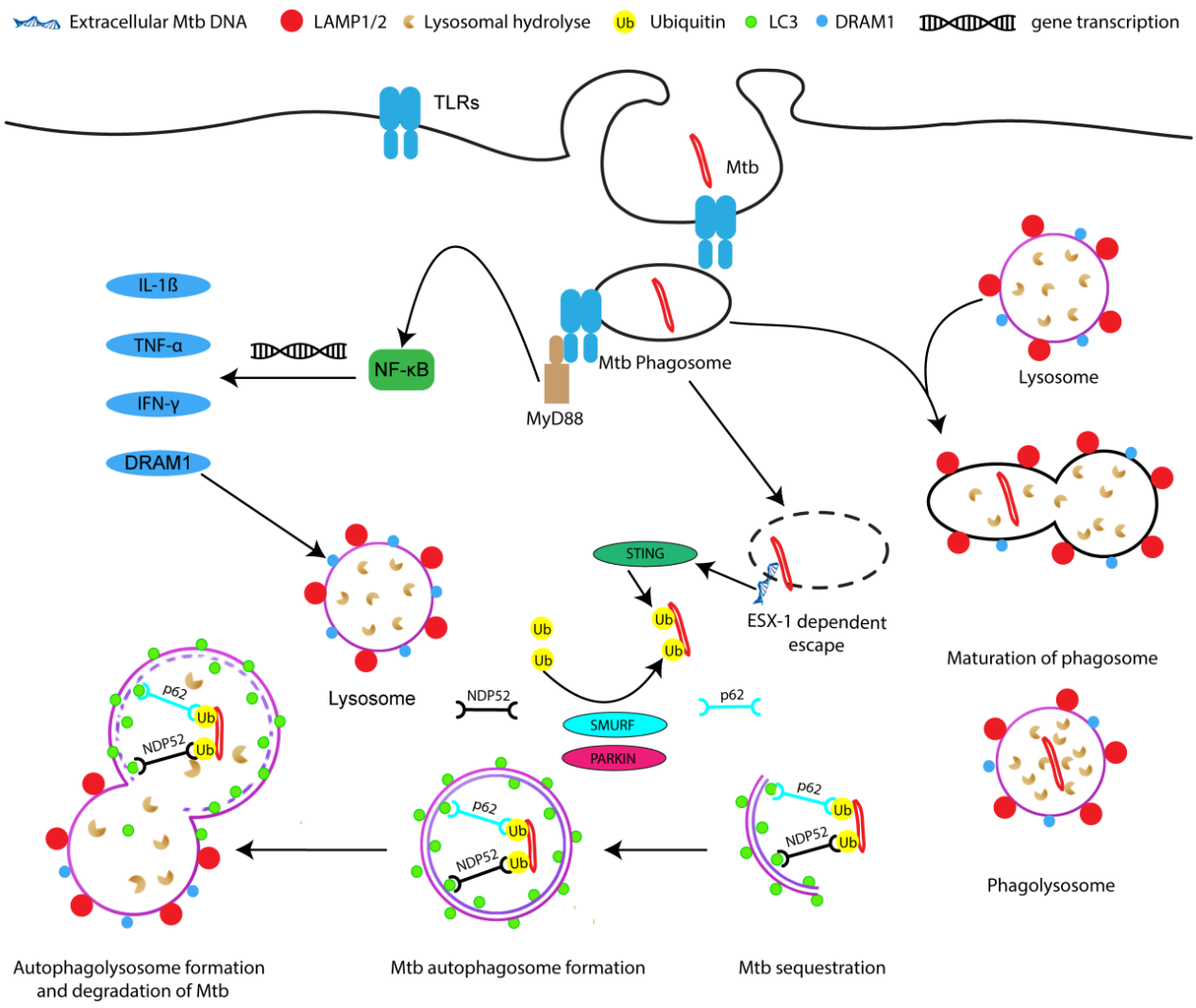

Figure 2: Schematic diagram of elimination of Mtb infection via the phagocytosis and autophagy pathways

The activation of autophagy via diverse signaling pathways plays an important function in the clearance of intracellular Mtb. Maturation of Mtb containing phagosomes partially attributes to killing of Mtb. However, Mtb inhibits phagosome maturation via multiple virulence mechanisms. For instance, Mtb utilizes its ESX-1 secretion system to escape from phagosomes into the cytosol. Cytoplasmic bacterial DNA can be recognized by the DNA sensor STING and promotes ubiquitination of Mtb. In this process, the ubiquitin ligases PARKIN and SMURF support the recruitment of ubiquitin to Mtb. Ubiquitin receptors, such as p62 and NDP52, recognize ubiquitinated Mtb and recruit LC3, contributing to the activation of autophagy to degrade Mtb. Finally, multiple factors stimulate autophagic clearance of Mtb. Mtb infection induces *DRAM1* as well as cytokine genes via a TLR-MYD88-NFκB signaling pathway. DRAM1 is thought to localize to the membrane of lysosomes to promote their fusion with autophagosomes.

3. The DRAM family of proteins

3.1 DRAM family proteins are regulators of autophagy

As described above, autophagy is orchestrated by several core proteins that are involved in all autophagic responses. In addition, autophagy regulators have been identified that are not critical components of the core autophagy machinery, but that play roles in regulating autophagy in specific situations or in response to specific stimuli. These autophagy regulators include the members of the DNA damage-regulated autophagy modulator (DRAM) family of proteins. DRAM1 was identified by Crighton et al. around one decade ago [122]. Until now, four other family members were identified and characterized as DRAM2/TMEM77, DRAM3/TMEM150B, DRAM4/TMEM150C and DRAM5/TMEM150A (Table 1). Currently, six Dram family members have been identified in zebrafish: Dram1, Dram2a, Dram2b, Dram3/Tmem150b, Dram4/Tmem150c and Dram5/Tmem150a. The DRAM family is conserved from humans to teleost fish, including zebrafish, with the exception that a DRAM1 homolog has not been identified in Coelacanth (*L. chalumnae*) yet (Fig3).

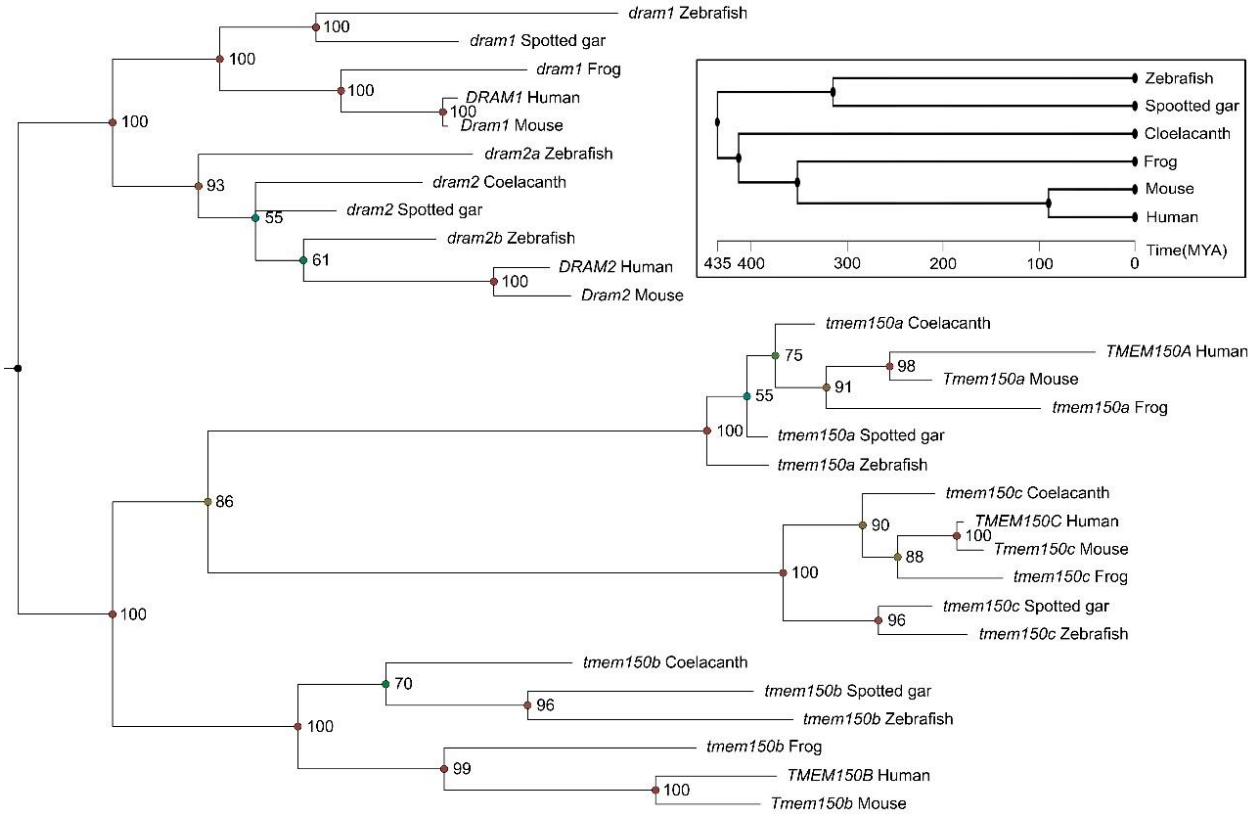

Figure 3: Phylogenetic comparison of DRAM family protein sequences from different species. Species include zebrafish (*Danio rerio*), spotted gar (*Lepisosteus oculatus*), coelacanth (*Latimeria chalumnae*), frog (*Xenopus)*, mouse (*Mus musculus*) and human (*Homo sapiens*). The protein sequences of DRAM1 (ENST00000258534.12), DRAM2 (ENST00000286692.8), DRAM3/TMEM150B (ENST00000326652.8), DRAM4/TMEM150C (ENST00000449862.6) and DRAM5/TMEM150A (ENST00000306353.7) were obtained from Ensembl. The phylogenetic tree was constructed with 4 independent MarKov chain Monte Carlo runs in MrByers 3.2.1 and each run consisted of 1,000,000 iterations sampled once every 200 iterations.

The human *DRAM1* gene encodes a protein that consists of 236 amino acids [122]. Protein domain analysis suggests that DRAM1 contains an endoplasmic reticulum (ER) targeting signal and six hydrophobic transmembrane regions (Table 1). DRAM1 is predominately found on lysosomes [122]. However, its presence in other compartments has also been described, including endosomes, peroxisomes, autophagolysosomes, the endoplasmic reticulum, and the Golgi apparatus [123]. Expression of *DRAM1* can be regulated by the tumor suppressing transcription factors p53 [122], p73 [124], and E2F1 [125], as well as the immunity-related transcription factor NF-κB [62]. It has been reported that DRAM1 is involved in the regulation of various cellular processes, including autophagy, apoptosis, immunity, and cellular differentiation [126]. For instance, DRAM1 is required to initiate autophagy and cell death downstream of p53-activation [122, 124]. Nonetheless, DRAM1 protein interactions remain poorly characterized. A direct interaction between DRAM1 and the apoptosis regulator BAX has been demonstrated [127], but the evidence for interactions with, for instance, p62 remains circumstantial [62, 128]. Given the many cellular functions DRAM1 is involved in, it is not surprising that this autophagy and cell death regulator has been implicated in several human diseases, including cancer [122, 124, 128-130], HIV[131] and tuberculosis [62].

DNA damage regulated autophagy modulator 2 (DRAM2) is closely related to DRAM1. Both DRAM1 and DRAM2 consist of six putative transmembrane domains and localize primarily to lysosomes [132, 133]. As is the case for DRAM1, overexpression of DRAM2 induces autophagic structures [134]. Moreover, silencing DRAM2 interferes with starvation-induced autophagy [134], which also implicates DRAM2 in regulation of autophagy. Like DRAM1, DRAM2 is also required for p53-dependent cell death, and overexpression of both DRAM1 and DRAM2 together was found to be sufficient to induce apoptosis [133]. DRAM2 was shown to interact with BECN1 and

UVRAG, essential components of the autophagy machinery, leading to the displacement of RUBCN from the BECN1-complex and promoting the activity of the class III phosphatidylinositol 3 kinase (PtdIns3K) [135]. DRAM2 also interacts with LAMP1 and LAMP2 to facilitate autophagosome maturation [135]. Although the transcriptional regulation of *DRAM2* remains to be determined, *DRAM2* mRNA levels have been identified as direct targets of down regulation by micro RNA (miRNA) 125b and miRNA144* [135, 136]. Downregulation of *DRAM2* is linked to human disease, as its expression was found to be reduced in ovarian cancers [133], and downregulation of *DRAM2* by miRNA125b promoted retino blastoma growth[136]. DRAM2 has also been implicated in tuberculosis, as further discussed below.

DRAM3 has an amino acid sequence overlap of 30% and a sequence similarity of 43% with DRAM1 [126, 137]. Like DRAM1, DRAM3 contains a signal peptide and several transmembrane domains. *DRAM3* has been detected in a range of normal tissues and tumor cells, but unlike *DRAM1*, its expression is not induced by p53 [137]. Similar to DRAM1, DRAM3 localizes to (auto)lysosomes and endosomes. However, it also localizes to the plasma membrane, which DRAM1 does not. The initial characterization of DRAM3 function revealed that it regulates autophagic flux and cell survival in response to starvation, but its effect on cell survival occurred independent of autophagy [137]

To date, DRAM4/TMEM150C and DRAM5/TMEM150A have been identified *in silico* as DRAM-family members but remain poorly characterized. DRAM5/TMEM150A was reported as the functional homologue of yeast Sfk1 [138]. DRAM5 forms a complex with PI 4-kinase type IIIα (PI4KIIIα) at the plasma membrane to regulate the generation of phosphatidylinositol 4,5-biphosphate $PI(4,5)P_2$ [138]. DRAM4 could also be detected at the plasma membrane but is primarily localized to lysosomes [138]. Clearly, the two remaining DRAM-family members are eagerly awaiting further characterisation.

Table 1: Interactions and functions of DRAM-family proteins in relation to human diseases

DRAM-family proteins	Protein domains	Protein localization	Interaction partners	Genetic regulation	Cellular functions	Involved diseases	First reported (year)
DRAM1	6 Transmembrane domains[122], Endoplasmic reticulum signal peptide[122]	Lysosomes [122, 139], Autolysosomes[123], Endosomes[123], Peroxisomes[123], Endoplasmic reticulum[123], Golgi apparatus[123]	p62[62], Bax[127]	p53[122], p73[124], NF-kB[62], E2F1[125], miRNA-26b[140]	Autophagy[122], Cell death[122], Cellular differentiation[129]	Cancer[122] APL[129] Ewing Sarcoma[130], Glioblastoma[128], HIV[131], Tuberculosis[62],	2006
DRAM2 (TMEM77)	6 transmembrane domains[133]	Lysosomes[133], Autophagosomes[134], Phagosomes[135]	DRAM1[133], Beclin1[135], UVRAG[135], Rubicon[135], LAMP1[135], LAMP2[135],	miRNA125b[136], miRNA144*[135],	Autophagy[134], Cell death[133],	Tuberculosis[135], Cancer[136],	2009
DRAM3 (TMEM150B)	Signal peptide[137], 6 Transmembrane domains[137]	Lysosomes[137], Autolysosomes[137], Endosomes[137], Plasma membrane[137]	-	-	Autophagy[137], Cell death[137],	-	2015
DRAM4 (TMEM150C)	-	Lysosomes[138], Plasma membrane[138],	-	-	-	-	2015
DRAM5 (TMEM150A)	-	Plasma membrane[138]	PI4KIIIα[138], EFR3[138]	-	Generation of $PI(4,5)P_2$[138]	-	2015

3.2 DRAM1 and DRAM2 play an important role in restricting mycobacterial infection

DRAM1 was first reported as a factor involved in host-pathogen interactions by Laforge et al. in 2013, who implicated DRAM1 in host defense against HIV infection via regulation of lysosome membrane permeabilization and subsequent cell death. This function of DRAM1 is dependent on activation of the p53 pathway and silencing of DRAM1 is shown to increase HIV infection[131]. Shortly thereafter, our group discovered that zebrafish Dram1 functions independently of p53 in host defense against intracellular mycobacteria [62]. As described before, we could demonstrate that mycobacterial infection induces zebrafish *dram1* and human *DRAM1* via a TLR-MYD88-NFκB signaling pathway. The autophagic defense against mycobacterial infection inferred by activation of zebrafish Dram1 also required Sting and the selective autophagy receptor p62 [62]. Furthermore, Dram1 promoted the fusion between bacteria-containing compartments and

lysosomes. Since expression of zebrafish *dram1* can also be induced by injection of the endotoxin LPS, we proposed that DRAM1 functions in defense against a spectrum of bacterial pathogens. This hypothesis was later confirmed by Masud et al. [141], who demonstrated that Dram1 also provides protection against infection by *Salmonella typhimurium*. A recent study using Mtb infected human macrophages revealed that DRAM2 also functions in defense against mycobacterial infections [135]. In this study, it was demonstrated that DRAM2 is required for acidification of Mtb-containing phagosomes. DRAM2 was shown to physically interact with a complex of autophagy regulators, including BECN1 and UVRAG, to remove the autophagy-inhibiting protein RUBICON from this complex and activate autophagy.

Concluding, both DRAM1 and DRAM2 have been demonstrated to participate in the immune response to mycobacterial infections, either *in vivo* using the zebrafish infection model (Dram1), or in vitro using human cell culture studies (both DRAM1 and DRAM2) [62, 135]. Interestingly, expression of human and zebrafish *DRAM1/dram1* is induced upon Mtb or Mm infection, while induction of miRNA144* reduces expression of *DRAM2* in response to Mtb infection [135]. The latter observation suggests that Mtb has evolved mechanisms to counteract the host's autophagy defenses. The interplay between the two DRAM-family members in defense against bacterial pathogens remains to be investigated.

4. Prospects of DRAM1 as a target for host-directed therapy against tuberculosis

4.1 Host-directed therapies as adjuvant for TB treatment

The rapid emergence of drug-resistant Mtb strains and co-morbidity caused by, for instance, HIV co-infections makes it difficult to treat TB patients [5]. Thus, the development of new and effective treatment regimens for TB is urgently needed. Currently, host-directed therapy (HDT) has gained interest as a complementary approach to antibiotic treatment. HDTs could transform traditional antibiotic therapies into more effective treatments and reduce the length of TB treatment regimens [142].

HDTs do not act like traditional antibiotics that directly target the pathogens and thereby put selective pressure on them. Therefore, application of these strategies might also reduce the development of drug resistance [5]. HDTs can increase host cellular responses to pathogens, counteract the cellular effects of disease-causing virulence factors, and activate immune responses (i.e. activation of autophagy, production of anti-microbial peptides, reactive oxygen species or cytokines), or reduce the pathological consequences of excessive inflammation [38, 142].

A range of candidate host-directed TB therapies have been developed aiming either at reducing the abundant inflammation and lung tissue damage typical of TB pathology, or at augmenting the specific innate and adaptive immune processes which directly target Mtb [38]. On the latter front, the most promising strategies for development of HDTs include 1) targeting the mechanisms of granuloma formation, 2) the induction of phagolysosomal fusion and autophagy, and 3) the modulation of cell-mediated immune responses [5, 38, 143].

Various pro-inflammatory cytokines are produced in response to Mtb infection, including TNF-α, IL1-b, IL-12, IL-17 and interferon gamma (IFN-γ) [144]. Inflammation functions as a double-edged sword during TB infection, and the levels of pro- and anti-inflammatory cytokine production can strongly affect the outcome of Mtb infections [14]. The balance of host inflammatory responses is also controlled by the production of lipoxin A4 (LXA4) and leukotriene B4 (LTB4): increased LXA4 levels are beneficial for a balanced inflammatory response and control of TB, while increased LTB4 levels produce the opposite effect with hyperinflammation and exacerbated infection [145, 146]. The inflammation induced by Mtb infection starts from the very early stages, and continues during the progression to active TB, until complete eradication [146]. This is at the basis of the current concept of modulating the inflammatory response as an HDT to reduce the lung tissue damage and adjust the host immune response [147]. For instance, a clinical trial has revealed that an IFN-γ adjuvant therapy can improve the outcome of TB treatment, resulting in significantly reduced respiratory symptoms and lung tissue damage, as well as reduced mortality compared to chemotherapy regimens without IFN-γ supplement. However, IFN-γ adjuvant therapy has also resulted in side effects, such as fever and headaches [148, 149].

The granuloma plays a central role in Mtb pathogenesis, encapsulating the bacteria to avoid Mtb

spreading into deeper tissue. As a side effect, granulomas also limit the effectiveness of anti-TB treatment due to poor penetration of antibiotics. TNF-α is known to be essential for granuloma maintenance and host defense against TB [150-152]. Hence, patients undergoing anti-TNF treatment for inflammatory diseases are at risk of activation of latent TB[151]. Nevertheless, neutralizing TNF-α during TB treatment with antibiotics could be promising strategy, as this was found to disrupt the architecture of granulomas and improve drug efficacy against Mtb [153]. However, the role of the granuloma in TB pathogenesis is not completely understood yet, which still restricts the use of this HDT in the clinic [26].

Given that autophagy is a critical immune defense mechanism against Mtb infection, this process is also a promising therapeutic target for TB treatment [154]. In fact, autophagy inducers were identified as hits in several drug screens for HDTs using Mtb infected human cells [155-157]. Furthermore, it was demonstrated that autophagy is required for effective anti-mycobacterial drug action of the first line drugs, such as isoniazid and pyrazinamide [156]. Both isoniazid and pyrazinamide treatment clearly induced autophagosome formation and co-localization of Lc3 with Mt.b in primary murine bone marrow-derived macrophages (BMDMs) [156]. However, it is a risk to induce canonical autophagy by non-selective drugs, due to the involvement of autophagy in diverse cellular functions. Rapamycin is a general autophagy-inducing drug which acts by inhibiting mTOR. Strikingly, treatment of zebrafish larvae with this drug increased susceptibility to mycobacterial infection, rather than decreasing it [62]. This could potentially be explained by the fact that Rapamycin is also known for its immunosuppressive effects on the host [158]. Thus, targeting autophagy to combat infectious diseases requires the development of specific modulators of autophagy.

4.2. Prospects of Dram-family members as host directed therapy against TB

Killing Mtb in infected macrophages in the early stages of infection is a key approach to avoid progression of TB disease. Two out of five DRAM family members (DRAM1 and DRAM2) have been implicated in anti-mycobacterial defense by enhancing autophagy and the microbicidal function of lysosomes either *in vitro* or *in vivo* [62, 135]. Thus, these DRAM family members are potential targets for HDTs that stimulate killing of Mtb by host-autonomous mechanisms.

Activation of zebrafish Dram1 leads to a significantly improved disease outcome following mycobacterial infection. The current bottleneck is to dissect how to pharmacologically stimulate DRAM1 in animal models or human patients. Based on our previous study, LPS injection is a strong inducer of *dram1* expression *in vivo* [62]. However, this approach carries severe risks in a clinical situation, as LPS injections can result in hyperactivation of inflammatory processes, or even toxic shock.

Another approach would be to directly inject DRAM1 recombinant protein into TB patients to elevate DRAM1 protein levels. DRAM1 protein could directly participate in defense against Mtb. However, it will be difficult to ensure that DRAM1 ends up at the appropriate location in infected cells to carry out its function. Thus, the more valid approach is to continue our study into the *in vivo* working mechanisms of DRAM1 (and other members of the DRAM family), to identify endogenous modulators that can serve as drug targets to stimulate DRAM1 activity. Identifying those might help to bring this research closer to clinical applications.

5. Outline of the thesis

The aim of the work described in this thesis was to exploit the benefits of the embryonic and larval zebrafish TB model to further study the function of selective autophagy in defense against mycobacterial infections. To this end we created null mutants for zebrafish Dram1, and the selective autophagy receptors p62 and Optineurin. The generated mutant lines were then used to study the role of these proteins in autophagic defense, as well as their potential effect on bacterial pathogenesis outside of autophagy.

This introductory **Chapter 1** provides background information about TB and autophagy and highlights that the DRAM family of proteins could be promising targets for host-directed therapy to modulate autophagy and eliminate mycobacterial infection.

Chapter 2 describes how mutation of the *dram1* gene leads to increased susceptibility to mycobacterial infection and highlights that the absence of Dram1 induces Caspase-1 dependent cell death of infected macrophages.

Chapter 3 reports on a transcriptome analysis of *dram1* mutants in the absence and presence of infection. This study revealed that deficiency in Dram1 has major effects on the expression of genes in pathways involved in metabolism, lytic cell death, and Toll-like receptor signaling.

Chapter 4 describes that mutation of the genes for the selective autophagy receptors Optineurin and p62 results in increased susceptibility to mycobacterial infection. These proteins mediate an autophagic defense response against mycobacterial infection by sequestering ubiquitin-labeled bacteria into autophagosomes.

Chapter 5 summarizes and discusses the findings presented in this thesis in relation to the latest scientific advances in TB and autophagy research.

References

1. Smith I. Mycobacterium tuberculosis Pathogenesis and Molecular Determinants of Virulence. Clinical Microbiology Reviews 2003; 16:463-96.
2. Al-Humadi HW, Al-Saigh RJ, Al-Humadi AW. Addressing the Challenges of Tuberculosis: A Brief Historical Account. Front Pharmacol 2017; 8:689.
3. Flynn JL, Chan J. Tuberculosis: latency and reactivation. Infect Immun 2001; 69:4195-201.
4. WHO. Global tuberculosis report 2017 (WHO/HTM/TB/2017.23). 2017.
5. Kolloli A, Subbian S. Host-Directed Therapeutic Strategies for Tuberculosis. Front Med (Lausanne) 2017; 4:171.
6. Matteelli A, Roggi A, Carvalho AC. Extensively drug-resistant tuberculosis: epidemiology and management. Clin Epidemiol 2014; 6:111-8.
7. Grange JM, Yates MD, de Kantor IN. Guidelines for speciation within the Mycobacterium tuberculosis complex. World Health Organization, Emerging and other Communicable Diseases, Surveillance and Control 1996.
8. Sanchez D, Rojas M, Hernandez I, Radzioch D, Garcia LF, Barrera LF. Role of TLR2- and TLR4-mediated signaling in Mycobacterium tuberculosis-induced macrophage death. Cell Immunol 2010; 260:128-36.
9. Chelsea E. Stamm ACC, Michael U. Shiloh. Sensing of Mycobacterium tuberculosis and consequences to both host and bacillus. Immunological Reviews 2015; 264:204-19.
10. Mortaz E, Adcock IM, Tabarsi P, Masjedi MR, Mansouri D, Velayati AA, et al. Interaction of Pattern Recognition Receptors with Mycobacterium Tuberculosis. J Clin Immunol 2015; 35:1-10.
11. Kaufmann SHE. HOW CAN IMMUNOLOGY CONTRIBUTE TO THE CONTROL OF TUBERCULOSIS ? Nat Rev Immunol 2001; 1:20-30.
12. Vandal OH, Nathan CF, Ehrt S. Acid resistance in Mycobacterium tuberculosis. J Bacteriol 2009; 191:4714-21.
13. Sundaramurthy V, Korf H, Singla A, Scherr N, Nguyen L, Ferrari G, et al. Survival of Mycobacterium tuberculosis and Mycobacterium bovis BCG in lysosomes in vivo. Microbes Infect 2017; 19:515-26.

14. Sasindran SJ, Torrelles JB. Mycobacterium Tuberculosis Infection and Inflammation: what is Beneficial for the Host and for the Bacterium? Front Microbiol 2011; 2:2.

15. Mahamed D, Boulle M, Ganga Y, Mc Arthur C, Skroch S, Oom L, et al. Intracellular growth of Mycobacterium tuberculosis after macrophage cell death leads to serial killing of host cells. Elife 2017; 6.

16. Flannagan RS, Cosio G, Grinstein S. Antimicrobial mechanisms of phagocytes and bacterial evasion strategies. Nat Rev Microbiol 2009; 7:355-66.

17. Smith J, Manoranjan J, Pan M, Bohsali A, Xu J, Liu J, et al. Evidence for pore formation in host cell membranes by ESX-1-secreted ESAT-6 and its role in Mycobacterium marinum escape from the vacuole. Infect Immun 2008; 76:5478-87.

18. Ligon LS, Hayden JD, Braunstein M. The ins and outs of Mycobacterium tuberculosis protein export. Tuberculosis (Edinb) 2012; 92:121-32.

19. Majlessi L, Prados-Rosales R, Casadevall A, Brosch1 R. Release of mycobacterial antigens. Immunological Reviews 2015; 264:25-45.

20. Queval CJ, Song OR, Carralot JP, Saliou JM, Bongiovanni A, Deloison G, et al. Mycobacterium tuberculosis Controls Phagosomal Acidification by Targeting CISH-Mediated Signaling. Cell Rep 2017; 20:3188-98.

21. Houben D, Demangel C, van Ingen J, Perez J, Baldeon L, Abdallah AM, et al. ESX-1-mediated translocation to the cytosol controls virulence of mycobacteria. Cell Microbiol 2012; 14:1287-98.

22. Guirado E, Schlesinger LS. Modeling the Mycobacterium tuberculosis Granuloma - the Critical Battlefield in Host Immunity and Disease. Front Immunol 2013; 4:98.

23. Silva Miranda M, Breiman A, Allain S, Deknuydt F, Altare F. The tuberculous granuloma: an unsuccessful host defence mechanism providing a safety shelter for the bacteria? Clin Dev Immunol 2012; 2012:139127.

24. Ramakrishnan L. Revisiting the role of the granuloma in tuberculosis. Nat Rev Immunol 2012; 12:352-66.

25. Volkman HE, Pozos TC, Zheng J, Davis JM, Rawls JF, Ramakrishnan L. Tuberculous granuloma induction via interaction of a bacterial secreted protein with host epithelium. Science

2010; 327:466-9.

26. Kiran D, Podell BK, Chambers M, Basaraba RJ. Host-directed therapy targeting the Mycobacterium tuberculosis granuloma: a review. Semin Immunopathol 2016; 38:167-83.

27. Cronan MR, Beerman RW, Rosenberg AF, Saelens JW, Johnson MG, Oehlers SH, et al. Macrophage Epithelial Reprogramming Underlies Mycobacterial Granuloma Formation and Promotes Infection. Immunity 2016; 45:861-76.

28. Pieters J. Mycobacterium tuberculosis and the macrophage: maintaining a balance. Cell Host Microbe 2008; 3:399-407.

29. Schreiber HA, Sandor M. The role of dendritic cells in mycobacterium-induced granulomas. Immunol Lett 2010; 130:26-31.

30. Bozzano F, Marras F, De Maria A. Immunology of tuberculosis. Mediterr J Hematol Infect Dis 2014; 6:e2014027.

31. Matteelli A, Sulis G, Capone S, D'Ambrosio L, Migliori GB, Getahun H. Tuberculosis elimination and the challenge of latent tuberculosis. Presse Med 2017; 46:e13-e21.

32. Roy A, Eisenhut M, Harris RJ, Rodrigues LC, Sridhar S, Habermann S, et al. Effect of BCG vaccination against Mycobacterium tuberculosis infection in children: systematic review and meta-analysis. BMJ 2014; 349:g4643.

33. Kaufmann SHE, Hussey G, Lambert P-H. New vaccines for tuberculosis. The Lancet 2010; 375:2110-9.

34. Andersen P, Doherty TM. The success and failure of BCG —implications for a novel tuberculosis vaccine. Nature 2005; 3:656-62.

35. Fox GJ, Dobler CC, Marais BJ, Denholm JT. Preventive therapy for latent tuberculosis infection-the promise and the challenges. Int J Infect Dis 2017; 56:68-76.

36. Ryu YJ. Diagnosis of pulmonary tuberculosis: recent advances and diagnostic algorithms. Tuberc Respir Dis (Seoul) 2015; 78:64-71.

37. WHO. Guidelines on the management of latent tuberculosis infection (WHO/HTM/TB/2015.01). 2014.

38. Zumla A, Rao M, Parida SK, Keshavjee S, Cassell G, Wallis R, et al. Inflammation and tuberculosis: host-directed therapies. J Intern Med 2015; 277:373-87.

39. Horsburgh CR, Jr., Barry CE, 3rd, Lange C. Treatment of Tuberculosis. N Engl J Med 2015; 373:2149-60.

40. Ormerod LP. Multidrug-resistant tuberculosis (MDR-TB): epidemiology, prevention and treatment. Br Med Bull 2005; 73-74:17-24.

41. Kapoor N, Pawar S, Sirakova TD, Deb C, Warren WL, Kolattukudy PE. Human granuloma in vitro model, for TB dormancy and resuscitation. PLoS One 2013; 8:e53657.

42. Bielecka MK, Tezera LB, Zmijan R, Drobniewski F, Zhang X, Jayasinghe S, et al. A Bioengineered Three-Dimensional Cell Culture Platform Integrated with Microfluidics To Address Antimicrobial Resistance in Tuberculosis. MBio 2017; 8.

43. Gupta UD, Katoch VM. Animal models of tuberculosis. Tuberculosis (Edinb) 2005; 85:277-93.

44. Driver ER, Ryan GJ, Hoff DR, Irwin SM, Basaraba RJ, Kramnik I, et al. Evaluation of a mouse model of necrotic granuloma formation using C3HeB/FeJ mice for testing of drugs against Mycobacterium tuberculosis. Antimicrob Agents Chemother 2012; 56:3181-95.

45. Kramnik I, Beamer G. Mouse models of human TB pathology: roles in the analysis of necrosis and the development of host-directed therapies. Semin Immunopathol 2016; 38:221-37.

46. Apt A, Kramnik I. Man and mouse TB: contradictions and solutions. Tuberculosis (Edinb) 2009; 89:195-8.

47. Pietrantonio TD, Schurr E. Mouse models for the genetic study of tuberculosis susceptibility. BRIEFINGS IN FUNCTIONAL GENOMICS AND PROTEOMICS 2005; 4:277-92.

48. Harper J, Skerry C, Davis SL, Tasneen R, Weir M, Kramnik I, et al. Mouse model of necrotic tuberculosis granulomas develops hypoxic lesions. J Infect Dis 2012; 205:595-602.

49. Myllymaki H, Niskanen M, Oksanen KE, Ramet M. Animal models in tuberculosis research - where is the beef? Expert Opin Drug Discov 2015; 10:871-83.

50. Swaim LE, Connolly LE, Volkman HE, Humbert O, Born DE, Ramakrishnan L. Mycobacterium marinum infection of adult zebrafish causes caseating granulomatous tuberculosis and is moderated by adaptive immunity. Infect Immun 2006; 74:6108-17.

51. Tobin DM, May RC, Wheeler RT. Zebrafish: a see-through host and a fluorescent toolbox

to probe host-pathogen interaction. PLoS Pathog 2012; 8:e1002349.

52. Meijer AH. Protection and pathology in TB: learning from the zebrafish model. Semin Immunopathol 2016; 38:261-73.

53. van der Vaart M, Spaink HP, Meijer AH. Pathogen recognition and activation of the innate immune response in zebrafish. Adv Hematol 2012; 2012:159807.

54. Ramakrishnan L. The zebrafish guide to tuberculosis immunity and treatment. Cold Spring Harb Symp Quant Biol 2013; 78:179-92.

55. Tønjum T, Welty DB, Jantzen E, Small PL. Differentiation of *Mycobacterium ulcerans*, *M. marinum*, and *M. haemophilum*: Mapping of Their Relationships to M. tuberculosis by Fatty Acid Profile Analysis, DNA-DNA Hybridization, and 16S rRNA Gene Sequence Analysis. J Clin Microbiol 1998; 36:918-25.

56. Cronan MR, Tobin DM. Fit for consumption: zebrafish as a model for tuberculosis. Dis Model Mech 2014; 7:777-84.

57. Torraca V, Masud S, Spaink HP, Meijer AH. Macrophage-pathogen interactions in infectious diseases: new therapeutic insights from the zebrafish host model. Dis Model Mech 2014; 7:785-97.

58. Tobin DM, Ramakrishnan L. Comparative pathogenesis of Mycobacterium marinum and Mycobacterium tuberculosis. Cell Microbiol 2008; 10:1027-39.

59. Torraca V, Mostowy S. Zebrafish Infection: From Pathogenesis to Cell Biology. Trends Cell Biol 2018; 28:143-56.

60. Tobin DM, Vary JC, Jr., Ray JP, Walsh GS, Dunstan SJ, Bang ND, et al. The lta4h locus modulates susceptibility to mycobacterial infection in zebrafish and humans. Cell 2010; 140:717-30.

61. Davis JM, Ramakrishnan L. The role of the granuloma in expansion and dissemination of early tuberculous infection. Cell 2009; 136:37-49.

62. van der Vaart M, Korbee CJ, Lamers GE, Tengeler AC, Hosseini R, Haks MC, et al. The DNA damage-regulated autophagy modulator DRAM1 links mycobacterial recognition via TLR-MYD88 to autophagic defense [corrected]. Cell Host Microbe 2014; 15:753-67.

63. Uchiyama Y, Shibata M, Koike M, Yoshimura K, Sasaki M. Autophagy-physiology and

pathophysiology. Histochem Cell Biol 2008; 129:407-20.

64. Reggiori F, Klionsky DJ. Autophagy in the Eukaryotic Cell. Eukaryotic Cell 2002; 1:11-21.

65. Levine B, Kroemer G. Autophagy in the pathogenesis of disease. Cell 2008; 132:27-42.

66. Deretic V, Saitoh T, Akira S. Autophagy in infection, inflammation and immunity. Nat Rev Immunol 2013; 13:722-37.

67. He C, Klionsky DJ. Regulation mechanisms and signaling pathways of autophagy. Annu Rev Genet 2009; 43:67-93.

68. Glick D, Barth S, Macleod KF. Autophagy: cellular and molecular mechanisms. J Pathol 2010; 221:3-12.

69. Klionsky BLaDJ. Development by Self-Digestion:
Molecular Mechanisms
and Biological Functions of Autophagy. Developmental Cell 2004; 6: 463–77.

70. Solvik T, Debnath J. At the crossroads of autophagy and infection: Noncanonical roles for ATG proteins in viral replication. J Cell Biol 2016; 214:503-5.

71. Li M, Hou Y, Wang J, Chen X, Shao ZM, Yin XM. Kinetics comparisons of mammalian Atg4 homologues indicate selective preferences toward diverse Atg8 substrates. J Biol Chem 2011; 286:7327-38.

72. Neff NT, Bourret L, Miao P, Dice FJ. Degradation of Proteins Microinjected into IMR-90 human diploid fibroblast THE JOURNAL OF CELL BIOLOGY 1981; 91:184-94.

73. Cuervo AM, Wong E. Chaperone-mediated autophagy: roles in disease and aging. Cell Res 2014; 24:92-104.

74. Kraft C, Peter M, Hofmann K. Selective autophagy: ubiquitin-mediated recognition and beyond. Nat Cell Biol 2010; 12:836-41.

75. Popovic D, Vucic D, Dikic I. Ubiquitination in disease pathogenesis and treatment. Nat Med 2014; 20:1242-53.

76. Kim B-W, Kwon DH, Song HK. Structure biology of selective autophagy receptors. BMB Reports 2016; 49:73-80.

77. Levine B. Eating oneself and uninvited guests: autophagy-related pathways in cellular defense. Cell 2005; 120:159-62.

78. Ichiro Nakagawa AA, Noboru Mizushima,, Akitsugu Yamamoto HY, Takahiro Kamimoto,, Atsuki Nara JF, Masanobu Nakata, Kayoko Tsuda,, Shigeyuki Hamada TY. Autophagy Defends Cells Against Invading Group A Streptococcus. Science 2004; 306 1037-40.

79. Gutierrez MG, Master SS, Singh SB, Taylor GA, Colombo MI, Deretic V. Autophagy is a defense mechanism inhibiting BCG and Mycobacterium tuberculosis survival in infected macrophages. Cell 2004; 119:753-66.

80. Sumpter R, Jr., Levine B. Autophagy and innate immunity: triggering, targeting and tuning. Semin Cell Dev Biol 2010; 21:699-711.

81. Yorimitsu T, Klionsky DJ. Eating the endoplasmic reticulum: quality control by autophagy. Trends Cell Biol 2007; 17:279-85.

82. Mizushima N, Komatsu M. Autophagy: renovation of cells and tissues. Cell 2011; 147:728-41.

83. Harnett MM, Pineda MA, Latre de Late P, Eason RJ, Besteiro S, Harnett W, et al. From Christian de Duve to Yoshinori Ohsumi: More to autophagy than just dining at home. Biomed J 2017; 40:9-22.

84. Wong PM, Puente C, Ganley IG, Jiang X. The ULK1 complex: sensing nutrient signals for autophagy activation. Autophagy 2013; 9:124-37.

85. Alers S, Löffler AS, Paasch F, Dieterle AM, Keppeler H, Lauber K, et al. Atg13 and FIP200 act independently of Ulk1 and Ulk2 in autophagy induction. Autophagy 2014; 7:1424-33.

86. Yin Z, Pascual C, Klionsky DJ. Autophagy: machinery and regulation. Microb Cell 2016; 3:588-96.

87. Klionsky DJ. Autophagy: from phenomenology to molecular understanding in less than a decade molecular cell biology 2007; 8:931-7.

88. Proikas-Cezanne T, Takacs Z, Donnes P, Kohlbacher O. WIPI proteins: essential PtdIns3P effectors at the nascent autophagosome. J Cell Sci 2015; 128:207-17.

89. Burman C, Ktistakis NT. Regulation of autophagy by phosphatidylinositol 3-phosphate. FEBS Lett 2010; 584:1302-12.

90. Geng J, Klionsky DJ. The Atg8 and Atg12 ubiquitin-like conjugation systems in macroautophagy. 'Protein modifications: beyond the usual suspects' review series. EMBO Rep

2008; 9:859-64.

91. Ney PA. Mitochondrial autophagy: Origins, significance, and role of BNIP3 and NIX. Biochim Biophys Acta 2015; 1853:2775-83.

92. Whang MI, Tavares RM, Benjamin DI, Kattah MG, Advincula R, Nomura DK, et al. The Ubiquitin Binding Protein TAX1BP1 Mediates Autophagasome Induction and the Metabolic Transition of Activated T Cells. Immunity 2017; 46:405-20.

93. Birgisdottir AB, Lamark T, Johansen T. The LIR motif - crucial for selective autophagy. J Cell Sci 2013; 126:3237-47.

94. Hurley JH, Lee S, Prag G. Ubiquitin-binding domains. Biochem J 2006; 399:361-72.

95. Shaid S, Brandts CH, Serve H, Dikic I. Ubiquitination and selective autophagy. Cell Death Differ 2013; 20:21-30.

96. Itakura E, Kishi-Itakura C, Mizushima N. The hairpin-type tail-anchored SNARE syntaxin 17 targets to autophagosomes for fusion with endosomes/lysosomes. Cell 2012; 151:1256-69.

97. Eskelinen EL. Roles of LAMP-1 and LAMP-2 in lysosome biogenesis and autophagy. Mol Aspects Med 2006; 27:495-502.

98. Levine B, Kroemer G. Autophagy in aging, disease and death: the true identity of a cell death impostor. Cell Death Differ 2009; 16:1-2.

99. Tang D, Kang R, Coyne CB, Zeh HJ, Lotze MT. PAMPs and DAMPs: signal 0s that spur autophagy and immunity. Immunol Rev 2012; 249:158-75.

100. Xu Y, Jagannath C, Liu XD, Sharafkhaneh A, Kolodziejska KE, Eissa NT. Toll-like receptor 4 is a sensor for autophagy associated with innate immunity. Immunity 2007; 27:135-44.

101. Mostowy S, Cossart P. Bacterial autophagy: restriction or promotion of bacterial replication? Trends Cell Biol 2012; 22:283-91.

102. Saitoh T, Fujita N, Jang MH, Uematsu S, Yang BG, Satoh T, et al. Loss of the autophagy protein Atg16L1 enhances endotoxin-induced IL-1beta production. Nature 2008; 456:264-8.

103. Hampe J, Franke A, Rosenstiel P, Till A, Teuber M, Huse K, et al. A genome-wide association scan of nonsynonymous SNPs identifies a susceptibility variant for Crohn disease in ATG16L1. Nat Genet 2007; 39:207-11.

104. Qian M, Fang X, Wang X. Autophagy and inflammation. Clin Transl Med 2017; 6:24.

105. Crisan TO, Plantinga TS, van de Veerdonk FL, Farcas MF, Stoffels M, Kullberg BJ, et al. Inflammasome-independent modulation of cytokine response by autophagy in human cells. PLoS One 2011; 6:e18666.

106. Harris J, Hartman M, Roche C, Zeng SG, O'Shea A, Sharp FA, et al. Autophagy controls IL-1beta secretion by targeting pro-IL-1beta for degradation. J Biol Chem 2011; 286:9587-97.

107. Kaufmann SH. Tuberculosis vaccines: time to think about the next generation. Semin Immunol 2013; 25:172-81.

108. Crotzer VL, Blum JS. Autophagy and its role in MHC-mediated antigen presentation. J Immunol 2009; 182:3335-41.

109. Jagannath C, Lindsey DR, Dhandayuthapani S, Xu Y, Hunter RL, Jr., Eissa NT. Autophagy enhances the efficacy of BCG vaccine by increasing peptide presentation in mouse dendritic cells. Nat Med 2009; 15:267-76.

110. Wellcome Trust Case Control C, Australo-Anglo-American Spondylitis C, Burton PR, Clayton DG, Cardon LR, Craddock N, et al. Association scan of 14,500 nonsynonymous SNPs in four diseases identifies autoimmunity variants. Nat Genet 2007; 39:1329-37.

111. Biswas D, Qureshi OS, Lee WY, Croudace JE, Mura M, Lammas DA. ATP-induced autophagy is associated with rapid killing of intracellular mycobacteria within human monocytes/macrophages. BMC Immunol 2008; 9:35.

112. Alonso S, Pethe K, Russell DG, Purdy GE. Lysosomal killing of *Mycobacterium* mediated by ubiquitin-derived peptides is enhanced by autophagy PNAS 2007; 104:6031-6.

113. Sudha B. Singh ASD, Gregory A. Taylor, Vojo Deretic. Human IRGM induces autophagy to eliminate intracellular mycobacteria SCIENCE 2006; 313:1438-41.

114. Conrad WH, Osman MM, Shanahan JK, Chu F, Takaki KK, Cameron J, et al. Mycobacterial ESX-1 secretion system mediates bacteri host cell lysis throughum contact-dependent gross membrane disruptions. Proc Natl Acad Sci U S A 2017; 114:1371-6.

115. Watson RO, Manzanillo PS, Cox JS. Extracellular M. tuberculosis DNA targets bacteria for autophagy by activating the host DNA-sensing pathway. Cell 2012; 150:803-15.

116. Manzanillo PS, Ayres JS, Watson RO, Collins AC, Souza G, Rae CS, et al. The ubiquitin ligase parkin mediates resistance to intracellular pathogens. Nature 2013; 501:512-6.

117. Franco LH, Nair VR, Scharn CR, Xavier RJ, Torrealba JR, Shiloh MU, et al. The Ubiquitin Ligase Smurf1 Functions in Selective Autophagy of Mycobacterium tuberculosis and Anti-tuberculous Host Defense. Cell Host Microbe 2017; 21:59-72.

118. Ponpuak M, Davis AS, Roberts EA, Delgado MA, Dinkins C, Zhao Z, et al. Delivery of cytosolic components by autophagic adaptor protein p62 endows autophagosomes with unique antimicrobial properties. Immunity 2010; 32:329-41.

119. Kimmey JM, Stallings CL. Bacterial Pathogens versus Autophagy: Implications for Therapeutic Interventions. Trends Mol Med 2016; 22:1060-76.

120. Codogno P MA. Atg5: more than an autophagy factor. NATURE CELL BIOLOGY 2006; 8:1045-7.

121. Hara T, Nakamura K, Matsui M, Yamamoto A, Nakahara Y, Suzuki-Migishima R, et al. Suppression of basal autophagy in neural cells causes neurodegenerative disease in mice. Nature 2006; 441:885-9.

122. Crighton D, Wilkinson S, O'Prey J, Syed N, Smith P, Harrison PR, et al. DRAM, a p53-induced modulator of autophagy, is critical for apoptosis. Cell 2006; 126:121-34.

123. Mah LY, O'Prey J, Baudot AD, Hoekstra A, Ryan KM. DRAM-1 encodes multiple isoforms that regulate autophagy. Autophagy 2012; 8:18-28.

124. Crighton D, O'Prey J, Bell HS, Ryan KM. p73 regulates DRAM-independent autophagy that does not contribute to programmed cell death. Cell Death Differ 2007; 14:1071-9.

125. Polager S, Ofir M, Ginsberg D. E2F1 regulates autophagy and the transcription of autophagy genes. Oncogene 2008; 27:4860-4.

126. Mrschtik M, Ryan KM. Another DRAM involved in autophagy and cell death. Autophagy 2016; 12:603-5.

127. Guan JJ, Zhang XD, Sun W, Qi L, Wu JC, Qin ZH. DRAM1 regulates apoptosis through increasing protein levels and lysosomal localization of BAX. Cell Death Dis 2015; 6:e1624.

128. Galavotti S, Bartesaghi S, Faccenda D, Shaked-Rabi M, Sanzone S, McEvoy A, et al. The autophagy-associated factors DRAM1 and p62 regulate cell migration and invasion in glioblastoma stem cells. Oncogene 2013; 32:699-712.

129. Humbert M, Mueller C, Fey MF, Tschan MP. Inhibition of damage-regulated autophagy

modulator-1 (DRAM-1) impairs neutrophil differentiation of NB4 APL cells. Leuk Res 2012; 36:1552-6.

130. Lorin S, Borges A, Ribeiro Dos Santos L, Souquere S, Pierron G, Ryan KM, et al. c-Jun NH2-terminal kinase activation is essential for DRAM-dependent induction of autophagy and apoptosis in 2-methoxyestradiol-treated Ewing sarcoma cells. Cancer Res 2009; 69:6924-31.

131. Laforge M, Limou S, Harper F, Casartelli N, Rodrigues V, Silvestre R, et al. DRAM triggers lysosomal membrane permeabilization and cell death in CD4(+) T cells infected with HIV. PLoS Pathog 2013; 9:e1003328.

132. O'Prey J, Skommer J, Wilkinson S, Ryan KM. Analysis of DRAM-related proteins reveals evolutionarily conserved and divergent roles in the control of autophagy. Cell Cycle 2009; 8:2260-5.

133. Park SM, Kim K, Lee EJ, Kim BK, Lee TJ, Seo T, et al. Reduced expression of DRAM2/TMEM77 in tumor cells interferes with cell death. Biochem Biophys Res Commun 2009; 390:1340-4.

134. Yoon JH, Her S, Kim M, Jang IS, Park J. The expression of damage-regulated autophagy modulator 2 (DRAM2) contributes to autophagy induction. Mol Biol Rep 2012; 39:1087-93.

135. Kim JK, Lee HM, Park KS, Shin DM, Kim TS, Kim YS, et al. MIR144* inhibits antimicrobial responses against Mycobacterium tuberculosis in human monocytes and macrophages by targeting the autophagy protein DRAM2. Autophagy 2017; 13:423-41.

136. Bai S, Tian B, Li A, Yao Q, Zhang G, Li F. MicroRNA-125b promotes tumor growth and suppresses apoptosis by targeting DRAM2 in retinoblastoma. Eye (Lond) 2016; 30:1630-8.

137. Mrschtik M, O'Prey J, Lao LY, Long JS, Beaumatin F, Strachan D, et al. DRAM-3 modulates autophagy and promotes cell survival in the absence of glucose. Cell Death Differ 2015; 22:1714-26.

138. Chung J, Nakatsu F, Baskin JM, De Camilli P. Plasticity of PI4KIIIalpha interactions at the plasma membrane. EMBO Rep 2015; 16:312-20.

139. Zhang XD, Qi L, Wu JC, Qin ZH. DRAM1 regulates autophagy flux through lysosomes. PLoS One 2013; 8:e63245.

140. Meng C, Liu Y, Shen Y, Liu S, Wang Z, Ye Q, et al. MicroRNA-26b suppresses autophagy in

breast cancer cells by targeting DRAM1 mRNA, and is downregulated by irradiation. Oncol Lett 2018; 15:1435-40.

141. Masud S. Autophagy and Lc3-associated phagocytosis in host defense against *Salmonella.* Leiden University, 2017:233.

142. Wallis RS, Hafner R. Advancing host-directed therapy for tuberculosis. Nat Rev Immunol 2015; 15:255-63.

143. Encinales L, Zuniga J, Granados-Montiel J, Yunis M, Granados J, Almeciga I, et al. Humoral immunity in tuberculin skin test anergy and its role in high-risk persons exposed to active tuberculosis. Mol Immunol 2010; 47:1066-73.

144. Majeed S. Dual Role of Inflammation in Prognosis and Prevention of Tuberculosis. Journal of Clinical & Cellular Immunology 2015; 06.

145. Tobin DM, Roca FJ, Oh SF, McFarland R, Vickery TW, Ray JP, et al. Host genotype-specific therapies can optimize the inflammatory response to mycobacterial infections. Cell 2012; 148:434-46.

146. Tobin DM, Roca FJ, Ray JP, Ko DC, Ramakrishnan L. An enzyme that inactivates the inflammatory mediator leukotriene b4 restricts mycobacterial infection. PLoS One 2013; 8:e67828.

147. Coussens AK, Wilkinson RJ, Hanifa Y, Nikolayevskyy V, Elkington PT, Islam K, et al. Vitamin D accelerates resolution of inflammatory responses during tuberculosis treatment. Proc Natl Acad Sci U S A 2012; 109:15449-54.

148. Park SK, Cho S, Lee IH, Jeon DS, Hong SH, Smego RA, Jr., et al. Subcutaneously administered interferon-gamma for the treatment of multidrug-resistant pulmonary tuberculosis. Int J Infect Dis 2007; 11:434-40.

149. Milanes-Virelles MT, Garcia-Garcia I, Santos-Herrera Y, Valdes-Quintana M, Valenzuela-Silva CM, Jimenez-Madrigal G, et al. Adjuvant interferon gamma in patients with pulmonary atypical Mycobacteriosis: a randomized, double-blind, placebo-controlled study. BMC Infect Dis 2008; 8:17.

150. Clay H, Volkman HE, Ramakrishnan L. Tumor necrosis factor signaling mediates resistance to mycobacteria by inhibiting bacterial growth and macrophage death. Immunity 2008; 29:283-

94.

151. Lin PL, Myers A, Smith L, Bigbee C, Bigbee M, Fuhrman C, et al. Tumor necrosis factor neutralization results in disseminated disease in acute and latent Mycobacterium tuberculosis infection with normal granuloma structure in a cynomolgus macaque model. Arthritis Rheum 2010; 62:340-50.

152. Algood HM LP, Flynn JL. Tumor Necrosis Factor and Chemokine Interactions
in the Formation and Maintenance of Granulomas
in Tuberculosis. Clinical Infectious Diseases 2005; 41:S189–93.

153. Bourigault ML, Segueni N, Rose S, Court N, Vacher R, Vasseur V, et al. Relative contribution of IL-1alpha, IL-1beta and TNF to the host response to Mycobacterium tuberculosis and attenuated M. bovis BCG. Immun Inflamm Dis 2013; 1:47-62.

154. Hawn TR, Matheson AI, Maley SN, Vandal O. Host-directed therapeutics for tuberculosis: can we harness the host? Microbiol Mol Biol Rev 2013; 77:608-27.

155. Levine B, Packer M, Codogno P. Development of autophagy inducers in clinical medicine. J Clin Invest 2015; 125:14-24.

156. Kim JJ, Lee HM, Shin DM, Kim W, Yuk JM, Jin HS, et al. Host cell autophagy activated by antibiotics is required for their effective antimycobacterial drug action. Cell Host Microbe 2012; 11:457-68.

157. Kumar D, Nath L, Kamal MA, Varshney A, Jain A, Singh S, et al. Genome-wide analysis of the host intracellular network that regulates survival of Mycobacterium tuberculosis. Cell 2010; 140:731-43.

158. Li J, Kim SG, Blenis J. Rapamycin: one drug, many effects. Cell Metab 2014; 19:373-9.

Chapter 2

Dram1 deficiency leads to increased susceptibility of zebrafish to mycobacterial infection due to activation of pyroptotic cell death in infected macrophages

Rui Zhang, Monica Varela, Vincenzo Torraca, Michiel van der Vaart and Annemarie H. Meijer

(Manuscript in preparation)

Abstract

Mycobacterium tuberculosis (Mtb) and *Mycobacterium marinum* (Mm) are infectious bacterial pathogens and the causative agents of tuberculosis (TB) in humans and fish, respectively. These mycobacteria can survive and proliferate inside host macrophages. In response, infected macrophages elicit diverse mechanisms in an attempt to eliminate the intracellular pathogens and prevent further dissemination. There are many factors – both host and bacteria derived – that together determine the fate of a mycobacterium-infected macrophage: will it kill the pathogen, or succumb to the infection? The autophagy and cell death mediator DRAM1 was previously linked to autophagic host defense against mycobacterial infection. In this study, we found that CRISPR/Cas9-mediated mutation of zebrafish Dram1 does not reduce basal levels of autophagy under non-infected conditions. However, in the zebrafish larval model of TB, Dram1 deficiency reduces autophagic targeting of Mm and results in increased susceptibility to infection. Moreover, we demonstrate that Dram1, which is predominantly localized to lysosomal membranes, is required for acidification of Mm-containing vesicles. By *in vivo* imaging of the infection process, we observed that Dram1-deficient macrophages fail to restrict Mm during early stages of the infection. Knockdown of the zebrafish functional homolog of Caspase 1 could rescue the increased infection levels of Dram1 mutants. Therefore, extending the previously described function of Dram1 in maturation of mycobacteria-containing vesicles, we now propose that the presence of functional Dram1 limits pyroptotic cell death of mycobacteria-infected macrophages and thereby contributes to host resistance to mycobacterial infection.

Introduction

Tuberculosis (TB), caused by *Mycobacterium tuberculosis* (Mtb), remains a severe infectious disease and global health threat. The increase in drug-resistant Mtb strains and the occurrence of comorbidities, like co-infection with HIV, lower the effectiveness of current TB treatments [1, 2]. Thus, it is essential to fully understand the mechanisms of Mtb pathogenesis and develop novel approaches to improve the outcome of TB treatment. Autophagy is a conserved process that maintains cellular homeostasis by degrading unwanted cytoplasmic contents [3]. Various studies have demonstrated that autophagy also acts as an innate immune defense mechanism to

control mycobacterial infection [4-8]. Therefore, enhancing autophagic defenses forms a promising target for host-directed TB treatment [9, 10].

Many autophagy factors involved in defense against mycobacterial infection have been identified. DNA Damage Regulated Autophagy Modulator 1 (DRAM1) is a more recently discovered regulator of autophagy and cell death [11, 12]. Besides being involved in cancer and HIV infection [11, 13], a role for DRAM1 has been identified in defense against mycobacterial infections [7]. Transient knockdown of zebrafish *dram1* leads to decreased autophagic targeting of mycobacteria and increased susceptibility to mycobacterial infection. Conversely, transient overexpression of *dram1* promotes autophagic sequestration of mycobacteria and decreases mycobacterial infection [7]. In addition, human DRAM1 colocalizes with Mtb in infected macrophages [7]. Therefore, DRAM1 is a potential target for host directed therapy to restrict TB infection.

Macrophages commonly serve as the first innate immune cells to engulf mycobacteria and play a central role in TB pathogenesis [14, 15]. Nevertheless, mycobacteria can utilize macrophages as a niche in which they are able to survive and replicate via activation of diverse virulence mechanisms. For example, mycobacteria have evolved versatile mechanisms to alter the host environment, which prevents the delivery of mycobacteria to microbicidal lysosomes[16]. Arrested phagosome maturation or mycobacterial escape from phagosomes results in activation of autophagic defenses by infected macrophages [4, 17]. The role of autophagy in defense against mycobacterial infections has been studied well, both *in vitro* and *in vivo* [4, 7, 18]. The sequestering of an invading microbe by autophagy is called xenophagy [19]. In this process, selective autophagy receptors like p62, NDP52 and NBR1 serve as adaptor proteins to directly connect ubiquitin-tagged mycobacteria to forming autophagosomes [4, 20, 21]. Apart from directly capturing cytoplasmic mycobacteria by xenophagy, p62 also contributes to defense against mycobacteria by delivering ubiquitinated cytosolic proteins to autophagolysosomes, where they are proteolytically converted into neo-antimicrobial peptides [22]. Previously, our laboratory found that Dram1-mediated autophagic defense against mycobacterial infection requires the selective autophagy receptor p62 [7].

Intracellular proliferation of mycobacteria ultimately leads to the death of the macrophage that has phagocytosed them. The remains of this dead macrophage and the now extracellular bacteria will be engulfed by newly recruited macrophages, which themselves become infected and disseminate the infection [23]. However, the newly recruited macrophages phagocytose a large number of mycobacteria from the deceased macrophage, which means that newly infected macrophages will also die rapidly [24]. In general, once overproliferation of mycobacteria initiates death of individual macrophages, this will result in a cascade of infection and killing of newly recruited macrophages [25, 26]. Eventually, this leads to large scale dissemination of the infection and the formation of inflammatory infection foci, called granulomas [27, 28]. The granuloma is a compact and organized structure that is a typical pathological feature of TB disease [28, 29]. It is formed by mycobacteria-infected macrophages that attract other immune cells, like neutrophils, T cells, and B cells. On the one hand, granulomas function as host-protective structures to restrict mycobacteria locally [30]. However, these structures also provide a safe shelter for mycobacteria to persist inside the host for long periods and they are poorly penetrated by anti-mycobacterial drugs [31, 32]. Furthermore, recent studies have demonstrated that the process of granuloma formation facilitates the spreading of mycobacteria between macrophages and thereby promotes the dissemination of infection [23, 29, 33, 34]. Therefore, the fate of individual infected macrophages is a major determinant for the outcome of mycobacterial infection.

Mycobacteria-infected macrophages can undergo at least three general types of cell death: apoptosis, necrosis and pyroptosis[35]. Apoptosis is an energy-dependent form of programmed cell death that does not induce an inflammatory response upon execution [36, 37]. There are cell-extrinsic and -intrinsic pathways activating apoptosis, governed by the involvement of different initiator and effector cysteine-dependent aspartate-directed proteases (Caspases). The similarity between these two types of activation pathways is that both require the participation of Caspase 3 [38] The role of apoptotic macrophages in controlling mycobacterial infection has been well-established by *in vitro* studies [39, 40]. In contrast, recent *in vivo* studies have shown that mycobacteria-induced apoptosis tends to promote the spreading of the infection during early stages of granuloma formation in zebrafish [23, 41], although necrotic cell death of infected macrophages promotes the spreading of infection to an even greater extent [42]. Necrosis is

accompanied by swelling of organelles and damaging of the plasma membrane. This is generally considered a passive type of cell death but can also occur as a form of programmed cell death (necroptosis) [42, 43]. Eventually, released cytoplasmic material enters the extracellular space [37, 44]. Necrotic cell death of mycobacteria-infected macrophages facilitates dissemination of the infection and promotes granuloma formation both in zebrafish and mouse models [23, 45]. Pyroptotic cell death activates the inflammatory response during a process that requires the involvement of Caspase 1 [37, 38]. It is conceivable that pyroptosis, similar to other lytic types of cell death (necrosis, necroptosis), is beneficial to bacterial spreading and proliferation [46]. In summary, the fate of mycobacteria-infected macrophages plays an important role in TB pathogenesis. While a role for DRAM1 in autophagic defense against mycobacterial infections has been demonstrated [7], its potential function as a modulator of cell death during TB pathogenesis has not been explored.

In this study, we used zebrafish embryos and larvae infected with *Mycobacterium marinum* (Mm) as a model for TB pathogenesis to study the role of Dram1 in controlling mycobacterial infection. We have generated two zebrafish *dram1* mutant alleles using CRISPR/Cas9-mediated mutagenesis. Using these mutants, we have demonstrated that Dram1 deficiency has no apparent effect on development and does not reduce basal levels of autophagy in zebrafish larvae under non-infected conditions. Confirming and extending our previous knockdown studies, we present evidence that Dram1 is required for autophagic targeting and host defense against Mm. Specifically, analysis of the mutant fish showed that Dram1 is required for maturation of Mm-containing vesicles and for macrophages to restrict Mm infection. Without functional Dram1, Mm-infected macrophages initiate programmed cell death via a Caspase 1-dependent mechanism, indicative of pyroptosis. Collectively, our data advocate that Dram1 protects against mycobacterial infection by modulating autophagic targeting and maturation of Mm-containing vesicles. In the absence of Dram1, infected macrophages rapidly become overburdened by the bacteria and initiate pyroptotic cell death, resulting in increased dissemination of the infection.

Results

Generation of Dram1 null mutants by CRISPR/Cas9 method

In a previous study, we have shown that the autophagy modulator Dram1 protects against mycobacterial infection via stimulation of autophagic defenses and maturation of bacteria-containing vesicles [7]. Here, we generated a zebrafish *dram1* mutant line using CRISPR/Cas9 technology to validate and expand on our previous findings. We designed a single guide RNA (sgRNA) that targets the CRISPR/Cas9 endonuclease complex to the first coding exon of the *dram1* gene (Fig1 A). We predicted that random insertions or deletions around the target site due to non-homologous end joining would introduce a frame shift and/or premature stop codon, ensuring that the Dram1 protein will not be translated (Fig1 A). We injected the sgRNA and Cas9 mRNA into the yolk of one cell stage embryos and analyzed the resulting mutations by Sanger sequencing to identify F0 founders (FigS1 A). Dram1 is known as a modulator of autophagy [11]. Thus, F0 founders carrying two independent mutations in exon1 of *dram1* were outcrossed with *Tg*(*CMV:EGFP-map1lc3b*) fish (hereafter referred to a GFP-Lc3) to allow visualization of autophagic processes [47]. Upon adulthood, F1 heterozygous carriers of the mutated *dram1* alleles ($dram1^{+/-}$) were incrossed to obtain F2 homozygous mutants ($dram1^{-/-}$) and wild type siblings ($dram1^{+/+}$) with or without GFP-Lc3 in the background. We performed Sanger sequencing on genomic DNA (F2) obtained from fin tissue to characterize the two independent mutant alleles: 1) a 21 nucleotides deletion combined with a 2 nucleotides insertion at the target site, named $dram1^{\Delta 19n/\Delta 19n}$ (Fig1 B); and 2) a 5 nucleotides insertion at the target site, named $dram1^{5n/5n}$ (FigS1 B). In this study, we focused primarily on the $dram1^{\Delta 19n/\Delta 19n}$ allele, and confirmed crucial observations with the $dram1^{5n/5n}$ allele. Using an N-terminal antibody capable of detecting zebrafish Dram1 by western blot, we could not detect Dram1 protein in the $dram1^{\Delta 19n/\Delta 19n}$ line, supporting that this represents a null allele (Fig1 C).

Apart from its important role in autophagy, Dram1 has also been found to modulate other cellular processes, including apoptosis and neutrophil differentiation[11, 48]. We therefore first asked whether Dram1 deficiency results in developmental defects. We compared body size measurements, but found no apparent difference in development between $dram1^{\Delta 19n/\Delta 19n}$ and

wild type siblings (*dram1*$^{+/+}$) (Fig1 E). Furthermore, *dram1*$^{\Delta 19n/\Delta 19n}$ larvae or adult fish (up to 18 months) did not exhibit observable differences in behavior, survival, or fertility compared to *dram1*$^{+/+}$ (data not shown). Finally, we used a Chi-square test to determine that the offspring from incrossed heterozygous *dram1*$^{\Delta 19N}$ (hereafter referred to as *dram1*$^{\Delta 19n/+}$) strictly followed Mendelian inheritance (Fig1 D). The same was true for incrossed *dram1*$^{5n/+}$ parents (FigS1 C). We also performed Tunel staining to detect if Dram1 deficiency affect the basal cell death, the result showed that *dram1*$^{+/+}$ and *dram1*$^{\Delta 19n/\Delta 19n}$ display similar numbers of Tunel^{+} cells (Fig1 F and G). Collectively, we have used CRISPR/Cas9 targeted mutagenesis to generate two *dram1* null mutants, both of which display no apparent phenotypes during development and can be used to study the function of Dram1 in autophagy and immune defense against infection.

Figure 1: Generation of Dram1 mutant lines (Figure on next page)

A. Schematic representation of the zebrafish *dram1*/Dram1(ENSDARG00000045561/ENSDARP0 0000066996.3) genetic and protein domain architecture and CRISPR/Cas9 target site. Dram1 (240 amino acids) contains six transmembrane domains, which are indicated with grey boxes and labels (T1-T6) with amino acid numbers above. The gene is depicted with coding exons as grey boxes and introns as solid black lines (introns not drawn to scale). The position of the CRISPR/Cas9 target site at the beginning of the first coding exon is indicated and the predicted truncated protein in the *dram1*$^{\Delta 19n/\Delta 19n}$ mutant line is drawn above. The *dram1*$^{5n/5n}$ allele was generated at the same target site, leading to a similarly truncated protein (FigS1).

B. Sanger sequencing of *dram1*$^{\Delta 19n/\Delta 19n}$ and *dram1*$^{+/+}$ from F2 offspring. Red lines indicate CRISPR/Cas9 target sites. The genomic DNA was isolated from fin tissue (>3 months old fish). The *dram1*$^{\Delta 19n/\Delta 19n}$ mutant allele has 21 nucleotides deleted and 2 nucleotides inserted.

C. Confirmation of truncation of the Dram1 protein by western blotting analysis. Protein samples were extracted from 4 dpf *dram1*$^{\Delta 19n/\Delta 19n}$ and *dram1*$^{+/+}$ larvae (>10 larvae/sample). The blots were probed with antibodies against Dram1 and Actin as a loading control.

D. Segregation from *dram1*$^{\Delta 19n/+}$ F1 heterozygous incross. Genotypes of adult fish (>3 months old) were combined from at least three independent breedings and confirmed by PCR and Sanger sequencing. Data were analyzed by Chi Square test. ns, non-significant,*p<0.05,**p<0.01,***p<0.001.

E. Measurements of larval body lengths. *dram1*$^{+/+}$ and *dram1*$^{\Delta 19n/\Delta 19n}$ larvae (≥10 larvae/group) were imaged by stereo microscopy at 3dpf and body lengths were measured as indicated by the red dotted lines.

F. Basal cell death was detected in *dram1*$^{\Delta 19n/\Delta 19n}$ and *dram1*$^{+/+}$ larvae in the tail region. Tunel staining was performed on 3 dpf larvae to detect cell death (≥7 larvae/group). ns, non-significant, *p<0.05, **p<0.01, ***p<0.001

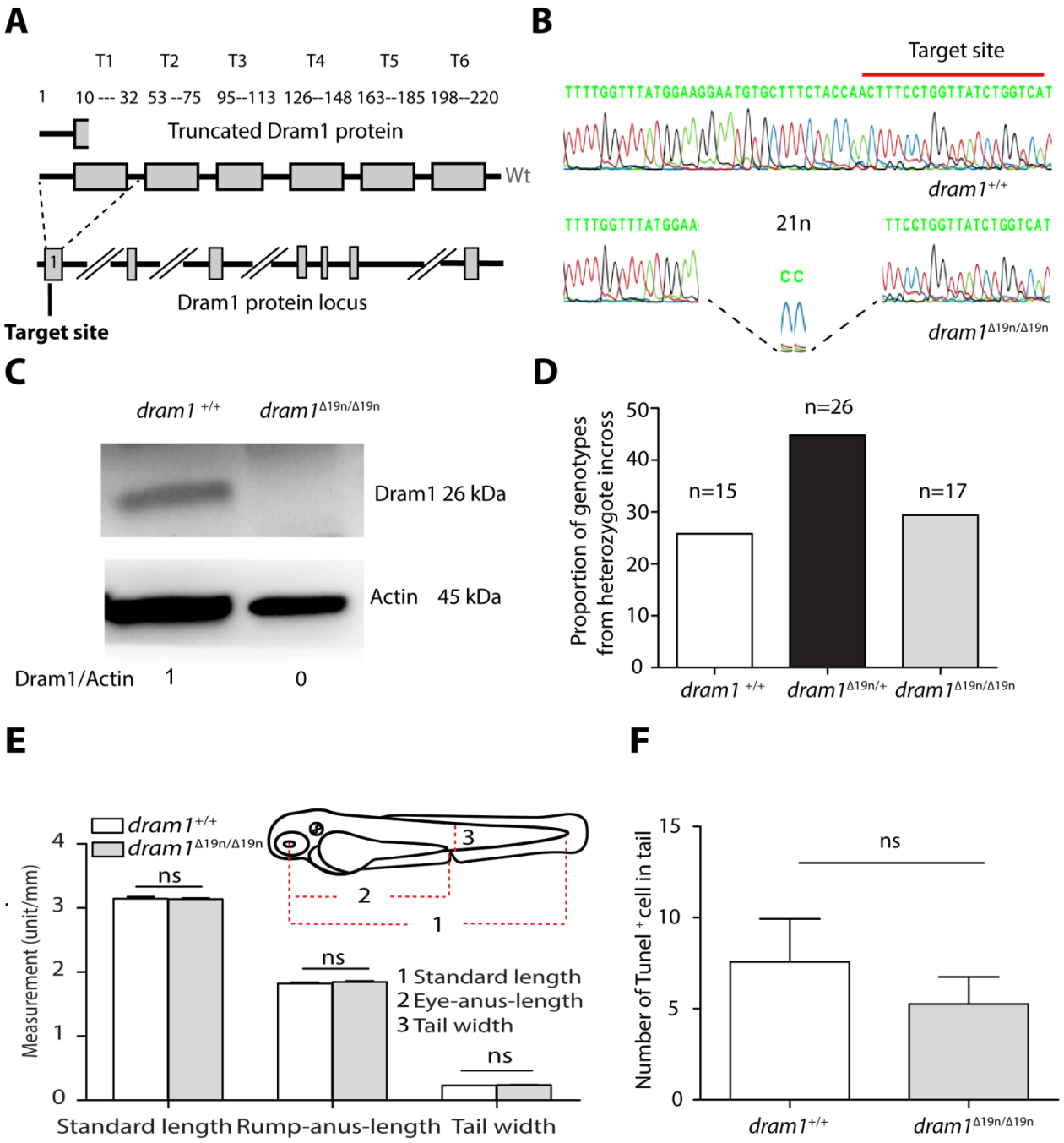

dram1 null mutants display increased susceptibility to mycobacterial infection

Since transient knockdown of zebrafish *dram1* by antisense morpholino oligonucleotide knockdown resulted in increased Mm infection and extracellular growth of bacteria [7], we sought

to confirm this phenotype in our *dram1* mutants. Therefore, we infected *dram1*$^{\Delta 19n/\Delta 19n}$, *dram1*$^{+/+}$, and unrelated wild types (AB/TL) with Mm at 1 dpf via blood island injection and found that *dram1*$^{\Delta 19n/\Delta 19n}$ had a significantly increased susceptibility to infection (Fig2 A and B). Furthermore, Dram1-deficient larvae randomly displayed accumulation of bacteria inside intersegmental blood vessels at 3 days post infection (dpi), which is indicative of extracellular growth of bacteria (Fig2 A). We detected no differences in bacterial burden between *dram*$^{+/+}$ and unrelated wild types, indicating that the genetic background in which the mutation was made did not affect its susceptibility to mycobacterial infection (Fig2 B). Mycobacterial infection in *dram1*$^{\Delta 19n/\Delta 19n}$ resulted in a clearly increased infection burden of around 290% compared to their WT siblings (Fig2 B). We next tested the infection susceptibility of larvae homozygous for the other *dram1* mutant allele, *dram1*$^{5n/5n}$, and found that it roughly exhibited the same increase (around 250%) compared to their wild type siblings (FigS2 B and FigS2 C). As expected, these experiments demonstrated that both *dram1* mutant alleles (19n indel and 5n indel) were more susceptible to mycobacterial infection. Since there are no clear differences between the two mutant alleles in susceptibility to Mm infection, we decided to use the *dram1*$^{\Delta 19n/\Delta 19n}$ allele for further study into Dram1 function.

Next, we asked if transient overexpression of *dram1* mRNA can compensate for Dram1-deficiency in *dram1*$^{\Delta 19n/\Delta 19n}$. For this purpose, we injected *dram1* mRNA into one cell *dram1*$^{\Delta 19n/\Delta 19n}$ and *dram*$^{+/+}$ embryos to overexpress *dram1*. As a negative control, we also injected *dram1* mutant mRNA, which was generated from cDNA obtained from *dram1*$^{\Delta 19n/\Delta 19n}$. The results showed that transient overexpression of *dram1* mRNA rescued Dram1 deficiency during mycobacterial infection, while overexpression of mutant *dram1* mRNA did not affect Mm infection burden (Fig2 C). Collectively, our analysis of two zebrafish *dram1* mutant alleles confirms that Dram1 is necessary for host defense during Mm infection.

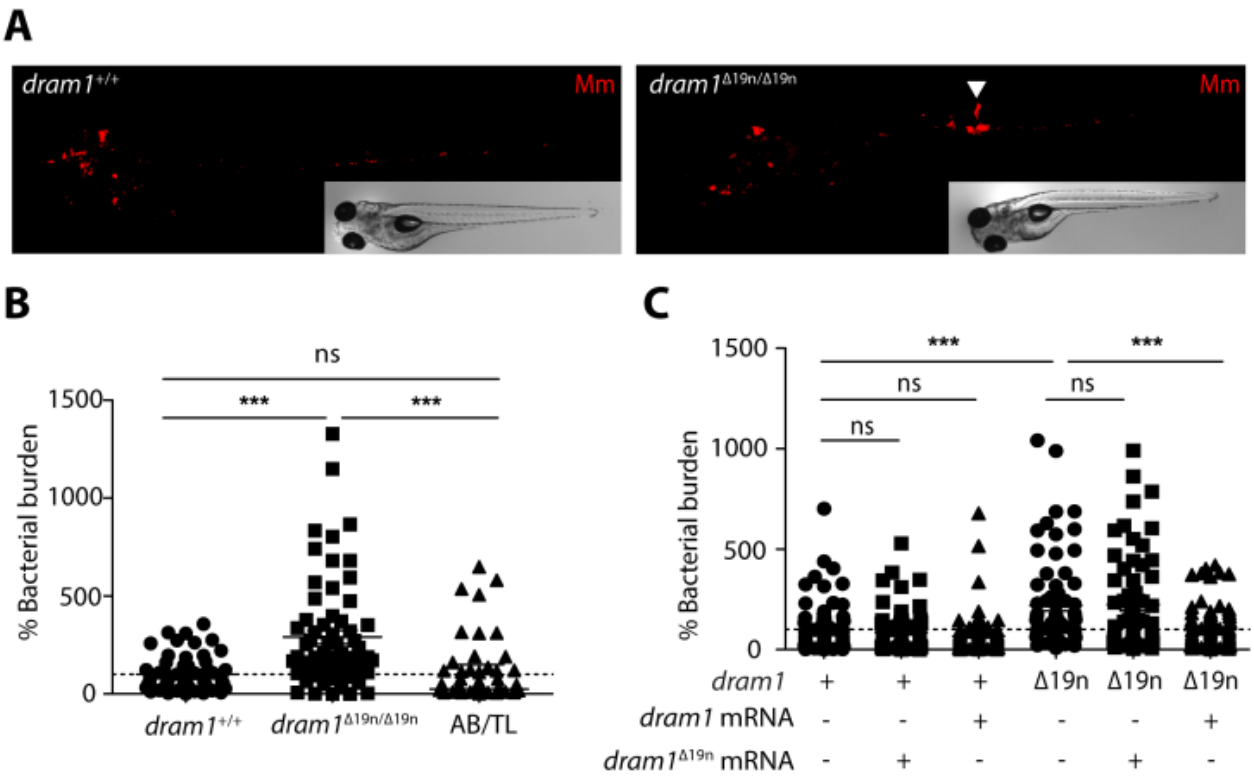

Figure 2: Dram1 deficiency leads to increased susceptibility to Mm infection

A. Representative stereo images of infected *dram1*$^{\Delta 19n/\Delta 19n}$ and *dram1*$^{+/+}$ larvae at 3 dpi**.**

B. Bacterial burdens were determined at 3dpi. The data is accumulated from two independent infection experiments. Each dot represents an individual larva. The arrowhead indicates the accumulation of bacteria in intersegmental veins. ns, non-significant, *p<0.05,**p<0.01,***p<0.001 .

C. Embryos were injected at the one cell stage with 50 ng of *dram1* or *dram1*$^{\Delta 19n}$ mRNA, or non injected. Data is accumulated from two independent infection experiments. Each dot represents an individual larva. ns, non-significant, *p<0.05,**p<0.01,***p<0.001.

Analyzing autophagic processes in *dram1* null mutants suggests defects in autophagosome maturation

Human DRAM1 is a modulator of autophagy and DRAM1 deficiency results in impaired autophagy induction *in vitro*[11]. Furthermore, a role for DRAM1 in maturation of autophagosomes has been described [49]. Therefore, we assessed the effect of zebrafish dram1 mutation on autophagy in developing embryos (Fig3 A). Increased GFP-Lc3 puncta and LC3-II protein levels can indicate enhanced autophagosome formation [50]. However, increased GFP-Lc3

puncta or Lc3-II protein levels can also indicate a block in degradation of autophagosomes (reduced autophagic flux). First, we used the GFP-Lc3 reporter to analyze whether differences in basal autophagy could be detected due to Dram1 deficiency. We imaged GFP-Lc3 puncta in the tail fin tissue of *dram1*$^{\Delta 19n/\Delta 19n}$ and *dram1*$^{+/+}$. Although the average number of autophagy-related structures was slightly higher in *dram1*$^{\Delta 19n/\Delta 19n}$, the difference between the two groups under basal conditions was not significant (Fig3 B). However, there might be differences that are obscured by ongoing autophagic flux, or that only become apparent under certain conditions. Therefore, we examined GFP-Lc3 accumulation following treatment with the vacuolar H+ ATPase (V-ATPase) inhibitor Bafilomycin A1 (BafA1). Treatment with BafA1 prevents maturation of autophagic vacuoles by inhibiting fusion between autophagosomes and lysosomes [51, 52]. While BafA1 treatment resulted in accumulation of GFP-Lc3 puncta in both *dram1*$^{\Delta 19n/\Delta 19n}$ and *dram1*$^{+/+}$, the dram1 mutants accumulated more GFP-Lc3 puncta than their wild type siblings (Fig3 C). To independently confirm these results, we next detected endogenous Lc3 protein levels by western blot. In agreement with the GFP-Lc3 puncta analysis, Lc3-II protein levels were not detectably different between *dram1*$^{\Delta 19n/\Delta 19n}$ and *dram1*$^{+/+}$ larvae under basal conditions, but Dram1 deficiency significantly increased Lc3-II protein levels when autophagic flux is blocked by BafA1 treatment (Fig3 D and E). Finally, we assessed the protein levels of p62 and Optineurin, since these ubiquitin-binding receptors are depleted during selective autophagy [53-55]. Therefore, protein levels of p62, as well as Optineurin, can be used as an inverse indicator of autophagy activity [56]. The results showed that Optineurin and p62 protein levels were similar in *dram1*$^{\Delta 19n/\Delta 19n}$ and *dram1*$^{+/+}$ under basal conditions but were elevated in *dram1*$^{\Delta 19n/\Delta 19n}$ larvae when autophagic flux is blocked in the presence of BafA1 (FigS3 A). This accumulation of Optineurin and p62 could be due either to increased production or to reduced degradation of these selective autophagy receptors. Taken together, Dram1 deficiency did not cause detectable differences in autophagic processes under basal conditions. However, blocking autophagic flux revealed alterations in the autophagy pathway that could be explained by an increase in autophagosome formation, a defect in autophagosome maturation, or both.

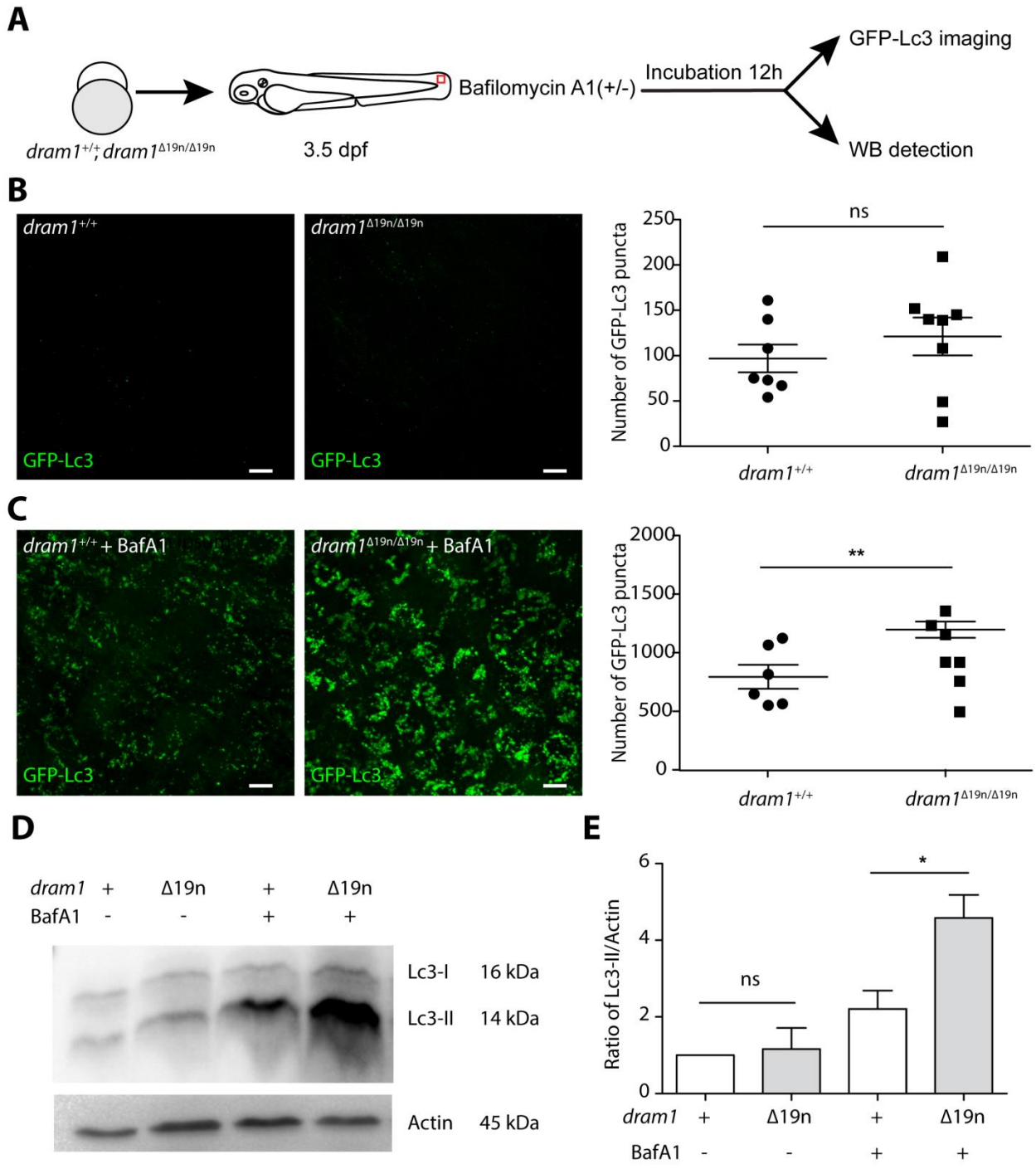

Figure 3: Dram1 mutation leads to impairment in autophagic flux

A. Workflow representing the experimental design followed in panels B-D. 3.5 dpf larvae were treated with BafA1 (100 nM) for 12h or no treatment. The *dram1*$^{\Delta 19n/\Delta 19n}$ and *dram1*$^{+/+}$ larvae in GFP-Lc3 background were used for

monitoring autophagic activity using confocal imaging. The *dram1*$^{\Delta 19n/\Delta 19n}$ and *dram1*$^{+/+}$ larvae not carrying GFP-Lc3 were used for assaying autophagy activity by western blot (WB).

B-C. Representative confocal micrographs of GFP-Lc3 puncta present in the tail fin, and quantification of the number of GFP-Lc3 puncta in *dram1*$^{\Delta 19n/\Delta 19n}$ and *dram1*$^{+/+}$ larvae in an unstimulated situation (basal autophagy, B) and following BafA1 treatment (C). Each larva was imaged at a pre-defined region of the tail fin (as indicated by the red boxed area in Fig3 A) (≥6 larvae/group). Results are representative of two independent experiments. Scale bars, 10 μm.

D. Lc3 protein levels were detected in *dram1*$^{\Delta 19n/\Delta 19n}$ and *dram1*$^{+/+}$ larvae in absence or presence of BafA1. Protein samples were obtained from 4 dpf *dram1*$^{\Delta 19n/\Delta 19n}$ and *dram1*$^{+/+}$ larvae (>10 larvae/sample). The WB were probed with antibodies against Lc3 and Actin as a loading control. WB were repeated three times with protein extracts derived from independent experiments.

E. Lc3-II/Actin ratios were quantified from the blots of *dram1*$^{\Delta 19n/\Delta 19n}$ and *dram1*$^{+/+}$ larvae in absence or presence of BafA1. WB band intensities were quantified by Lab Image (Bio-Rad). The data were combined from three independent experiments.

Dram1 deficiency leads to reduced GFP-Lc3 targeting of mycobacteria, but accumulated Lc3-II protein levels

We previously found that Dram1 mediates autophagic defense against Mm and that *dram1* knockdown decreased targeting of autophagic vesicles to Mm [7]. Thus, we infected *dram1*$^{\Delta 19n/\Delta 19n}$ and *dram1*$^{+/+}$ in a GFP-Lc3 background with Mm to determine whether *dram1* knockout confirms our previous observations. We used confocal laser scanning microscopy to image the entire caudal hematopoietic tissue (CHT) at 2 dpi, since the majority of immune cells that have phagocytosed Mm are present in the CHT at this time point (Fig4 A). We quantified the colocalization between GFP-Lc3 and Mm and found that *dram1*$^{\Delta 19n/\Delta 19n}$ larvae displayed significantly less GFP-Lc3-positive Mm clusters compared to their wild type siblings (Fig4 B). Approximately 9% of the Mm clusters were positive for GFP-Lc3 in wild type siblings, opposed to only around 3% in *dram1*$^{\Delta 19n/\Delta 19n}$ (Fig4 C). Since Dram1 deficiency reduced autophagic targeting of Mm, we expected to detect lower Lc3-II protein levels by western blot at 3 dpi. The results showed that Mm infection increased Lc3-II levels in *dram1*$^{\Delta 19n/\Delta 19n}$ and *dram1*$^{+/+}$ (Fig4 D), consistent with the observed autophagic targeting of Mm (Fig4 B). However, the results also showed that Dram1-deficient larvae accumulated more Lc3-II than their wild type siblings during

Mm infection (Fig4 D), which was opposite to our expectation. Since ubiquitination of cytoplasmic cargo plays an important role in selective autophagy against mycobacteria [20], we performed western blot detection of ubiquitinated proteins on non-infected and infected *dram1*$^{\Delta 19n/\Delta 19n}$ and *dram1*$^{+/+}$. The results showed that Dram1 deficiency led to accumulation of ubiquitinated proteins during the infection (FigS4 A). In conclusion, Mm infection results in increased accumulation of Lc3-II and ubiquitinated proteins. While these proteins accumulate at even higher levels in Dram1-deficient larvae, we clearly observed reduced autophagic targeting of Mm in the absence of Dram1.

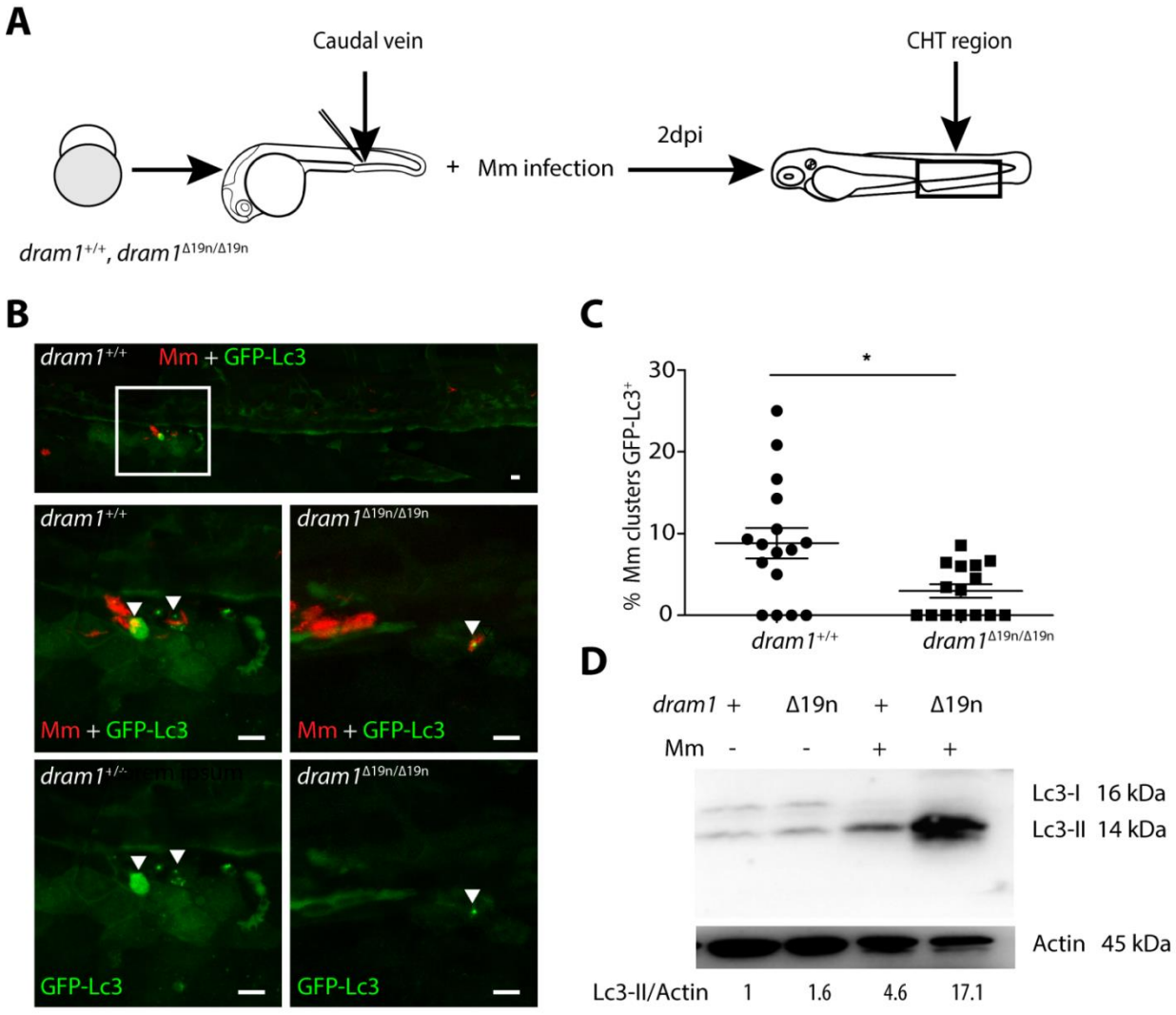

Figure 4: Dram1 is required for GFP-Lc3 targeting to Mm clusters

A. Workflow representing the experimental design followed in B. 2 dpi fixed larvae were used for confocal imaging. The entire caudal hematopoietic tissue (CHT) was imaged, as indicated by the black box.

B. Representative confocal micrographs of GFP-Lc3 co-localization with Mm clusters in infected *dram1*$^{\Delta 19n/\Delta 19n}$ and *dram1*$^{+/+}$ larvae. The top image shows the entire CHT region. the bottom images show GFP-Lc3 colocalization of Mm clusters in *dram1*$^{\Delta 19n/\Delta 19n}$ and *dram1*$^{+/+}$ larvae. The arrowheads indicate the overlap between GFP-Lc3 and Mm clusters. Scale bars, 10 μm.

C. Quantification of the percentage of Mm clusters positive for GFP-Lc3 vesicles. The data is accumulated from two independent experiments, each dot represents an individual larva (≥15 larvae/group).

D. Lc3 protein levels were determined by WB in infected and uninfected larvae. Protein samples were extracted from 4 dpf larvae (>10 larvae/sample). The blots were probed with antibodies against Lc3 and Actin as a loading control. WBs were repeated two times with independent extracts.

Dram1-deficiency does not affect phagocytosis of Mm

Macrophages play an important role in defense against mycobacterial infections. Thus, we were interested to know whether Dram1 deficiency affects the immune functions of macrophages. Therefore, the *dram1*$^{\Delta 19n/\Delta 19n}$ line was outcrossed with the macrophage marker line *Tg*(*mpeg1:mCherry-F*)^{umsF001} [57] and subsequently incrossed to obtain *dram1*$^{+/+}$, *dram1*$^{\Delta 19n/+}$, and *dram1*$^{\Delta 19n/\Delta 19n}$ with an *mpeg1*-driven and membrane-localizing *mCherry-F* in the background (FigS1 A and D). Since human DRAM1 is involved in cellular differentiation of immune cells [48], we first asked whether Dram1-deficiency affected the development of immune cells in zebrafish. For this purpose, we performed TSA-staining to count the number of neutrophils and utilized the *mpeg1:mCherry-F* reporter to count the number of macrophages. The results revealed that Dram1 deficiency did not alter the number of macrophages and neutrophils (Fig5 A and Fig5 B). Since the first stages of TB pathogenesis take place inside macrophages, we asked whether increased mycobacterial burden caused by Dram1 deficiency was due to defects in phagocytosis by macrophages. We infected *dram1*$^{\Delta 19n/\Delta 19n}$ and *dram1*$^{+/+}$ with Mm and assessed the phagocytic activity of leukocytes at 1 hour post infection (hpi). The results showed that Mm were phagocytosed by macrophages both in *dram1*$^{\Delta 19n/\Delta 19n}$ and their wild type siblings, and there was no significant difference in the percentage of Mm clusters that reside inside macrophages at 1 hpi (Fig5 C and Fig5 D). Next, we determined at which time point during the infection we were

first able to detect a difference in bacterial burden between *dram1*$^{\Delta 19n/\Delta 19n}$ and *dram1*$^{+/+}$. We found that there was no detectable difference in Mm infection burden at 1 dpi, but Dram1 deficiency significantly increased Mm infection burden at 2 dpi (Fig5 E and Fig5 F). In conclusion, Mm are phagocytosed at a similar rate by *dram1*$^{\Delta 19n/\Delta 19n}$ and *dram1*$^{+/+}$, and the immunocompromised state of Dram1-deficient larvae first becomes apparent at 2 days post infection.

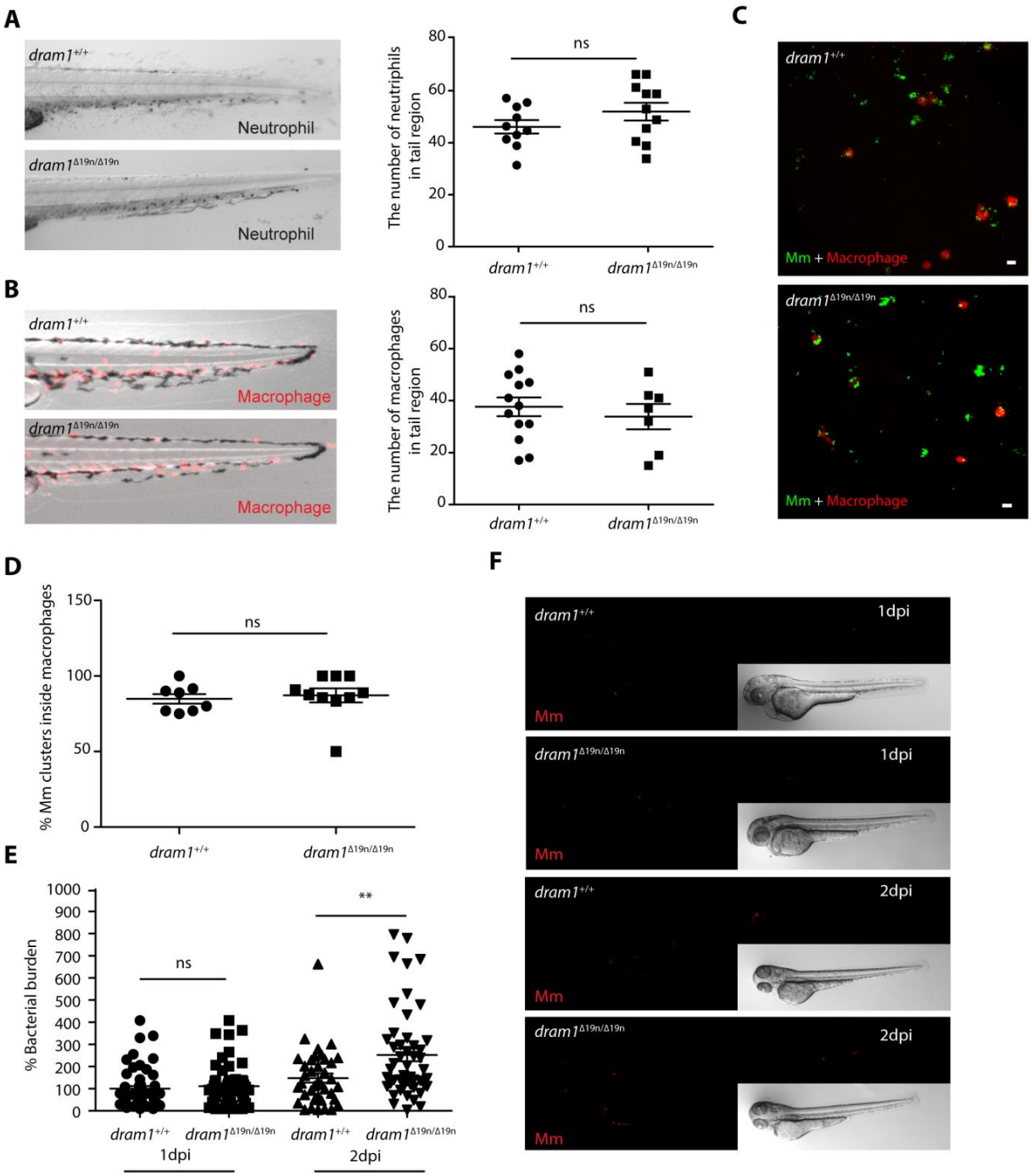

Figure 5: Dram1 deficiency does not affect the capability of macrophages to phagocytose Mm

A. Representative stereo images of the whole tail of *dram1*$^{\Delta 19n/\Delta 19n}$ and *dram1*$^{+/+}$ larvae following an immunohistochemical peroxidase activity detection protocol. The number of neutrophils in this region was quantified per individual larva (≥10 larvae/group). Each data point represents an individual larva. The results are representative for two individual repeats.

B. Representative stereo micrographs of macrophages in the whole tail region and quantification of the number of macrophages in this region. 3 dpf *dram1*$^{\Delta 19n/\Delta 19n}$ and *dram1*$^{+/+}$/ *mpeg1:mCherry-F* larvae were obtained from incrossed *dram1*$^{\Delta 19n/+}$ animals and the number of macrophages for each larva were counted before knowing the genotype. Genotyping was performed by PCR and Sanger sequencing (≥7 larvae/ group). The results are representative for two individual repeats.

C. Representative confocal micrographs of the yolk of infected *dram1*$^{\Delta 19n/\Delta 19n}$ and *dram1*$^{+/+}$ embryos in *mpeg1:mCherry-F* background at 1 hour post infection (hpi). Scale bars, 10 µm.

D. Quantification of phagocytosis of Mm by macrophages at 1 hpi. *dram1*$^{\Delta 19n/\Delta 19n}$ and *dram1*$^{+/+}$ embryos in *mpeg1:mCherry-F* background were infected Mm at 30 hpf and fixed at 1 hpi. Each dot represents the percentage of macrophages that have phagocytosed Mm clusters in an individual larva (≥8 larvae/ group). The results are representative for two individual repeats.

E. Bacterial pixel counts were determined at 1 and 2 dpi for infected embryos. *dram1*$^{\Delta 19n/\Delta 19n}$ and *dram1*$^{+/+}$. Each dot represents an individual infected larva. ns, non-significant, *p<0.05,**p<0.01,***p<0.001 ..

F. Representative stereo images of infected *dram1*$^{\Delta 19n/\Delta 19n}$ and *dram1*$^{+/+}$ embryos at 1 and 2 dpi.

Dram1 is required for macrophages to restrict Mm infection

Since Dram1 is a lysosomal membrane protein [11], we asked whether Dram1-deficiency affected the maturation of Mm-containing vesicles. We used LysoTracker to determine the extent of colocalization between Mm and acidic vesicles in the CHT at 1 dpi, a time point at which we did not observe a difference in bacterial burden between *dram1*$^{\Delta 19n/\Delta 19n}$ and *dram1*$^{+/+}$ yet (Fig5 E). In wild type siblings, we observed that roughly 60% of the bacterial clusters were LysoTracker-positive, while in Dram1-deficient larvae only roughly 20% of the bacterial clusters were positive for LysoTracker staining (Fig6 B). This implicates that Dram1 is indeed required for maturation of Mm-containing vesicles. Next, we asked whether the reduced maturation of Mm-containing vesicles limits the ability of macrophages in *dram1*$^{\Delta 19n/\Delta 19n}$ hosts to combat the infection. The results showed that at 1 dpi the majority of Mm clusters were restricted inside macrophages both in *dram1*$^{\Delta 19n/\Delta 19n}$ and *dram1*$^{+/+}$ (63% and 75%, respectively; Fig6 C and Fig6 D). However, at

2 dpi, we observed that the majority of Mm remained inside of macrophages in *dram1*$^{+/+}$ (65%), while in *dram1*$^{\Delta 19n/\Delta 19n}$ larvae we found that most Mm had escaped from macrophages and only 31% remained intracellular (Fig6 E and F). Furthermore, we frequently observed evidence of macrophage cell death in the proximity of bacterial clusters in *dram1*$^{\Delta 19n/\Delta 19n}$ (Fig6 E). Together, these data demonstrated that Dram1 is necessary for macrophages to restrict mycobacterial infection and prevent extracellular growth of the bacteria.

Figure 6: Macrophages fail to restrict Mm infection in Dram1-deficient larvae (Figure on next page)

A. Representative confocal images of LysoTracker staining performed on *dram1*$^{\Delta 19n/\Delta 19n}$ and *dram1*$^{+/+}$ embryos at 1 dpi. The arrowheads indicate the colocalization between Mm and LysoTracker staining. Scale bars, 10 µm.

B. The percentage of Mm clusters positive for LysoTracker staining (LysoTracker^{+}) was determined in infected embryos (≥10 embryos/group) at 1 dpi. Each dot represents the percentage of Mm clusters that are LysoTracker^{+} in an individual infected larva. Data is representative of two independent experiments. ns, non-significant,*p<0.05,**p<0.01,***p<0.001.

C and D Representative confocal images of *dram1*$^{\Delta 19n/\Delta 19n}$ and *dram1*$^{+/+}$ embryos/larvae in *mpeg1:mCherry-F* background, infected as described in Fig6 A, at 1 and 2 dpi. The entire CHT region of fixed embryos or larvae was imaged. The arrowheads indicate extracellular Mm clusters and stars(*) indicate dead macrophages. Scale bars, 10 µm.

E and F: The percentage of Mm clusters restricted inside macrophages was determined at 1 and 2 dpi (≥5 embryos/group). Each dot represents the percentage of intracellular Mm clusters in an individual embryos. Data is representative of two independent experiments. ns, non-significant,*p<0.05,**p<0.01,***p<0.001.

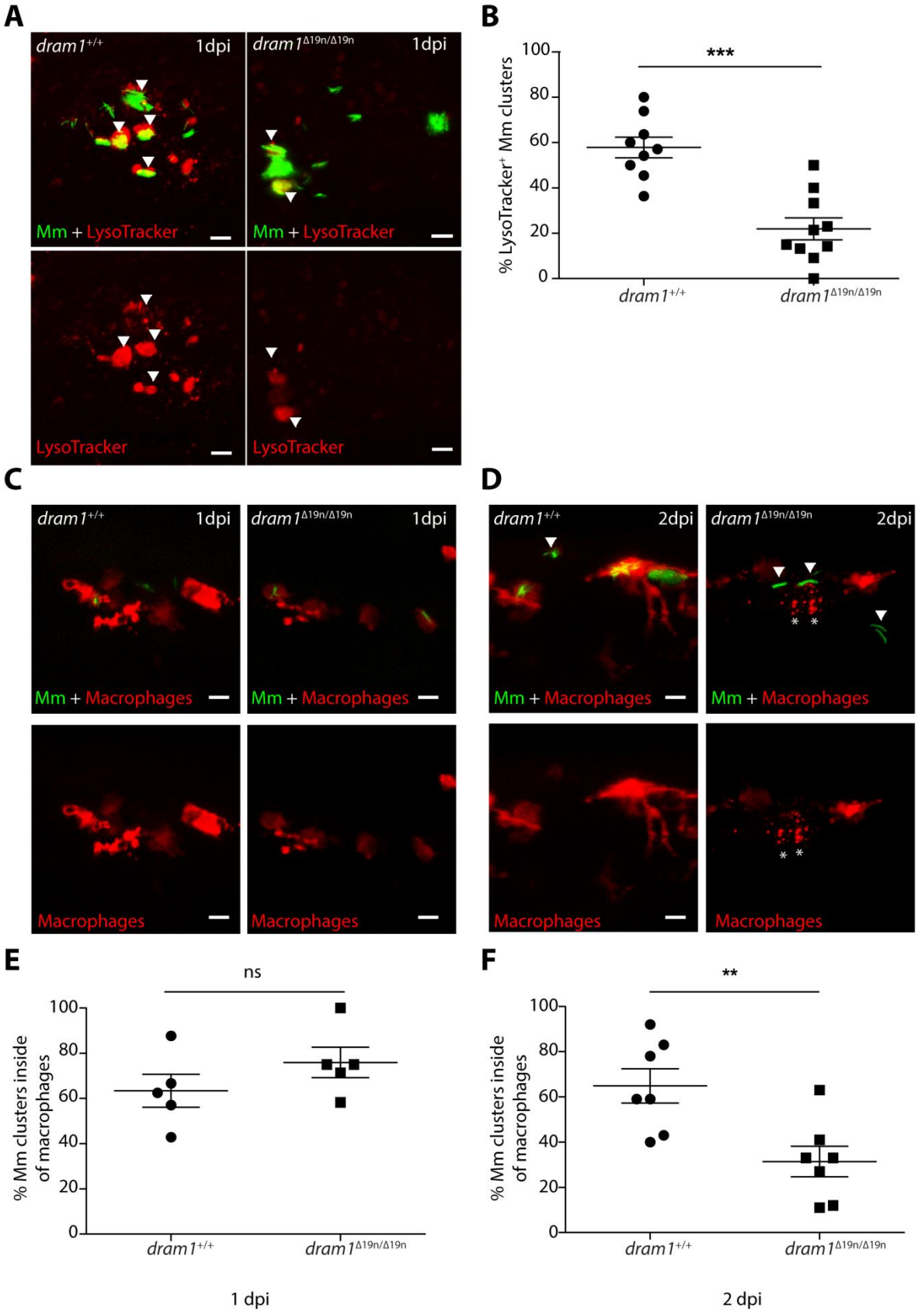
A
dram1+/+
1dpi
dram1Δ19n/Δ19n
1dpi
Mm + LysoTracker
Mm + LysoTracker
LysoTracker
LysoTracker
B
% LysoTracker+ Mm clusters
100
80
60
40
20
0
***
dram1+/+
dram1Δ19n/Δ19n
C
dram1+/+
1dpi
dram1Δ19n/Δ19n
1dpi
Mm + Macrophages
Mm + Macrophages
Macrophages
Macrophages
D
dram1+/+
2dpi
dram1Δ19n/Δ19n
2dpi
Mm + Macrophages
Mm + Macrophages
Macrophages
Macrophages
E
% Mm clusters inside of macrophages
100
80
60
40
20
0
ns
dram1+/+
dram1Δ19n/Δ19n
1 dpi
F
% Mm clusters inside of macrophages
100
80
60
40
20
0
**
dram1+/+
dram1Δ19n/Δ19n
2 dpi

Dram1 deficiency results in increased Caspase-1 dependent programmed cell death

Since we observed many dead macrophages around Mm in *dram1*$^{\Delta 19n/\Delta 19n}$ at 2 and 3 dpi (Fig6 E and data not shown), we aimed to decipher the mechanism responsible for this cell death. Thus, we performed Terminal deoxynucleotidyl transferase dUTP nick end labeling (Tunel) on infected embryos and imaged the entire CHT region of *dram1*$^{\Delta 19n/\Delta 19n}$ and *dram1*$^{+/+}$. This staining can detect damaged DNA present both in apoptotic and pyroptotic cells [58, 59]. We could observe Tunel-positive cells around Mm clusters both in *dram1*$^{\Delta 19n/\Delta 19n}$ and *dram1*$^{+/+}$ (Fig7 A). The results showed that the percentage of Tunel-positive Mm clusters was around 2.1 times higher in *dram1*$^{\Delta 19n/\Delta 19n}$ when compared to *dram1*$^{+/+}$ (Fig7 B). Human DRAM1 has previously been reported as a regulator of apoptosis [12]. Thus, we determined whether Dram1-deficiency affected apoptosis in response to infection. Caspase 3 serves as a main executioner and indicator of apoptotic cell death [38, 60]. We therefore utilized an antibody against full length and active Caspase 3 to monitor apoptosis activity by western blot in *dram1*$^{\Delta 19n/\Delta 19n}$ and *dram1*$^{+/+}$. The results showed that Caspase 3 was activated (cleaved) in response to Mm infection in *dram1*$^{\Delta 19n/\Delta 19n}$ and *dram1*$^{+/+}$. However, we did not detect any difference in the levels of Caspase 3 activation between *dram1*$^{\Delta 19n/\Delta 19n}$ and *dram1*$^{+/+}$ (Fig7 C). This indicated that cells undergo apoptosis in *dram1*$^{\Delta 19n/\Delta 19n}$ and *dram1*$^{+/+}$ during Mm infection but did not provide evidence that the increased cell death observed in *dram1*$^{\Delta 19n/\Delta 19n}$ was due to increased apoptosis. Next, we asked if these macrophages died via pyroptotic cell death. Pyroptosis is a Caspase 1-dependent form of cell death [37]. Thus, we detected Caspase 1 activity in the absence and presence of Mm infection in *dram1*$^{\Delta 19n/\Delta 19n}$ and *dram1*$^{+/+}$ at 2dpf, the time point at which we observed increased cell death in *dram1*$^{\Delta 19n/\Delta 19n}$. The results showed that Caspase 1 activity was increased in *dram1*$^{\Delta 19n/\Delta 19n}$ infected with Mm, but not in *dram1*$^{+/+}$ (Fig7 D). Next, we asked if the increased bacterial burden in Dram1-deficient larvae is dependent on Caspase 1 activity. Thus, we injected *caspase a* (a functional homologue of caspase 1) morpholino into the one cell stage of *dram1*$^{+/+}$ and *dram1*$^{\Delta 19/\Delta 19}$ embryos and infected with Mm at 1 dpf. In agreement with previous results (Fig 2), the infection burden of *dram1*$^{\Delta 19n/\Delta 19}$ embryos was higher that of *dram1*$^{+/+}$ (Fig7 E and F). Morpholino knockdown of *caspase a* knockdown in decreased infection burden in *dram1*$^{+/+}$ by 48% and in *dram1*$^{\Delta 19/\Delta 19}$ by 63%, bringing the infection burden of both groups to a similar low

level (Fig7 E and F). Collectively, these data suggest that mycobacterial infection in zebrafish embryos is promoted by pyroptosis of infected macrophages and that the lack of functional Dram1 results in macrophages being overgrown by the bacteria, thereby increasing pyroptotic cell death.

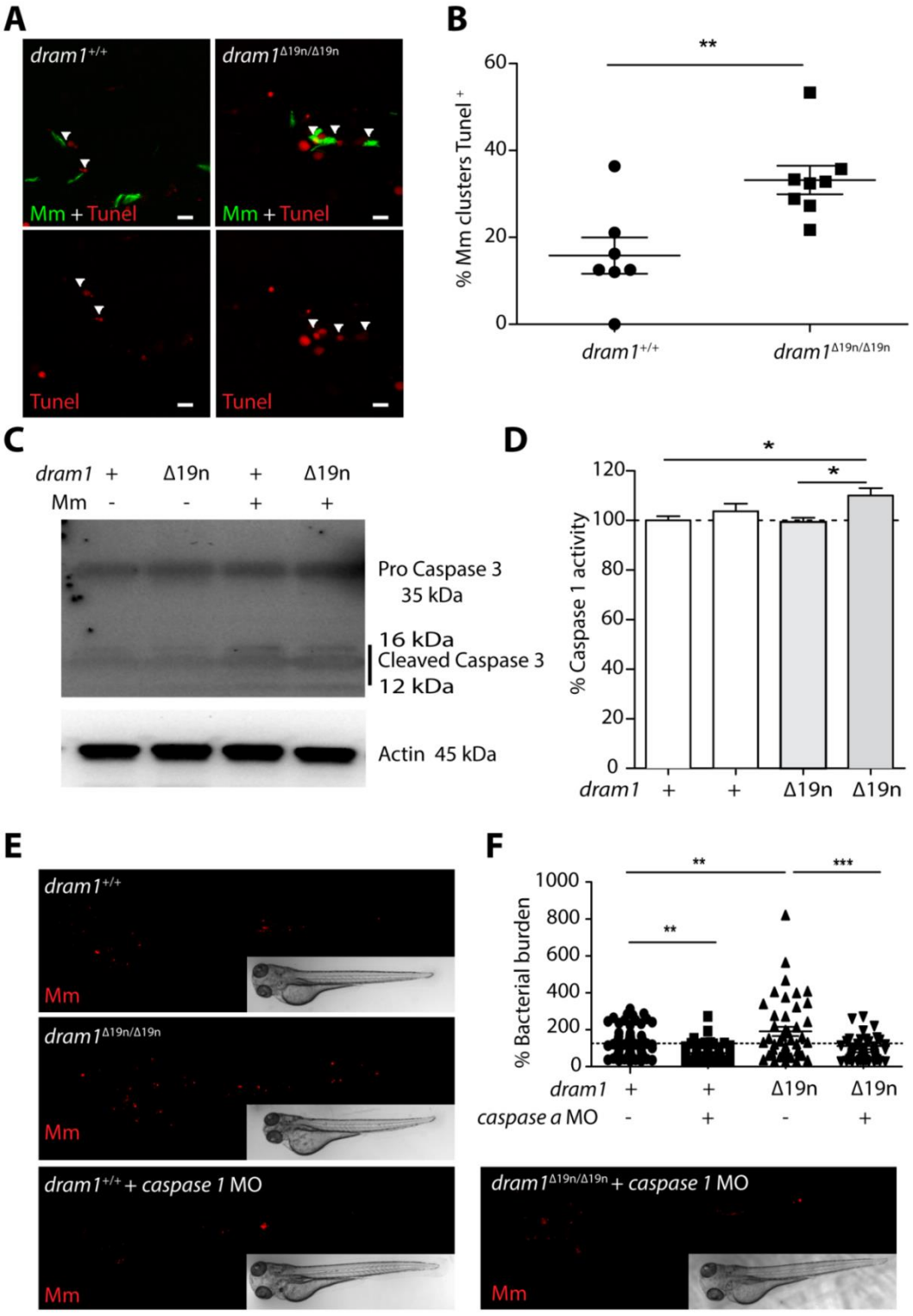

Figure 7: Dram1 deficiency results in increased Caspase 1-dependent programmed cell death

A. Representative confocal images of Tunel staining in *dram1*$^{\Delta 19n/\Delta 19n}$ and *dram1*$^{+/+}$ larvae at 2 dpi. The entire CHT region of 2 dpi fixed *dram1*$^{\Delta 19n/\Delta 19n}$ and *dram1*$^{+/+}$ larvae was imaged. The arrowheads indicate the cells positive for Tunel staining (Tunel^{+}). Scale bars, 10 µm.

B. Quantification of the percentage of Mm clusters Tunel^{+} in *dram1*$^{\Delta 19n/\Delta 19n}$ and *dram1*$^{+/+}$ larvae. Each dot represents the percentage of Mm clusters Tunel^{+} in the CHT region of an individual infected larva. ns, non-significant,*p<0.05,**p<0.01,***p<0.001.

C. Detection of pro-Caspase 3 and cleaved Caspase 3 protein in *dram1*$^{\Delta 19n/\Delta 19n}$ and *dram1*$^{+/+}$ embryos. Protein samples were extracted from 4 dpf infected and uninfected *dram1*$^{\Delta 19n/\Delta 19n}$ and *dram1*$^{+/+}$ larvae (>10 larvae/sample). The western blots were probed with antibodies against Caspase 3 and Actin as a loading control. The experiments were repeated two times.

D. Caspase 1 activity was assessed in *dram1*$^{\Delta 19n/\Delta 19n}$ and *dram1*$^{+/+}$/GFP-Lc3 embryos. Protein samples were obtained from 2 dpf infected and uninfected *dram1*$^{\Delta 19n/\Delta 19n}$ and *dram1*$^{+/+}$ embryos (>30 embryos/sample). The data is accumulated from two independent experiments. ns, non-significant,*p<0.05,**p<0.01,***p<0.001

E. Bacterial pixel counts were determined at 2 dpi following knockdown of *caspase a* in *dram1*$^{\Delta 19n/\Delta 19n}$ and *dram1*$^{+/+}$ embryos. The data is accumulated from two independent experiments. ns, non-significant,*p<0.05,**p<0.01,***p<0.001

F. Representative stereo images of infected *dram1*$^{\Delta 19n/\Delta 19n}$ and *dram1*$^{+/+}$ larvae at 2 dpi with and without *caspase a* MO injection**.**

Discussion

The lysosomal protein DRAM1 regulates autophagy and cell survival/death decisions under multiple stress conditions, including diseases like cancer and infection. Its mechanism of action remains largely unknown. In this study, we have demonstrated that mutation of *dram1* in zebrafish impairs resistance to mycobacterial infection. Importantly, we show that Dram1 deficiency reduces the acidification of Mm-containing vesicles, ultimately resulting in Caspase 1-dependent cell death of infected macrophages and increased extracellular growth of mycobacteria during early stages of the infection.

In this study we generated two independent *dram1* mutant lines using CRISPR/Cas9 technology to confirm and build upon results obtained with transient knockdown studies [7]. The combined use of knockdown (transient silencing) and knockout (stable loss of function) technologies is important, considering that targeting the same gene with these two approaches can result in

different phenotypes due to several reasons [61]. First, knockdown approaches can generate off-target effects and thereby induce phenotypes that are quite different from corresponding mutants. On the other hand, higher eukaryotic organisms can adapt to genetic variation (e.g. loss of function) by altering the activity of other genes, a mechanism which is called genetic compensation [62, 63]. This genetic compensation cannot be activated during transient knockdown of a gene and might therefore account for discrepancies between phenotypes resulting from knockout or knockdown approaches [62, 63]. Embryos and larvae homozygous for the two *dram1* CRISPR/Cas9 mutant alleles were viable and displayed no apparent phenotypes. Furthermore, we used the stable mutant lines to demonstrate that Dram1 deficiency does not affect development into adulthood or fertility. These observations are similar to *DRAM1* mutation in mouse models, which resulted in viable, fertile, and apparently normal individuals compared to their wild-type siblings (Mah thesis 2012) [86]. While DRAM1 deficiency was previously shown to affect the differentiation of neutrophils in acute promyelocytic leukaemia (APL) [48], the absence of functional Dram1 in zebrafish did not affect the total numbers of neutrophils or macrophages. In agreement with previous morpholino knockdown studies [7], both *dram1* mutant alleles showed increased susceptibility to mycobacterial infection in the zebrafish larval model of TB. The observation of a similar infection phenotype by two methods for disrupting *dram1* gene activity provides strong evidence that Dram1 is an important factor for host resistance against pathogenic mycobacteria. Furthermore, *dram1* mutants display decreased survival during *Salmonella* Typhimurium infection (Masud thesis) [87], indicating that Dram1 plays a role in immune defense against a broad range of intracellular bacterial pathogens.

The function of DRAM1 as a modulator of autophagy has been studied well *in vitro* [11]. We therefore tested whether zebrafish *dram1* mutants display defects in autophagic processes. Autophagy is a host response to diverse stress factors, including starvation. Wild type zebrafish larvae until 5 dpf can rely on their yolk proteins for nutrients [64], and we therefore assumed that their autophagic processes are not activated above a level normal for their developmental stage, unless autophagy is triggered by a stressor such as infection. In agreement, we did not detect any differences when comparing the basal levels of autophagy activity in uninfected *dram1* mutant larvae of 4 dpf to those of their wild type siblings. This finding is consistent with an *in*

vitro study of the function of mouse DRAM1 [65], which showed that basal autophagy was not altered in the absence of DRAM1 in primary mouse embryonic fibroblasts (MEFs). The five members of the DRAM family are conserved between human, mouse and zebrafish [7, 11, 66-68], and as also described in chapter 1 of this thesis. Therefore, it is conceivable that other DRAM family members can replace the loss of Dram1/DRAM1 under basal conditions, or that DRAM1 is only involved in autophagic processes in response to specific stress factors. Galavotti et al. (2013) found that autophagy induction in response to starvation or while blocking mTOR was not changed in the absence of DRAM1 [69]. However, the lack of DRAM1 affected the activation of autophagy in human cells (Hela and A549) following the induction of cellular stress by treatment with the mitochondria inhibitor 3-nitropropionic acid (3-NP) [49]. Besides infection, DNA-damage, and interference with impaired energy metabolism [7, 11, 13], it remains to be further investigated which stress factors can activate DRAM1/Dram1 *in vitro* and *in vivo*.

Treatment of *dram1* mutant larvae with BafA1, which blocks lysosomal degradation of autophagosomes, revealed an increase of GFP-Lc3 punctae and Lc3-II protein levels. This result is reminiscent of a previous study which showed that transient knockdown of human *DRAM1* significantly affected the clearance of autophagosomes in Hela cells [49]. The *dram1* mutants also accumulated higher Lc3-II protein levels than their wild type siblings under conditions of Mm infection. As in the case of BafA treatment, the accumulation of Lc3-II could indicate an increase in autophagosome production, or a defect in the degradation of autophagosomes. The latter possibility is supported by increased accumulation of ubiquitinated proteins in the *dram1* mutants. Collectively, we propose based on our data and the existing literature that the lysosomal protein Dram1/DRAM1 is important for maturation and degradation of autophagosomes. Furthermore, we believe that the induction of additional autophagosomes in response to BafA1 treatment or Mm infection – could function as a compensatory mechanism for the defect in degradation of cellular stress factors. Intriguingly, despite of the increased Lc3-II levels in infected *dram1* mutants, imaging in GFP-Lc3 transgenic fish revealed that mycobacteria are targeted by autophagic vesicles nearly 3-folds less frequently in *dram1* mutants than in wild type zebrafish larvae. This provides new evidence that Dram1 is required for autophagic defense against mycobacteria, as previously proposed based on morpholino

knockdown results [7]. How autophagic targeting of intracellular pathogens is orchestrated by DRAM1/Dram1 remains an important question for future research.

Previous studies have revealed that interaction occurs between autophagosomes and phagosomes [6, 70]. Specifically, defects in autophagy led to increased phagocytosis of Mtb in mouse macrophages [71]. Therefore, it was important to address the question whether altered autophagic targeting of Mm in zebrafish mutants was associated with different phagocytic ability of zebrafish macrophages. We found that, while Dram1 deficiency impaired autophagic defense against mycobacterial infection, it did not affect the capability of macrophages to phagocytose Mm. We did, however, find that Dram1 deficiency reduced autophagic targeting and acidification of Mm-containing vesicles, which ultimately resulted in the death of infected macrophages. These findings are in line with a recent study that revealed that DRAM1 directly mediates lysosomal membrane permeabilization (LMP) in HIV infected $CD4^+$ T cells [13]. Lysosome destabilisation triggered cell death and lowered viral replication [13]. While the mechanism of cell death could be similar in both situations, we detected higher mycobacterial burdens following death of the infected immune cells, as is to be expected from extracellularly growing Mm [23].

Apoptosis of infected cells is generally regarded as a host protective defence mechanism against mycobacterial infection, and virulent Mtb therefore actively inhibit apoptosis [33, 40, 72]. Apoptosis is a non-lytic form of cell death which prevents activation of an inflammatory response. Therefore, any intracellular mycobacteria will be encapsulated within the apoptotic envelope until the remains of the dying cell have been phagocytosed by recruited macrophages [40, 46, 73]. This is reasoned to be beneficial to the host by preventing uncontrolled extracellular growth of the bacteria. However, an *in vivo* study has demonstrated that apoptotic cell death can facilitate the expansion and dissemination of mycobacteria when macrophages phagocytosing the remains of the infected cell become infected themselves [23]. Nevertheless, only a small proportion of infected macrophages initiates apoptosis, as the majority of infected macrophages undergoes mycobacteria-induced lytic cell death [46]. In our study we observed that Caspase 3 was activated during mycobacterial infection, which is an indicator for apoptotic processes. DRAM1 was previously shown to mediate apoptosis by blocking the

degradation of the pro-apoptotic protein Bax [12]. While Dram1 deficiency leads to more cell death during Mm infection, we did not observe any changes in apoptosis activity on a whole embryo level, which led us to explore the role of Dram1 in other types of programmed cell death.

Strikingly, we found that Dram1 deficiency leads to more Caspase 1 activity and Caspase 1-dependent pyroptotic cell death. Pyroptosis is a lytic form of cell death which activates an inflammatory response [74]. Thus, the mechanisms, characteristics, and consequences of pyroptotic cell death are different from apoptosis [37, 75]. Previous studies revealed that pyroptosis can be induced by diverse pathogens and forms a critical mechanism to restrict microbial infection [75, 76]. In line with this, there is also evidence that mycobacteria inhibit pyroptosis of infected macrophages via diverse mechanisms [77]. However, recent studies found that lytic cell death (e.g. pyroptosis and necrosis) helps mycobacteria to evade host immunity and dissminate the infection [24, 46]. Indeed, in this present study we found that Caspase 1-dependent pyroptotic cell death promoted the expansion of bacteria. Moreover, genetic inhibition of Caspase 1 could rescue the exacerbated bacterial growth in *dram1* mutants. Taken together, the death of infected macrophages is intricately related to TB pathogenesis and can result either in increased dissemination or restriction of the infection. The sometimes contradicting evidence concerning the beneficial or detrimental effects of the different modes of cell death suggests that the context of cell death (e.g. location, timing during TB pathogenesis, and the immune status of the host) plays a crucial role in determining the outcome.

In conclusion, restriction of mycobacteria in infected macrophages during the early stages of infection requires functional Dram1. In this work, we have shown that Dram1 is involved in several processes important to defense against intracellular pathogens, potentially providing an intersection between modulation of autophagy, lysosomal function, and programmed cell death. Future studies are required to precisely elucidate the role of the lysosomal protein Dram1/DRAM1 in this network. Facing the complexity of the current TB situation, there is an urgent need to improve treatment strategies to control TB progression. Host-directed therapies (HDT) have emerged as a promising alternative to counter TB. HDTs can assist the host in

responding appropriately to Mtb infection, thereby promoting the effectiveness of drug treatments and reducing the time required for treatment [9]. Using an *in vivo* model for the early stages of TB disease we have demonstrated the importance of Dram1 for the elimination of intracellular mycobacteria and the cell fate of infected macrophages. This makes Dram1/DRAM1 – and its interaction partners that remain to be identified –promising targets for HDT development to improve the outcome of TB disease.

Materials and methods

Zebrafish culture and lines

Zebrafish lines in this study (TableS1) were maintained and used in compliance with local animal welfare regulations as overseen by the Leiden University (registration number: 10612). Embryos were kept in egg water, in a 28.5°C-30°C incubator, and treated with 0.02% Ethyl 3-aminobenzoate methanesulfonate (Tricaine, SIGMA-ALDRICH) in egg water for anesthesia before bacterial injections, imaging and fixation.

CRISPR/Cas9 mediated mutagenesis of zebrafish *dram1*

Single guide RNAs (sgRNAs) targeting the first coding exon of zebrafish *dram1* (ENSDARG00000045561) were designed using the chop-chop website [78]. To make sgRNAs, the template single strand DNA (ssDNA) (122 bases) was obtained by PCR complementation and amplification of full length ssDNA oligonucleotides. Oligonucleotides up to 81 nucleotides were purchased from Sigma-Aldrich using standard synthesis procedures (25 nmol concentration, purification with desalting method) (TableS2). The pairs of semi-complimentary oligos were annealed together by a short PCR program (50 µL reaction, 200uM dTNPs, 1 unit of Dream Taq polymerase (EP0703, ThermoFisher); PCR program: initial denaturation 95°C/3 minute (min), 5 amplification cycles 95°C/30 Second (s), 55°C/60 s, 72°C/30 s, final extension step 72°C/15 min) and subsequently the products were amplified using the primers in TableS2 with a standard PCR program (initial denaturation 95°C/3 min, 35 amplification cycles 95°C/30 s,55°C/60 s, 72°C/30 s, final extension step 72°C/15 min). The final PCR products were purified with Quick gel extraction

and PCR purification combo kit (00505495, ThermoFisher). The purified PCR products were confirmed by gel electrophoresis or Sanger sequencing (Base Clear, Netherlands). For *in vitro* transcription of sgRNAs, 0.2 µg template DNA was used to generate sgRNAs using the MEGA short script ®T7 kit (AM1354, ThermoFisher) and purified by RNeasy Mini Elute Clean up kit (74204, QIAGEN Benelux B.V., Venlo, Netherlands). The Cas9 mRNA was transcribed using mMACHINE® SP6 Transcription Kit (AM1340, ThermoFisher) from a Cas9 plasmid (39312, Addgene) (Hrucha et al 2013) and purified with RNeasy Mini Elute Clean up kit (74204,QIAGEN Benelux B.V., Venlo, Netherlands). A mixture of sgRNA and Cas9 mRNA was injected into one cell stage AB/TL embryos (sgRNA 150 pg/embryo and Cas9 mRNA 300 pg/embryo). The effect of CRISPR injection was confirmed by PCR and Sanger sequencing.

Genomic DNA isolation and genotyping

Genomic DNA was isolated from an individual embryo (2 dpf) or small pieces of the tail fin tissue of adults (>3 months) by fin clipping. Embryos or tissue samples were incubated in 200 µL 100% Methanol at -20°C overnight (O/N), then methanol was removed, and remaining methanol was evaporated at 70°C for 20 min. Next, samples were incubated in 25 µL of TE buffer containing 1.7 µg/µL proteinase K at 55°C for more than 5 h. Proteinase K was heat inactivated at 80°C for 30 min, after which samples were diluted with 100 µL of Milli-Q water. Genotyping was performed by PCR-amplification of the region of interest using the following primers: Forward: AGTGAACGTCCGTGTCTTTCTT, Reverse: ACATCTTGTCGATACAAAGCGA; followed by Sanger sequencing to identify mutations (Base Clear, Netherlands).

Western blot analysis

Embryos (4dpf/3dpi) were anaesthetised with Tricaine (Lot#MKBG4400V, SIGMA-ALDRICH) and homogenised with a Bullet-blender (Next-Advance) in RIPA buffer (#9806, Cell Signalling) containing a protein inhibitor cocktail (000000011836153001, cOmplete, Roche). The extracts were then spun down at 4°C for 10 min at 12000 rpm/min and the supernatants were frozen for storage at −80°C. Western blotting was performed using Mini-PROTEAN-TGX (456-9036, Bio-Rad) or 18% Tris-Hcl 18% polyacrylamide gels, and protein transfer to commercial PVDF membranes

(Trans-Blot Turbo-Transfer pack, 1704156, Bio-Rad). Membranes were blocked with 5% dry milk (ELK, Campina) in Tris buffered saline (TBS) solution with Tween 20 (TBST,1XTBS contains 0.1% Tween 20) buffer and incubated with primary and secondary antibodies. Digital images were acquired using Bio-Rad Universal Hood II imaging system (720BR/01565 UAS). Band intensities were quantified by densitometric analysis using Image Lab Software (Bio-Rad, USA) and values were normalised to actin as a loading control. Antibodies used were as follows: polyclonal rabbit anti DRAM1 (N-terminal) (ARP47432- P050, Aviva systems biology), polyclonal rabbit anti-Optineurin (C-terminal) (1:200, lot#100000; Cayman Chemical), polyclonal rabbit anti-p62 (C-terminal) (PM045, lot#019, MBL), polyclonal rabbit anti Lc3 (1:1000, NB100-2331, lot#AB-3, Novus Biologicals), monoclonal Caspase 3 antibody (1:1000, #9662, Lot#12, Cell Signaling), Anti mono-and polyubiquitinated conjugates mouse monoclonal antibody (1:200; BML-PW8810-0100, lot#01031445, Enzo life Sciences), Polyclonal actin antibody (1:1000, 4968S, lot#3, Cell Signaling), Anti-rabbit IgG, HRP-Linked Antibody (1:1000, 7074S, Lot#0026, Cell Signaling), Anti-mouse IgG, HRP-linked Antibody (1:3000, 7076S, Lot#029, Cell Signaling).

Infection conditions and bacterial burden quantification

Mycobacterium marinum strain M or *Mycobacterium marinum* strain 20 fluorescently labeled with Wasabi or mCherry, respectively [79, 80], were microinjected into the blood island of embryos at 28 hpf as previously described [81]. The injection dose was 200 CFU for all experiments, except for the phagocytosis assay (500 CFU). Embryos were manually dechorionated by tweezers and treated with tricaine to keep anesthesia before the injection. Infected embryos were imaged using a Leica MZ16FA stereo fluorescence microscope equipped with a DFC420C colour camera, and the bacterial pixels per infected fish data were obtained from the individual embryo stereo fluorescence images using previously described software [82].

Confocal laser scanning microscopy and image quantification

Fixed or live embryos were mounted with 1.5% low melting agarose (140727, SERVA) and imaged using a Leica TCS SPE confocal microscopy. For quantification of numbers of GFP-Lc3 positive vesicles, the fixed 4dpf larvae were imaged by confocal microscopy with a 63x water

immersion objective (NA 1.2) in the pre-defined tail fin region to detect the number of GFP-LC3-positive vesicles (Fig3 B and C). The numbers of GFP-Lc3 vesicles were measured by Fiji/ImageJ software (Fig3 B and C) [83]. For quantification of the autophagic response targeted to Mm clusters (Fig4 B and C), the fixed 2 dpi infected larvae were imaged by confocal microscopy with a 40X water immersion objective (NA 1.0) at over the whole caudal hematopoietic tissue (CHT) region. The percentage of Mm clusters that were positive for GFP-Lc3 per embryo was determined in this study. The same approach was used to quantify Mm acidification in the CHT region (Fig6 A and B). To investigate the intramacrophage or extracellular localization of bacteria, fixed 2 dpi larvae were again imaged over the CHT as described above, and first the number of Mm clusters was counted in this region and then the number of Mm clusters that were inside of macrophages were counted. To assay cell death, images from fixed 2 dpi larvae were acquired as above, and the number of Tunel staining^{+} cells in the CHT region was counted manually.

mRNA preparation and injection

dram1 or *dram1*$^{\Delta 19N}$ (negative control) RNA was isolated from wild type or *dram1*$^{\Delta 19n/\Delta 19n}$ embryos using QIAzol lysis reagent (79306, QIAGEN) and purified with the RNeasy MinElute Cleanup kit (74204, QIAGEN). cDNA synthesis was performed using the iScript cDNA synthesis kit (1708891, BIO-RAD). Full-length *dram1* cDNA and *dram1*$^{\Delta 19N}$ cDNA was obtained by PCR amplification using Phusion High-Fidelity DNA Polymerase (M0530S, New England Biolabs). The following primers were used: Forward: CTG CGG CGA GAT GTT TTG GTT; Reverse: CAA AAA CAG TGG GAC ATA CAG TGA A. *dram1* or *dram1*$^{\Delta 19N}$ PCR products were ligated into a ZERO BLUNT TOPO vector (450245, ThermoFisher) and the insert was confirmed by Sanger sequencing (Base Clear, Netherlands). *dram1* and *dram1*$^{\Delta 19N}$ mRNA was generated using the SP6 mMessage mMachine kit (AM1340, Thermo Fisher) and Poly(A) Tailing Kit (AM1350, ThermoFisher);purified using the RNeasy Min Elute Cleanup kit (74204, QIAGEN) and 50pg mRNA was microinjected into one cell stage embryos.

TUNEL assay

Cell death was examined by Terminal deoxynucleotidyl transferase dUTP nick end labelling

(TUNEL staining) with the In Situ Cell Death Detection Kit (000000011684795910, SIGMA-ALDRICH) in 2dpi fixed embryos. The assay was performed as follows: embryos were re-hydrated with 75% Methanol (MeOH)/5min, 50% MeOH/10 min, 25% MeOH/5 min, Wash 3× 5 min in PBS-TX. Then, embryos were permeabilized in 10 µg/mL Proteinase K for 40 min at 37 °C followed by a quick rinse in PBST. 50µl of reagents mixture was added per sample, incubated O/N at 37°C while protected from light. Samples were washed 3X with PBST for 15 min each time and stored in PBST. Samples were examined with confocal microscopy as described above.

LysoTracker staining and Myeloperoxidase (Mpx) activity assay

Infected embryos were immersed in egg water with 10 µM LysoTracker Red DND-99 (L7528, ThermoFisher) for 1h. Embryos were washed 3 times with egg water before imaging. Myeloperoxidase (Mpx) activity assay was performed with the Leukocyte detection Kit (390A, SIGMA-ALDRICH) for detection of neutrophils as previously described [82].

Drug treatment

Embryos were bath treated with Bafilomycin A1 (BafA1) (B1793-10UG, SIGMA-ALDRICH) diluted into egg water at the working concentration of 100 nM for 12h.

Caspase 1 activity assay

Caspase-1 activity was assayed with the fluorometric substrate Z-YVAD 7-Amido-4-trifluoromethylcoumarin (Z-YVAD-AFC, Caspase-1 Substrate IV, Colorimetric, sc-311283, Santa Cruz) as described previously [84] 20 embryos/group were lysed in hypotonic cell lysis buffer (25 mM 4-(2-hydroxyethyl) piperazine-1-ethanesulfonic acid, 5 mM ethylene glycol-bis (2-aminoethyl ether)-N,N,N',N'-tetraacetic acid, 5 mM dithiothreitol, 1:20 protease inhibitor cocktail (000000011836153001, cOmplete, Roche), pH 7.5) on ice for 10 min. For each reaction, 10 µg protein was incubated for 90 min at 28°C with 50 µM YVAD-AFC in 50 µl of reaction buffer (0.2% 3-[(3-cholamidopropyl) dimethylammonio]-1-propanesulfonate (CHAPS), 0.2 M 4-(2-hydroxyethyl) piperazine-1-ethanesulfonic acid, 20% sucrose, 29 mM dithiothreitol, pH 7.5). After the incubation, the fluorescence of the AFC released from the Z-YVAD-AFC substrate was

measured with a Microplate Readers (Tecan M1000) at an excitation wavelength of 400 and emission wavelength of 505 nm.

Morpholino Injection condition

caspase a morpholino (MO) in this study was previously used and validated [85] and purchased from Gene tools (Gene Tools, USA). MO oligonucleotide sequence: 5'GCCAT GTTTAGCTCAGGGCGCTGAC-3' [85]. MO was diluted in Milli-Q water with 0.05% phenol red and 1nL of 0.6 mM MO was microinjected into the yolk of one cell stage embryos as previously described.

Statistical analyses

Statistical analyses were performed using GraphPad Prism software (Version 5.01; GraphPad). All experimental data (mean ± SEM) was analyzed using unpaired, two-tailed t-tests for comparisons between two groups and one-way ANOVA with Tukey's multiple comparison methods as a posthoc test for comparisons between more than two groups. (ns, no significant difference; *$p < 0.05$; **$p < 0.01$; ***$p < 0.001$). For segregation from F1 or F3 heterozygous, data were analysed with a Chi-square test (ns, no significant difference).

Acknowledgements

We thank Daniel Klionsky for sharing of the GFP-Lc3 transgenic zebrafish line and George Lutfalla for the mpeg1-mCherryF line. We are grateful to all members of the fish facility team for zebrafish caretaking. We would like to thank Gerda Lamers and Joost Willemse for advice on confocal imaging and image analysis. R.Z. was supported by a grant from the China Scholarship Council (CSC). M.V. was funded by a European Marie Curie fellowship (H2020-MSCA-IF-2014-655424), V.T. was a Marie Curie fellow in the Initial Training Network FishForPharma (PITN-GA-2011-289209), and MvdV was supported by the Netherlands Technology Foundation TTW (project 13259).

References

1. Ahmad S, Mokaddas E. Recent advances in the diagnosis and treatment of multidrug-resistant tuberculosis. Respir Med 2009; 103:1777-90.

2. Gupta-Wright A, Tomlinson GS, Rangaka MX, Fletcher HA. World TB Day 2018: The Challenge of Drug Resistant Tuberculosis. F1000Res 2018; 7:217.

3. Yorimitsu T, Klionsky DJ. Autophagy: molecular machinery for self-eating. Cell Death Differ 2005; 12 Suppl 2:1542-52.

4. Watson RO, Manzanillo PS, Cox JS. Extracellular M. tuberculosis DNA targets bacteria for autophagy by activating the host DNA-sensing pathway. Cell 2012; 150:803-15.

5. Biswas D, Omar S Qureshi, Wing-Yiu Lee, Joanne E Croudace, Mura. M, Lammas DA. ATP-induced autophagy is associated with rapid killing of
intracellular mycobacteria within human monocytes/macrophages. BMC Immunology 2008; 9.

6. Gutierrez MG, Master SS, Singh SB, Taylor GA, Colombo MI, Deretic V. Autophagy is a defense mechanism inhibiting BCG and Mycobacterium tuberculosis survival in infected macrophages. Cell 2004; 119:753-66.

7. van der Vaart M, Korbee CJ, Lamers GE, Tengeler AC, Hosseini R, Haks MC, et al. The DNA damage-regulated autophagy modulator DRAM1 links mycobacterial recognition via TLR-MYD88 to autophagic defense [corrected]. Cell Host Microbe 2014; 15:753-67.

8. Kohler LJ, Roy CR. Autophagic targeting and avoidance in intracellular bacterial infections. Curr Opin Microbiol 2017; 35:36-41.

9. Wallis RS, Hafner R. Advancing host-directed therapy for tuberculosis. Nat Rev Immunol 2015; 15:255-63.

10. Kolloli A, Subbian S. Host-Directed Therapeutic Strategies for Tuberculosis. Front Med (Lausanne) 2017; 4:171.

11. Crighton D, Wilkinson S, O'Prey J, Syed N, Smith P, Harrison PR, et al. DRAM, a p53-induced modulator of autophagy, is critical for apoptosis. Cell 2006; 126:121-34.

12. Guan JJ, Zhang XD, Sun W, Qi L, Wu JC, Qin ZH. DRAM1 regulates apoptosis through increasing protein levels and lysosomal localization of BAX. Cell Death Dis 2015; 6:e1624.

13. Laforge M, Limou S, Harper F, Casartelli N, Rodrigues V, Silvestre R, et al. DRAM triggers

lysosomal membrane permeabilization and cell death in CD4(+) T cells infected with HIV. PLoS Pathog 2013; 9:e1003328.

14. Lee J, Repasy T, Papavinasasundaram K, Sassetti C, Kornfeld H. Mycobacterium tuberculosis induces an atypical cell death mode to escape from infected macrophages. PLoS One 2011; 6:e18367.

15. McClean CM, Tobin DM. Macrophage form, function, and phenotype in mycobacterial infection: lessons from tuberculosis and other diseases. Pathog Dis 2016; 74.

16. Sundaramurthy V, Korf H, Singla A, Scherr N, Nguyen L, Ferrari G, et al. Survival of Mycobacterium tuberculosis and Mycobacterium bovis BCG in lysosomes in vivo. Microbes Infect 2017; 19:515-26.

17. Romagnoli A, Etna MP, Giacomini E, Pardini M, Remoli ME, Corazzari M, et al. ESX-1 dependent impairment of autophagic flux by Mycobacterium tuberculosis in human dendritic cells. Autophagy 2012; 8:1357-70.

18. Deretic V, Levine B. Autophagy, immunity, and microbial adaptations. Cell Host Microbe 2009; 5:527-49.

19. Levine B. Eating oneself and uninvited guests: autophagy-related pathways in cellular defense. Cell 2005; 120:159-62.

20. Franco LH, Nair VR, Scharn CR, Xavier RJ, Torrealba JR, Shiloh MU, et al. The Ubiquitin Ligase Smurf1 Functions in Selective Autophagy of Mycobacterium tuberculosis and Anti-tuberculous Host Defense. Cell Host Microbe 2017; 21:59-72.

21. Manzanillo PS, Ayres JS, Watson RO, Collins AC, Souza G, Rae CS, et al. The ubiquitin ligase parkin mediates resistance to intracellular pathogens. Nature 2013; 501:512-6.

22. Ponpuak M, Davis AS, Roberts EA, Delgado MA, Dinkins C, Zhao Z, et al. Delivery of cytosolic components by autophagic adaptor protein p62 endows autophagosomes with unique antimicrobial properties. Immunity 2010; 32:329-41.

23. Davis JM, Ramakrishnan L. The role of the granuloma in expansion and dissemination of early tuberculous infection. Cell 2009; 136:37-49.

24. Mahamed D, Boulle M, Ganga Y, Mc Arthur C, Skroch S, Oom L, et al. Intracellular growth of Mycobacterium tuberculosis after macrophage cell death leads to serial killing of host cells.

Elife 2017; 6.

25. Cambier CJ, O'Leary SM, O'Sullivan MP, Keane J, Ramakrishnan L. Phenolic Glycolipid Facilitates Mycobacterial Escape from Microbicidal Tissue-Resident Macrophages. Immunity 2017; 47:552-65 e4.

26. Berg RD, Levitte S, O'Sullivan MP, O'Leary SM, Cambier CJ, Cameron J, et al. Lysosomal Disorders Drive Susceptibility to Tuberculosis by Compromising Macrophage Migration. Cell 2016; 165:139-52.

27. Cambier CJ, Falkow S, Ramakrishnan L. Host evasion and exploitation schemes of Mycobacterium tuberculosis. Cell 2014; 159:1497-509.

28. Sandor M, Weinstock JV, Wynn TA. Granulomas in schistosome and mycobacterial infections: a model of local immune responses. TRENDS in Immunology 2003; 24.

29. Flynn JL, Chan J, Lin PL. Macrophages and control of granulomatous inflammation in tuberculosis. Mucosal Immunol 2011; 4:271-8.

30. Ehlers S, Schaible UE. The granuloma in tuberculosis: dynamics of a host-pathogen collusion. Front Immunol 2012; 3:411.

31. Silva Miranda M, Breiman A, Allain S, Deknuydt F, Altare F. The tuberculous granuloma: an unsuccessful host defence mechanism providing a safety shelter for the bacteria? Clin Dev Immunol 2012; 2012:139127.

32. Ndlovu H, Marakalala MJ. Granulomas and Inflammation: Host-Directed Therapies for Tuberculosis. Front Immunol 2016; 7:434.

33. Ramakrishnan L. Revisiting the role of the granuloma in tuberculosis. Nat Rev Immunol 2012; 12:352-66.

34. Cronan MR, Beerman RW, Rosenberg AF, Saelens JW, Johnson MG, Oehlers SH, et al. Macrophage Epithelial Reprogramming Underlies Mycobacterial Granuloma Formation and Promotes Infection. Immunity 2016; 45:861-76.

35. Srinivasan L, Ahlbrand S, Briken V. Interaction of Mycobacterium tuberculosis with host cell death pathways. Cold Spring Harb Perspect Med 2014; 4.

36. Elmore S. Apoptosis: A Review of Programmed Cell Death. Toxicol Pathol 2007; 35:495–516.

37. Fink SL, Cookson BT. Apoptosis, pyroptosis, and necrosis: mechanistic description of dead and dying eukaryotic cells. Infect Immun 2005; 73:1907-16.

38. Galluzzi L, Vitale I, Aaronson SA, Abrams JM, Adam D, Agostinis P, et al. Molecular mechanisms of cell death: recommendations of the Nomenclature Committee on Cell Death 2018. Cell Death Differ 2018; 25:486-541.

39. Mauro Oddo TR, Antoine Attinger, Talitha Bakker, H. Robson MacDonald and Pascal R. A. Meylan. Fas Ligand-Induced Apoptosis of Infected Human Macrophages Reduces the Viability of Intracellular Mycobacterium tuberculosis. J Immunol 1998; 160:5448-54.

40. Behar SM, Martin CJ, Booty MG, Nishimura T, Zhao X, Gan HX, et al. Apoptosis is an innate defense function of macrophages against Mycobacterium tuberculosis. Mucosal Immunol 2011; 4:279-87.

41. Aguilo N, Marinova D, Martin C, Pardo J. ESX-1-induced apoptosis during mycobacterial infection: to be or not to be, that is the question. Front Cell Infect Microbiol 2013; 3:88.

42. Roca FJ, Ramakrishnan L. TNF dually mediates resistance and susceptibility to mycobacteria via mitochondrial reactive oxygen species. Cell 2013; 153:521-34.

43. Stutz MD, Ojaimi S, Allison C, Preston S, Arandjelovic P, Hildebrand JM, et al. Necroptotic signaling is primed in Mycobacterium tuberculosis-infected macrophages, but its pathophysiological consequence in disease is restricted. Cell Death Differ 2017.

44. Lamkanfi M, Dixit VM. Manipulation of host cell death pathways during microbial infections. Cell Host Microbe 2010; 8:44-54.

45. Amaral EP, Ribeiro SC, Lanes VR, Almeida FM, de Andrade MR, Bomfim CC, et al. Pulmonary infection with hypervirulent Mycobacteria reveals a crucial role for the P2X7 receptor in aggressive forms of tuberculosis. PLoS Pathog 2014; 10:e1004188.

46. Stutz MD, Clark MP, Doerflinger M, Pellegrini M. Mycobacterium tuberculosis: Rewiring host cell signaling to promote infection. J Leukoc Biol 2018; 103:259-68.

47. He C, Clinton R. Bartholomew, Weibin Zhou, Klionsky aDJ. Assaying autophagic activity in transgenic GFP-Lc3 and GFPGabarap
zebrafish embryos. Autophagy 2009; 5:520-6.

48. Humbert M, Mueller C, Fey MF, Tschan MP. Inhibition of damage-regulated autophagy

modulator-1 (DRAM-1) impairs neutrophil differentiation of NB4 APL cells. Leuk Res 2012; 36:1552-6.

49. Zhang XD, Qi L, Wu JC, Qin ZH. DRAM1 regulates autophagy flux through lysosomes. PLoS One 2013; 8:e63245.

50. Barth S, Glick D, Macleod KF. Autophagy: assays and artifacts. J Pathol 2010; 221:117-24.

51. Klionsky DJ, Hagai Abeliovich, Patrizia Agostinis, Devendra K. Agrawal, Aliev G. Guidelines for the use and interpretation of assays for monitoring
autophagy in higher eukaryotes. Autophagy 2008; 4:151-75.

52. Mauvezin C, Neufeld TP. Bafilomycin A1 disrupts autophagic flux by inhibiting both V-ATPase-dependent acidification and Ca-P60A/SERCA-dependent autophagosome-lysosome fusion. Autophagy 2015; 11:1437-8.

53. Ying H, Turturro S, Nguyen T, Shen X, Zelkha R, Johnson EC, et al. Induction of autophagy in rats upon overexpression of wild-type and mutant optineurin gene. BMC Cell Biol 2015; 16:14.

54. Myeku N, Figueiredo-Pereira ME. Dynamics of the degradation of ubiquitinated proteins by proteasomes and autophagy: association with sequestosome 1/p62. J Biol Chem 2011; 286:22426-40.

55. Bjorkoy G, Lamark T, Brech A, Outzen H, Perander M, Overvatn A, et al. p62/SQSTM1 forms protein aggregates degraded by autophagy and has a protective effect on huntingtin-induced cell death. J Cell Biol 2005; 171:603-14.

56. Klionsky DJ, Abdelmohsen K, Abe A, Abedin MJ, Abeliovich H, Acevedo Arozena A, et al. Guidelines for the use and interpretation of assays for monitoring autophagy (3rd edition). Autophagy 2016; 12:1-222.

57. Bernut A, Herrmann JL, Kissa K, Dubremetz JF, Gaillard JL, Lutfalla G, et al. Mycobacterium abscessus cording prevents phagocytosis and promotes abscess formation. Proc Natl Acad Sci U S A 2014; 111:E943-52.

58. Miao EA, Rajan JV, Aderem A. Caspase-1-induced pyroptotic cell death. Immunol Rev 2011; 243:206-14.

59. Kyrylkova K, Kyryachenko S, Leid M, Kioussi C. Detection of apoptosis by TUNEL assay. Methods Mol Biol 2012; 887:41-7.

60. Porter AG, Janicke RU. Emerging roles of caspase-3 in apoptosis. Cell Death and Differentiation 1999; 6.

61. Stainier DYR, Raz E, Lawson ND, Ekker SC, Burdine RD, Eisen JS, et al. Guidelines for morpholino use in zebrafish. PLoS Genet 2017; 13:e1007000.

62. El-Brolosy MA, Stainier DYR. Genetic compensation: A phenomenon in search of mechanisms. PLoS Genet 2017; 13:e1006780.

63. Rossi A, Kontarakis Z, Gerri C, Nolte H, Holper S, Kruger M, et al. Genetic compensation induced by deleterious mutations but not gene knockdowns. Nature 2015; 524:230-3.

64. Quinlivan VH, Farber SA. Lipid Uptake, Metabolism, and Transport in the Larval Zebrafish. Front Endocrinol (Lausanne) 2017; 8:319.

65. Nagata M, Arakawa S, Yamaguchi H, Torii S, Endo H, Tsujioka M, et al. Dram1 regulates DNA damage-induced alternative autophagy. Cell Stress 2018; 2:55-65.

66. Mrschtik M, Ryan KM. Lysosomal proteins in cell death and autophagy. FEBS J 2015; 282:1858-70.

67. Chung J, Nakatsu F, Baskin JM, De Camilli P. Plasticity of PI4KIIIalpha interactions at the plasma membrane. EMBO Rep 2015; 16:312-20.

68. Park SM, Kim K, Lee EJ, Kim BK, Lee TJ, Seo T, et al. Reduced expression of DRAM2/TMEM77 in tumor cells interferes with cell death. Biochem Biophys Res Commun 2009; 390:1340-4.

69. Galavotti S, Bartesaghi S, Faccenda D, Shaked-Rabi M, Sanzone S, McEvoy A, et al. The autophagy-associated factors DRAM1 and p62 regulate cell migration and invasion in glioblastoma stem cells. Oncogene 2013; 32:699-712.

70. Deretic V, Levine B. Autophagy balances inflammation in innate immunity. Autophagy 2018:1-9.

71. Bonilla DL, Bhattacharya A, Sha Y, Xu Y, Xiang Q, Kan A, et al. Autophagy regulates phagocytosis by modulating the expression of scavenger receptors. Immunity 2013; 39:537-47.

72. Gan H, Lee J, Ren F, Chen M, Kornfeld H, Remold HG. Mycobacterium tuberculosis blocks crosslinking of annexin-1 and apoptotic envelope formation on infected macrophages to maintain virulence. Nat Immunol 2008; 9:1189-97.

73. Martin CJ, Booty MG, Rosebrock TR, Nunes-Alves C, Desjardins DM, Keren I, et al. Efferocytosis is an innate antibacterial mechanism. Cell Host Microbe 2012; 12:289-300.

74. Wallach D, Kang TB, Dillon CP, Green DR. Programmed necrosis in inflammation: Toward identification of the effector molecules. Science 2016; 352:aaf2154.

75. Bergsbaken T, Fink SL, Cookson BT. Pyroptosis: host cell death and inflammation. Nat Rev Microbiol 2009; 7:99-109.

76. Cookson B, Brennan M. Pro-inflammatory programmed cell death. TRENDS in Microbiology 2001; 9:113-4.

77. Danelishvili L, Everman JL, McNamara MJ, Bermudez LE. Inhibition of the Plasma-Membrane-Associated Serine Protease Cathepsin G by Mycobacterium tuberculosis Rv3364c Suppresses Caspase-1 and Pyroptosis in Macrophages. Front Microbiol 2011; 2:281.

78. Labun K, Montague TG, Gagnon JA, Thyme SB, Valen E. CHOPCHOP v2: a web tool for the next generation of CRISPR genome engineering. Nucleic Acids Res 2016; 44:W272-6.

79. van der Sar AM, Abdallah AM, Sparrius M, Reinders E, Vandenbroucke-Grauls CM, Bitter W. Mycobacterium marinum strains can be divided into two distinct types based on genetic diversity and virulence. Infect Immun 2004; 72:6306-12.

80. Takaki K, Davis JM, Winglee K, Ramakrishnan L. Evaluation of the pathogenesis and treatment of Mycobacterium marinum infection in zebrafish. Nat Protoc 2013; 8:1114-24.

81. Benard EL, van der Sar AM, Ellett F, Lieschke GJ, Spaink HP, Meijer AH. Infection of zebrafish embryos with intracellular bacterial pathogens. J Vis Exp 2012.

82. Cui C, Benard EL, Kanwal Z, Stockhammer OW, van der Vaart M, Zakrzewska A, et al. Infectious disease modeling and innate immune function in zebrafish embryos. Methods Cell Biol 2011; 105:273-308.

83. Schindelin J, Arganda-Carreras I, Frise E, Kaynig V, Longair M, Pietzsch T, et al. Fiji: an open-source platform for biological-image analysis. Nat Methods 2012; 9:676-82.

84. Tyrkalska SD, Candel S, Angosto D, Gomez-Abellan V, Martin-Sanchez F, Garcia-Moreno D, et al. Neutrophils mediate Salmonella Typhimurium clearance through the GBP4 inflammasome-dependent production of prostaglandins. Nat Commun 2016; 7:12077.

85. Masumoto J, Zhou W, Chen FF, Su F, Kuwada JY, Hidaka E, et al. Caspy, a zebrafish

caspase, activated by ASC oligomerization is required for pharyngeal arch development. J Biol Chem 2003; 278:4268-76.

86. Mah LY. *Characterisation of DRAM-1 in vitro and in vivo*. University of Glasgow, 2012:263.

87. Samrah M. Autophagy and Lc3-associated phagocytosis in host defense against *Salmonella.* Leiden University, 2017:233.

Supplementary data

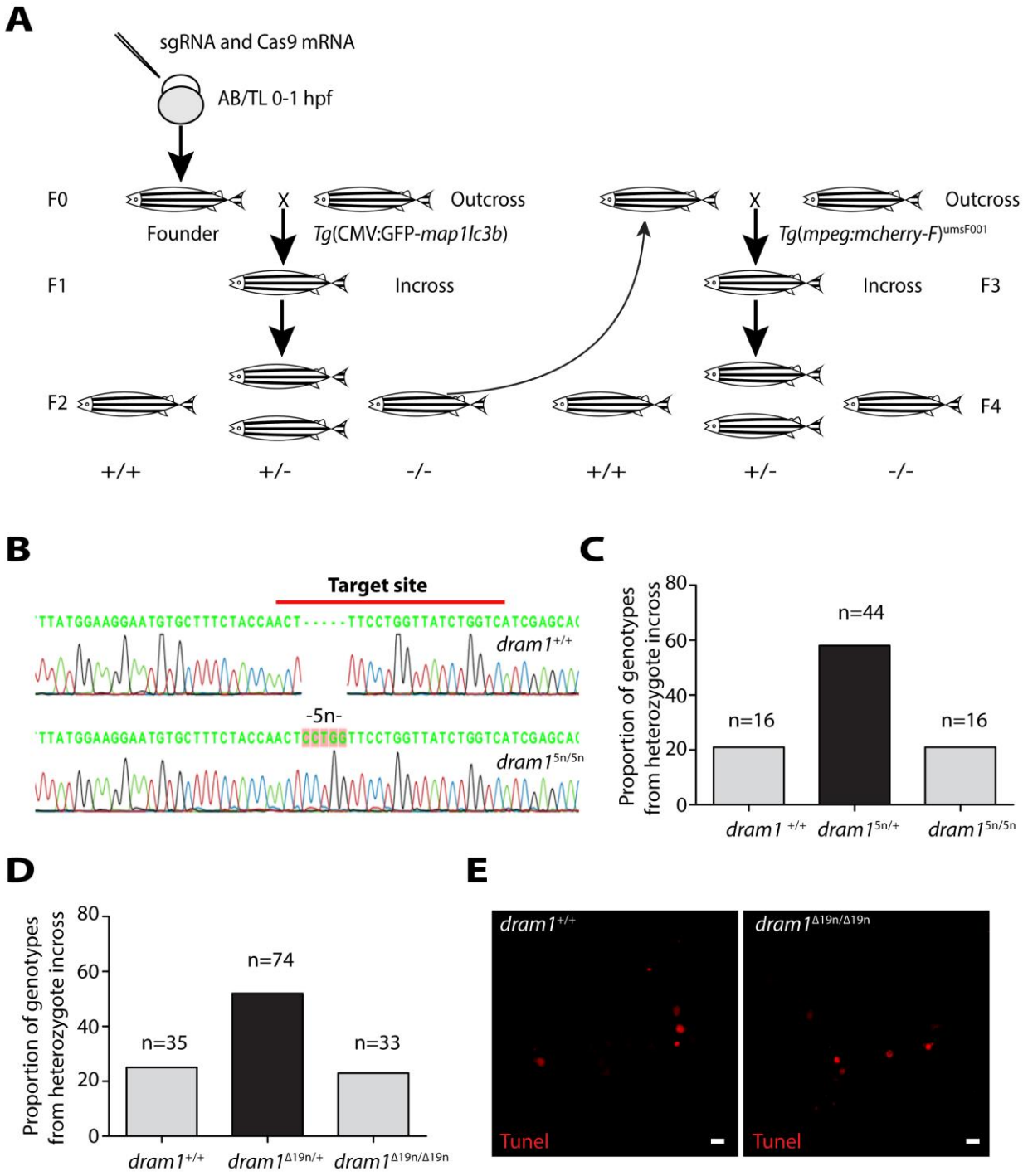

Supplementary figure 1: Dram1 deficiency does not result in apparent defects in development or survival

A. Schematic diagram showing the workflow used for the generation of *dram1* mutant lines. Target-specific sgRNA and Cas9 mRNA were co-injected into one cell stage embryos (AB/TL, wild type line). Founders were outcrossed to

Tg(*CMV:EGFP-map1lc3b*) or wild type fish to obtain F1. After 3-4 months, the F1 was incrossed to obtain homozygous mutant and wild type F2 siblings. *dram1*$^{\Delta 19n/\Delta 19n}$ were outcrossed with the macrophage marker *Tg*(*mpeg1:mCherry-F*)^{umsF001} and after 3-4 months subsequently incrossed to obtain *dram1*$^{+/+}$, *dram1*$^{\Delta 19/+}$, and *dram1*$^{\Delta 19n/\Delta 19n}$ carrying *Tg*(*mpeg1:mCherry-F*)^{umsF001}.

B. Sanger sequencing of *dram1*$^{+/+}$ and *dram1*$^{5n/5n}$ from F2 fish. The red line indicates the CRISPR/Cas9 target site. The genomic DNA was isolated from fin tissue of adults (>3 months old). The *dram1*$^{5n/5n}$ sequence revealed insertion of 5 nucleotides within the target site.

C. Segregation from *dram1*$^{5N/+}$ F1 heterozygous incross. Genotypes of adult fish (>3 months old) combined from at least three independent breedings were confirmed by PCR and Sanger sequencing. Data were analyzed by Chi square test. ns, non-significant,*p<0.05,**p<0.01,***p<0.001

D. Segregation from *dram1*$^{\Delta 19n+}$*/mpeg1:mCherry-F* F1 heterozygous incross. Genotypes of adult fish (>3 months old) combined from at least three independent breedings were confirmed by PCR and sequencing. Data were analyzed by Chi square test. ns, non-significant,*p<0.05,**p<0.01,***p<0.001

E. Representative confocal micrographs tail region of Tunel staining performed on *dram1*$^{\Delta 19n/\Delta 19n}$ and *dram1*$^{+/+}$ larvae at 3dpf. Scale bar, 10 μm.

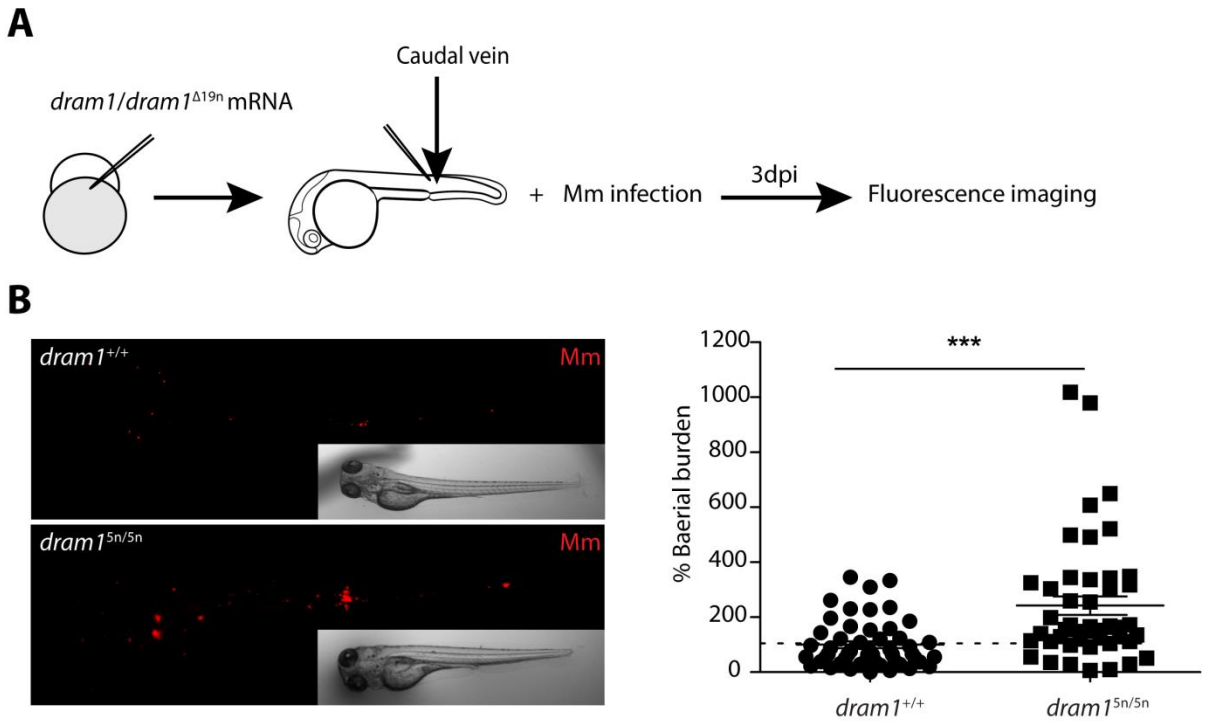

Supplementary figure 2: Dram1 is required for the host to restrict Mm infection

A. Workflow representing the experimental design for Mm infection experiments. Bacterial pixel counts were examined at 3 dpi.

B. Representative stereo images of infected *dram1*$^{+/+}$ and *dram1*$^{5n/5n}$ larvae at 3 dpi**.**

C. Bacterial burdens were determined at 3 dpi. The data is accumulated from two independent experiments. Each dot represents an individual larva. ns, non-significant, *p<0.05, **p<0.01, ***p<0.001

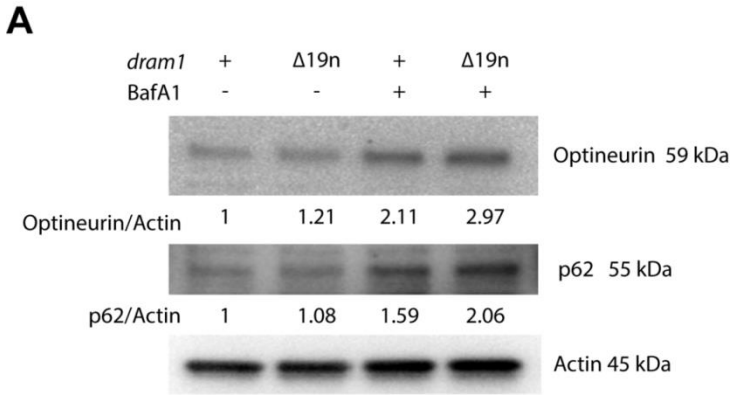

Supplementary figure 3: Increased accumulation of p62 and Optineurin suggests that autophagic flux is decreased without Dram1

A. p62 and Optineurin protein levels were detected in *dram1*$^{\Delta 19n/\Delta 19n}$ and *dram1*$^{+/+}$ larvae in absence or presence of BafA1. Protein samples were extracted from 4dpf *dram1*$^{\Delta 19n/\Delta 19n}$ and *dram1*$^{+/+}$ larvae (>10 larvae/sample). The blots were probed with antibodies against p62, Optineurin, and Actin as a loading control. p62/Actin and Optineurin/Actin. The ratios are indicated below the blot.

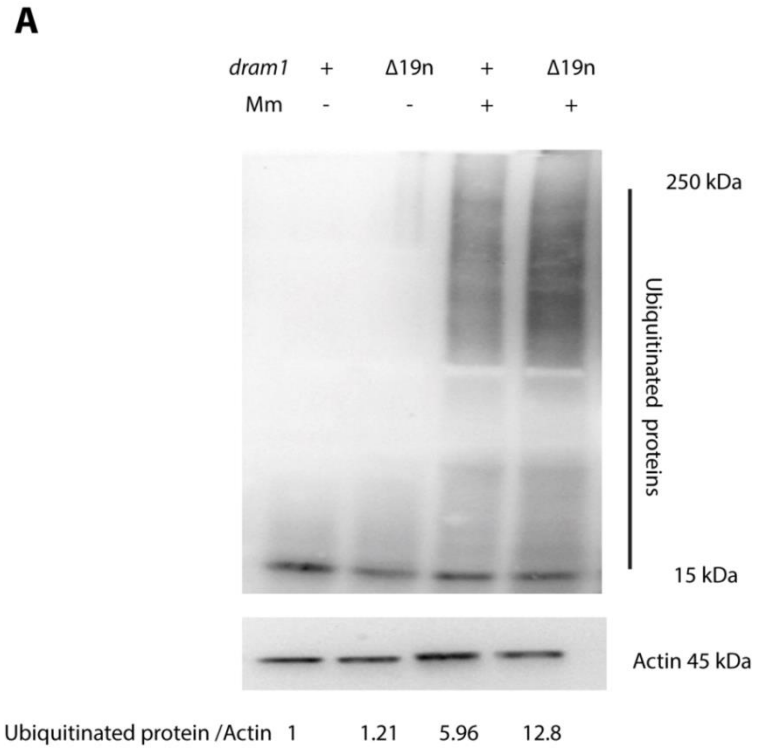

Supplementary figure 4: Accumulation of ubiquitinated proteins in *dram1*$^{+/+}$ and *dram1*$^{\Delta 19n/\Delta 19n}$ during Mm infection

A. Detection of ubiquitination in infected and uninfected larvae. Protein samples were extracted from 4dpf/3dpi *dram1*$^{\Delta 19n/\Delta 19n}$ and *dram1*$^{+/+}$ larvae (>10 larvae/sample). The blots were probed with antibodies against poly and mono ubiquitin; Actin was used as a loading control. Ubiquitinated protein/Actin ratios are indicated below the blot.

Supplementary table1: The zebrafish lines used in this study

Name	Description	Reference
AB/TL	Wild type strain	7
Tg(*CMV:EGFP-map1lc3b*)	GFP reporter transgenic zebrafish for Lc3	47
Tg(*mpeg1:mCherryF*)^{umsF001}	Macrophage marker with membrane-localizing *mCherry-F*	57
dram1$^{+/+}$/GFP-Lc3	Siblings of *dram1* carrying a transgenic GFP-Lc3 reporter	In this study
dram1$^{\Delta 19n/\Delta 19n}$/GFP-Lc3	*dram1* mutant line (Δ19n indel) carrying a transgenic GFP-Lc3 reporter	In this study
dram1$^{5n/5n}$/GFP-Lc3	*dram1* mutant line (5n indel) carrying a transgenic GFP-Lc3 reporter	In this study
dram1$^{+/+}$*/mpeg1:mCherry-F*	Siblings of *dram1*$^{\Delta 19n/\Delta 19n}$ carrying a transgenic *mpeg1:mCherry-F* reporter	In this study
dram1$^{\Delta 19n/\Delta 19n}$*/mpeg1:mCherry-F*	Siblings of *dram1*$^{+/+}$ carrying a transgenic *mpeg1:mCherry-F* reporter	In this study

Supplementary table2: Primers for complementation and amplification of sgRNA

Name	Forward (5'-3')	Reverse (5'-3')
dram1 sgRNA template	GCG**TAATACGACTCACTATAG**GACCAGATAA CCAGGAAAGTTGGTTTTAGAGCTAGAAATAG CAAGTTAAAATAAGGCTAGTC	GATCCGCACCGACTCGGTGCCACTTTTTCAA GTTGATAACGGACTAGCCTTATTTTAACTTG CTATTTCTAGCTCTAAAAC
sg RNA amplify	GCGTAATACGACTCACTATAG	GATCCGCACCGACTCGGT

T7 promoter: **TAATACGACTCACTATAG**

The underlined sequence indicates the target sites for gRNAs designed to mutate *dram1*

Chapter 3

Deficiency of the autophagy modulator Dram1 affects the transcriptional regulation of metabolic and immune response pathways during mycobacterial infection

Rui Zhang, Monica Varela, Gabriel Forn-Cuní, Michiel van der Vaart and Annemarie H. Meijer

(Manuscript in preparation)

Abstract

The widespread and gradually increasing number of multidrug-resistant (MDR) or extensively drug-resistant (XDR) Tuberculosis (TB) cases remains a major threat to global health. Currently, it is urgent to develop an effective treatment to combat TB. Using the zebrafish model for TB, we have previously demonstrated that the lysosomal protein known as DNA Damage Regulated Autophagy Modulator 1 (Dram1) protects against mycobacterial infections via autophagic defense mechanisms. Dram1 therefore presents a promosing target for host-directed therapy against TB. To further explore the function of Dram1 in health and during the early stages of TB pathogenesis, we performed whole organism transcriptome analysis on uninfected and *Mycobacterium marinum* (Mm)-infected zebrafish larvae carrying a *dram1* loss-of-function mutation compared to wild type control groups. Under unchallenged conditions, we found that deficiency of Dram1 affects the network of gene regulation to a small degree, with detectable differences in proteinase and metabolic pathways. The transcriptome response to mycobacterial infection was vastly different between *dram1* mutants and wild type zebrafish, which indicates that the immune response to mycobacterial infection is altered in the absence of Dram1. Furthermore, we found that the metabolic response to mycobacterial infection that occurs in wild type zebrafish was lacking in Dram1-deficient zebrafish, again pointing towards a function in metabolic pathways for Dram1. Finally, we highlight that loss-of-function mutation of *dram1* affects cell death and Toll-like receptor (TLR) signaling pathways during mycobacterial infection. Our analyses suggest that Dram1 is involved in cell death processes activated during mycobacterial infection, while recognition of mycobacteria by TLRs appears altered in the absence of Dram1. Collectively, our RNAseq study reveals a role for Dram1 in metabolic processes under basal and pathogenic stress conditions, and emphasizes the importance of autophagic mechanisms in the host immune response against mycobacterial pathogens.

Introduction

Mycobacterium tuberculosis (Mtb) is the causative organism of Tuberculosis (TB) and remains a big threat to public health, resulting in nearly 2 million deaths every year [1]. Around 30% of the

world population is latently or actively infected with Mtb and there is an increase in the occurrence of multidrug-resistant (MDR) and extensively drug-resistant (XDR) strains [1]. The development of novel effective anti-TB therapies is therefore a key priority [2]. However, the pathogenesis of TB is not completely elucidated yet, which hinders the development of new therapies. Recently, studies performed using the zebrafish TB model have generated new insights into the host-pathogen interactions underlying TB disease. An excellent example is that macrophages are sufficient to initiate the formation of tuberculous granulomas under circumstances in which only the innate immune system is functional [3]. Intriguingly, it was found that mycobacterial virulence factors also contribute to the formation of granulomas, making these hallmark structures of TB a double-edged sword. Moreover, macrophages also perform dual roles in TB pathogenesis by both restricting the initial infection via phagocytosis of mycobacteria and promoting dissemination of infection via subsequent initiation of granuloma formation [4, 5], which eventually leads to the infection of newly attracted macrophages [3, 6].

Infections with *Mycobacterium marinum* (Mm) in zebrafish embryos and larvae present a well-described *in vivo* TB model that recapitulates hallmark structural features of human TB [7, 8]. Moreover, the activation of gene transcription in response to *Mm infection in the zebrafish model* is similar to the transcriptional response elicited by *Mtb* infection in humans. It was shown that Mm-infected larvae express many genes homologous to human immune responsive factors to Mtb infection [9, 10]. Using the zebrafish TB model, our group has previously demonstrated that the transcriptional response of the host during the early stages of TB granuloma formation follows three main stages [11]. The early stage corresponds to the first few hours after phagocytosis of Mm by macrophages and is characterized by activation of transcription factors and genes of the complement system, followed by a minor induction of pro-inflammatory cytokines. The mid phase, ranging from 6 hours to 1-day post infection (dpi), is characterized by a minimal transcriptional response, which could be due to suppression of the host immune response by mycobacterial virulence factors. The late phase begins when granulomas start to develop around 2 dpi and are characterized by progressively increasing induction of transcription factors, complement genes, pro-inflammatory cytokines, matrix metalloproteases, and other defense and inflammation-related transcriptional signatures.

Selective autophagy plays a vital role in restricting mycobacterial infection and our group has previously demonstrated that DNA Damage Regulated Autophagy Modulator 1 (Dram1) functions in host defense against TB [12]. Human DRAM1 was first identified as a p53-induced regulator of autophagy and cell death [13], but in response to mycobacterial infection, its transcription is regulated by NFκB [12]. DRAM1 has been demonstrated to be involved in diverse cellular processes, including autophagy, apoptosis, immunity, and cellular differentiation [14]. We have generated Dram1-deficient mutant zebrafish (*dram1*$^{\Delta 19n/\Delta 19n}$) and demonstrated that the absence of functional Dram1 increases susceptibility to Mm infection via a decrease in the maturation of Mm-containing vesicles and a subsequent increase in cell death of infected macrophages (Chapter 2 of this thesis).

To gain a deeper understanding of the transcriptional changes underlying these findings, we have now used RNA deep sequencing to analyse the transcriptomes of infected and uninfected *dram1*$^{\Delta 19n/\Delta 19n}$ larvae and their wild type siblings. With this approach, we set out to uncover which cellular functions of Dram1 are involved in defense against mycobacterial infection based on differences in the transcriptional regulation of diverse host processes. We found evidence that Dram1 deficiency has major effects on the expression profiles of proteinase and metabolic pathways. Furthermore, we were able to detect differences in gene expression of immune response and cell death pathways that help explain the increased susceptibility of *dram1*$^{\Delta 19n/\Delta 19n}$ larvae to mycobacterial infection.

Results

Principle component analysis of RNAseq data indicates transcriptional effects of *dram1* mutation in the absence and presence of TB infection

Previous studies in our group have shown that Dram1 deficiency leads to increased mycobacterial infection burdens [12] (Chapter 2 of this thesis). Thus, to further explore the phenotype of *dram1*$^{\Delta 19n/\Delta 19n}$ mutants, we performed RNA deep sequencing to identify changes in the transcriptome that could help explain their increased susceptibility to mycobacterial infection. We chose to analyze the differences in gene expression between infected and

uninfected *dram1*$^{+/+}$ and *dram1*$^{\Delta 19n/\Delta 19n}$ larvae at 4 days post infection (dpi), corresponding to 5 days post fertilization (dpf). Early stage granuloma-like structures have been formed at this time point after infection, and a previous time course infection study has shown this correlates with transcriptional activation of diverse defense-related processes [11]. Therefore, we designed infection experiments in which we infected *dram1*$^{+/+}$ with 300 CFU (colony forming units) of Mm via injection into the caudal vein at 28 hours post fertilization (hpf), while we infected *dram1*$^{\Delta 19n/\Delta 19n}$ with two different dosages: 150 or 300 CFU (Fig1 A). To control for any transcriptional response to the injection itself, the uninfected *dram1*$^{+/+}$ and *dram1*$^{\Delta 19n/\Delta 19n}$ groups were injected with PBS. Since dram1 mutation is known to increase the susceptibility of zebrafish larvae to Mm infection (Chapter 2 of this thesis), mutant larvae infected with the dose of 300 CFU were expected to display a higher infection burden compared to their wild type siblings infected with the same dose, whereas infection with 150 CFU in *dram1*$^{\Delta 19n/\Delta 19n}$ was expected to develop the same level of infection compared to infection with 300 CFU in *dram1*$^{+/+}$. With this setup, we would be able to identify transcriptional differences that are specifically caused by the absence of functional Dram1, rather than by the higher infection burden. Analyzing the level of infection at 4 dpi confirmed our expectation that 150 CFU infected *dram1*$^{\Delta 19n/\Delta 19n}$ larvae display the same level of infection as *dram1*$^{+/+}$ infected with 300 CFU, while *dram1*$^{\Delta 19n/\Delta 19n}$ larvae infected with 300 CFU displayed highly increased infection burdens (Fig1 B). Thus, we isolated total RNA from samples of pooled larvae from three independent biological replicates to perform RNA deep sequencing analysis. We used Illumina sequencing technology and mapped the obtained reads to zebrafish genome assembly GRCz10.80 (Genome Reference Consortium Zebrafish Build 10.80). Quality control analysis showed that the samples from one independent group (*dram1*$^{\Delta 19n/\Delta 19n}$ family 2) did not align with the two other replicates, according to the principal component analysis (PCA). Therefore, we discarded all samples belonging to this group and performed the further analysis with samples from two independent experiments for the *dram1* mutant fish (Fig1 C). For the remaining samples, the PCA showed clustering of the different samples belonging to the same experimental group, and clear differences in the regulation of gene expression between the infected and non-infected groups, as well as between the *dram1* mutants and wild type controls.

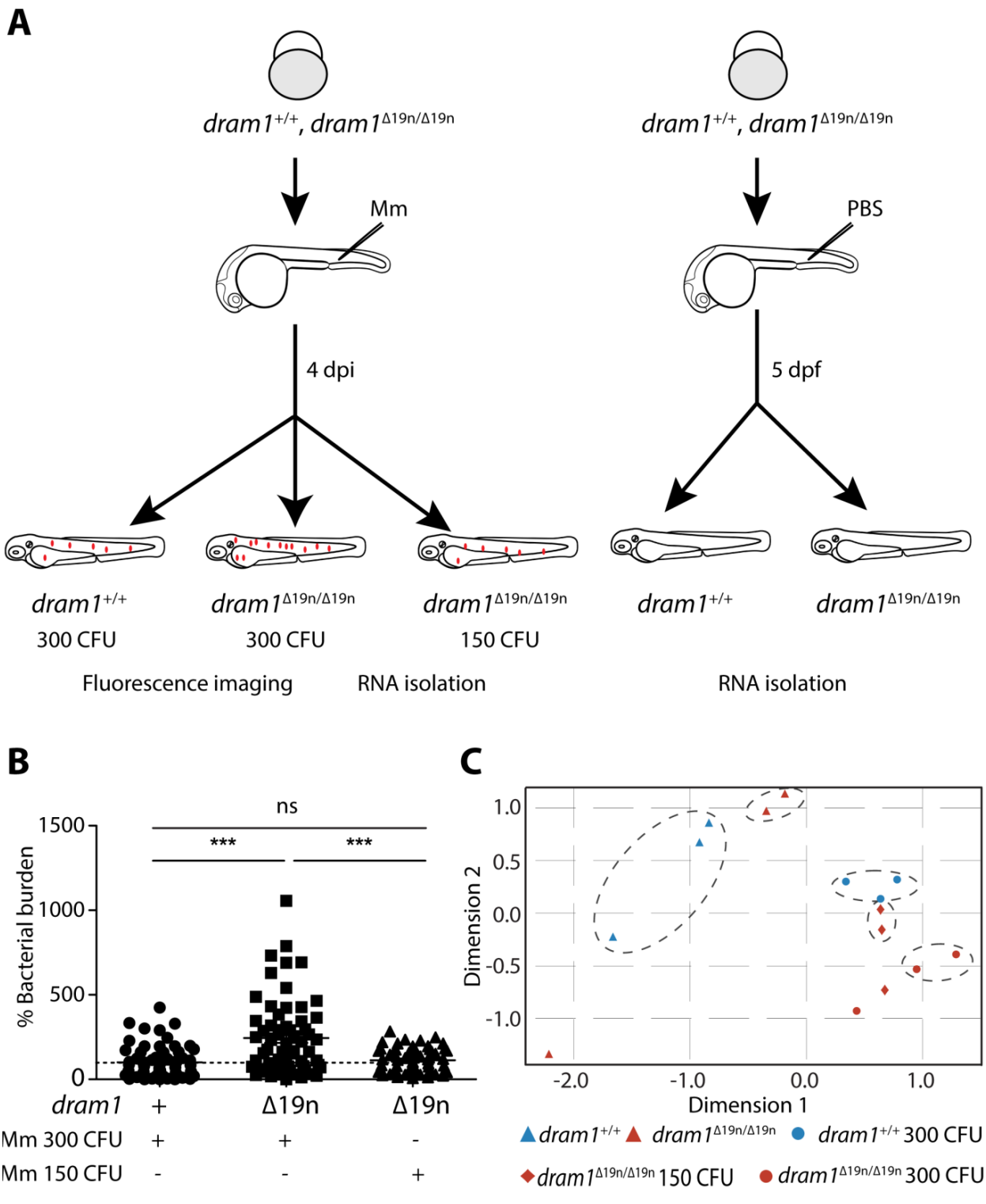
A
dram1+/+, dram1Δ19n/Δ19n
Mm
4 dpi
dram1+/+
300 CFU
dram1Δ19n/Δ19n
300 CFU
dram1Δ19n/Δ19n
150 CFU
Fluorescence imaging
RNA isolation
dram1+/+, dram1Δ19n/Δ19n
PBS
5 dpf
dram1+/+
dram1Δ19n/Δ19n
RNA isolation
B
ns
***
***
% Bacterial burden
1500
1000
500
0
dram1
+
Δ19n
Δ19n
Mm 300 CFU
+
+
-
Mm 150 CFU
-
-
+
C
Dimension 2
1.0
0.5
0.0
-0.5
-1.0
-2.0
-1.0
0.0
1.0
Dimension 1
dram1+/+
dram1Δ19n/Δ19n
dram1+/+ 300 CFU
dram1Δ19n/Δ19n 150 CFU
dram1Δ19n/Δ19n 300 CFU

Figure 1: The experimental design for investigating the effect of Dram1 deficiency on gene expression

A. Experimental design to obtain samples for RNA deep sequencing. *Mycobacterium marinum* strain M (Mm) fluorescently labeled with mCherry was microinjected into the blood island of embryos at 28 hpf at an injection dosage of 300 CFU of 150 CFU. Control groups were injected with PBS. B. Bacterial burdens at 4 dpi. The data is accumulated from three independent experiments. Each dot represents an individual larva. ns, non-significant, *p<0.05,**p<0.01,***p<0.001. C. Principal component analysis of the gene expression data obtained by RNA sequencing. The RNA sequencing samples clustered well, as pictured by the dashed ellipses grouping the conditions. The data sets of one family of *dram1*$^{\Delta 19n/\Delta 19n}$ (Mm infected and uninfected) were outliers (data points outside the dashed ellipses) and were discarded from the analysis

Mycobacterial infection increases the transcriptional differences between wild type and Dram1-deficient zebrafish

We performed DESeq2 analysis to detect differential gene expression between the different conditions. When comparing the transcriptome of uninfected *dram1*$^{\Delta 19n/\Delta 19n}$ larvae to that of uninfected *dram1*$^{+/+}$ larvae, we found that 236 genes were differentially regulated between the two conditions. In total, 77 genes were expressed at a significantly higher level in *dram1*$^{\Delta 19n/\Delta 19n}$, while 159 genes were downregulated (Fig2 A). This indicates that, while the absence of Dram1 influences the network of gene regulation, it only does so to a relatively small extent under uninfected conditions. When challenged by a mycobacterial infection, wild type larvae differentially expressed a total of 1971 genes compared to uninfected wild type larvae, which is comparable with previous findings for this stage of pathogenesis in the zebrafish TB model [11]. Of this set of genes with altered expression during infection, 1109 genes were upregulated, and 862 genes were downregulated. In *dram1*$^{\Delta 19n/\Delta 19n}$ larvae infected with the same dose (300 CFU), we observed a total of 1269 differentially regulated genes compared to uninfected *dram1*$^{\Delta 19n/\Delta 19n}$, 861 of which were upregulated and 408 downregulated. For *dram1*$^{\Delta 19n/\Delta 19n}$ larvae infected with 150 CFU, 1143 genes were differentially regulated compared to uninfected *dram1*$^{\Delta 19n/\Delta 19n}$, 876 of which were upregulated and 267 downregulated.

Both wild type larvae and *dram1* mutants displayed a marked increase in gene regulation when comparing the transcriptome of infected larvae with that of their uninfected siblings. To analyze whether the same set of genes is differentially regulated in response to infection in the absence

of functional Dram1, we plotted four comparisons in a Venn-diagram: (1) uninfected *dram1* mutants vs uninfected wild types, (2 & 3) low and high dose infected *dram1* mutants vs uninfected *dram1* mutants, and (4) infected wild types vs uninfected wild types (Fig2 B). Strikingly, we found that roughly 60% of the infection-responsive genes in wild types (1170 out of a total of 1971) were not differentially regulated in response to infection in *dram1*$^{\Delta 19n/\Delta 19n}$. Furthermore, while a low dose infection of *dram1*$^{\Delta 19n/\Delta 19n}$ (150 CFU) results in a similar bacterial burden as a high dose-infection in wild type larvae (300 CFU), the transcriptome response of highly infected *dram1*$^{\Delta 19n/\Delta 19n}$ larvae (300 CFU) showed more overlap with the wild type response to infection. This initial analysis of global changes in gene expression suggests that *dram1*$^{\Delta 19n/\Delta 19n}$ larvae display limited alterations in gene expression compared to *dram1*$^{+/+}$ under basal conditions, but these differences are markedly increased when facing a mycobacterial infection.

Figure 2: Dram1 deficiency affects the host transcriptome response to Mm infection

A. The general profile of differential gene expression between the different conditions. Genes upregulated are coloured in yellow, and downregulated in blue. The fold change level of the genes in each group is indicated by colour intensity.

B. Venn diagram of the differentially expressed genes common and different between the *dram1*$^{\Delta 19n/\Delta 19n}$ and *dram1*$^{+/+}$,*dram1*$^{\Delta 19n/\Delta 19n}$150 CFU and *dram1*$^{\Delta 19n/\Delta 19n}$ PBS, *dram1*$^{\Delta 19n/\Delta 19n}$ 300 CFU and *dram1*$^{\Delta 19n/\Delta 19n}$, *dram1*$^{+/+}$ 300 CFU and *dram1*$^{+/+}$ PBS comparisons.

A

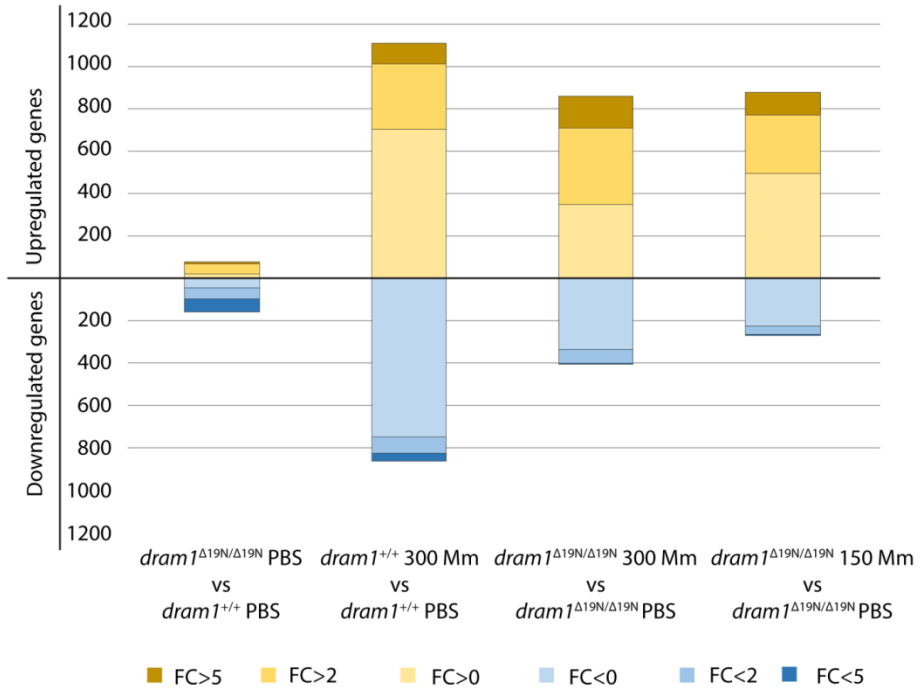
Upregulated genes
Downregulated genes
1200
1000
800
600
400
200
dram1Δ19N/Δ19N PBS vs dram1+/+ PBS
dram1+/+ 300 Mm vs dram1+/+ PBS
dram1Δ19N/Δ19N 300 Mm vs dram1Δ19N/Δ19N PBS
dram1Δ19N/Δ19N 150 Mm vs dram1Δ19N/Δ19N PBS
FC>5
FC>2
FC>0
FC<0
FC<2
FC<5

B

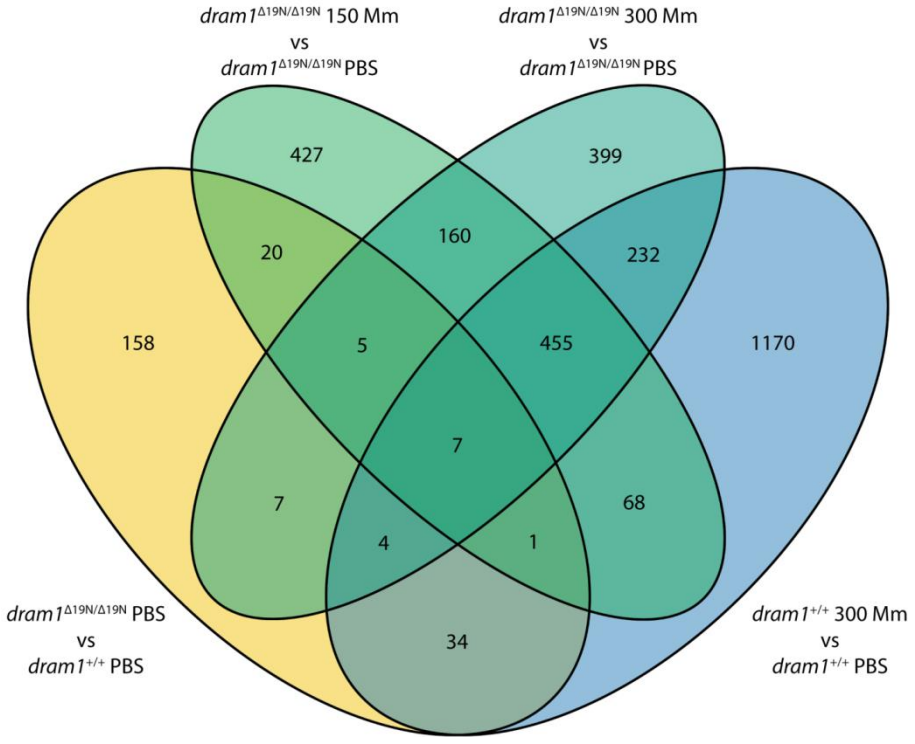
dram1Δ19N/Δ19N 150 Mm vs dram1Δ19N/Δ19N PBS
dram1Δ19N/Δ19N 300 Mm vs dram1Δ19N/Δ19N PBS
dram1Δ19N/Δ19N PBS vs dram1+/+ PBS
dram1+/+ 300 Mm vs dram1+/+ PBS
427
399
158
1170
20
160
232
5
455
7
7
68
4
1
34

dram1 mutants display transcriptional changes in metabolic and proteolytic pathways under non-infected conditions

When comparing the transcriptome of uninfected *dram1* mutants to that of uninfected wild types, we only found a total of 236 significantly differentially expressed genes (Fig2 A). This small difference in gene expression under basal conditions fits with the described function of DRAM1/Dram1 in response to cellular stress factors [13, 15]. Nonetheless, analysing the top 25 annotated genes that were differentially expressed under basal conditions provided interesting links to processes that were affected by *dram1* deficiency, including *isg15* and *alox5b* which are involved in ubiquitination and the arachidonic acid pathway, respectively (TableS1). For an unbiased assessment of potentially altered biological processes in *dram1*$^{\Delta 19n/\Delta 19n}$ larvae under basal conditions, we analysed gene ontology (GO) enrichment on the subsets of differentially up- or down-regulated genes. Only two GO terms were enriched in the absence of functional Dram1, both of which are related to proteinase activity (TableS1). Conversely, several GO terms were underrepresented in the differentially expressed genes in *dram1*$^{\Delta 19n/\Delta 19n}$ compared to *dram1*$^{+/+}$, most of which are related to metabolic processes (TableS1).

In a more detailed analysis, we found no significant differences between *dram1* mutants and wild type larvae when analyzing whether specific KEGG (Kyoto Encyclopedia of Genes and Genomes) pathways for biological processes were enriched amongst the differentially expressed genes (data not shown). We therefore turned to Gene Set Enrichment Analysis (GSEA) to compare our dataset against curated gene sets related to specific pathways or disease states in the Molecular Signature Database (MSigDB). We identified several published gene sets that were enriched in uninfected *dram1*$^{\Delta 19n/\Delta 19n}$ or *dram1*$^{+/+}$ larvae. The gene sets that were enriched in *dram1*$^{\Delta 19n/\Delta 19n}$ larvae displayed clear links to known functions of DRAM1, or processes that it has been implicated in, such as UV damage; cancer; apoptosis; and the mTOR and MAPK pathways which are involved in autophagy regulation (Fig3 A). This is also the case for the inhibited (or underrepresented) gene sets in *dram1*$^{\Delta 19n/\Delta 19n}$ larvae, which include clear links to the phagosome pathway; ubiquitination; apoptosis; immunity; autophagy (rapamycin-responsive genes); and p53 signaling (Fig3 B). To identify a potential common set of genes in the

previous pathways, we performed a leading edge analysis of the GSEA results. With this analysis, we could identify four main clusters of genes whose expression was inhibited in the *dram1*$^{\Delta 19n/\Delta 19n}$ larvae in comparison to the *dram1*$^{+/+}$ larvae that were shared by many of the negatively correlated pathways: proteasome, ribosome, mitochondrial, and polymerase genes. Taken together, our GSEA analysis shows that *dram1*$^{\Delta 19n/\Delta 19n}$ larvae display altered transcriptional profiles in pathways related to metabolic and catabolic processes, which could be a compensatory response to defects in autophagosomal and lysosomal processes due to the absence of Dram1.

Figure 3: Transcriptomic gene expression changes in *dram1* mutants under non-infected conditions (Figure on next page). All the genes in the RNA sequencing were ranked according to their statistical significance and fold change level, from left (most significant upregulated, in yellow) to the right (most significant, downregulated in blue), and the gene sets of the curated C2 MSigDB were tested for enrichment in the ranked gene list with GSEA. The number of genes belonging to each gene set found in our RNA sequencing (size column), the enrichment score values (NES), and the significance of the enrichment before (pval) and after Benjamini-Hochberg multitest correction (FDR) are shown. The gene ranks depict the position of each gene from the gene set in the ranked list (one gene = one column).

A. Gene sets enriched (high expression) in the *dram1*$^{\Delta 19n/\Delta 19n}$ mutants in comparison to the *dram1*$^{+/+}$

B. Gene sets enriched (high expression) in the *dram1*$^{+/+}$ fish in comparison to the *dram1*$^{\Delta 19n/\Delta 19n}$ mutants.

A **Gene sets enriched in the *dram1*$^{\Delta 19N/\Delta 19N}$ vs the *dram1*$^{+/+}$ transcriptome**

Gene Set	Size	Gene ranks	NES	pval	FDR
DACOSTA UV Response via ERCC3 COMMON DN	413		5,080	0	0
REACTOME Voltage Gated Potassium Channels	32		4,082	0	0
GABRIELY miR21 Targets	226		3,699	0	0
PID AVB3 Integrin Pathway	69		3,076	0	0
GINESTIER Breast Cancer ZNF217 Amplified DN	238		3,037	0	0
REACTOME Axon Guidance	202		2,947	0	0
BIOCARTA MAPK Pathway	79		2,675	0	0,004
MONNIER Postradiation Tumor Escape UP	301		2,634	0	0,005
CARD miR302a Targets	70		2,618	0	0,005
DEBIASI Apoptosis By Reovirus Infection DN	236		2,520	0,002	0,011
HAMAI Apoptosis Via Trail UP	457		2,493	0	0,012
PID RHOA Pathway	42		2,431	0	0,018
FOSTER Tolerant Macrophage DN	297		2,402	0	0,020
KEGG Inositol Phosphate Metabolism	45		2,306	0	0,034
PID mTor 4Pathway	63		2,262	0	0,043

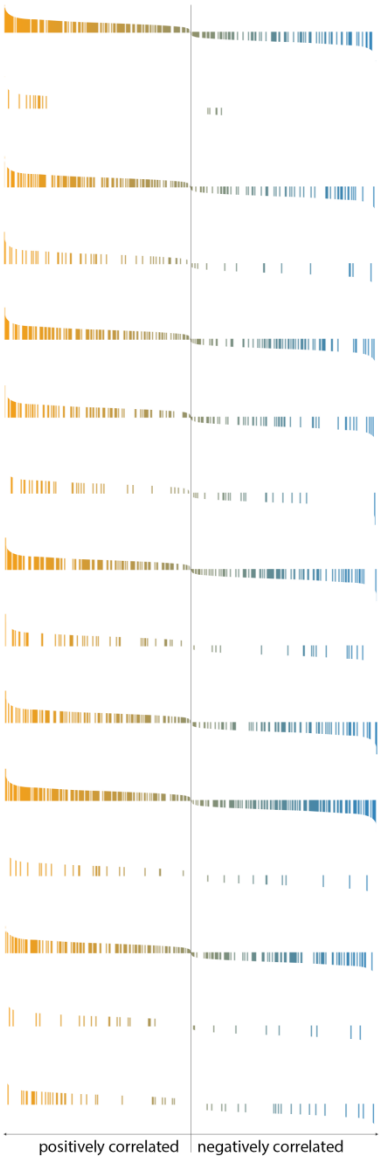

B

Gene sets enriched in the *dram1*$^{+/+}$ vs the *dram1*$^{\Delta 19N/\Delta 19N}$ transcriptome

Gene Set	Size	Gene ranks	NES	pval	FDR
REACTOME SRP Dependent Cotranslational Protein Targeting To Membrane	96		-5,688	0	0
REACTOME ER Phagosome Pathway	47		-4,898	0	0
REACTOME Autodegradation Of The E3 Ubiquitin Ligase COP1	42		-4,889	0	0
KEGG Proteasome	37		-4,817	0	0
REACTOME Regulation Of Apoptosis	49		-4,752	0	0
REACTOME Antigen Processing Cross Presentation	58		-4,670	0	0
REACTOME Influenza Life Cycle	117		-4,474	0	0
REACTOME Activation Of NF Kappab In B Cells	56		-4,143	0	0
MOOTHA Mitochondria	366		-4,108	0	0
REACTOME Cell Cycle Checkpoints	99		-3,562	0	0
BILANGES Serum And Rapamycin Sensitive Genes	61		-3,551	0	0
REACTOME HIV Infection	163		-3,008	0	0
RHEIN All Glucocorticoid Therapy DN	299		-2,855	0	2E-04
LEE Liver Cancer Survival DN	139		-2,733	0	6E-04
KEGG P53 Signaling Pathway	55		-2,728	0	6E-04

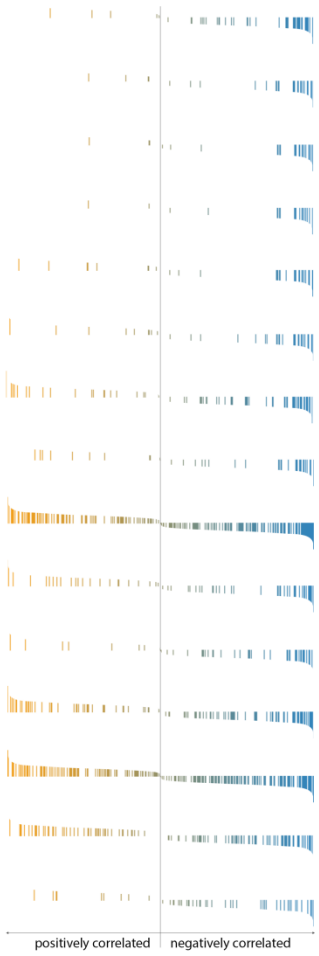

Dram1 deficiency has a major impact on the metabolic pathways induced by Mm challenge

Next, we analyzed the KEGG pathways to compare the immune response to Mm infection without functional *dram1* (Fig4). As a general remark, we found that *dram1*$^{\Delta 19n/\Delta 19n}$ larvae infected with the high infection displayed more similarity to the dram1$^{+/+}$ response than the low infection dose, with 15 pathways commonly altered by the infection in the high dose compared to only 8 in the low dose. The pathways commonly affected in both the *dram1*$^{+/+}$ and *dram1*$^{\Delta 19n/\Delta 19n}$ larvae were those involved in defense against mycobacterial infections, such as the Nod-like receptor signaling pathway, phagosome-related processes, cytokine signaling, and apoptosis. As in previously published results [11], we found that the Mm infection strongly affected metabolic pathways, especially the ones related to energy and carbon metabolism (Glycolysis, TCA cycle, etc.). Strikingly, the alteration of these metabolic pathways was absent in the *dram1*$^{\Delta 19n/\Delta 19n}$ infected larvae. However, we found that the infection of *dram1*$^{\Delta 19n/\Delta 19n}$ with 300 CFU influenced other metabolic processes, including the cholesterol, alanine, aspartate, and glutamate pathways. Thus, the data shows that mutation of Dram1 hinders the activation of several metabolic pathways known to be involved in defense against Mm, while modulating other pathways involved in cholesterol and amino acid biosynthesis.

A

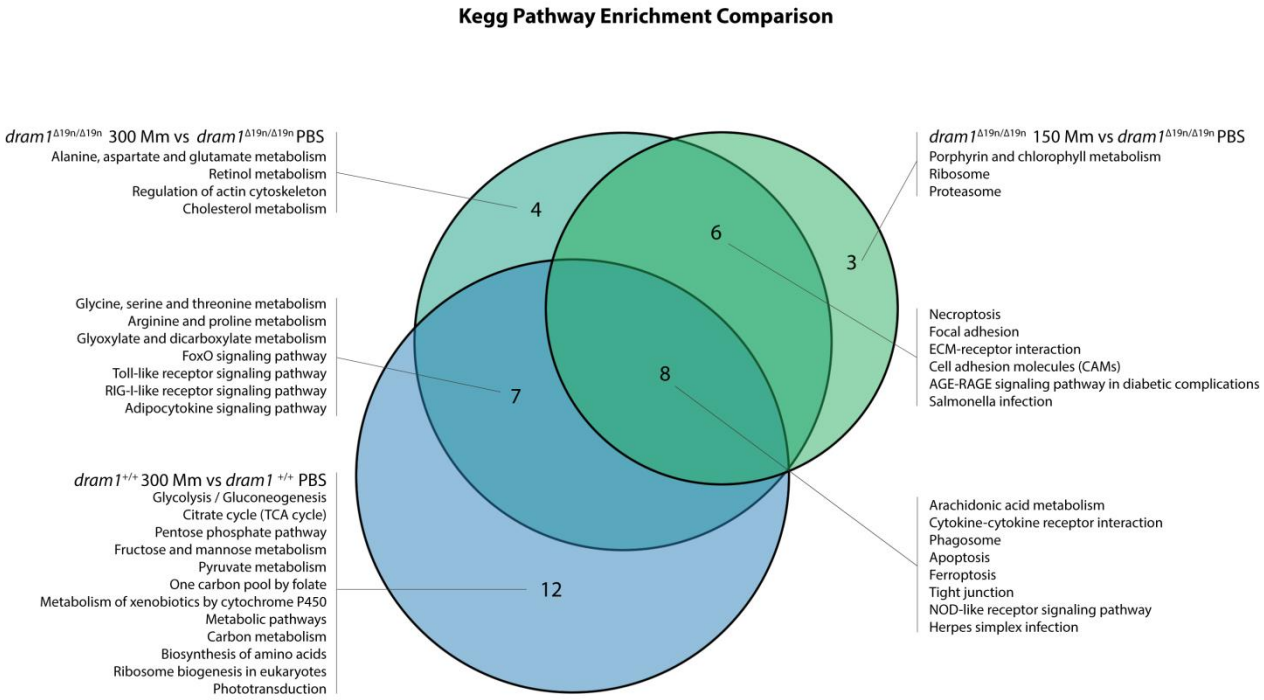

Figure 4: Venn diagram of the enriched KEGG pathways in larvae infected with Mm.

A. The KEGG pathways enrichment comparisons were performed on *dram1*$^{\Delta 19n/\Delta 19n}$ 150 CFU versus *dram1*$^{\Delta 19n/\Delta 19n}$ PBS, *dram1*$^{\Delta 19n/\Delta 19n}$ 300 CFU versus *dram1*$^{\Delta 19n/\Delta 19n}$, and *dram1*$^{+/+}$ 300 CFU versus *dram1*$^{+/+}$ PBS.

Dram1 deficiency alters the expression of genes involved in programmed cell death mechanisms

DRAM1 has been reported to be involved in the regulation of cellular death and we found that Dram1 deficiency affected both the apoptosis and necroptosis KEGG pathways in our study. We therefore decided to investigate the modulation of these pathways in more detail by comparing the expression of the genes involved in these pathways between the different groups (Fig5 A). Regarding the apoptosis pathway, we found a pronounced activation of *caspase 8* (*casp8l2*) and *caspase 9* expression in *dram1*$^{\Delta 19n/\Delta 19n}$ larvae infected with 300 CFU, while the 150 CFU infected larvae slightly increased the expression of these two caspase genes but did not reach significance levels. In comparison, in infected wild type larvae the expression of these two genes

were not significantly changed. We also found a profound inhibition of *granzyme 3* expression in infected *dram1* mutant fish, while this gene was highly expressed in infected *dram1*$^{+/+}$ larvae. Despite this, in general terms, the apoptosis effectors were not very differentially regulated between the *dram1* mutants and the wild types.

Concerning the necroptosis pathway (representing lytic forms of cell death), we found enhanced expression of 27 genes activated following DNA damage in *dram1*$^{\Delta 19n/\Delta 19n}$ larvae infected with 300 CFU. For example, we found a high expression level of *h2afva* and *baxa*. Histone H2A (encoded by *h2afva*) is involved in repair of a variety of DNA damage [16]. The increased expression of *h2afva* in infected *dram1*$^{\Delta 19n/\Delta 19n}$ larvae might indicate an increase in DNA damage, such as chromatinolysis triggered by programmed cell death [17]. The activation of programmed cell death mediates sequential activation of *baxa* expression, which translocates from mitochondria to the nucleus to enhance chromatinolysis. We found that gene expression of the necroptosis regulators *ripk1* and *ripk3* was activated both in infected *dram1*$^{+/+}$ and *dram1*$^{\Delta 19n/\Delta 19n}$ larvae. However, the expression of hsp90, which regulates protein stability of Ripk1 and Ripk3, was suppressed in infected *dram1*$^{\Delta 19n/\Delta 19n}$ larvae compared with infected wild types. We also observed that *caspase 1* expression was significantly increased in *dram1*$^{\Delta 19n/\Delta 19n}$ larvae infected with 300 CFU. In summary, while the gene expression level of apoptosis effectors does not appear altered between infected *dram1*$^{\Delta 19n/\Delta 19n}$ and wild type larvae, we did observe differences in gene expression that point towards an increase in lytic cell death in the absence of functional Dram1.

Figure 5: KEGG pathway analysis of differential gene expression in infected *dram1*$^{\Delta 19n/\Delta 19n}$ and *dram1*$^{+/+}$. (Figure on next page) The three data sets used for comparison are shown in the legend of the figure. The expression fold change of the genes is depicted by colour (yellow, upregulated, blue downregulated).

A. Cellular death signaling.

B. TLR signaling.

A

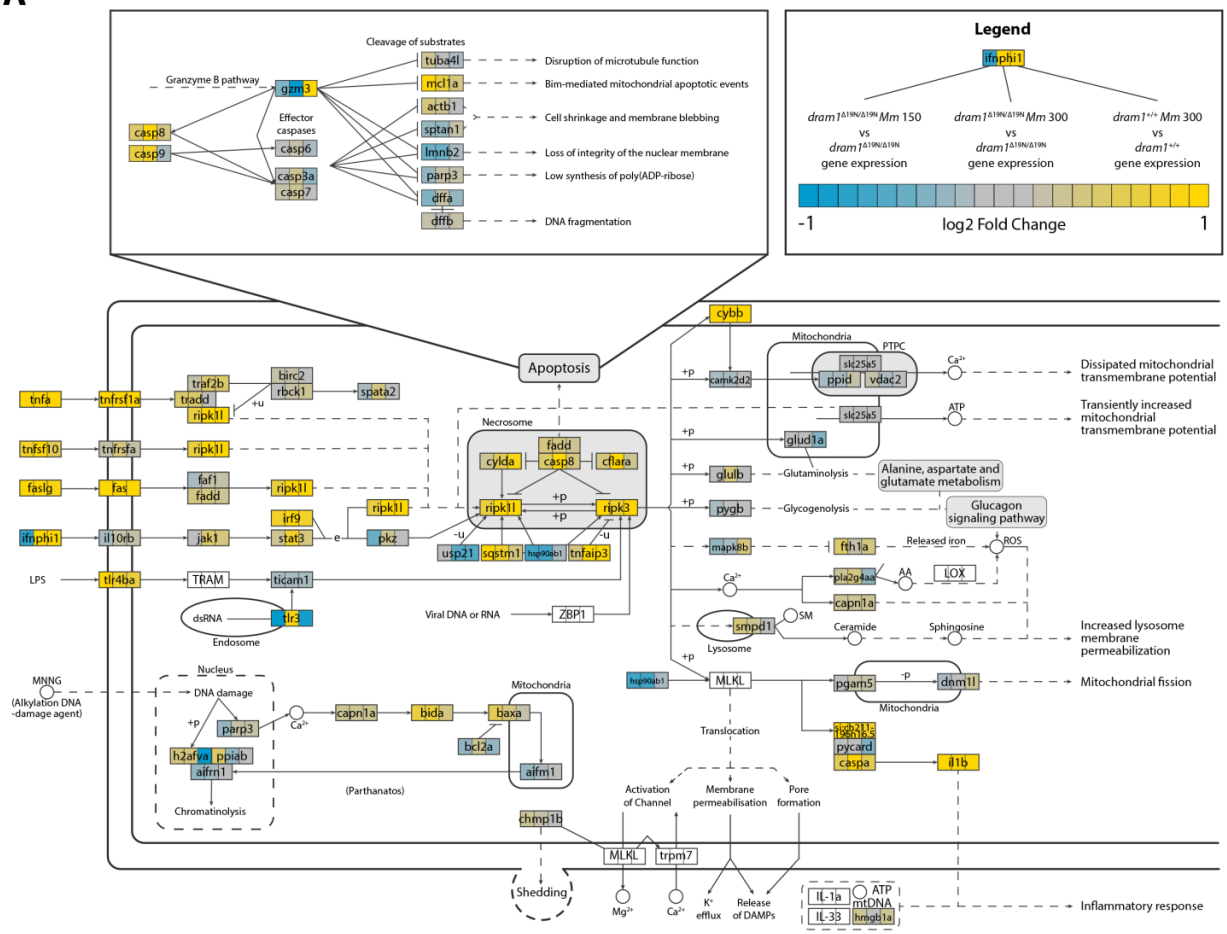
Cellular Death Pathways
Legend
log2 Fold Change
Apoptosis
Necrosis
Pyroptosis
Mitochondria
Lysosome
Nucleus
Endosome
Shedding
Inflammatory response
Mitochondrial fission
Dissipated mitochondrial transmembrane potential
Transiently increased mitochondrial transmembrane potential
Increased lysosome membrane permeabilization
Glucagon signaling pathway
Alanine, aspartate and glutamate metabolism
Chromatinolysis
Translocation
Activation of Channel
Membrane permeabilisation
Pore formation

B

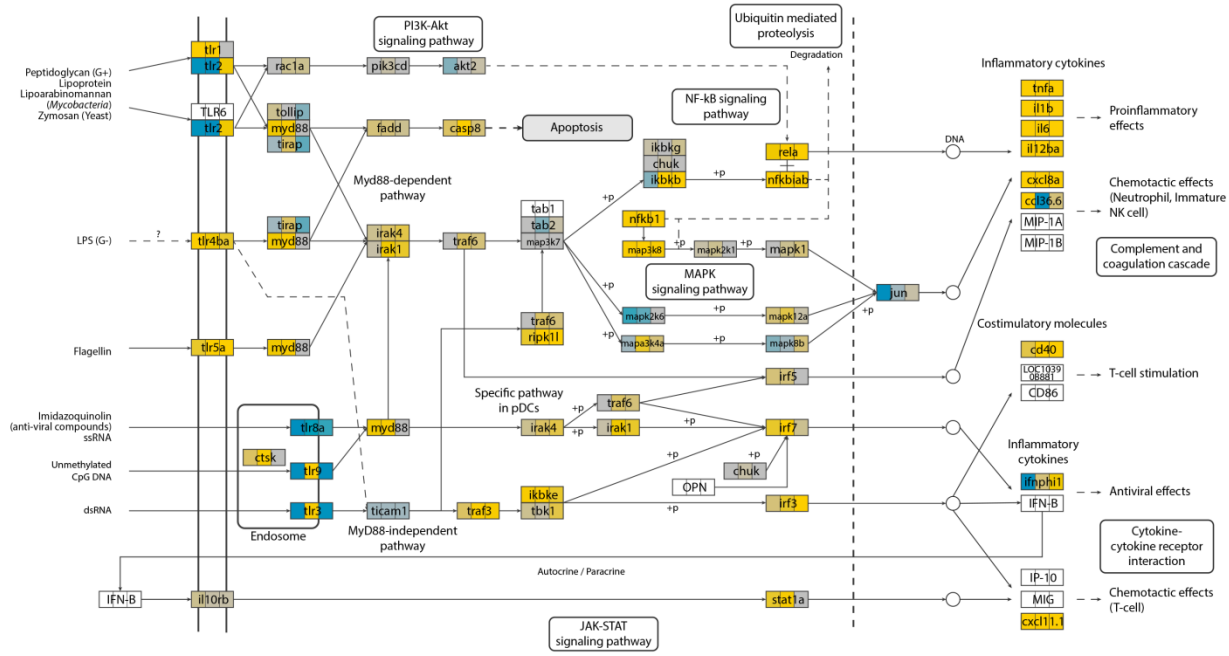
Toll-like Receptor Signaling Pathway
PI3K-Akt signaling pathway
Ubiquitin mediated proteolysis
NF-kB signaling pathway
MAPK signaling pathway
Myd88-dependent pathway
MyD88-independent pathway
Specific pathway in pDCs
JAK-STAT signaling pathway
Apoptosis
Endosome
Autocrine / Paracrine
Inflammatory cytokines
Costimulatory molecules
Proinflammatory effects
Chemotactic effects (Neutrophil, Immature DC, NK cell)
Complement and coagulation cascade
T-cell stimulation
Antiviral effects
Cytokine-cytokine receptor interaction
Chemotactic effects (T-cell)

Dram1 deficiency alters the expression of genes involved in immune signaling

We found that sensor pathways, like TLR and RIG-I-like signaling, were not activated in *dram1*$^{\Delta 19n/\Delta 19n}$ infected with the low dose of Mm, despite that these larvae developed similar bacterial burden as the wild type larvae infected with higher dose (Fig4). Since TLR signaling was previously found to be critical for defense of the zebrafish host against Mm [9], we set out to compare the gene expression of TLR components (Fig5 B). Explicitly, TLR2, TLR4 and TLR9 have been reported as crucial for the host to recognize the diverse molecular patterns of mycobacteria and activate an immune response against this pathogen [18, 19]. Strikingly, we found that *tlr2* expression was highly suppressed in *dram1*$^{\Delta 19n/\Delta 19n}$ larvae during infection, but highly activated in *dram1*$^{+/+}$ in response to infection. We found an opposite expression pattern in the expression of *tlr1*, which was activated in *dram1* mutants but not affected in the *dram1*$^{+/+}$ infected larvae. The high dose infection of *dram1*$^{\Delta 19n/\Delta 19n}$ larvae induced a high expression of *tlr3* and *tlr9*. Furthermore, the expression of MyD88-dependent immune signaling genes, including *irak1*, *irak4*, *traf6*, and *ikbkb* were only upregulated in the *dram1*$^{+/+}$ and *dram1*$^{\Delta 19n/\Delta 19n}$ larvae infected with a high dose of Mm. These results indicate that the presence or absence of functional Dram1, in combination with the level of infection, affects which TLR signaling routes are employed to detect the pathogen.

Dram1 deficiency leads to suppressed expression of LTB4

The control of the inflammatory balance is a crucial factor that affects the outcome of mycobacterial infection [20]. The arachidonic acid metabolism pathway produces principal mediators of inflammation –both pro- and anti-inflammatory– and directly impacts the progression and outcome of the infection. Since we found that the *alox5b.1* and *alox5b.2* genes were downregulated in *dram1*-deficient larvae (both in absence and presence of infection) and that the arachidonic acid pathway was affected during mycobacterial infection, we sought to explore this in more detail (Fig6 and FigS1). As a read-out for the function of this pathway, we performed ELISAs (enzyme-linked immunosorbent assays) to detect the level of lipoxin A4 (LXA4), which acts as an anti-inflammatory molecule, and leukotriene B4 (LTB4), whose function is pro-inflammatory. The synthesis of both these lipids depends on the arachidonic acid pathway.

We collected samples at 5 dpf from infected and non-infected larvae to measure the concentration of LTB4 and LXA4. The results showed that the level of LTB4 was around 2.5 times higher in uninfected *dram1*$^{+/+}$ than in uninfected *dram1*$^{\Delta 19n/\Delta 19n}$ larvae (Fig6 B). During mycobacterial infection, the levels of LTB4 in *dram1*$^{+/+}$ were decreased to similar levels as in *dram1*$^{\Delta 19n/\Delta 19n}$ larvae. For LXA4 we did not detect any differences between infected and non-infected larvae, or between the two genotypes (Fig6 B). These data demonstrate that Dram1 deficiency leads to impaired production of the pro-inflammatory molecule LTB4, but differences in the production of the anti-inflammatory LXA4 were not detected.

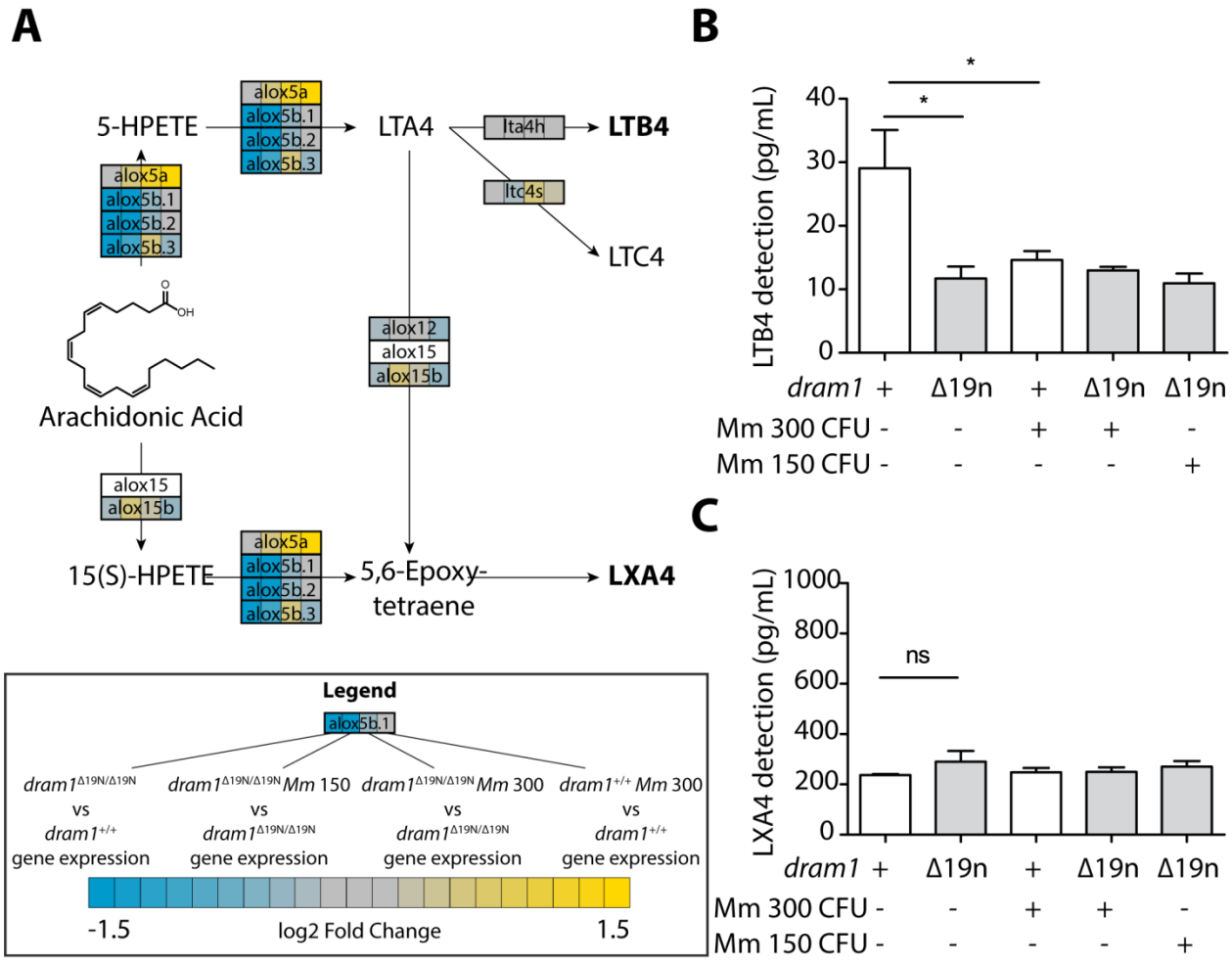

Figure 6: Dram1 deficiency leads to reduced LTB4 production

A. Differential expression of the genes from the Arachidonic Acid Metabolism pathway involved in the production of LTB4 and LXA4. The five data sets used for comparison are shown in the legend of the figure. The expression fold change is depicted by colour (yellow, upregulated, blue downregulated).

B-C. Detection of LTB4 (B) and LXA4 (C) levels by ELISA in infected and uninfected *dram1*$^{\Delta 19n/\Delta 19n}$ and *dram1*$^{+/+}$. larvae. Data shown are the averages from three replicates. ns, non-significant, *p<0.05,**p<0.01,***p<0.001.

Discussion

The lysosomal protein DRAM1 modulates autophagy and cell death in response to cellular stress factors, such as cancer, infection or nutrient depletion [12, 13]. Specifically, it was shown that DRAM1/Dram1 is activated downstream of a TLR-MyD88-NFκB signaling pathway to modulate autophagic defense against mycobacterial infection in primary human macrophages and zebrafish larvae [12]. In this study, we have demonstrated that loss-of-function mutation of *dram1* alters the expression of TLR signaling, cell death and metabolic pathway components during Mm infection in zebrafish. These results suggest that Dram1 contributes to host defense against mycobacterial pathogens by transcriptional modulation of the immune response in addition to its known function in anti-bacterial autophagy.

Before analyzing the effect of Dram1 deficiency on the transcriptome response to infection, we asked whether a difference in gene expression could be observed between *dram1*$^{\Delta 19n/\Delta 19n}$ and wild type larvae. Despite that the known functions of Dram1 are related to stress conditions, we found that, even without infection challenge, a total of 236 genes displayed altered expression between *dram1* mutant and wild type larvae. Amongst these altered genes, we identified many genes related to metabolic processes and the proteasome. This transcriptional response could be a compensatory mechanism for defects in lysosomal function due to the deficiency in Dram1. This hypothesis is in line with recent studies that have revealed that lysosomes function as central regulatory units in signal transduction [21]. The differences between *dram1* mutants and wild types in the expression of metabolic pathway genes was markedly enhanced in response to Mm infection. Many recent studies have shown that the metabolic status of macrophages, the primary cell type parasitized by mycobacteria, is critical for their innate host defense function [22]. Therefore, it is conceivable that metabolic dysregulation in *dram1* mutants is a major cause of the hypersusceptibility phenotype.

TLRs can recognize invading mycobacterial pathogens and play an essential role in resistance to the infection. Recognition of mycobacteria via TLR/MyD88 signaling activates NFκB to initiate the expression of *dram1*, which in turn modulates autophagic responses to control mycobacterial infection [12]. We have demonstrated that Dram1 deficiency fails to restrict Mm inside lysosomal vesicles, culminating in increased death of infected macrophages (Chapter 2 of this thesis). Thus, without Dram1 mycobacterial infection more commonly results in extracellular growth of the bacteria. Both the localization of mycobacteria and the mode of cell death can contribute to the recognition of bacteria by pattern recognition receptors (PRRs) and activation of immune and inflammatory responses. PRRs can recognize mycobacteria and other pathogens in different locations, including TLR2 which is located on the surface of the plasma membrane, while TLR3, TLR7, and TLR9 are predominantly located on the lumen of endosomes [23, 24]. In our case, the expression of *tlr2* was significantly reduced in infected *dram1* mutant larvae compared to infected wild types. Moreover, the expression of *tlr*3 and *tlr*9 was increased dramatically in Dram1-deficient larvae during mycobacterial infection. This could reflect the altered localization of bacteria, which potentially results in adjustments in the expression of plasma membrane and endosomal TLRs. For instance, the down regulation of *tlr2* in *dram1* mutants might be related to the overgrowth of extracellular mycobacteria, which are not effectively eliminated by the host. Therefore, we can speculate that Tlr2 molecules on the plasma membrane are continuously signaling, causing the cell to down regulate *tlr2* as a negative feedback loop.

Inflammatory responses play a vital role in eliminating mycobacterial infections. The inflammatory response to mycobacterial infection is balanced by the production of the pro-inflammatory lipid leukotriene B4 (LTB4) and the anti-inflammatory lipid lipoxin A4 (LXA4) [25]. The enzyme LTA4H catalyses the final step in the synthesis of LTB4. LTA4H polymorphisms that resulted in reduced production of LTB4 and increased production of LXA4 have been linked to host susceptibility to mycobacterial infections [26]. In addition, it has been shown that overexpression of LTA4H, which increases LTB4 levels, causes hyperinflammation and exacerbated infection [27, 28]. In our transcriptome analyses, the arachidonic acid pathway was affected due to the disrupted function of Dram1. We found that the *alox5b1* and *alox5b2* genes

were downregulated in *dram1* mutants. Alox5 is a lipoxygenase that catalyses membrane lipid peroxidation and has been suggested to be involved in the regulation of cell death [29, 30]. We found that the production of LTB4 was impaired due to Dram1 deficiency, while the production of LXA4 was not changed in the absence of Dram1. We also observed that Mm infection reduced LTB4 in wild type larvae to the same level as that of uninfected and infected *dram1* mutants. Based on these results, we believe that the increased susceptibility of *dram1* mutants to mycobacterial infection is not related to the arachidonic acid pathway, since both wild type larvae and *dram1* mutants infected with Mm display similar levels of LTB4 and LXA4.

Cell death of infected macrophages is a crucial factor in dissemination of invading mycobacterial pathogens. In this study, we found that Dram1 deficiency affects the signaling pathways orchestrating cell death. Specifically, the apoptosis and necroptosis KEGG pathways were differentially regulated between infected *dram1*$^{+/+}$ and *dram1*$^{\Delta 19n/\Delta 19n}$ larvae. We have previously demonstrated that apoptosis could be induced by mycobacterial infection both in *dram1*$^{+/+}$ and *dram1*$^{\Delta 19n/\Delta 19n}$, with no difference in apoptosis activity between *dram1*$^{+/+}$ and *dram1*$^{\Delta 19n/\Delta 19n}$ (Chapter 2 of this thesis). In agreement with these results, we found only minor differences in *caspase 8* and *9* expression, and did not detect striking differences in regulation of apoptosis effector genes in response to infection between infected *dram1*$^{+/+}$ and *dram1*$^{\Delta 19n/\Delta 19n}$ larvae. The differentially regulated necroptosis KEGG pathway contains various regulators and effectors of different forms of lytic cell death, including those involved in pyroptosis. Looking specifically at necroptosis, the activation of this pathway requires the involvement of *RIPK1*, *RIPK3* and *MLKL* [31]. While zebrafish do not express a *mlkl* gene, *ripk1* and *ripk3* were activated by mycobacterial infection both in *dram1*$^{+/+}$ and *dram1*$^{\Delta 19n/\Delta 19n}$ larvae. In contrast, the expression of *hsp90* was suppressed in infected *dram1*$^{\Delta 19n/\Delta 19n}$ larvae compared with infected wild types. HSP90 has been reported to regulate necroptosis via maintaining the stability of RIPK1, RIPK3 and MLKL [31, 32]. Therefore, although *ripk1* and *ripk3* are equally expressed in infected *dram1*$^{+/+}$ and *dram1*$^{\Delta 19n/\Delta 19n}$ larvae, there might be differences at the protein level due to altered stability caused by differences in *hsp90* expression. Furthermore, we also observed that *caspase 1* expression was significantly increased in *dram1*$^{\Delta 19n/\Delta 19n}$ larvae infected with 300 CFU. This suggests that Dram1 deficiency leads to pyroptotic cell death via activation of *caspase*

1. Other evidence supporting this hypothesis is that higher levels of Caspase 1 protease activity can be detected in infected *dram1*$^{\Delta 19n/\Delta 19n}$ larvae and that the hypersusceptibility phenotype of these mutants can be rescued by knockdown of *caspase 1* gene activity (Chapter 2 of this thesis). Taken together, we propose that infected macrophages in *dram1*$^{\Delta 19n/\Delta 19n}$ larvae more frequently activate lytic cell death pathways compared to their wild type counterparts. While increased pyroptotic cell death of infected macrophages in *dram1*$^{\Delta 19n/\Delta 19n}$ larvae has been experimentally demonstrated (Chapter 2 of this thesis), a potential increase in the occurrence of necroptosis in the absence of Dram1 remains to be investigated.

In conclusion, we have demonstrated that the presence of functional Dram1 is important for the transcriptional regulation of metabolic processes under basal and pathogenic stress conditions at the whole organism level. While these observations require further investigations, we implicate altered cell death programs and differential requirements for pattern recognition receptors as important factors in the hypersusceptibility of *dram1* mutants to mycobacterial infection, adding to the previously reported effects of Dram1 deficiency on anti-bacterial autophagy.

Materials and methods

Zebrafish culture and lines

Zebrafish lines in this study (TableS2) were maintained and used in compliance with local animal welfare regulations as overseen by the Leiden University (registration number: 10612). Embryos were kept in egg water, in a 28.5°C-30°C incubator, and treated with 0.02% Ethyl 3-aminobenzoate methanesulfonate (Tricaine, SIGMA-ALDRICH) in egg water for anesthesia before bacterial injections, imaging and fixation.

Infection conditions and bacterial burden quantification

Approximately 300 CFU of *Mycobacterium marinum* strain fluorescently labelled with mCherry [33] were microinjected into the blood island of embryos at 28 hpf as previously described [34]. Embryos were manually dechorionated by tweezers and treated with tricaine to keep

anesthesia before the injection. Infected embryos were imaged using a Leica MZ16FA stereo fluorescence microscope equipped with a DFC420C colour camera, and the bacterial pixels per infected fish data were obtained from the individual embryo stereo fluorescence images using previously described software [35].

RNA preparation and RNA sequencing

Total RNA was extracted from 5 dpf infected and non infected larvae (20 larvae/sample) from three independent crosses using Trizol reagent (15596026, Invitrogen) according to the manufacturer's instructions and extracted with RNeasy Min Elute Clean up kit (Lot:154015861, QIAGEN). RNAs were quantified using a 2100 Bioanalyzer (Agilent, US). At least 10 million reads per sample were sequenced using Illumina Single read 50 nt runs in a Hiseq2500. Sequencing, mapping the reads against the *D. rerio* GRCz10.80 reference genome and read counting were performed by ZF-screens (Leiden, Netherlands).

Analysis of RNA sequencing results

Analysis of the count libraries was performed in RStudio 1.1.383 [36] running R 3.4.3 [37] using in-house scripts (available at github.com/gabrifc). An initial quality check of the samples was performed using the tools provided in the edgeR package v3.20.7 [38]. Based on a PCA analysis and gene expression heatmap, a biological replicate from the *dram1*$^{-/-}$ samples, including non-infected and infected fish was discarded from subsequent analysis. Differential gene expression was assessed via pairwise comparisons using DESeq2 v1.18.1 [39]. Genes with a FDR-adjusted p-value < 0.05 were considered statistically significant. Venn Diagrams were created using the R package VennDiagram v1.6.18 [40].

Gene lists were ranked using the published function "-log(adjpval)*log2FC" and compared to the C2 "Curated Gene Sets" collection from the Molecular Signatures Database (MSigDB) using GSEA v3.0 [41], and visualized with fgsea v1.4.1 [42]. Gene ontology enrichment was analysed with goseq v1.3.0 [43]. Updated gene length and Gene Ontology data from the Zv9 assembly was retrieved from Ensembl with the packages ensembldb v2.2.1 [44] and biomaRt v2.34.2 [45],

respectively. When necessary, mapping between different database gene identifiers was also performed using biomaRt. KEGG Pathway analysis was performed with the kegga function provided in limma v3.34.5 [46]. Gene regulation data of significant pathways was visualized with pathview v1.18.0 [47].

Detection of LTB4 and LXA4 by ELISA

LTB4 and LXA4 in whole larvae were detected using a previously described method [48]. 5dpf infected and uninfected larvae (20 larvae/group) were collected and washed with PBS. All liquid was removed and samples were snap frozen (10s) in liquid nitrogen. For the ELISA, 375 µL PBS and 0.2 SSB02 stainless steel beads (Next Advance) were added to each sample. Larvae were homogenized using a Bullet Blender (Next Advance) for 3 minutes on speed 8. The samples were then centrifuged at 3500 rpm for 5 minutes. The supernatant was collected and centrifuged again at 5000 rpm for 5 minutes after which the supernatant was collected again. An LTB4 ELISA kit (ADI-900-068, Enzo Life Sciences) and an LXA4 ELISA kit (CEB452Ge, Cloud-Clone Corp) were used according to the manufacturer's instructions. All samples were measured in duplicate (50 or 100 µL used per measurement), and the data from the duplicates were averaged. Data shown are the averages (SEM) from 3 replicates.

Statistical analyses

Statistical analyses were performed using GraphPad Prism software (Version 5.01; GraphPad). All experimental data (mean ± SEM) was analyzed using unpaired, two-tailed t-tests for comparisons between two groups and one-way ANOVA with Tukey's multiple comparison methods as a posthoc test between more than two groups. (ns, no significant difference; *$p < 0.05$; **$p < 0.01$; ***$p < 0.001$).

Acknowledgements

We thank Daniel Klionsky for sharing of GFP-Lc3 transgenic zebrafish line. We are grateful to all members of the fish facility team for zebrafish caretaking. R.Z was supported by a grant from the China Scholarship Council (CSC). M.V and G.C were funded by European Marie Curie

fellowships (H2020-MSCA-IF-2014-655424, MSCA-COFUND-2015-FP, respectively), and MvdV was supported by the Netherlands Technology Foundation TTW (project 13259).

References

1. WHO. Global tuberculosis report 2017 (WHO/HTM/TB/2017.23). 2017.
2. Tiberi S, du Plessis N, Walzl G, Vjecha MJ, Rao M, Ntoumi F, et al. Tuberculosis: progress and advances in development of new drugs, treatment regimens, and host-directed therapies. The Lancet Infectious Diseases 2018.
3. Davis JM, Ramakrishnan L. The role of the granuloma in expansion and dissemination of early tuberculous infection. Cell 2009; 136:37-49.
4. Clay H, Volkman HE, Ramakrishnan L. Tumor necrosis factor signaling mediates resistance to mycobacteria by inhibiting bacterial growth and macrophage death. Immunity 2008; 29:283-94.
5. Ramakrishnan L. Revisiting the role of the granuloma in tuberculosis. Nat Rev Immunol 2012; 12:352-66.
6. Cronan MR, Beerman RW, Rosenberg AF, Saelens JW, Johnson MG, Oehlers SH, et al. Macrophage Epithelial Reprogramming Underlies Mycobacterial Granuloma Formation and Promotes Infection. Immunity 2016; 45:861-76.
7. Meijer AH. Protection and pathology in TB: learning from the zebrafish model. Semin Immunopathol 2016; 38:261-73.
8. Berg RD, Ramakrishnan L. Insights into tuberculosis from the zebrafish model. Trends Mol Med 2012; 18:689-90.
9. van der Vaart M, van Soest JJ, Spaink HP, Meijer AH. Functional analysis of a zebrafish myd88 mutant identifies key transcriptional components of the innate immune system. Dis Model Mech 2013; 6:841-54.
10. Meijer AH, Verbeek FJ, Salas-Vidal E, Corredor-Adamez M, Bussman J, van der Sar AM, et al. Transcriptome profiling of adult zebrafish at the late stage of chronic tuberculosis due to Mycobacterium marinum infection. Mol Immunol 2005; 42:1185-203.
11. Benard EL, Rougeot J, Racz PI, Spaink HP, Meijer AH. Transcriptomic Approaches in the Zebrafish Model for Tuberculosis-Insights Into Host- and Pathogen-specific Determinants of the Innate Immune Response. Adv Genet 2016; 95:217-51.
12. van der Vaart M, Korbee CJ, Lamers GE, Tengeler AC, Hosseini R, Haks MC, et al. The DNA

damage-regulated autophagy modulator DRAM1 links mycobacterial recognition via TLR-MYD88 to autophagic defense [corrected]. Cell Host Microbe 2014; 15:753-67.

13. Crighton D, Wilkinson S, O'Prey J, Syed N, Smith P, Harrison PR, et al. DRAM, a p53-induced modulator of autophagy, is critical for apoptosis. Cell 2006; 126:121-34.

14. Mrschtik M, Ryan KM. Another DRAM involved in autophagy and cell death. Autophagy 2016; 12:603-5.

15. Nagata M, Arakawa S, Yamaguchi H, Torii S, Endo H, Tsujioka M, et al. Dram1 regulates DNA damage-induced alternative autophagy. Cell Stress 2018; 2:55-65.

16. Moore JD, Yazgan O, Ataian Y, Krebs JE. Diverse roles for histone H2A modifications in DNA damage response pathways in yeast. Genetics 2007; 176:15-25.

17. Matt S, Hofmann TG. The DNA damage-induced cell death response: a roadmap to kill cancer cells. Cell Mol Life Sci 2016; 73:2829-50.

18. Quesniaux V, Fremond C, Jacobs M, Parida S, Nicolle D, Yeremeev V, et al. Toll-like receptor pathways in the immune responses to mycobacteria. Microbes Infect 2004; 6:946-59.

19. Bafica A, Scanga CA, Feng CG, Leifer C, Cheever A, Sher A. TLR9 regulates Th1 responses and cooperates with TLR2 in mediating optimal resistance to Mycobacterium tuberculosis. J Exp Med 2005; 202:1715-24.

20. Sasindran SJ, Torrelles JB. Mycobacterium Tuberculosis Infection and Inflammation: what is Beneficial for the Host and for the Bacterium? Front Microbiol 2011; 2:2.

21. Perera RM, Zoncu R. The Lysosome as a Regulatory Hub. Annu Rev Cell Dev Biol 2016; 32:223-53.

22. O'Neill LA, Pearce EJ. Immunometabolism governs dendritic cell and macrophage function. J Exp Med 2016; 213:15-23.

23. Basu J, Shin DM, Jo EK. Mycobacterial signaling through toll-like receptors. Front Cell Infect Microbiol 2012; 2:145.

24. Nishiya T, DeFranco AL. Ligand-regulated chimeric receptor approach reveals distinctive subcellular localization and signaling properties of the Toll-like receptors. J Biol Chem 2004; 279:19008-17.

25. Scanga CA, Flynn JL. Mycobacterial infections and the inflammatory seesaw. Cell Host

Microbe 2010; 7:177-9.

26. Tobin DM, Vary JC, Jr., Ray JP, Walsh GS, Dunstan SJ, Bang ND, et al. The lta4h locus modulates susceptibility to mycobacterial infection in zebrafish and humans. Cell 2010; 140:717-30.

27. Tobin DM, Roca FJ, Oh SF, McFarland R, Vickery TW, Ray JP, et al. Host genotype-specific therapies can optimize the inflammatory response to mycobacterial infections. Cell 2012; 148:434-46.

28. Tobin DM, Roca FJ, Ray JP, Ko DC, Ramakrishnan L. An enzyme that inactivates the inflammatory mediator leukotriene b4 restricts mycobacterial infection. PLoS One 2013; 8:e67828.

29. Chen M, Hong MJ, Sun H, Wang L, Shi X, Gilbert BE, et al. Essential role for autophagy in the maintenance of immunological memory against influenza infection. Nat Med 2014; 20:503-10.

30. Maccarrone M, Catani MV, Agro AF, Melino G. Involvement of 5-lipoxygenase in programmed cell death of cancer cells. Cell Death and Differentiation 1997; 4:396-402.

31. Jacobsen AV, Silke J. The importance of being chaperoned: HSP90 and necroptosis. Cell Chem Biol 2016; 23:205-7.

32. Li D, Xu T, Cao Y, Wang H, Li L, Chen S, et al. A cytosolic heat shock protein 90 and cochaperone CDC37 complex is required for RIP3 activation during necroptosis. Proc Natl Acad Sci U S A 2015; 112:5017-22.

33. van der Sar AM, Abdallah AM, Sparrius M, Reinders E, Vandenbroucke-Grauls CM, Bitter W. Mycobacterium marinum strains can be divided into two distinct types based on genetic diversity and virulence. Infect Immun 2004; 72:6306-12.

34. Benard EL, van der Sar AM, Ellett F, Lieschke GJ, Spaink HP, Meijer AH. Infection of zebrafish embryos with intracellular bacterial pathogens. J Vis Exp 2012.

35. Cui C, Benard EL, Kanwal Z, Stockhammer OW, van der Vaart M, Zakrzewska A, et al. Infectious disease modeling and innate immune function in zebrafish embryos. Methods Cell Biol 2011; 105:273-308.

36. RStudio Team. RStudio: Integrated Development for R. 2015.

37. R Development Core Team. R: A language and environment for statistical computing. Vienna, Austria : the R Foundation for Statistical Computing, 2011.

38. Robinson MD, McCarthy DJ, Smyth GK. edgeR: a Bioconductor package for differential expression analysis of digital gene expression data. Bioinformatics 2010; 26:139-40.

39. Love MI, Huber W, Anders S. Moderated estimation of fold change and dispersion for RNA-seq data with DESeq2. Genome Biol 2014; 15:550.

40. Chen H. Venn Diagram:Generate High-Resolution Venn and Euler Plots. 2017.

41. Subramaniana A, Tamayoa P, Moothaa VK, Mukherjee S, Mesirov JP. Gene set enrichment analysis: A knowledge-based approach for interpreting genome-wide expression profiles. Proc Natl Acad Sci U S A 2005; 102:15545-50.

42. Sergushichev A. An algorithm for fast preranked gene set enrichment analysis using cumulative statistic calculation. BioRxiv 2016.

43. Young MD, Wakefield MJ, Smyth GK, Oshlack A. MGeethnode ontology analysis for RNA-seq: accounting for selection bias. Genome Biology 2010; 11.

44. Rainer J. ensembldb: Utilities to create and use Ensembl-based annotation databases. 2008.

45. Durinck S, Spellman PT, Birney E, Huber W. Mapping identifiers for the integration of genomic datasets with the R/Bioconductor package biomaRt. Nat Protoc 2009; 4:1184-91.

46. Ritchie ME, Phipson B, Wu D, Hu Y, Law CW, Shi W, et al. limma powers differential expression analyses for RNA-sequencing and microarray studies. Nucleic Acids Res 2015; 43:e47.

47. Luo W, Brouwer C. Pathview: an R/Bioconductor package for pathway-based data integration and visualization. Bioinformatics 2013; 29:1830-1.

48. Chatzopoulou A, Heijmans JP, Burgerhout E, Oskam N, Spaink HP, Meijer AH, et al. Glucocorticoid-Induced Attenuation of the Inflammatory Response in Zebrafish. Endocrinology 2016; 157:2772-84.

Supplementary data

Regulation	GO ID	FDR	DGE	Category	Term
Overrepresented	GO:0070011	1,97E-07	16	585	peptidase activity, acting on L-amino acid peptides
	GO:0008233	3,19E-07	16	608	peptidase activity
Underrepresented	GO:0005623	1,34E-08	29	10118	Cell
	GO:0044464	1,34E-08	29	10118	cell part
	GO:0009987	2,07E-08	34	10941	cellular process
	GO:0043226	5,64E-08	12	6372	Organelle
	GO:0043229	1,06E-07	12	6265	intracellular organelle
	GO:0044424	4,32E-07	21	7983	intracellular part
	GO:0044260	5,24E-07	8	4969	cellular macromolecule metabolic process
	GO:0006139	1,04E-06	2	3076	nucleobase-containing compound metabolic process
	GO:0005622	1,45E-06	24	8360	intracellular
	GO:0043227	2,87E-06	11	5449	membrane-bounded organelle
	GO:0065007	3,34E-06	17	6719	biological regulation
	GO:0043231	3,35E-06	10	5179	intracellular membrane-bounded organelle
	GO:0046483	4,93E-06	3	3153	heterocycle metabolic process
	GO:0016070	6,57E-06	1	2397	RNA metabolic process
	GO:0090304	9,45E-06	2	2700	nucleic acid metabolic process
	GO:0034641	1,41E-05	5	3597	cellular nitrogen compound metabolic process
	GO:0009059	1,76E-05	2	2624	macromolecule biosynthetic process
	GO:0034645	1,92E-05	2	2609	cellular macromolecule biosynthetic process
	GO:0019222	2,07E-05	2	2575	regulation of metabolic process
	GO:1901576	2,30E-05	4	3218	organic substance biosynthetic process
	GO:0006725	2,50E-05	4	3172	cellular aromatic compound metabolic process
	GO:0044271	2,84E-05	2	2545	cellular nitrogen compound biosynthetic process
	GO:0050789	3,07E-05	17	6269	regulation of biological process
	GO:0044249	3,13E-05	4	3160	cellular biosynthetic process
	GO:0010467	3,86E-05	3	2814	gene expression
	GO:0018130	4,40E-05	1	2080	heterocycle biosynthetic process
	GO:0019438	4,58E-05	1	2073	aromatic compound biosynthetic process
	GO:0060255	4,61E-05	2	2435	regulation of macromolecule metabolic process
	GO:0031323	5,13E-05	2	2421	regulation of cellular metabolic process
	GO:0034654	6,18E-05	1	2022	nucleobase-containing compound biosynthetic process
	GO:0080090	6,23E-05	2	2387	regulation of primary metabolic process
	GO:0044237	6,73E-05	18	6347	cellular metabolic process
	GO:0051171	7,71E-05	2	2348	regulation of nitrogen compound metabolic process

Supplementary table1: Results of gene ontology analysis in *dram1*$^{\Delta 19n/\Delta 19n}$ and *dram1*$^{+/+}$ without Mm infection. GO categories overrepresented or underrepresented in *dram1*$^{\Delta 19n/\Delta 19n}$ versus *dram1*$^{+/+}$ are indicated. The DGE Column indicates the number of differentially expressed genes between *dram1*$^{\Delta 19n/\Delta 19n}$ and *dram1*$^{+/+}$ with the indicated GO category (described by GO ID and Term), while the Category column indicates the total number of genes in the GO category that were detected in our RNA sequencing. FDR indicates the false discovery rate.

Supplementary table2: Zebrafish lines used in this study

Fish line	Description	Reference
dram1$^{+/+}$/GFP-Lc3	Siblings of *dram1* carrying a transgenic GFP-Lc3 reporter	In this study
dram1$^{\Delta 19n/\Delta 19n}$/GFP-Lc3	*dram1* mutant line (Δ19n indel) carrying a transgenic GFP-Lc3 reporter	In this study

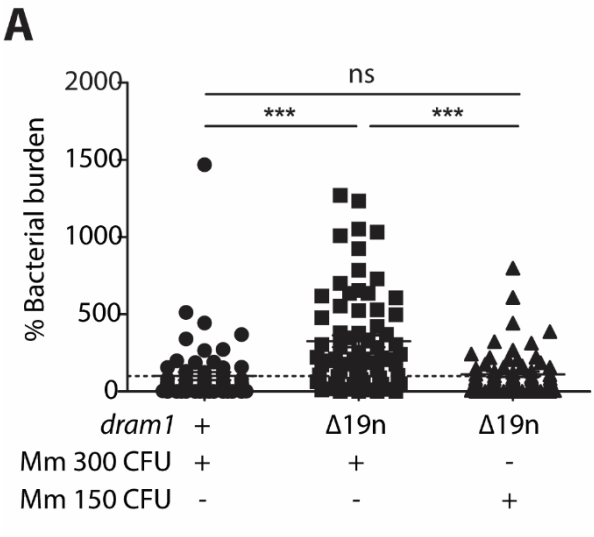

Supplementary figure 1: Mutation of *dram1* leads to increased susceptibility to Mm infection

A. Bacterial burdens at 4 dpi in *dram1*$^{+/+}$ and *dram1*$^{\Delta 19n/\Delta 19n}$ larvae. Each dot represents an individual larva. ns, non-significant, *p<0.05,**p<0.01,***p<0.001.

Chapter 4

The selective autophagy receptors Optineurin and p62 are both required for innate host defense against mycobacterial infection

Rui Zhang, Monica Varela, Wies Vallentgoed, Gabriel Forn-Cuní, Michiel van der Vaart and Annemarie H. Meijer

(*Submitted*)

Abstract:

Mycobacterial pathogens are the causative agents of chronic infectious diseases like tuberculosis and leprosy. Autophagy has recently emerged as an innate mechanism for defense against these intracellular pathogens. *In vitro* studies have shown that mycobacteria escaping from phagosomes into the cytosol are ubiquitinated and targeted by selective autophagy receptors. However, there is currently no *in vivo* evidence for the role of selective autophagy receptors in defense against mycobacteria, and the importance of autophagy in control of mycobacterial diseases remains controversial. Here we have used *Mycobacterium marinum* (Mm), which causes a tuberculosis-like disease in zebrafish, to investigate the function of two selective autophagy receptors, Optineurin (Optn) and SQSTM1 (p62), in host defense against a mycobacterial pathogen. To visualize the autophagy response to Mm *in vivo*, *optn* and *p62* zebrafish mutant lines were generated in the background of a GFP-Lc3 autophagy reporter line. We found that loss-of-function mutation of *optn* or *p62* reduces autophagic targeting of Mm, and increases susceptibility of the zebrafish host to Mm infection. Transient knockdown studies confirmed the requirement of both selective autophagy receptors for host resistance against Mm infection. For gain-of-function analysis, we overexpressed *optn* or *p62* by mRNA injection and found this to increase the levels of GFP-Lc3 puncta in association with Mm and to reduce the Mm infection burden. Taken together, our results demonstrate that both Optineurin and p62 are required for autophagic host defense against mycobacterial infection and support that protection against tuberculosis disease may be achieved by therapeutic strategies that enhance selective autophagy.

Introduction

Autophagy is a fundamental cellular pathway in eukaryotes that functions to maintain homeostasis by degradation of cytoplasmic contents in lysosomes [1]. During autophagy, protein aggregates or defective organelles are sequestered by double-membrane structures, called isolation membranes or phagophores, which mature into autophagosomes capable of fusing with lysosomes. Autophagy was previously considered a strictly non-selective bulk degradation

pathway. However, recent comprehensive studies have highlighted its selective ability. Selective autophagy depends on receptors that interact simultaneously with the cytoplasmic material and with the autophagosome marker microtubule-associated protein 1 light chain 3 (Lc3), thereby physically linking the cargo with the autophagy compartment [2,3]. Different selective autophagy pathways are classified according to their specific cargo; for example, mitophagy is the pathway that degrades mitochondria, aggrephagy targets misfolded proteins or damaged organelles, and xenophagy is directed against intracellular microorganisms. Recent studies have firmly established xenophagy as an effector arm of the innate immune system [4-6]. The xenophagy pathway targets microbial invaders upon their escape from phagosomes into the cytosol, where they are coated by ubiquitin. These ubiquitinated microbes are then recognized by selective autophagy receptors of the Sequestosome (p62/SQSTM1)-like receptor (SLR) family, including p62, Optineurin, NDP52, NBRC1, and TAX1BP1 [5]. In addition to targeting microbes to autophagy, SLRs also deliver ubiquitinated proteins to the same compartments. It has been shown that the processing of these proteins into neo-antimicrobial peptides is important for elimination of the pathogen *Mycobacterium tuberculosis* in macrophages [7].

M. tuberculosis (Mtb) is the causative agent of chronic and acute tuberculosis (Tb) infections that remain a formidable threat to global health, since approximately one-third of the human population carry latent infections and 9 million new cases of active disease manifest annually. Current therapeutic interventions are complicated by increased incidence of multi-antibiotic resistance of Mtb and co-infections with Human Immunodeficiency Virus (HIV). Despite decades of extensive research efforts, the mechanisms of how Mtb subverts the host's innate immune defenses are incompletely understood, which poses a bottleneck for developing novel therapeutic strategies [8]. Because of the discovery of autophagy as an innate host defense mechanism, the potential of autophagy-inducing drugs as adjunctive therapy for Tb is now being explored [9].

Many studies have shown that induction of autophagy in macrophages by starvation, interferon-γ (IFN-γ) treatment, or by autophagy-inducing drugs, promotes maturation of mycobacteria-containing phagosomes and increases lysosome-mediated bacterial killing [7,10-12].

Furthermore, it has been shown that the ubiquitin ligase Parkin and the ubiquitin-recognizing SLRs p62 and NDP52 are activated by the escape of Mtb from phagosomes into the cytosol [13,14]. Subsequently, the ubiquitin-mediated xenophagy pathway targets Mtb to autophagosomes [13,14]. Parkin-deficient mice are extremely vulnerable to Mtb infection [14]. However, a recent study has questioned the function of autophagy in the host immune response against Mtb, since mutations in several autophagy proteins, with the exception of ATG5, did not affect the susceptibility of mice to acute Mtb infection [15]. The susceptibility of ATG5-deficient mice in this study was attributed to the ability of ATG5 to prevent a neutrophil-mediated immunopathological response rather than to direct autophagic elimination of Mtb. In the same study, loss of p62 did not affect the susceptibility of mice to Tb, despite that p62 has previously been shown to be required for autophagic control of Mtb in macrophages [7,15]. These different reports suggest that Mtb employs virulence mechanisms to suppress autophagic defense mechanisms and that the host requires autophagy induction as a countermeasure [12]. Taken together, the role that autophagy plays in Tb is complex and further studies are required to determine if pharmacological intervention in this process is useful for a more effective control of this disease.

In this study, we utilized zebrafish embryos and larvae to investigate the role of selective autophagy during the early stages of mycobacterial infection, prior to the activation of adaptive immunity. Zebrafish is a well-established animal model for Tb that has generated important insights into host and bacterial factors determining the disease outcome [16,17]. Infection of zebrafish embryos with *Mycobacterium marinum* (Mm), a pathogen that shares the majority of its virulence factors with Mtb, results in the formation of granulomatous aggregates of infected macrophages, considered as a pathological hallmark of Tb [17-19]. Using a combination of confocal imaging in GFP-Lc3 transgenic zebrafish and transmission electron microscopy, we have previously shown that the autophagy machinery is activated during the early stages of granuloma formation in this model [20,21]. Furthermore, we found that the DNA-damage regulated autophagy modulator Dram1 protects the zebrafish host against Mm infection by a p62-dependent mechanism [21]. However, the role of p62 and other SLRs in host defense against Mm remains to be further elucidated.

p62 is known to function cooperatively with Optineurin in xenophagy of *Salmonella enterica* [22-24]. Both these SLRs are phosphorylated by Tank-binding kinase 1 (TBK1) and bind to different microdomains of ubiquitinated bacteria as well as interacting with Lc3 [23,25]. While several studies have implicated p62 in autophagic defense against Mtb, Optineurin has thus far not been linked to control of mycobacterial infection [7,13,24-26]. We found gene expression of *p62* and *optn* to be coordinately upregulated during granuloma formation in zebrafish larvae [27], and set out to study the function of these SLRs by CRISPR/Cas9-mediated mutagenesis. We found that either p62 or Optineurin deficiency increased the susceptibility of zebrafish embryos to Mm infection, while overexpression of *p62* or *optn* mRNAs enhanced Lc3 association with Mm and had a host-protective effect. These results provide new *in vivo* evidence for the role of selective autophagy as an innate host defense mechanism against mycobacterial infection.

Results

***Mycobacterium marinum* bacteria are ubiquitinated during infection of zebrafish**

Phagosomal permeabilization and cytosolic escape of Mtb is known to induce the STING-dependent DNA-sensing pathway, resulting in ubiquitination and targeting of bacteria to autophagy [13]. We have previously shown that this pathway is also functional in zebrafish larvae infected with Mm and that a failure to induce autophagy reduces host resistance [21]. However, it had not been formally demonstrated that Mm bacteria are ubiquitinated in this model. To examine whether ubiquitin interacts with Mm and Lc3 during infection of zebrafish, we infected embryos at 28 hours post fertilization (hpf) and performed immunostaining for ubiquitin at 1, 2, and 3 days post- infection (dpi), time points at which the early stages of tuberculous granuloma formation can be observed (Fig1 A). This process of granuloma formation is known to be induced by infected macrophages, which attract new macrophages that subsequently also become infected [28]. Developing granulomas also attract neutrophils and usually contain extracellular bacteria released by dying cells [29]. We observed that around 3% and 9% of Mm clusters are targeted by GFP-Lc3 at 1 and 2 dpi, respectively, which increases to uncountable levels at 3 dpi because of the increasing numbers and size of granulomas (Fig1 B and Fig1 C). These results were confirmed by Western blot, showing that LC3-II protein levels – indicative of

autophagosome formation – gradually increased during Mm infection compared to uninfected controls (Fig1 D). Using a FK2 ubiquitin antibody, which can recognize monoubiquitinated cell surface molecules as well as polyubiquitin chains, we observed that ubiquitin co-colocalized with approximately 4% and 10% of the Mm clusters at 1 and 2 dpi, respectively (Fig1 E and Fig1 F). Furthermore, we observed by Western blot detection that Mm infection increased general levels of protein ubiquitination (Fig1 G). In addition, we found that ubiquitin and GFP-Lc3 co-localized at Mm clusters (Fig1 H). Collectively, these data demonstrate that Mm is marked by ubiquitin and that overall ubiquitination levels are induced during infection in the zebrafish model, which coincides with autophagic targeting of bacteria.

Figure 1: Ubiquitination and autophagy activity can be induced by Mm infection. (Figure on next page)

A. Schematic diagram of the zebrafish Mm infection model for TB study. *Mycobacterium marinum* (Mm) strain 20 fluorescently labelled with mCherry was microinjected into the blood island of embryos at 28 hpf. Red dots represent small clusters of Mm-infected cells visible from 1 dpi. At 3 dpi these Mm clusters have grown into early stage granulomas.

B. Representative confocal micrographs of GFP-Lc3 co-localization with Mm clusters in infected embryos/larvae at 1, 2 and 3 days post infection (dpi). Scale bars, 10 μm.

C. Quantification of the percentage of Mm clusters positive for GFP-Lc3 at 1 and 2 dpi. The results are representative for two individual repeats (≥ 20 embryo/group). ns, non-significant,*p<0.05,**p<0.01,***p<0.001.

D. Western blot determination of Lc3 protein levels in infected and uninfected embryos/larvae at 1, 2 and 3 dpi. Protein samples were extracted from 1, 2 and 3 dpi infected and uninfected larvae (>10 larvae/sample). The blots were probed with antibodies against Lc3 and Actin as a loading control. Western blot was representative for three independent experimental repeats.

E. Representative confocal micrographs of Ubiquitin co-localization with Mm clusters in infected embryos/larvae at 1, 2 and 3 days post infection (dpi). Scale bars, 10 μm.

F. Quantification of the percentage of Mm clusters positive for ubiquitin staining at 1 and 2 dpi (≥ 10 embryo/group). The results are representative for two individual repeats. ns, non-significant, *p<0.05, **p<0.01, ***p<0.001.

G. Western blot analysis of ubiquitination levels in infected and uninfected embryos/larvae at 1, 2 and 3 dpi. Protein samples were extracted from 1, 2 and 3 dpi infected and uninfected larvae (>10 larvae/sample). The blots were probed with an antibody detecting both poly and mono ubiquitin and with anti-Actin antibody as a loading control. Western blot representative for three independent experimental repeats.

H. Representative confocal micrographs of GFP-Lc3 and Ubiquitin co-localization with Mm clusters in infected larvae at 3 dpi. Scale bars, 10 μm.

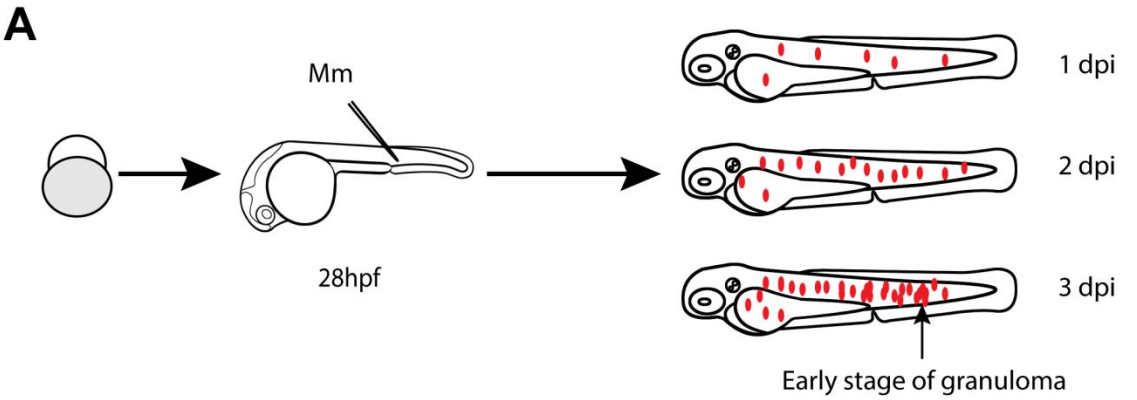
A
Mm
28hpf
1 dpi
2 dpi
3 dpi
Early stage of granuloma

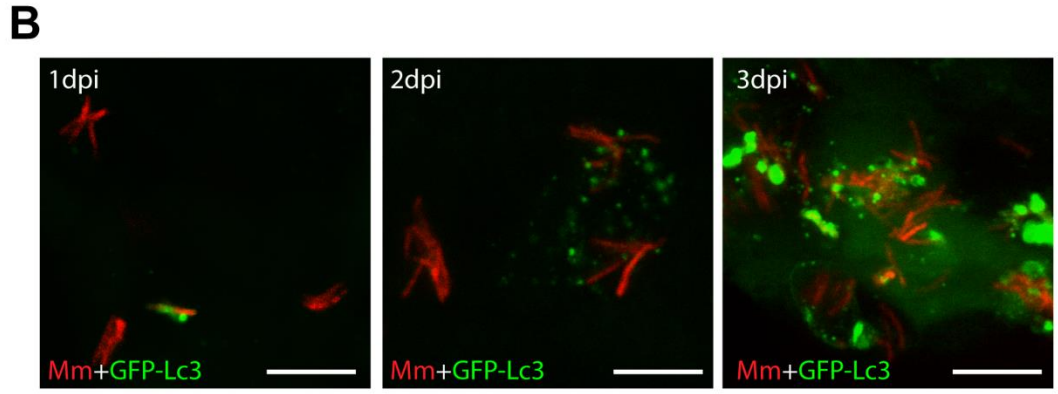
B
1dpi
2dpi
3dpi
Mm+GFP-Lc3
Mm+GFP-Lc3
Mm+GFP-Lc3

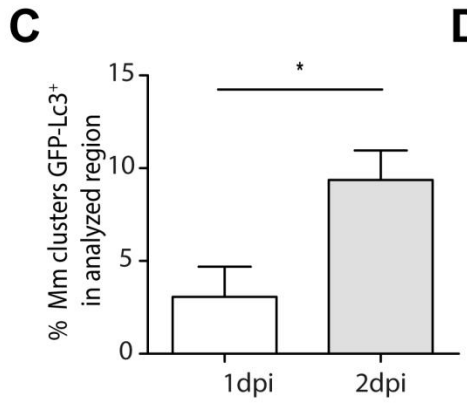
C
% Mm clusters GFP-Lc3+ in analyzed region
15
10
5
0
*
1dpi
2dpi

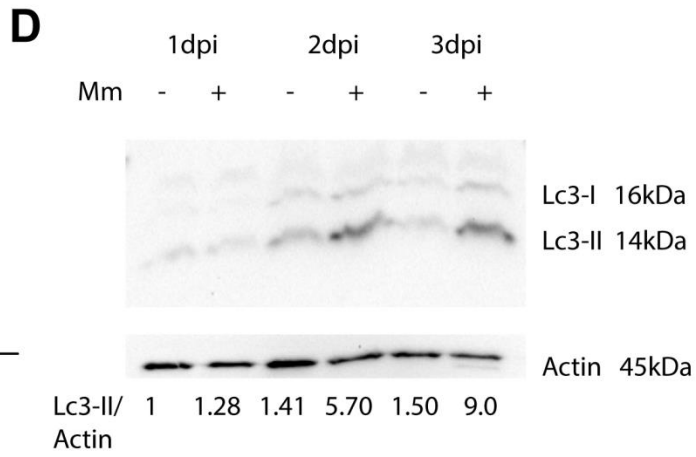
D
1dpi
2dpi
3dpi
Mm - + - + - +
Lc3-I 16kDa
Lc3-II 14kDa
Actin 45kDa
Lc3-II/ Actin 1 1.28 1.41 5.70 1.50 9.0

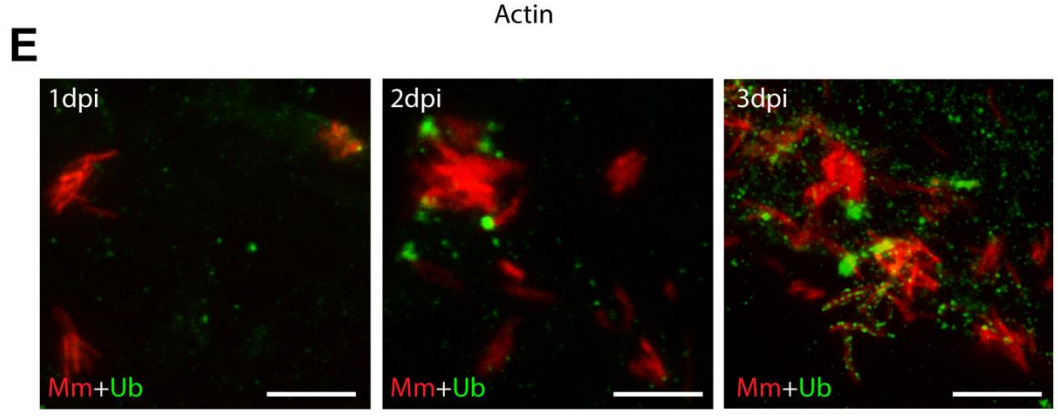
E
1dpi
2dpi
3dpi
Mm+Ub
Mm+Ub
Mm+Ub

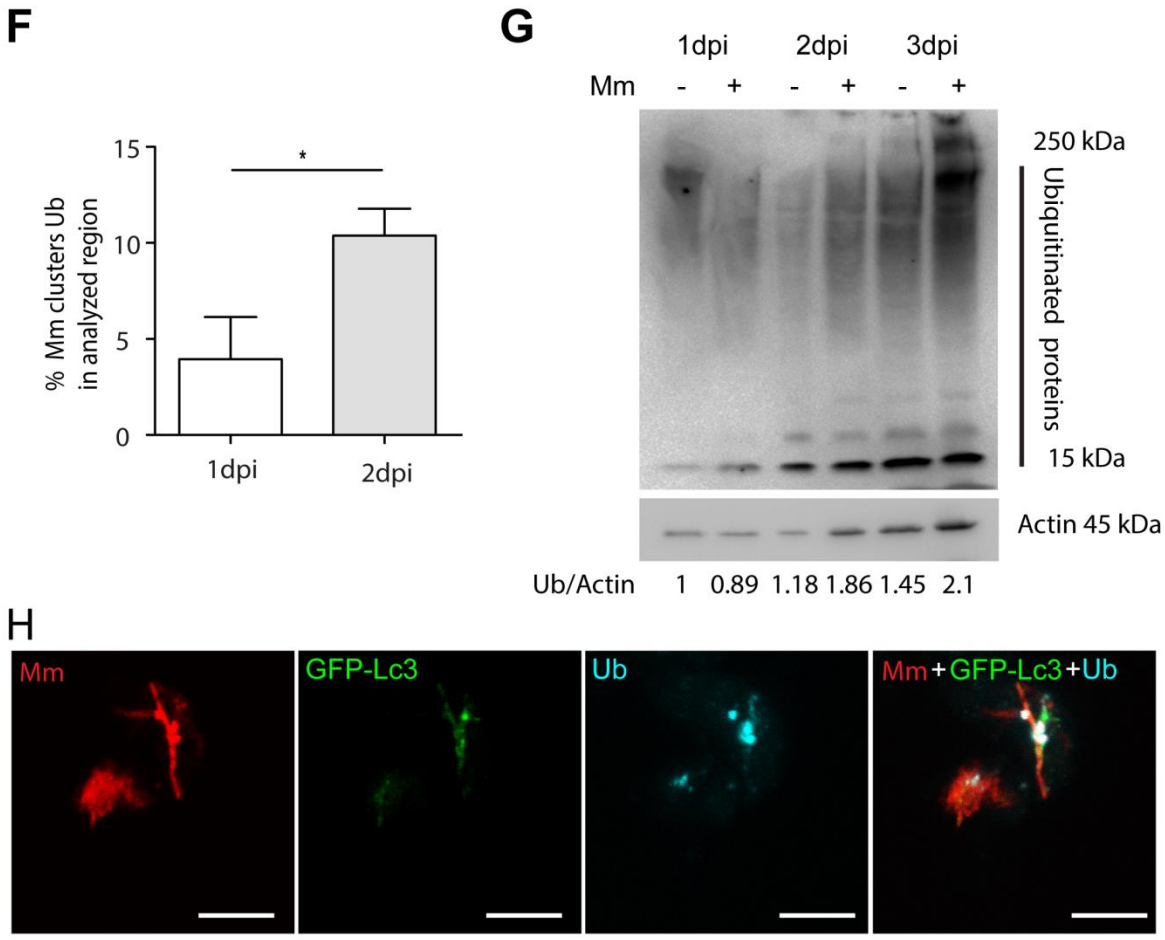

Deficiency in the ubiquitin receptors Optineurin or p62 does not impair zebrafish development

Since ubiquitinated bacteria are targets for members of the sequestosome-like receptor family, we compared the protein sequences of its members p62, Optineurin, Calcoco2 (Ndp52), Nbrc1, and Tax1bp1 between human, zebrafish and other vertebrates, showing a high overall degree of conservation (S1B Fig and S1C Fig). We focused this study on two members of the family, *p62* and *optn*, which are transcriptionally induced during Mm infection of zebrafish based on published RNA sequencing data [27] and show strong similarity with their human orthologues in the ubiquitin-binding domains (UBA in p62 and UBAN in Optineurin) and Lc3 interaction regions (LIR) (S1D Fig). With the aim to investigate the functions of Optineurin and p62 in anti-mycobacterial autophagy, we utilized CRISPR/Cas9 genome editing technology to generate

mutant zebrafish lines. We designed short guide RNAs for target sites at the beginning of coding exons 2 of the *optn* and *p62* genes, upstream of the exons encoding the ubiquitin and Lc3 binding regions, such that the predicted effect of CRISPR mutation is a complete loss of protein function (Fig2 A). A mixture of sgRNA and Cas9 mRNA was injected into zebrafish embryos at the one cell stage and founders carrying the desired mutations were outcrossed to the *Tg*(*CMV:EGFP-map1lc3b*) autophagy reporter line (hereafter referred to as GFP-Lc3) (Fig2 B) [30]. The established *optn* mutant allele carried a 5 nucleotides deletion at the target site, which we named $optn^{\Delta 5n/\Delta 5n}$ (Fig2 C). The *p62* mutant allele carried an indel resulting in the net loss of 37 nucleotides, which we named $p62^{\Delta 37n/\Delta 37n}$ (Fig2 C). The homozygous mutants were fertile and produced embryos that did not exhibit detectable morphological differences compared with embryos produced by their wild-type ($optn^{+/+}$ or $p62^{+/+}$) siblings (S1A Fig). Furthermore, no significant deviation from the Mendelian 1:2:1 ratio for +/+, +/- and -/- genotypes was observed when the offspring of heterozygous incrosses were sequenced at 3 months of age (Fig2 E). Western blot analysis using anti-Optineurin and anti-p62 C-terminal antibodies confirmed the absence of the proteins in the respective mutant lines (Fig2 D). In addition, quantitative PCR (Q-PCR) analysis revealed approximately 4.5-fold reduction of *optn* mRNA in the $optn^{\Delta 5n/\Delta 5n}$ larvae and 10-fold reduction of *p62* mRNA in the $p62^{\Delta 37n/\Delta 37n}$ larvae, indicative of nonsense-mediated mRNA decay (Fig2 F). Collectively, the $optn^{\Delta 5n/\Delta 5n}$ and $p62^{\Delta 37n/\Delta 37n}$ mutant zebrafish produce no functional Optineurin or p62, respectively, and the loss of these ubiquitin receptors does not induce detectable developmental defects that could interfere with the use of the mutant lines in infection models.

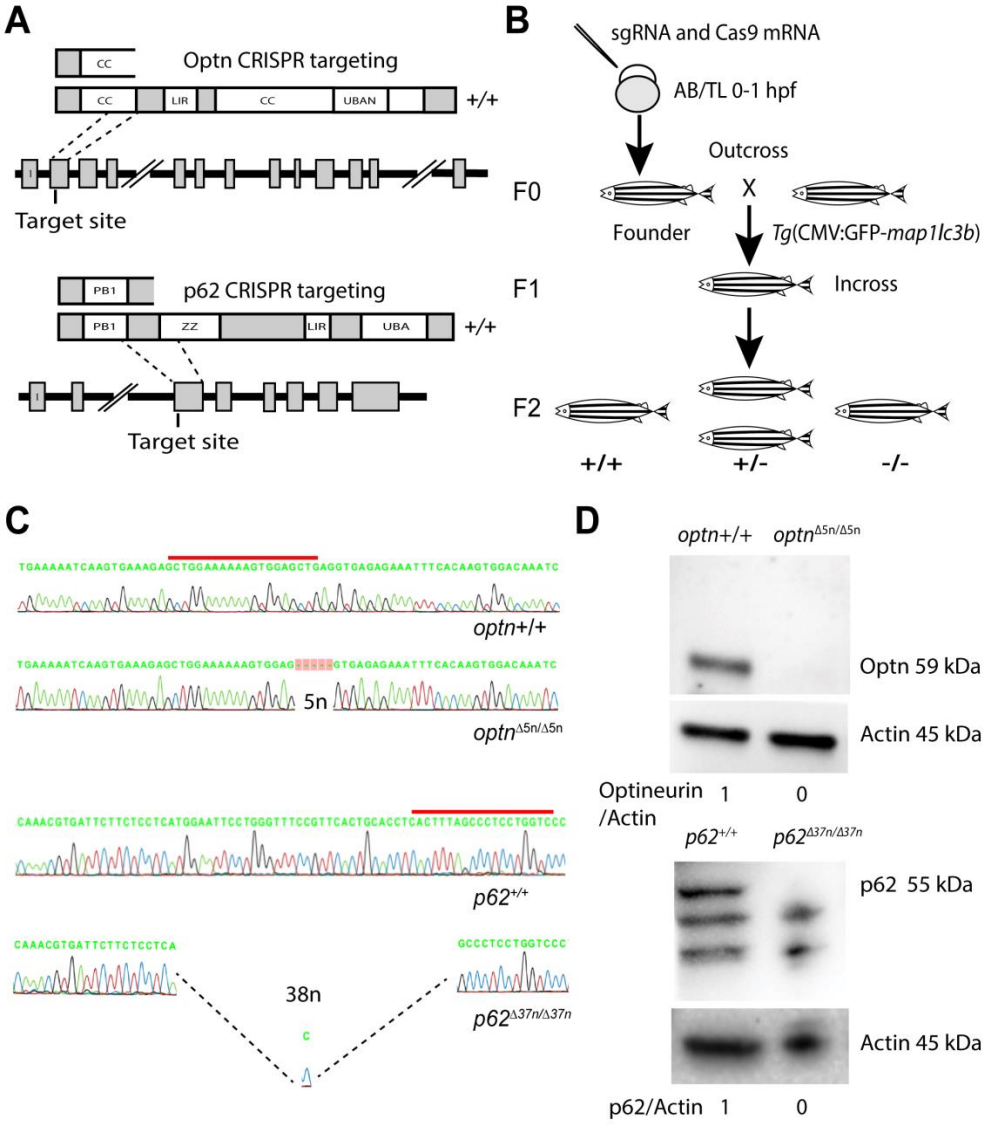
A
Optn CRISPR targeting
CC
CC
LIR
CC
UBAN
+/+
Target site
p62 CRISPR targeting
PB1
PB1
ZZ
LIR
UBA
+/+
Target site
B
sgRNA and Cas9 mRNA
AB/TL 0-1 hpf
Outcross
F0
X
Founder
Tg(CMV:GFP-map1lc3b)
F1
Incross
F2
+/+
+/-
-/-
C
optn+/+
5n
optnΔ5n/Δ5n
p62+/+
38n
p62Δ37n/Δ37n
D
optn+/+
optnΔ5n/Δ5n
Optn 59 kDa
Actin 45 kDa
Optineurin /Actin 1 0
p62+/+
p62Δ37n/Δ37n
p62 55 kDa
Actin 45 kDa
p62/Actin 1 0
E
Proportion of genotypes from heterozygote incross
n=40
n=112
n=46
optn+/+
optnΔ5n/+
optnΔ5n/Δ5n
n=22
n=42
n=19
p62+/+
p62Δ37n/+
p62Δ37n/Δ37n
F
optn mRNA
p62 mRNA
Relative fold change
***
ns
optn + Δ5n + Δ5n
p62 mRNA
optn mRNA
*
ns
p62 + Δ37n + Δ37n

Figure 2: Generation of Optineurin and p62 mutant lines

A. Schematic representation of the Optn and p62 genetic and protein domain architecture and CRISPR target site. Optn (517 aa) and P62 (452 aa) both contain a Lc3 interaction region domain (LIR) and ubiquitin binding domains (UBAN in Optn and UBA in P62). Additionally, two coiled-coil motifs (CC) in Optineurin and the PHOX/Bem1p (PB) and Zinc Finger (ZZ) domains of P62 are indicated. The gene loci are shown with coding exons as grey boxes (14 in Optn and 8 in P62) and introns as solid black lines (large introns not drawn to scale). The position of the CRISPR target site sequences at the beginning of exon 2 in Optineurin and exon 3 in p62 are indicated and the predicted truncated proteins in the mutant lines are drawn above.

B. Schematic diagram of the generation of Optn and P62 mutant lines. Target-specific sgRNA and Cas9 mRNAs were co-injected into one cell stage embryos (AB/TL *WT* line). Founders were outcrossed to *Tg*(*CMV*:*EGFP-Lc3*) fish and the F1 was incrossed to obtain homozygous mutant and wild type F2 siblings.

C. Sanger sequencing of *WT* and mutant F2 fish. Red lines indicate CRISPR target sites. The Optn and p62 mutant sequences contain deletions of 5 and 37 nucleotides indel, respectively.

D. Confirmation of CRISPR mutation effect by WB analysis. Protein samples were extracted from 4 dpf *optn* or 3dpf *p62* mutant and WT larvae (>10 embryos/sample) and WBs were repeated at least three times with independent extracts. The blots were probed with antibodies against Optn or P62 and Actin as a loading control. Optn/Actin and P62/Actin ratios) are indicated below. kDa, kilodalton.

E. Segregation from F1 heterozygous incross. Genotypes of adult fish (>3 months) combined from 4 (for *optn*) or 3 (*p62*) independent breedings were confirmed by PCR and sequencing.

F. *optn* and *p62* mRNA was detected by quantitative PCR. Total RNA was isolated from 4dpf of $optn^{+/+}$, $optn^{\Delta 5n/\Delta 5n}$, $p62^{+/+}$ and $p62^{\Delta 37n/\Delta 37n}$ embryos (>10 embryos/sample) from three biological replicates.

Optineurin or p62 deficiencies affect autophagy

To analyze the effects of Optineurin or p62 deficiency on autophagy, we performed Lc3 Western blot detection on whole embryo extracts and imaged GFP-Lc3 signal *in vivo* (Fig3 A). Differences in the levels of the cytosolic (Lc3-I) and membrane-bound (Lc3-II) forms of Lc3 or effects on GFP-Lc3 puncta accumulation can be due to altered basal autophagy levels, but can also be caused by differences in autophagosome degradation. Therefore, we also examined Lc3-I/Lc3-II levels and GFP-Lc3 accumulation in larvae following treatment with Bafilomycin A1 (Baf A1), which is an inhibitor of vacuolar H+ ATPase (V-ATPase) that prevents maturation of autophagic vacuoles by inhibiting fusion between autophagosomes and lysosomes [31,32]. First, we performed a dose range assay to determine the effect of Baf A1 on Lc3-II accumulation in zebrafish embryos. Results showed that after 12 h of incubation, a dosage of 100nM resulted in Lc3-II accumulation

without affecting the Lc3-I level, whereas higher dosage additionally increased the Lc3-I level (S2A Fig). Thus, we utilized a dosage of 100nM to test Lc3-II accumulation in wildtype and mutant embryos not carrying the GFP-Lc3 reporter (Fig3 B). No differences in Lc3-II accumulation were observed between *optn*$^{+/+}$ and *optn*$^{\Delta 5n/\Delta 5n}$ embryos or between *p62*$^{+/+}$ and *p62*$^{\Delta 37n/\Delta 37n}$ embryos (Fig3 C). However, accumulation of Lc3-II in *optn* or *p62* mutant embryos was significantly reduced in presence of Baf A1 (52% and 66%, respectively) compared to the wildtype controls (Fig3 C). In agreement, the number of GFP-Lc3 puncta in *optn* or *p62* mutants were significantly lower than in the corresponding WT controls, showing 59% and 47% reductions, respectively (Fig3 D and Fig3 E).

The function of Optineurin and p62 as ubiquitin receptors implies that these proteins are degraded themselves during the process of autophagy. Therefore, we asked if p62 protein levels are affected in *optn* mutants or, vice versa, if *p62* mutation impacts Optineurin protein levels. Western blot analysis showed accumulation of p62 and Optineurin protein in wild type embryos in response to Baf A1 treatment, confirming that these ubiquitin receptors are substrates for autophagy under basal conditions (S2B Fig). Levels of p62 protein were reduced in *optn*$^{\Delta 5n/\Delta 5n}$ embryos compared with *optn*$^{+/+}$, both in absence or presence of Baf A1 (Fig3 F). This difference was not due to a transcriptional effect, since p62 mRNA levels were not significantly different between *optn*$^{+/+}$ and *optn*$^{\Delta 5n/\Delta 5n}$ embryos (Fig2 F). Similarly, levels of Optineurin protein were reduced in *p62*$^{\Delta 37n/\Delta 37n}$ embryos compared with *p62*$^{+/+}$ in absence or presence of Baf A1 (Fig3 F), and again this was not associated with a difference in mRNA expression (Fig2 F). In conclusion, the absence of either of the ubiquitin receptors, Optineurin or p62, leads to increased use of the other ubiquitin receptor as a substrate for autophagic degradation. Furthermore, loss of either of the receptors leads to lower levels of Lc3-II and GFP-Lc3 accumulation when lysosomal degradation is blocked, suggesting reduced activity of the autophagy pathway in the *optn* and *p62* mutants.

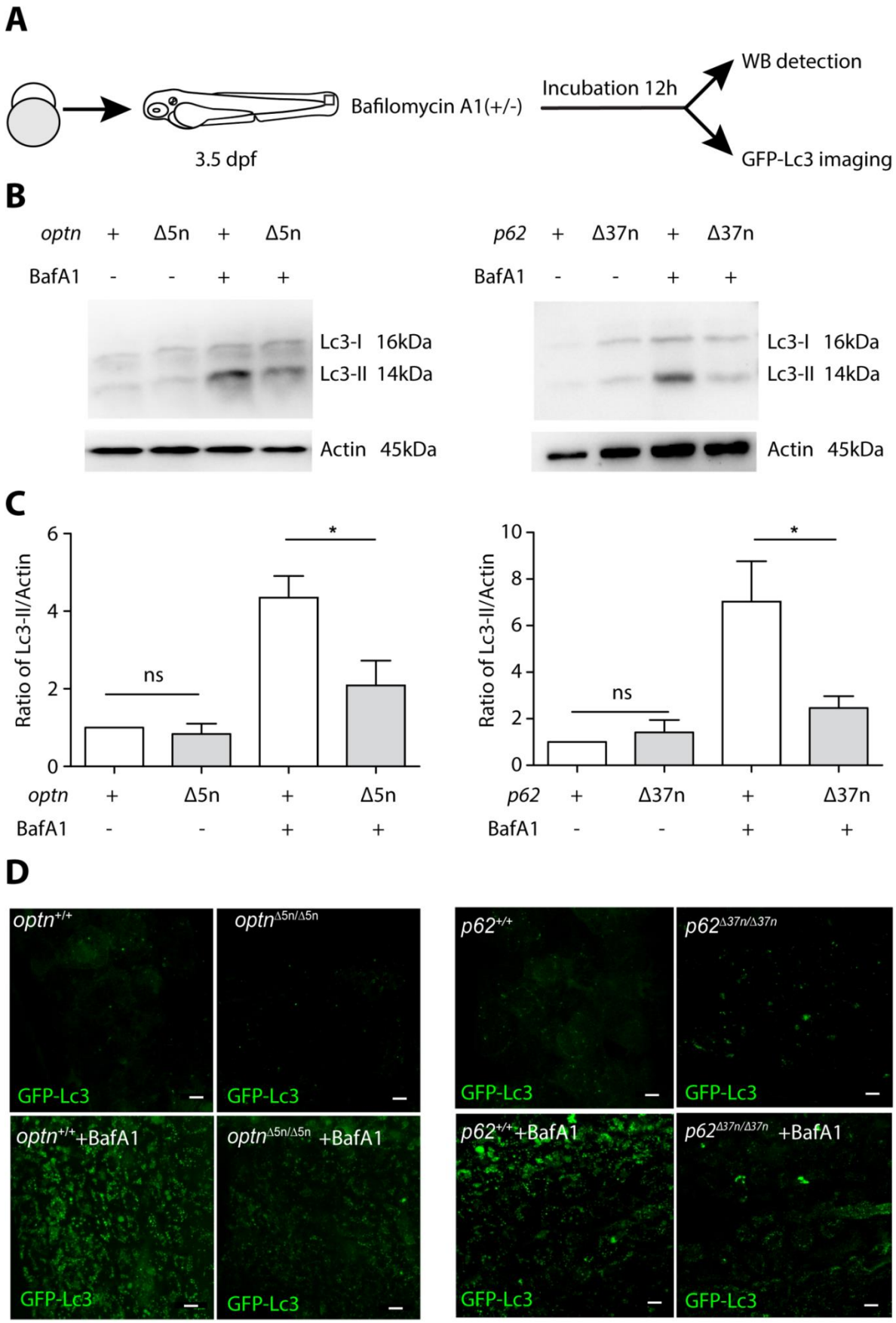
A
3.5 dpf
Bafilomycin A1(+/-)
Incubation 12h
WB detection
GFP-Lc3 imaging
B
optn + Δ5n + Δ5n
BafA1 - - + +
Lc3-I 16kDa
Lc3-II 14kDa
Actin 45kDa
p62 + Δ37n + Δ37n
BafA1 - - + +
Lc3-I 16kDa
Lc3-II 14kDa
Actin 45kDa
C
Ratio of Lc3-II/Actin
ns
*
optn + Δ5n + Δ5n
BafA1 - - + +
Ratio of Lc3-II/Actin
ns
*
p62 + Δ37n + Δ37n
BafA1 - - + +
D
optn+/+
optnΔ5n/Δ5n
p62+/+
p62Δ37n/Δ37n
GFP-Lc3
optn+/+ +BafA1
optnΔ5n/Δ5n +BafA1
p62+/+ +BafA1
p62Δ37n/Δ37n +BafA1

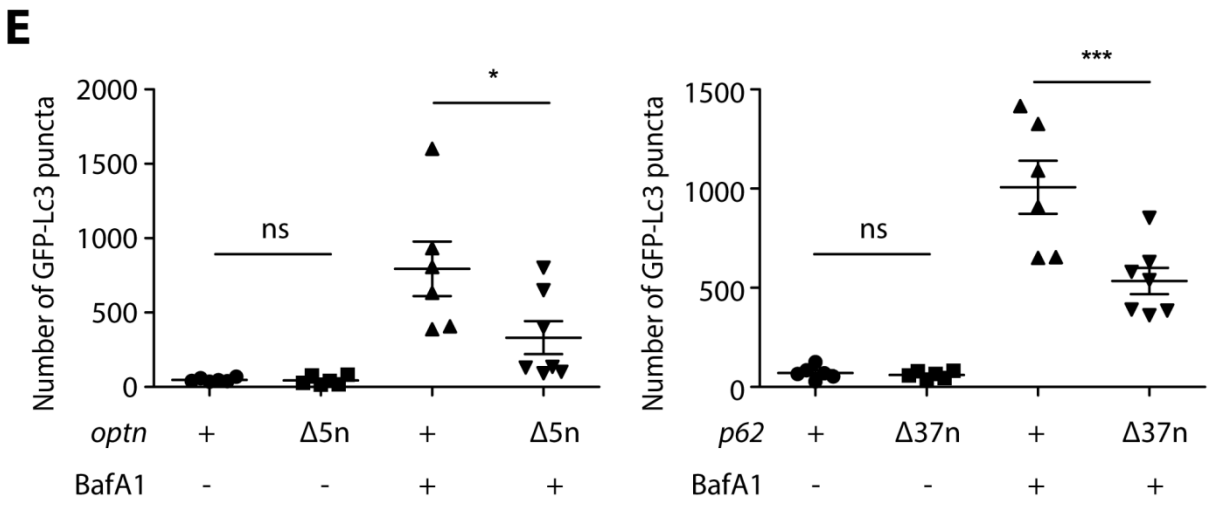

Figure 3: Optineurin or p62 deficiency affects autophagosome formation

A. Workflow of the experiments shown in (B-G). 3.5 dpf larvae were treated with Bafilomycin A1 (Baf A1) (100 nM) for 12h. The GPF-Lc3 negative larvae were selected to assay autophagy activity by WB, the GFP-Lc3 positive larvae were collected to monitor autophagic activity using confocal imaging. The red square indicates the region for confocal imaging.

B. The level of basal autophagy in WT and mutant embryos in absence or presence of Baf A1. Protein samples were extracted from 4 dpf WT and mutant larvae (>10 embryos/sample). The blots were probed with antibodies against Lc3 and Actin as a loading control. WBs were repeated at least three times with independent extracts.

C. Quantification of Lc3-II fold changes in WT and mutant embryos in absence or presence of Baf A1. WB band intensities were quantified by Lab Image. Data is combined from three independent experiments.

D. Representative confocal micrographs of GFP-Lc3 puncta present in the tail fin of *optn*$^{+/+}$, *optn*$^{\Delta 5n/\Delta 5n}$, *p62*$^{+/+}$ and *p62*$^{\Delta 37n/\Delta 37n}$ at 4 dpf. Scale bars, 10 µm.

E. Quantification of the number of GFP-Lc3 puncta in *optn*$^{+/+}$, *optn*$^{\Delta 5n/\Delta 5n}$, *p62*$^{+/+}$ and *p62*$^{\Delta 37n/\Delta 37n}$ larvae with and without Baf A1 treatment. Each larva was imaged at a pre-defined region of the tail fin (as indicated by the red boxed area in Fig3 A) (≥6 larvae/group). Results are representative of two independent experiments.

Optineurin or p62 deficiencies increase the susceptibility of zebrafish embryos to Mm infection

Next, we asked if *optn* or *p62* mutations would affect the resistance of zebrafish embryos to mycobacterial infection. We injected Mm into embryos via the caudal vein at 28 hpf to measure infection burden at 3 dpi (Fig4 A). The infection data showed that *optn* or *p62* mutant embryos

were hypersusceptible to Mm infection compared with their WT controls, culminating in an increase of the Mm fluorescent signal of 2.8 and 2.9 times, respectively (Fig4 B). In addition, we examined whether transient knockdown of *optn* or *p62* would phenocopy the infection phenotype of the mutant lines. We injected *optn* or *p62* antisense morpholino oligonucleotides into the one cell stage of embryos and collected injected individuals at 28h for confirmation of the knockdown effect by reverse transcription polymerase chain reaction (RT-PCR) and Western blot (S3A Fig , S3B Fig and S3C Fig). Subsequently, analysis of the Mm infection burden at 3 dpi showed that transient knockdown of *optn* or *p62* led to similar increases of the Mm infection burden as had been observed in the mutant lines (Fig4 C). Since Optineurin and p62 are known to function cooperatively in xenophagy of *Salmonella enterica* [22-24], we asked if double deficiency of Optineurin and p62 resulted in an increased infection burden compared to single mutation of either *optn* or *p62*. No additive effect on the infection burden was observed when *p62* morpholino was injected into *optn* mutant embryos or *optn* morpholino into *p62* mutant embryos (Fig4 D). Taken together, our data demonstrate that both Optineurin and p62 are required for controlling Mm infection and that loss of either of these ubiquitin receptors cannot be compensated for by the other receptor in this context.

Figure 4: Optineurin or p62 deficiency leads to increased susceptibility to Mm infection (Figure on next page)

A. Workflow of the experiments shown in (B-D). *optn* or *p62* MO were injected into the one cell stage of embryos and infection was performed at 28 hpf with 200 CFU of Mm via blood island microinjection. Bacterial quantification was done at 3dpi.

B-D. Mm infection burden in *optn* and *p62* mutant larvae (B), under *optn* and *p62* MO knockdown conditions (C), and following injection of p62 MO or optn MO in *optn* and *p62* mutants, respectively (D). The data are accumulated from three independent infection experiments. Each dot represents an individual larva. ns, non-significant,*p<0.05,**p<0.01,***p<0.001.

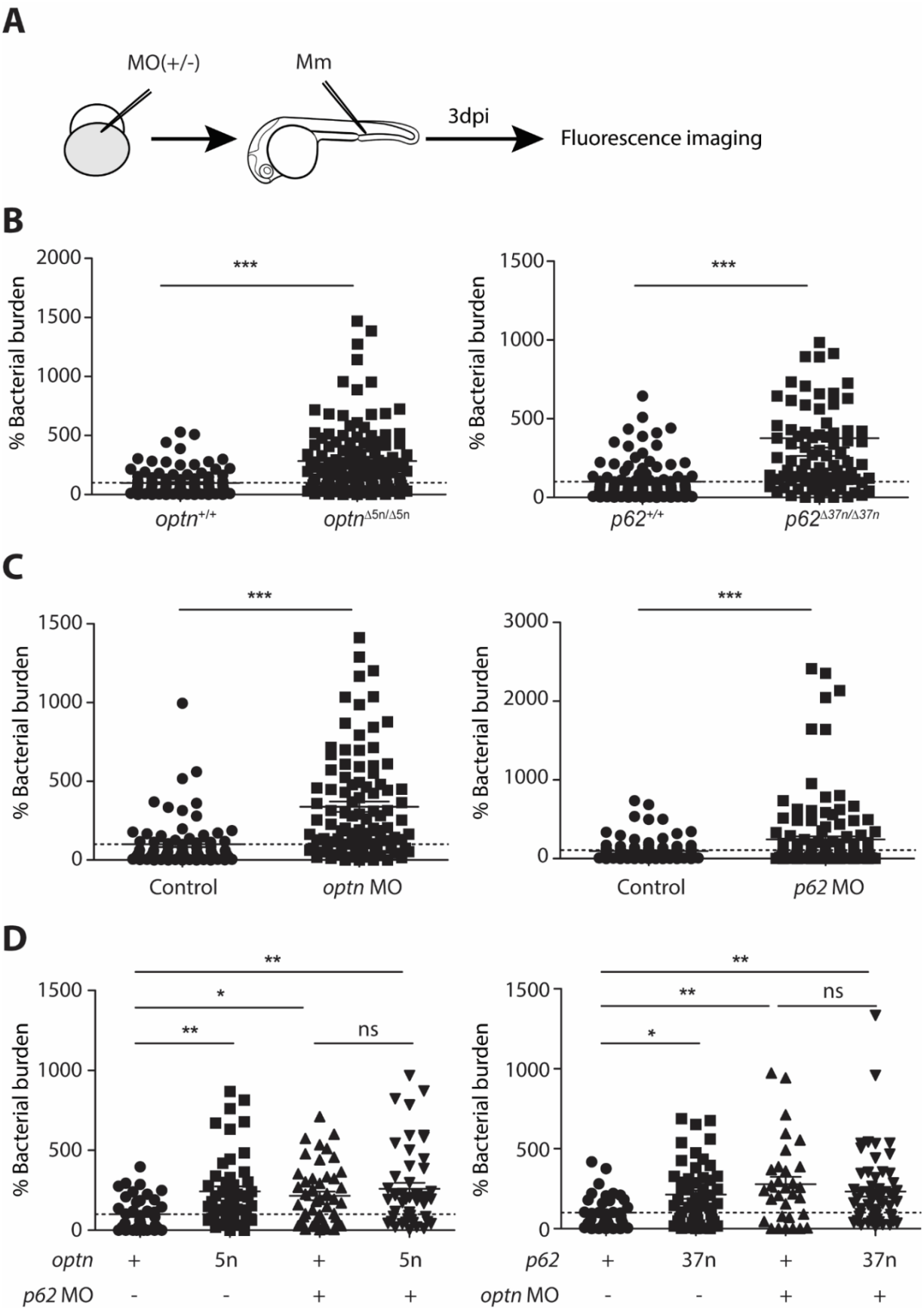
A
MO(+/-)
Mm
3dpi
Fluorescence imaging
B
% Bacterial burden
2000
1500
1000
500
0
***
optn+/+
optnΔ5n/Δ5n
1500
1000
500
0
***
p62+/+
p62Δ37n/Δ37n
C
% Bacterial burden
1500
1000
500
0
***
Control
optn MO
3000
2000
1000
0
***
Control
p62 MO
D
% Bacterial burden
1500
1000
500
0
**
*
**
ns
optn + 5n + 5n
p62 MO - - + +
1500
1000
500
0
**
**
ns
*
p62 + 37n + 37n
optn MO - - + +

Optineurin or p62 deficiency reduces the autophagy response to Mm infection

Having established that mutation of either *optn* or *p62* results in increased Mm infection burden, we investigated if the inability of mutant embryos to control infection is due to a reduction in the targeting of mycobacteria to autophagy (Fig5 A). To this end, we first examined the association of GFP-Lc3 with Mm at 1 dpi. Mm has formed small infection foci at this time point, which could be manually scored as positive or negative for GFP-Lc3 association. In wild type embryos 5-6% of these infection foci were positive for GFP-Lc3 (S4A Fig and S4B Fig). The percentage of GFP-Lc3 positive Mm clusters was approximately 50% lower in the *optn* or *p62* mutant embryos compared with their wild type controls, but differences were not statistically significant due to the relatively low number of these GFP-Lc3 association events (S4A Fig and S4B Fig). We continued to examine GFP-Lc3 targeting to Mm at 2 dpi and found that mutation of *optn* or *p62* resulted in significantly decreased GFP-Lc3 co-localization with Mm clusters (Fig5 A, B and C). In addition, we used GFP-Lc3-negative mutant and wild type larvae for Western blot analysis of Lc3-II protein levels in response to infection. We found that Mm infection increased Lc3-II protein levels approximately 3- to 5-fold in wild type ($optn^{+/+}$ amd $p62^{+/+}$) larvae at 3 dpi, whereas this induction level was approximately 50% lower in the *optn* and *p62* mutant larvae (Fig5 D). Mm-infected mutant embryos also showed reduced Lc3-II accumulation in the presence of Baf A1 (S4B Fig). Taken together, these data support the hypothesis that Optineurin and p62 are required for autophagic defense against mycobacterial infection.

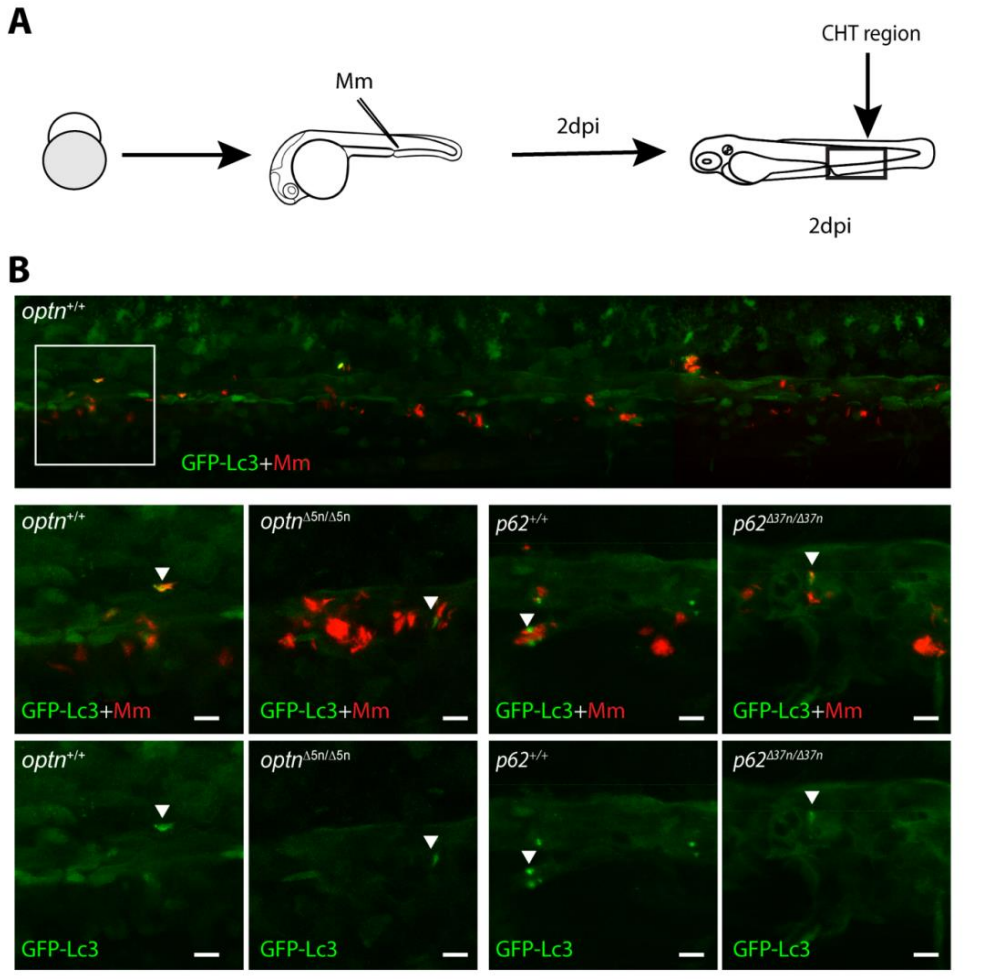
A
Mm
2dpi
CHT region
2dpi
B
optn+/+
GFP-Lc3+Mm
optn+/+
optnΔ5n/Δ5n
p62+/+
p62Δ37n/Δ37n
GFP-Lc3+Mm
GFP-Lc3
C
% Mm clusters GFP-Lc3+
optn+/+
optnΔ5n/Δ5n
p62+/+
p62Δ37n/Δ37n
D
optn + Δ5n + Δ5n
Mm - - + +
Lc3-I 16kDa
Lc3-II 14kDa
Actin 45kDa
Lc3-II/Actin 1 0.81 5.56 2.32
p62 + Δ37n + Δ37n
Mm - - + +
Lc3-I 16kDa
Lc3-II 14kDa
Actin 45kDa
Lc3-II/Actin 1 1.35 3.01 1.52

Figure 5: Optineurin or p62 deficiency inhibits targeting of Mm by GFP-Lc3

A. Workflow of the experiment shown in B. 2 dpi fixed larvae were used for confocal imaging. The entire caudal hematopoietic tissue (CHT) was imaged, as indicated by the black box.

B. Representative confocal micrographs of GFP-Lc3 co-localization with Mm clusters in infected larvae. The top image shows the entire CHT region in *optn*$^{+/+}$ infected larvae. The bottom images show GFP-Lc3 co-localization of Mm clusters in *optn*$^{+/+}$, *optn*$^{\Delta 5n/\Delta 5n}$, *p62*$^{+/+}$ and *p62*$^{\Delta 37n/\Delta 37n}$ infected larvae. The arrowheads indicate the overlap between GFP-Lc3 and Mm clusters. Scale bars, 10 μm.

C. Quantification of the percentage of Mm clusters positive for GFP-Lc3 vesicles. The data is accumulated from two independent experiments; each dot represents an individual larva (≥12 larvae/group). ns, non-significant, *p<0.05,**p<0.01,***p<0.001.

D. Lc3 protein levels were determined by WB in infected and uninfected larvae. Protein samples were extracted from 4 dpf larvae (>10 larvae/sample). The blots were probed with antibodies against Lc3 and Actin as a loading control. WBs were repeated two times with independent extracts.

Overexpression of *optn* or *p62* increases resistance of zebrafish embryos to Mm infection

To further test the hypothesis that Optineurin and p62 mediate autophagic defense against Mm, we generated full-length *optn* and *p62* mRNAs *in vitro* and injected these into embryos at the one cell stage, resulting in ubiquitous overexpression (Fig6 A). The increase in Optineurin or p62 protein levels following mRNA injection was verified by Western blot analysis (Fig6 B) and no effects of overexpression on embryo survival or development were observed (data not shown). Overexpression of *optn* or *p62* mRNAs significantly reduced Mm infection burden at 2 or 3 dpi compared to the control groups (Fig6 C and S5A Fig). Furthermore, injection of *optn* or *p62* mRNAs carrying deletions in the sequences encoding the ubiquitin binding domains or Lc3 interaction regions did not lead to a reduction of the Mm infection burden compared with the control groups (Fig6 C). Thus, we conclude that *optn* or *p62* overexpression protects against Mm infection in a manner dependent on the interaction of the Optn and p62 proteins with both ubiquitin and Lc3.

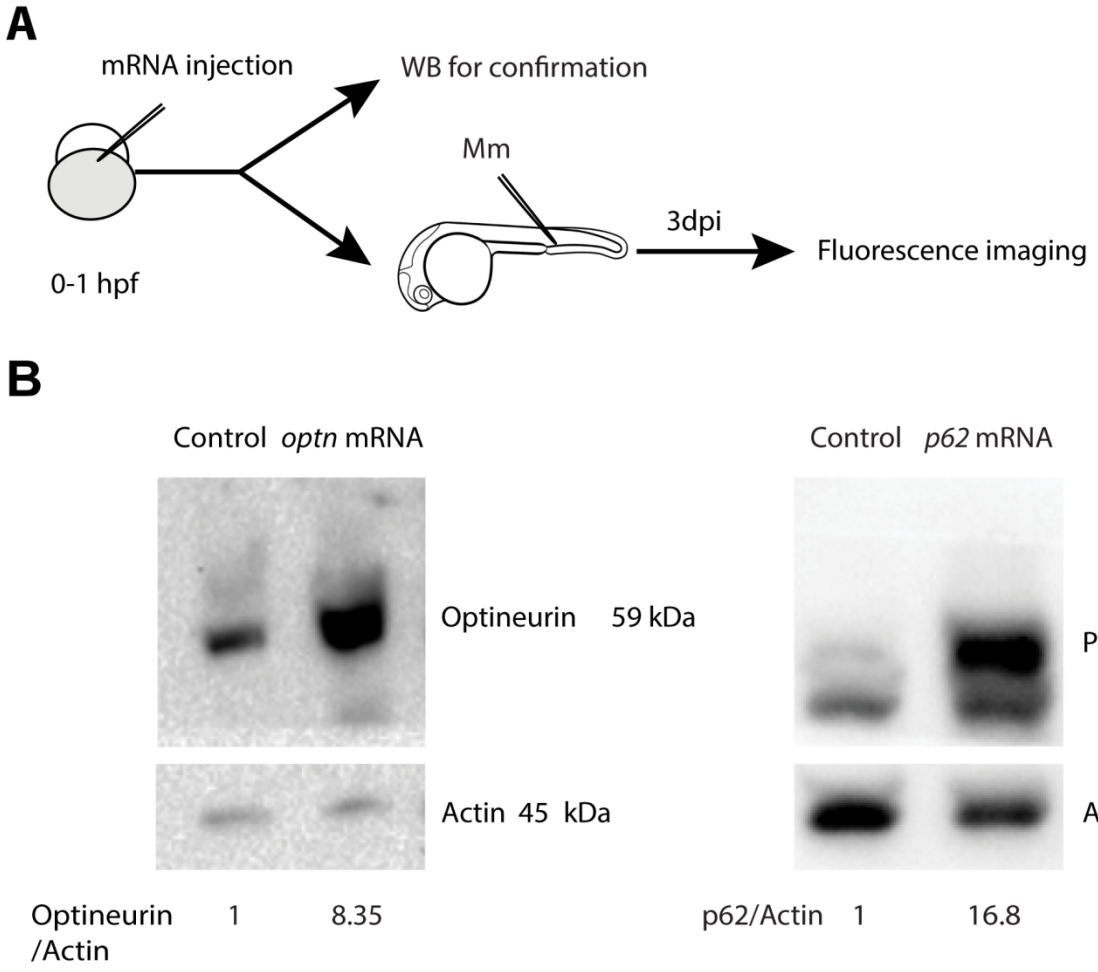
A
mRNA injection
WB for confirmation
Mm
3dpi
Fluorescence imaging
0-1 hpf
B
Control optn mRNA
Optineurin 59 kDa
Actin 45 kDa
Optineurin /Actin 1 8.35
Control p62 mRNA
P62 55 kDa
Actin 45 kDa
p62/Actin 1 16.8
C
***
ns
ns
% Bacterial burden
600
400
200
0
optn mRNA - - - +
optnΔLIR - + - -
optnΔUBAN - - + -
*
ns
ns
p62 mRNA - - - +
p62ΔLIR - + - -
p62ΔUBAN - - + -

Figure 6: Transient overexpression *optn* or *p62* mRNA protects against Mm infection

A. Workflow representing the experimental design in (B-C). *optn* or *p62* mRNA was injected into the one cell stage of embryos (*AB/TL*) at a dosage of 100 pg/embryo. Injected embryos were collected at 28 hpf for confirmation of the overexpression by WB analysis. Embryos were infected at 28hpf with 200 CFU Mm via the blood island by microinjection and bacterial burden was determined at 3 dpi.

B. Western blot analysis to test the effect of transient overexpression of *optn* or *p62* mRNA. Protein extracts were made from >20 mRNA-injected or control embryos per group. The blots were probed with antibodies against Optineurin or p62 and Actin as a loading control. Similar results were observed in two independent experiments.

C. Quantification of Mm infection burden in embryos injected with full length or ΔLIR/ΔUBAN deletion mRNAs of *optn* and *p62*. Accumulated data from two independent infection experiments is shown. ns, non-significant,*p<0.05,**P<0.01,***p<0.001.

Overexpression of *optn* or *p62* promotes GFP-Lc3 association with Mm

Since overexpression of *optn* or *p62* mRNAs resulted in decreased Mm infection burden, we postulated that elevation of the Optn or p62 protein levels would result in increased targeting of Mm to autophagy by these ubiquitin receptors, in a manner dependent on the functions of the Lc3 interaction (LIR) and ubiquitin binding domains (UBAN/UBA)**.** To test this hypothesis, we injected the full-length mRNAs, or mRNAs generated from deletion constructs lacking these domains, and quantified GFP-Lc3-positive and GFP-negative Mm infection foci at 1 dpi and 2 dpi (S6A Fig and Fig7 A). The results showed that overexpression of full-length *optn* or *p62* mRNAs significantly increased the percentage of GFP-Lc3-positive Mm clusters at 2 dpi, compared with the control groups (Fig7 B and Fig7 C). Conversely, injection of *optn* ΔUBAN, *optn* ΔLIR, *p62* ΔUBA and *p62* ΔLIR mRNAs did not increase the association of GFP-Lc3 with Mm clusters (Fig7 B and Fig7 C). Similar results could be observed as early as 1 day post infection (S6B Fig). In conclusion, our combined results demonstrate that Optineurin and p62 can target Lc3 to Mm and that increasing the level of either of these receptors promotes host defense against this mycobacterial pathogen.

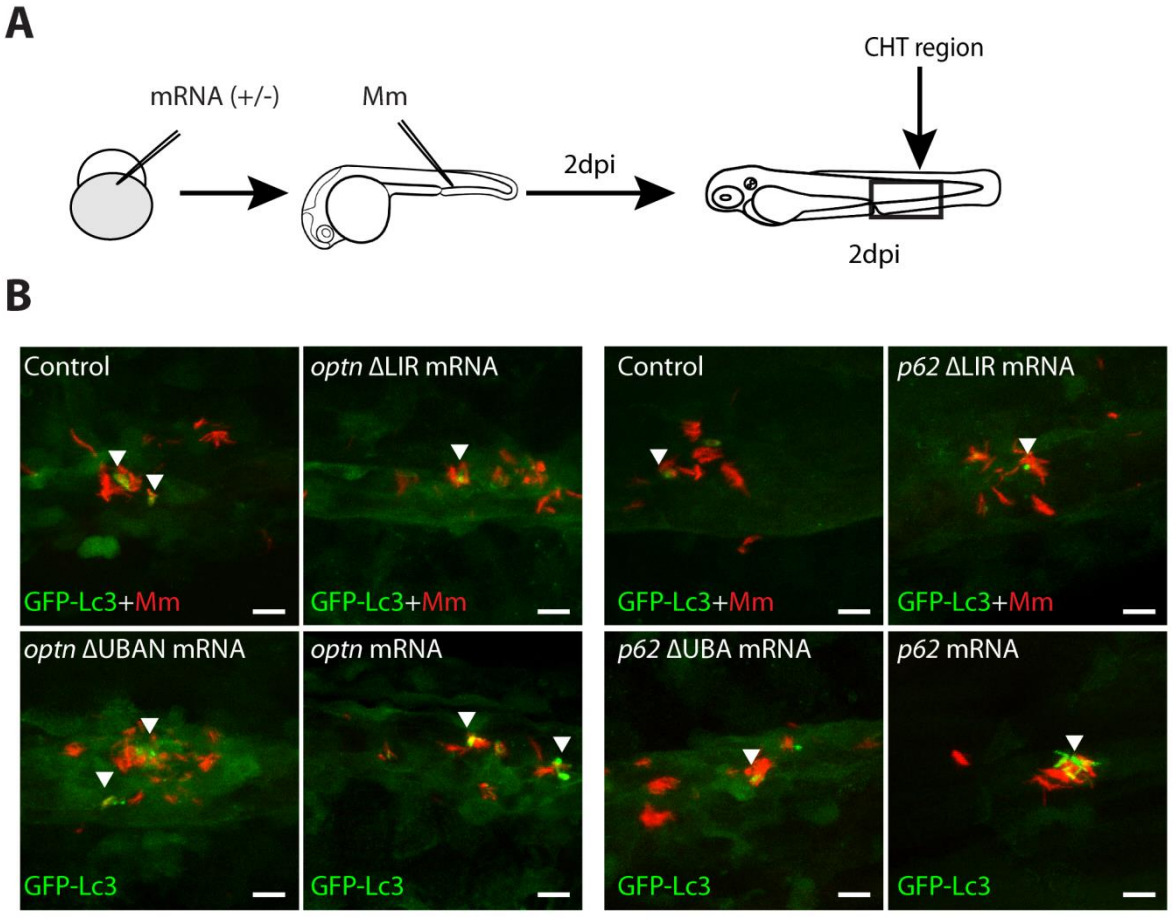
A
mRNA (+/-)
Mm
2dpi
CHT region
2dpi
B
Control
optn ΔLIR mRNA
Control
p62 ΔLIR mRNA
GFP-Lc3+Mm
GFP-Lc3+Mm
GFP-Lc3+Mm
GFP-Lc3+Mm
optn ΔUBAN mRNA
optn mRNA
p62 ΔUBA mRNA
p62 mRNA
GFP-Lc3
GFP-Lc3
GFP-Lc3
GFP-Lc3
C
% Mm clusters GFP-Lc3+
60
40
20
0
*
ns
ns
optn mRNA - - - +
optn ΔLIR - + - -
optn ΔUBAN - - + -
% Mm clusters GFP-Lc3+
40
30
20
10
0
*
ns
ns
p62 mRNA - - - +
p62 ΔLIR - + - -
p62 ΔUBAN - - + -

Figure 7: Transient overexpression of *optn* or *p62* mRNA promotes GFP-Lc3 recruitment to Mm clusters

A. Workflow of the experiments in (B-C). *optn* or *p62* mRNA was injected into the one cell stage of embryos at a dosage of 100 pg/embryo. 2 dpi fixed larvae were used for confocal imaging. The entire caudal hematopoietic tissue (CHT) was imaged, as indicated by the black box.

B. Representative confocal micrographs of GFP-Lc3 co-localization with Mm clusters in larvae injected with full length or ΔLIR/ΔUBAN deletion mRNAs of *optn* and *p62*. The arrowheads indicate the overlap between GFP-Lc3 and Mm clusters. Scale bars, 10 μm.

C. Quantification of the percentage of Mm clusters positive for GFP-Lc3 vesicles. Each dot represents an individual larva (≥7 larvae/group). ns, non-significant,*p<0.05,**P<0.01, *** p<0.001.

Discussion

Members of the family of sequestosome (p62/SQSTM1)-like receptors (SLRs) function in autophagic host defense mechanisms targeting a range of intracellular pathogens, including *Salmonella, Shigella*, *Streptococci*, *Listeria*, *Mycobacteria*, and Sindbis virus [5,13,14,33]. These discoveries inspired investigations into autophagy modulators as host-directed therapeutics for treatment of infectious diseases, including Tb [9,34,35]. However, the relevance of autophagic defense mechanisms for host resistance against Mtb infection has recently been questioned [15,36]. This indicates that there are significant gaps in our understanding of the interaction between components of the autophagy pathway and mycobacterial pathogens, emphasizing the need for more research in animal models of Tb [12]. Here, we have studied the function of two SLR family members in the zebrafish Tb model. We show that selective autophagy mediated by p62 and Optineurin provides resistance against mycobacterial infection in the context of our *in vivo* infection model that is representative of the early stages of Tb granuloma formation [17,19]. Our findings support the host-protective role of p62 in Tb by autophagic targeting of *Mycobacteria*, in line with previous *in vitro* studies [13,14]. Importantly, we also present the first evidence linking Optineurin to resistance against *Mycobacteria*, expanding our understanding of the function of SLRs in host defense against intracellular pathogens.

The zebrafish embryo and larval Tb model provides the opportunity to image critical stages of the mycobacterial infection process, from the initial phagocytosis of Mm by macrophages up to the early stages of Tb granuloma formation [37]. The model is representative of miliary Tb, where

the infection is disseminated to multiple organs of the host. The embryonic and larval stages of the zebrafish allow us to study the contribution of innate immunity to host defense, since they lack a matured adaptive immune response at this time point of development [17]. We therefore used this model to study the importance of autophagic defense mechanisms during innate host defense against mycobacterial infections. In this study, we successfully generated *p62* and *optn* loss-of-function zebrafish mutant lines using CRISPR/Cas9 technology. Besides its role in host defense, p62 is a stress-inducible protein that functions as a signalling hub in diverse processes like amino acid sensing and the oxidative stress response [38]. Defects in autophagy pathways caused by mutations in *OPTN* have been associated with human disorders like glaucoma, Paget disease of bone, and amyotrophic lateral sclerosis [24,39]. Despite the important functions reported for p62 and Optineurin in cellular homeostasis, the mutant fish lines we generated are viable and fertile. The absence of either p62 or Optineurin resulted in increased use of the other ubiquitin receptor to sequester autophagic cargo in zebrafish larvae. Nonetheless, loss of either of the receptors leads to lower levels of Lc3-II and GFP-Lc3 accumulation when lysosomal degradation is blocked, which indicates reduced activity of the autophagy pathway in these mutants. Therefore, we could use these mutant lines to gain a better understanding of the role of p62, Optineurin, and selective autophagy in host defense against mycobacterial infection.

Genetic links between autophagy pathway genes and susceptibility to Tb in human populations support the function of autophagy in innate host defense against Mtb [40]. However, the contribution of autophagy as a direct anti-mycobacterial mechanism has recently been challenged, since macrophage-specific depletion of a number of autophagy genes, including *p62*, did not affect the outcome of disease in a mouse model of Tb [15,36]. A possible explanation for these findings, as suggested by the authors of this study, is that Mtb, like other successful intracellular pathogens, could have evolved virulence mechanisms that subvert or exploit autophagic defense mechanisms employed by the host [41]. In case of one of the autophagy genes, ATG5, macrophage-specific depletion increased Mtb infection in mice by over-activating inflammation rather than by impairing autophagic processes [15]. It is therefore conceivable that modulating the activity of SLRs could also affect inflammation. Indeed, Optineurin has been implicated in inflammatory bowel disease and both p62 and Optineurin are involved in

regulation of inflammatory signaling downstream of NF-κB [42-46]. Through a process that involves polyubiquitination of regulatory proteins, both p62 and Optineurin can modulate the activity of the IKK kinase complex that activates NFκB [42,43]. It is therefore possible that altered inflammatory responses in *p62* and *optn* mutants could explain (part of) the increase in mycobacterial burden observed in zebrafish hosts, while the beneficial role for autophagic defense mechanisms targeting the bacteria might be limited.

To investigate the possible role of Optineurin and p62 in anti-mycobacterial autophagy, we quantified the association between GFP-Lc3 and Mm under loss-of-function and gain-of-function conditions of both receptors. In wild type zebrafish embryos, only 3-5% of the bacteria co-localized with autophagic vesicles one day after a systemic infection with mycobacteria. Although the number of GFP-Lc3 positive bacterial clusters rises over the next two days, the percentage of bacteria targeted by autophagy at any distinct time point remains relatively low (e.g. ~10% at 2 days post infection). According to these results, the host only employs autophagic defense mechanisms against a small proportion of the invading mycobacteria during early stages of the infection, either because there is no greater need, or because the pathogens are indeed effectively suppressing this response. It is important to note though that GFP-Lc3 association with Mm is a transient process [20], which means that the percentage of bacteria that encounter autophagic defenses throughout the early infection process might be much higher. Strikingly, the percentage of bacteria labeled by ubiquitin closely resembled the percentage of bacteria targeted by autophagy, and we were able to detect clear colocalization between ubiquitin and GFP-Lc3 at bacterial clusters. Upon loss-of-function of either p62 or Optineurin, the co-localization between bacteria and autophagic vesicles decreased and the bacterial burden increased. Conversely, overexpression of either ubiquitin binding receptor increased autophagic targeting of bacteria and resulted in lower bacterial burdens, both of which required the presence of functional Lc3 and ubiquitin binding domains. Taken together, we conclude that autophagic targeting of mycobacteria by p62 and Optineurin indeed provides protection against infection in our *in vivo* Tb model.

In summary, our findings confirm that p62 mediates ubiquitin-dependent autophagic targeting of mycobacteria in an *in vivo* model for Tb. We also provide the first evidence that the SLR family member Optineurin is involved in autophagic targeting of ubiquitinated mycobacteria. While we cannot exclude a role for p62 and Optineurin in regulating inflammatory processes during Tb disease progression, we have shown that the autophagic targeting of mycobacteria by these ubiquitin-binding receptors forms an important aspect of innate host defense against Tb. Our results are therefore especially important for the development of new treatment strategies for Tb patients with a compromised adaptive immune system – such as in HIV-coinfection. Based on these results, selective autophagy stimulation remains a promising strategy for development of novel anti-Tb therapeutics.

Materials and methods

Zebrafish culture and lines

Zebrafish lines in this study (S1 Table) were handled in compliance with local animal welfare regulations as overseen by the Animal Welfare Body of Leiden University (License number:10612) and maintained according to standard protocols (zfin.org). All protocols adhered to the international guidelines specified by the EU Animal Protection Directive 2010/63/EU. Embryos were grown at 28.5°C and kept under anesthesia with egg water containing 0.02% buffered 3-aminobenzoic acid ethyl ester (Tricaine, Sigma) during bacterial injections, imaging and fixation.

CRISPR/Cas9 mediated mutagenesis of zebrafish *optn* and *p62*

Single guide RNAs (sgRNAs) targeting the second coding exon of zebrafish *optn* (ENSDART00000014036.10) and the third coding exon of *p62 (*ENSDART00000140061.2) were designed using the chop-chop website [47]. To make sgRNAs, the template single strand DNA (ssDNA) (122 bases) was obtained by PCR complementation and amplification of full length ssDNA oligonucleotides. Oligonucleotides up to 81 nucleotides were purchased from Sigma-Aldrich using standard synthesis procedures (25 nmol concentration, purification with desalting

method) (S2 Table and S3 Table). The pairs of semi-complimentary oligos were annealed together by a short PCR program (50 µL reaction, 200uM dTNPs, 1 unit of Dream Taq polymerase (EP0703, ThermoFisher); PCR program: initial denaturation 95°C/3 minute (min), 5 amplification cycles 95°C/30 Second (s), 55°C/60 s, 72°C/30 s, final extension step 72°C/15 min) and subsequently the products were amplified using the primers in S2 Table with a standard PCR program (initial denaturation 95°C/3 min, 35 amplification cycles 95°C/30 s,55°C/60 s, 72°C/30 s, final extension step 72°C/15 min). The final PCR products were purified with Quick gel extraction and PCR purification combo kit (00505495, ThermoFisher). The purified PCR products were confirmed by gel electrophoresis and Sanger sequencing (Base Clear, Netherlands). For *in vitro* transcription of sgRNAs, 0.2 µg template DNA was used to generate sgRNAs using the MEGA short script ®T7 kit (AM1354, ThermoFisher) and purified by RNeasy Mini Elute Clean up kit (74204, QIAGEN Benelux B.V., Venlo, Netherlands). The Cas9 mRNA was transcribed using mMACHINE® SP6 Transcription Kit (AM1340, Thermo Fisher) from a Cas9 plasmid (39312, Addgene) (Hrucha et al 2013) and purified with RNeasy Mini Elute Clean up kit (74204,QIAGEN Benelux B.V., Venlo, Netherlands). A mixture of sgRNA and Cas9 mRNA was injected into one cell stage AB/TL embryos (sgRNA 150 pg/embryo and Cas9 mRNA 300 pg/embryo). The effect of CRISPR injection was confirmed by PCR and Sanger sequencing.

Genomic DNA isolation and genotyping

Genomic DNA was isolated from an individual embryo (2 dpf) or small pieces of the tail fin tissue of adults (>3 months) by fin clipping. Embryos or tissue samples were incubated in 200 µL 100% Methanol at -20°C overnight (O/N), then methanol was removed, and remaining methanol was evaporated at 70°C for 20 min. Next, samples were incubated in 25 µL of TE buffer containing 1.7 µg/µL proteinase K at 55°C for more than 5 h. Proteinase K was heat inactivated at 80°C for 30 min, after which samples were diluted with 100 µL of Milli-Q water. Genotyping was performed by PCR-amplification of the region of interest using the primers in S5 Table followed by Sanger sequencing to identify mutations (Base Clear, Netherlands).

Western blot analysis

Embryos (28hpf/2dpf/4dpf/3dpi) were anaesthetised with Tricaine (Lot#MKBG4400V, SIGMA-ALDRICH) and homogenised with a Bullet-blender (Next-Advance) in RIPA buffer (#9806, Cell Signalling) containing a protein inhibitor cocktail (000000011836153001, cOmplete, Roche). The extracts were then spun down at 4°C for 10 min at 12000 rpm/min and the supernatants were frozen for storage at −80°C. Western blot was performed using Mini-PROTEAN-TGX (456-9036, Bio-Rad) or 18% Tris—Hcl 18% polyacrylamide gels, and protein transfer to commercial PVDF membranes (Trans-Blot Turbo-Transfer pack, 1704156, Bio-Rad). Membranes were blocked with 5% dry milk (ELK, Campina) in Tris buffered saline (TBS) solution with Tween 20 (TBST, 1XTBS contains 0.1% Tween 20) buffer and incubated with primary and secondary antibodies. Digital images were acquired using Bio-Rad Universal Hood II imaging system (720BR/01565 UAS). Band intensities were quantified by densitometric analysis using Image Lab Software (Bio-Rad, USA) and values were normalised to actin as a loading control. Antibodies used were as follows: polyclonal rabbit anti-Optineurin (C-terminal) (1:200, lot#100000; Cayman Chemical), polyclonal rabbit anti-p62 (C-terminal) (PM045, lot#019, MBL), polyclonal rabbit anti Lc3 (1:1000, NB100-2331, lot#AB-3, Novus Biologicals), Anti mono-and polyubiquitinated conjugates mouse monoclonal antibody (1:200; BML-PW8810-0100, lot#01031445, Enzo life Sciences), Polyclonal actin antibody (1:1000, 4968S, lot#3, Cell Signaling), Anti-rabbit IgG, HRP-Linked Antibody (1:1000, 7074S, Lot#0026, Cell Signaling), Anti-mouse IgG, HRP-linked Antibody (1:3000, 7076S, Lot#029, Cell Signaling).

Morpholino design and validation

optn and *p62* splice blocking morpholinos were purchased from Gene Tools. For morpholino sequences see S4 Table. Morpholinos were diluted in Milli Q water with 0.05% phenol red and 1 nL of 0.1 mM *optn* or 0.5 mM p62 Morpholino was injected into the one cell stage of embryos as previously described [21]. The knockdown effect was validated by RT-PCR and Western blot.

Infection conditions and bacterial burden quantification

Mycobacterium marinum strain 20 bacteria, fluorescently labelled with mCherry, were microinjected into the blood island of embryos at 28 hpf as previously described [48]. The injection dose was 200 CFU for all experiments. Before the injection, embryos were manually dechorionated around 24hpf. Approximately 5 min before bacterial injections, zebrafish embryos were brought under anaesthesia with tricaine. Infected embryos were imaged using a Leica MZ16FA stereo fluorescence microscopy with DFC420C camera, total fluorescent bacterial pixels per infected fish were determined on whole-embryo stereo fluorescent micrographs using previously described software [49] .

Confocal laser scanning microscopy and image quantification

Fixed or live embryos were mounted with 1.5% low melting agarose (140727, SERVA) and imaged using a Leica TCS SPE confocal microscope. For quantification of basal autophagy, fixed uninfected 4dpf larvae were imaged by confocal microscopy with a 63x water immersion objective (NA 1.2) in a pre-defined region of the tail fin to detect GFP-LC3-positive vesicles (Fig3 D and Fig3 E). The number of GFP-Lc3 vesicles per condition was quantified using Fiji/ImageJ software (Fig3 D and Fig3 E). For quantification of the autophagic response targeted to Mm clusters (Fig1 B and C, S4A Fig and B, S6A Fig and B), live or fixed infected embryos were viewed by confocal microscopy with a 63x water immersion objective (NA 1.2) and the number of Mm clusters that were targeted by GFP-Lc3 puncta in the tail region were counted manually. The same approach was used to quantify Ubiquitin targeting to Mm clusters (Fig1 E and F). To quantify the percentage of GFP-Lc3^{+} Mm clusters, we imaged the entire caudal hematopoietic tissue (CHT) region of 2 dpi larvae (confocal microscopy; 40X water immersion objective with NA 1.0) and stitched multiple images together to manually count the number of Mm clusters positive for GFP-Lc3 out of the total number of clusters (Fig5 B and C, Fig7 B and C) .

Immunostaining

Embryos (1,2,3 dpi) were fixed with 4% PFA in PBS and incubated overnight with shaking at 4°C. After washing the embryos three times briefly in (PBS with triton-100) PBSTx, the embryos/larvae were digested in 10 µg/ml proteinase K (000000003115879001, SIGMA-ALDRICH) for 10 minutes at 37°C. Subsequently, the embryos were quickly washed, blocked with PBSTx containing 1% Bovine serum albumins (BSA) (A4503-100g, SIGMA-ALDRICH) for 2h at room temperature and incubated overnight at 4°C in mono-and polyubiquitinated conjugates mouse monoclonal antibody (1:200; BML-PW8810-0100; Enzo lifes Siences), diluted in the blocking buffer. Next, embryos were washed three times in PBSTx, incubated for 1 h in blocking buffer at room temperature, incubated for 2 h at room temperature in 1:200 dilution of Alexa Fluor 488 or 633 goat anti-mouse (Invitrogen) in blocking buffer, followed with three times washes in PBSTx for imaging.

mRNA preparation and injection

optn (ENSDART00000014036.10, Ensembl) and *p62* (ENSDART00000140061.2, Ensembl) cDNAs were amplified from 3dpf AB/TL embryos by PCR (primers in S5 Table) and ligated into a vector using the Zero-blunt cloning PCR kit (450245, Invitrogen). The sequence was confirmed by Sanger sequencing (BaseClear, Netherlands), after which *optn* and *p62* cDNAs were subcloned into a pCS2+ expression vector.

optn ΔUBAN cDNA was produced by in vitro transcription of *optn*–pCS2+ constructs digested by Sca1(R3122, NEB), which excludes the region encoding the UBAN protein domain.

optn ΔLIR cDNA was amplified from *optn*-pCS2+ constructs by designed primers (S5 Table), excluding the LIR protein domain. The PCR products were gel purified by Quick gel Extraction PCR Purification Combo Kit (K220001,Invitrogen) and the two fragments and pCS2+ plasmid were digested by BamH1(R0136S,NEB) and EcoR1(R0101S,NEB), after which the two fragments were ligated into pCS2+ plasmid by T4 DNA ligase.

p62 ΔUBA cDNA was obtained from a *p62*-pCS2+ construct by Nco1(R0193S, NEB) digestion and religation, which excludes the region encoding the UBA protein domain.

p62 ΔLIR cDNA was obtained from a *p62*-pCS2+ construct by NcoN1 digestion and religation.

Optn mRNA,*optn* ΔUBAN, and *optn* ΔLIR mRNA was generated using SP6 mMessage mMachine kit (Life Technologies) from Kpn1 or Sac1(R0156S, NEB) digested *optn*–pCS2+ constructs. RNA purification was performed using the RNeasy Mini Elute Clean up kit (QIAGEN Benelux B.V., Venlo, Netherlands).

In vitro transcription of *p62*, *p62* ΔUBA, and *p62* ΔLIR was performed using mMESSAGE mMACHINE® T3 Transcription Kit (AM1348, Thermo Fisher) and purified using the RNeasy MiniElute Cleanup kit (QIAGEN Benelux B.V., Venlo, Netherlands). All mRNAs were injected into one cell stage embryos, and the overexpression effects of *optn* or *p62* were validated by Q-PCR and Western blot.

Gene Expression Analysis

Total RNA was extracted using Trizol reagent (15596026, Invitrogen) according to the manufacturer's instructions and purified with RNeasy Min Elute Clean up kit (Lot:154015861, QIAGEN). RNAs were quantified using a NanoDrop 2000c instrument (Thermo Scientific, U.S). Reverse transcription reaction was performed using 0.5 µg of total RNA with iScript cDNA synthesis kit (Cat:#170-8891, Bio-Rad). The mRNA expression level was determined by quantitative real-time PCR using iQSYBR Green Supermix (Cat:170-8882, Rio-Rad) and Single color Real-Time PCR Detection System (Bio-Rad, U.S) as previously described [50]. All primers are listed in S5 Table.

Statistical analyses

Statistical analyses were performed using GraphPad Prism software (Version 5.01; GraphPad). All experimental data (mean ± SEM) was analyzed using unpaired, two-tailed t-tests for comparisons between two groups and one-way ANOVA with Tukey's multiple comparison methods as a posthoc test for comparisons between more than two groups. (ns, no significant difference; *$p < 0.05$; **$p < 0.01$; ***$p < 0.001$). To determine whether the offspring of F1

heterozygous mutants follows Mendelian segregation, the obtained data was analysed with a Chi-square test (ns, no significant difference).

Acknowledgement

We thank Daniel Klionsky for sharing of the GFP-Lc3 transgenic zebrafish line. We are grateful to all members of the fish facility team for zebrafish caretaking. We would like to thank Gerda Lamers and Joost Willemse for advice on confocal imaging and image analysis. R.Z. was supported by a grant from the China Scholarship Council (CSC). M.V. and G.C. were funded by European Marie Curie program (H2020-MSCA-IF-2014-655424, MSCA-COFUND-2015-FP, respectively), and MvdV was supported by the Netherlands Organisation for Scientific Research (NWO) Domain Applied and Engineering Sciences (TTW project 13259).

References

1. Ohsumi Y. Historical landmarks of autophagy research. Cell Res. 2014;24(1):9-23.
2. Yang Z, Klionsky DJ. Mammalian autophagy: core molecular machinery and signaling regulation. Curr Opin Cell Biol. 2010;22(2):124-131.
3. Johansen T, Lamark T. Selective autophagy mediated by autophagic adapter proteins. Autophagy. 2014;7(3):279-296.
4. Bradfute SB, Castillo EF, Arko-Mensah J, et al. Autophagy as an immune effector against tuberculosis. Curr Opin Microbiol. 2013;16(3):355-365.
5. Deretic V, Saitoh T, Akira S. Autophagy in infection, inflammation and immunity. Nat Rev Immunol. 2013;13(10):722-737.
6. Mostowy S, Cossart P. Bacterial autophagy: restriction or promotion of bacterial replication? Trends Cell Biol. 2012;22(6):283-291.
7. Ponpuak M, Davis AS, Roberts EA, et al. Delivery of cytosolic components by autophagic adaptor protein p62 endows autophagosomes with unique antimicrobial properties. Immunity. 2010;32(3):329-341.
8. Tiberi S, Buchanan R, Caminero JA, et al. The challenge of the new tuberculosis drugs. Presse Med. 2017;46(2 Pt 2):e41-e51.
9. Kumar D, Nath L, Kamal MA, et al. Genome-wide analysis of the host intracellular network that regulates survival of Mycobacterium tuberculosis. Cell. 2010;140(5):731-743.
10. Gutierrez MG, Master SS, Singh SB, Taylor GA, Colombo MI, Deretic V. Autophagy is a defense mechanism inhibiting BCG and Mycobacterium tuberculosis survival in infected macrophages. Cell. 2004;119(6):753-766.
11. Alonso S, Pethe K, Russell DG, Purdy GE. Lysosomal killing of *Mycobacterium* mediated by ubiquitin-derived peptides is enhanced by autophagy. Proceedings of the National Academy of Sciences. 2007;104:6031-6036.
12. Deretic V. Autophagy in leukocytes and other cells: mechanisms, subsystem organization, selectivity, and links to innate immunity. J Leukoc Biol. 2016;100(5):969-978.
13. Watson RO, Manzanillo PS, Cox JS. Extracellular M. tuberculosis DNA targets bacteria for autophagy by activating the host DNA-sensing pathway. Cell. 2012;150(4):803-815.
14. Manzanillo PS, Ayres JS, Watson RO, et al. The ubiquitin ligase parkin mediates resistance to intracellular pathogens. Nature. 2013;501(7468):512-516.

15. Kimmey JM, Huynh JP, Weiss LA, et al. Unique role for ATG5 in neutrophil-mediated immunopathology during M. tuberculosis infection. Nature. 2015;528(7583):565-569.
16. Ramakrishnan L. Looking Within the Zebrafish to Understand the Tuberculous Granuloma. The New Paradigm of Immunity to Tuberculosis. 2013;83.
17. Meijer AH. Protection and pathology in TB: learning from the zebrafish model. Semin Immunopathol. 2016;38(2):261-273.
18. Davis JMC, Hilary , Lewis JL, Ghori N, Herbomel P, Ramakrishnan L. Real-Time Visualization of Mycobacterium-Macrophage Interactions Leading to Initiation of Granuloma Formation in Zebrafish Embryos. Immunity. 2002;17:693-702.
19. Ramakrishnan L. Revisiting the role of the granuloma in tuberculosis. Nat Rev Immunol. 2012;12(5):352-366.
20. Hosseini R, Lamers GE, Hodzic Z, Meijer AH, Schaaf MJ, Spaink HP. Correlative light and electron microscopy imaging of autophagy in a zebrafish infection model. Autophagy. 2014;10(10):1844-1857.
21. van der Vaart M, Korbee CJ, Lamers GE, et al. The DNA damage-regulated autophagy modulator DRAM1 links mycobacterial recognition via TLR-MYD88 to autophagic defense [corrected]. Cell Host Microbe. 2014;15(6):753-767.
22. Zheng YT, Shahnazari S, Brech A, Lamark T, Johansen T, Brumell JH. The adaptor protein p62/SQSTM1 targets invading bacteria to the autophagy pathway. J Immunol. 2009;183(9):5909-5916.
23. Wild P, Farhan H, McEwan DG, et al. Phosphorylation of the autophagy receptor optineurin restricts Salmonella growth. Science. 2011;333(6039):228-233.
24. Slowicka K, Vereecke L, Mc Guire C, et al. Optineurin deficiency in mice is associated with increased sensitivity to Salmonella but does not affect proinflammatory NF-kappaB signaling. Eur J Immunol. 2016;46(4):971-980.
25. Pilli M, Arko-Mensah J, Ponpuak M, et al. TBK-1 promotes autophagy-mediated antimicrobial defense by controlling autophagosome maturation. Immunity. 2012;37(2):223-234.
26. Seto S, Tsujimura K, Horii T, Koide Y. Autophagy Adaptor Protein p62/SQSTM1 and Autophagy-Related Gene Atg5 Mediate Autophagosome Formation in Response to Mycobacterium tuberculosis Infection in Dendritic Cells. PLOS ONE. 2013;8(12):e86017.
27. Benard EL, Rougeot J, Racz PI, Spaink HP, Meijer AH. Transcriptomic Approaches in the Zebrafish Model for Tuberculosis-Insights Into Host- and Pathogen-specific Determinants of the Innate

Immune Response. Adv Genet. 2016;95:217-251.

28. Davis JM, Ramakrishnan L. The role of the granuloma in expansion and dissemination of early tuberculous infection. Cell. 2009;136(1):37-49.
29. Yang CT, Cambier CJ, Davis JM, Hall CJ, Crosier PS, Ramakrishnan L. Neutrophils exert protection in the early tuberculous granuloma by oxidative killing of mycobacteria phagocytosed from infected macrophages. Cell Host Microbe. 2012;12(3):301-312.
30. He C, Bartholomew CR, Zhou W, Klionsky DJ. Assaying autophagic activity in transgenic GFP-Lc3 and GFP-Gabarap zebrafish embryos. Autophagy. 2009;5(4):520-526.
31. Levitte S, Adams KN, Berg RD, Cosma CL, Urdahl KB, Ramakrishnan L. Mycobacterial Acid Tolerance Enables Phagolysosomal Survival and Establishment of Tuberculous Infection In Vivo. Cell Host Microbe. 2016;20(2):250-258.
32. Yuan N, Song L, Zhang S, et al. Bafilomycin A1 targets both autophagy and apoptosis pathways in pediatric B-cell acute lymphoblastic leukemia. Haematologica. 2015;100(3):345-356.
33. Mostowy S. Autophagy and bacterial clearance: a not so clear picture. Cell Microbiol. 2013;15(3):395-402.
34. Stanley SA, Barczak AK, Silvis MR, et al. Identification of host-targeted small molecules that restrict intracellular Mycobacterium tuberculosis growth. *PLoS Pathog.* 2014;10(2):e1003946.
35. Kolloli A, Subbian S. Host-Directed Therapeutic Strategies for Tuberculosis. Front Med (Lausanne). 2017;4:171.
36. Behar SM, Baehrecke EH. Autophagy is not the answer. NATURE. 2015;528:482-483.
37. Swaim LE, Connolly LE, Volkman HE, Humbert O, Born DE, Ramakrishnan L. Mycobacterium marinum infection of adult zebrafish causes caseating granulomatous tuberculosis and is moderated by adaptive immunity. Infect Immun. 2006;74(11):6108-6117.
38. Katsuragi Y, Ichimura Y, Komatsu M. p62/SQSTM1 functions as a signaling hub and an autophagy adaptor. FEBS J. 2015;282(24):4672-4678.
39. Slowicka K, van Loo G. Optineurin Functions for Optimal Immunity. *Front Immunol.* 2018;9:769.
40. Deretic V. Autophagy in tuberculosis. Cold Spring Harb Perspect Med. 2014;4(11):a018481.
41. Kimmey JM, Stallings CL. Bacterial Pathogens versus Autophagy: Implications for Therapeutic Interventions. Trends Mol Med. 2016;22(12):1060-1076.
42. Zhu G, Wu CJ, Zhao Y, Ashwell JD. Optineurin negatively regulates TNFalpha- induced NF-kappaB activation by competing with NEMO for ubiquitinated RIP. Curr Biol. 2007;17(16):1438-1443.
43. Duran A, Linares JF, Galvez AS, et al. The signaling adaptor p62 is an important NF-kappaB

mediator in tumorigenesis. Cancer Cell. 2008;13(4):343-354.

44. Tschurtschenthaler M, Adolph TE. The Selective Autophagy Receptor Optineurin in Crohn's Disease. Frontiers in Immunology. 2018;9(766).

45. Chew TS, O'Shea NR, Sewell GW, et al. Optineurin deficiency in mice contributes to impaired cytokine secretion and neutrophil recruitment in bacteria-driven colitis. Disease Models & Mechanisms. 2015;8(8):817-829.

46. Smith AM, Sewell GW, Levine AP, et al. Disruption of macrophage pro-inflammatory cytokine release in Crohn's disease is associated with reduced optineurin expression in a subset of patients. Immunology. 2015;144(1):45-55.

47. Labun K, Montague TG, Gagnon JA, Thyme SB, Valen E. CHOPCHOP v2: a web tool for the next generation of CRISPR genome engineering. Nucleic Acids Res. 2016;44(W1):W272-276.

48. Benard EL, van der Sar AM, Ellett F, Lieschke GJ, Spaink HP, Meijer AH. Infection of zebrafish embryos with intracellular bacterial pathogens. J Vis Exp. 2012(61).

49. Stoop EJM, Schipper T, Rosendahl Huber SK, et al. Zebrafish embryo screen for mycobacterial genes involved in the initiation of granuloma formation reveals a newly identified ESX-1 component. Disease Models & Mechanisms. 2011;4(4):526-536.

50. Stockhammer OW, Zakrzewska A, Hegedûs Z, Spaink HP, Meijer AH. Transcriptome Profiling and Functional Analyses of the Zebrafish Embryonic Innate Immune Response to *Salmonella* Infection. The Journal of Immunology. 2009;182(9):5641-5653.

Supplementary data

A

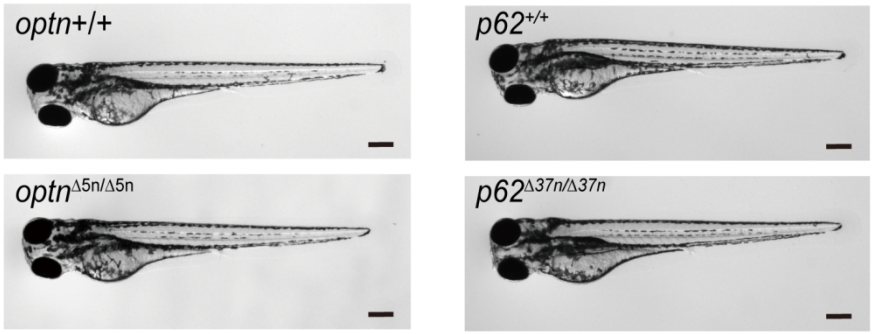

B

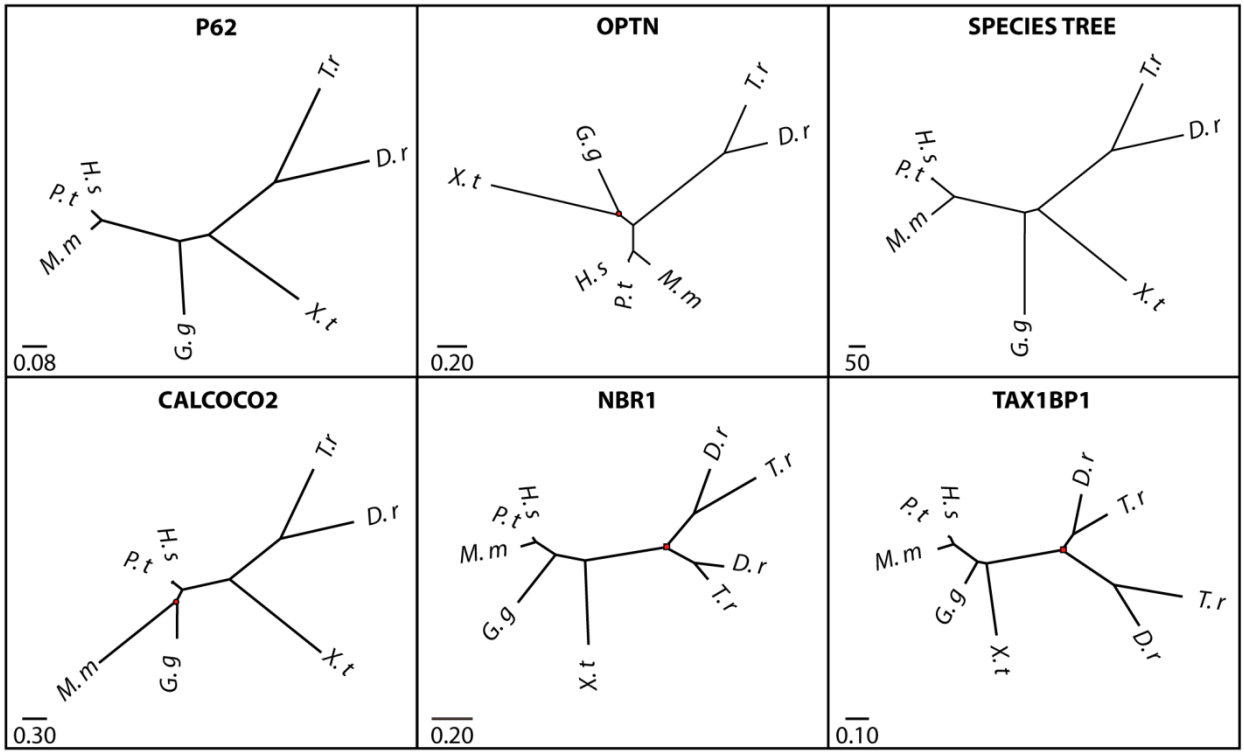

C

Protein	Optineurin	p62	Calcoco2	Tax1bp1a	Tax1bp1b	Nbr1a	Nbr1b
% Identity to human protein	46.99	52.58	34.27	48.99	52.96	43.06	44.87
% Similarity to human protein	45.3	55.65	35.78	56.37	65.13	49.97	49.62

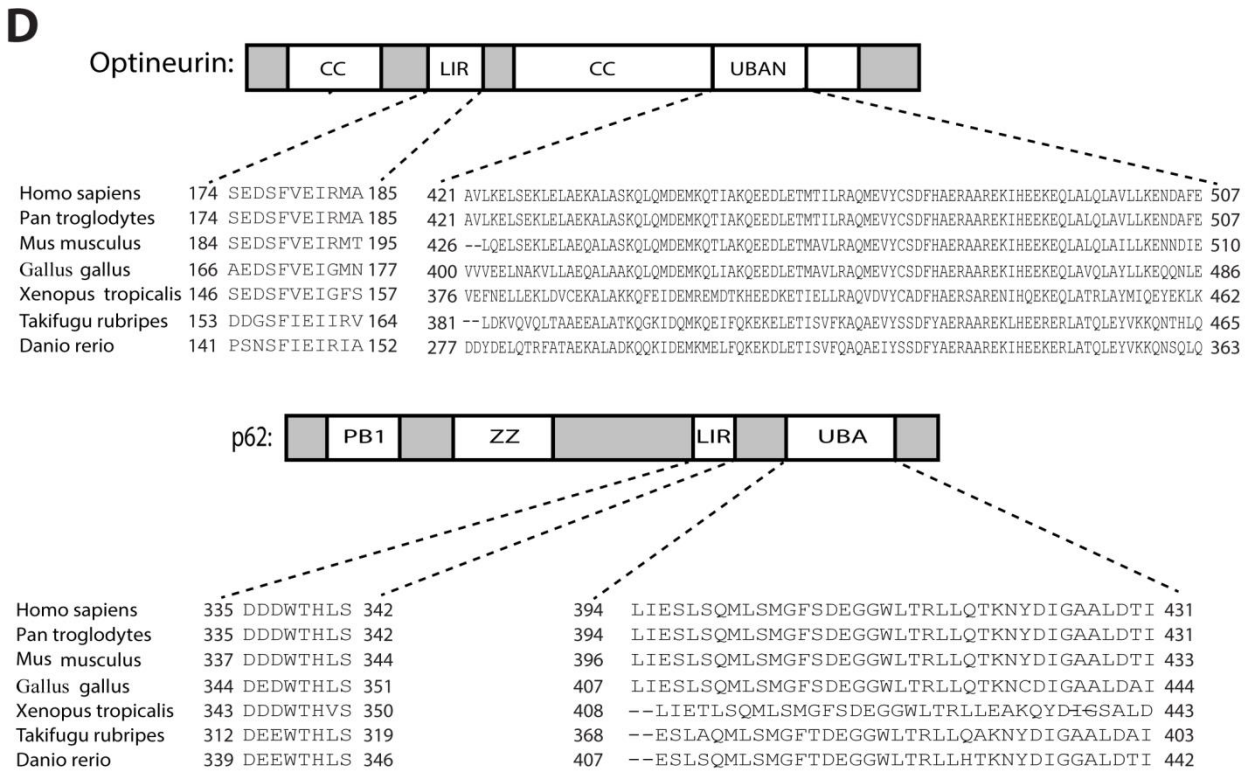

Supplementary figure 1: Optineurin and p62 are highly conserved between zebrafish and human

A. Representative images of *WT* and mutant F2 embryos at 4dpf. Scale bars, 250 µm.

B. Phylogenetic tree of SLR amino acid sequences. Optineurin, p62, NDP52(Calcoco2), NBRC1 and TAX1BP1 sequences were searched from the NCBI Ensembl database and the accession number listed in TableS6. MUSCLE online server was used to generate the protein alignment. The best-fitting amino acid replacement model to the alignment (JTT) was determined using ProtTest 3.2 based on the Akaike Information Criterion (AIC). Finally, the maximum likelihood gene tree was estimated with PhyML 3.0 and represented in FigTree v1.3.1 (http://tree.bio.ed.ac.uk/software/figtree/). Nodal confidence was calculated with non-parametric bootstrap of 100 replicates.

C. Protein sequence identity of SLRs between zebrafish and human. The percentage identity and similarity was calculated using a Clustal Omega alignment.

D. Alignment of LIR, UBAN and UBA motifs from the Optn and p62 sequences of different vertebrates. Amino acid sequences of the LIR motif of Optn and p62 from the indicated species were aligned using Mega7 software (DNASTAR, Madison, WI) and aligned Clustal W2 method{EMBL,Cambridge,UK}. The Ubiquitin binding domains of Optineurin or p62 were determined by NCBI-BlASTP (https://blast.ncbi.nlm.nih.gov/Blast.cgi?PAGE=Proteins).

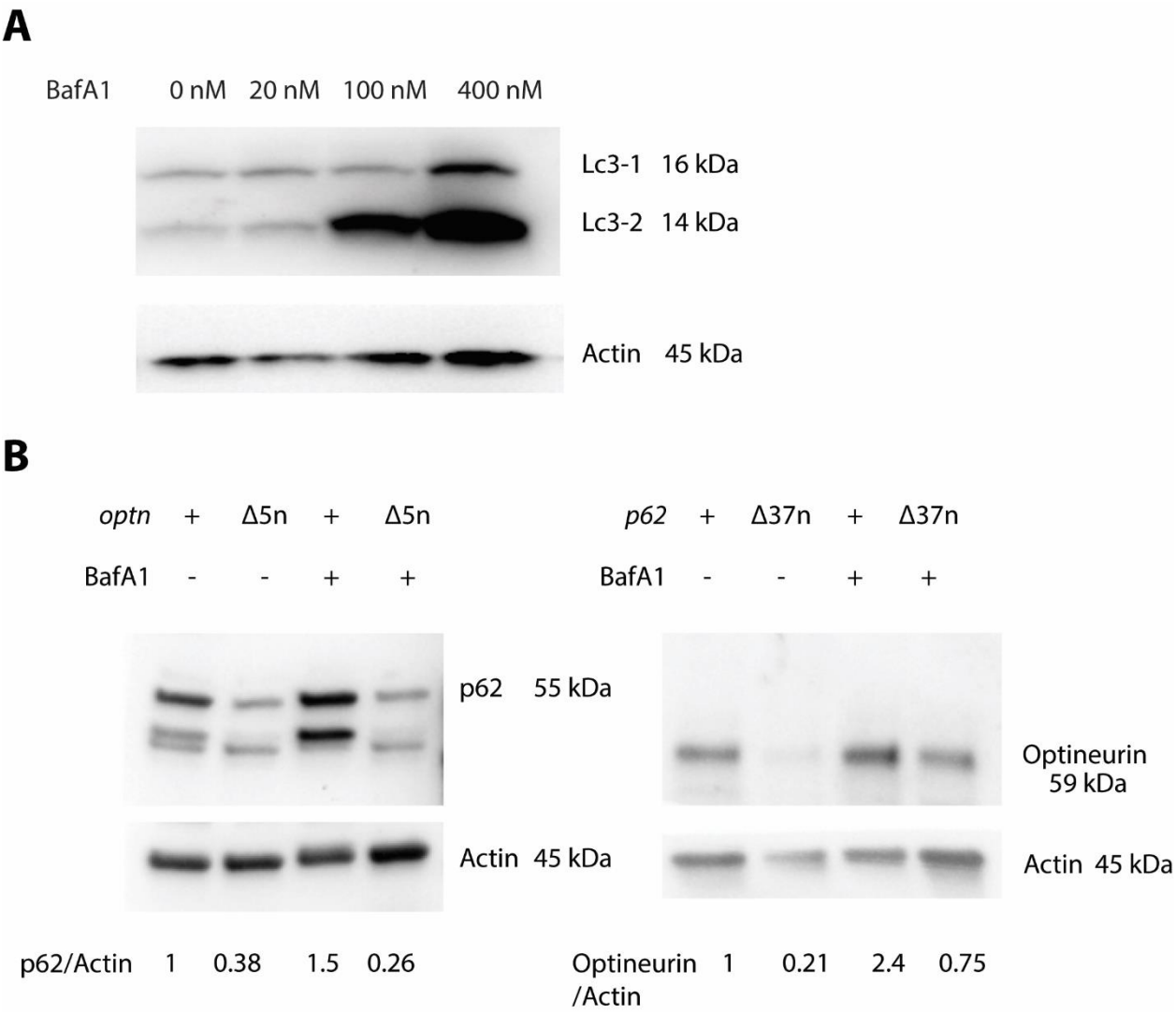

Supplementary figure 2: Characterization of Optineurin and p62 mutant lines

A. Validation of Baf A1 effect on zebrafish by WB. Baf A1 treatment at dosages of 20, 100 and 400 nM was performed by incubation for 12h in egg water. The protein samples were extracted from 4 dpf AB/TL larvae (>10 embryos/sample). The blots were probed with antibodies against Lc3 and Actin

B. Detection of p62 or Optineurin protein in mutant lines in absence or presence of Baf A1. Protein samples were extracted from *optn*$^{+/+}$, *optn*$^{\Delta 5n/\Delta 5n}$, *p62*$^{+/+}$ and *p62*$^{\Delta 37n/\Delta 37n}$ larvae at 4 dpf(>10 embryos/sample). The blots were probed with antibodies against Optineurin, p62 and Actin as a loading control. Optineurin/Actin and p62/Actin ratios are indicated below.

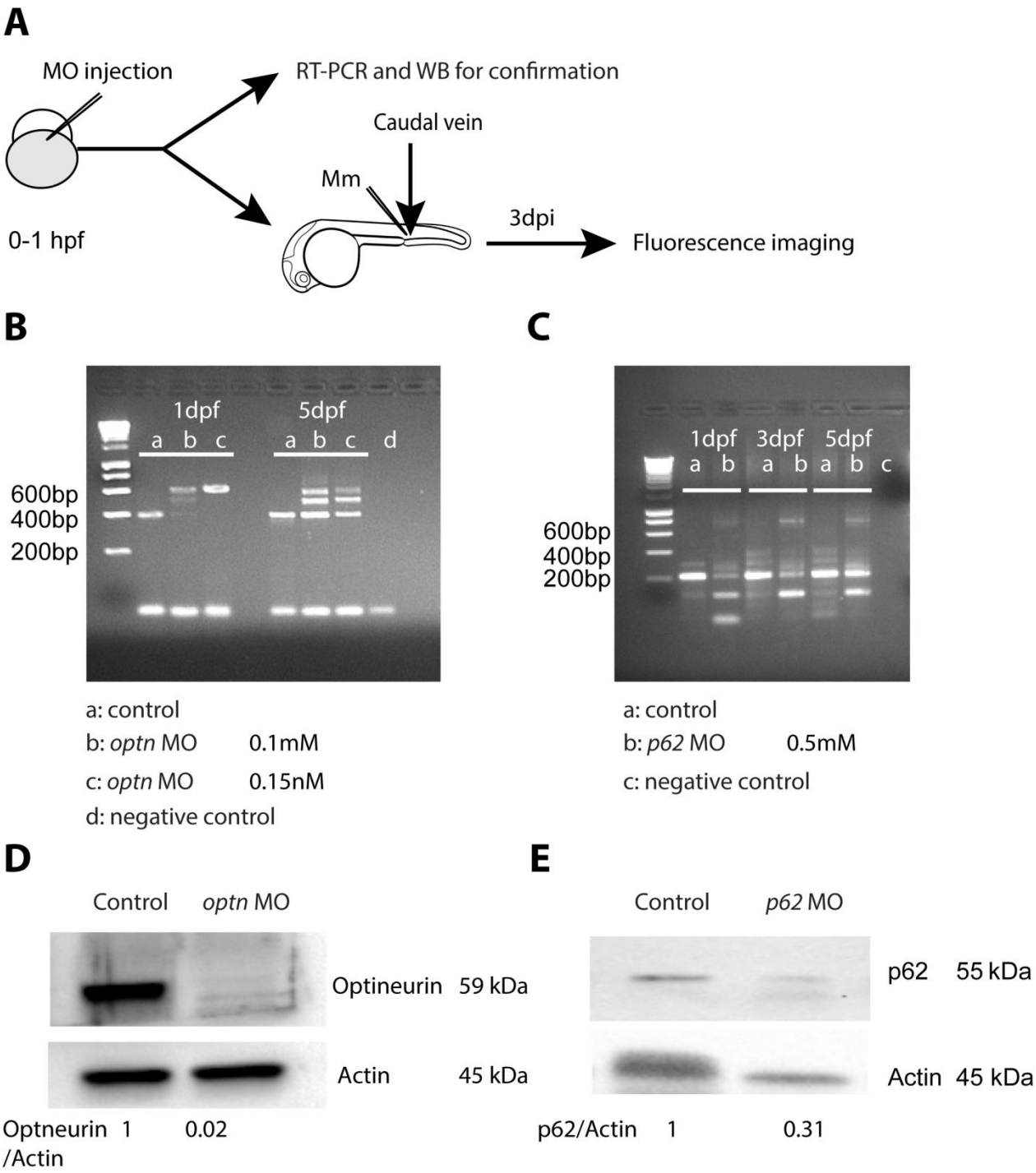

Supplementary figure 3: Injection of *optn* or *p62* MO transiently knocks down the corresponding mRNA and protein.

A. Workflow representing the experimental design in (B-E). *optn* or *p62* MO were injected into one cell stage embryos (AB/TL), and injected embryos were collected for confirmation of the knockdown effect by RT-PCR and Western blot analysis (>20 embryos /Sample).

B. Validation of the effect of *optn* splice-blocking MO e2i2 (targeting the splice event between exon 2 and intron 2) by RT-PCR on (a) the wild type control group, (b) embryos injected with 0.1mM MO, or (c) embryos injected with 0.15 mM MO. The wild type PCR product is expected to be 400 bp in length.

C. Validation of the effect of *p62* splice-blocking MO i1 e2 (targeting the splice event between intron 1 and exon 2) by RT-PCR on (a) the wild type control group, (b) embryos injected with 0.5mM MO. The wild type PCR products is expected to be 200 bp in length.

D and E. Validation of MO knockdown effect by WB analysis. The protein samples were exacted from 2 dpf AB/TL embryos injected with 0.1mM *optn* or 0.5 mM *p62* MO (>20 embryos/sample). The blots were probed with antibodies against Optn or P62 and Actin.

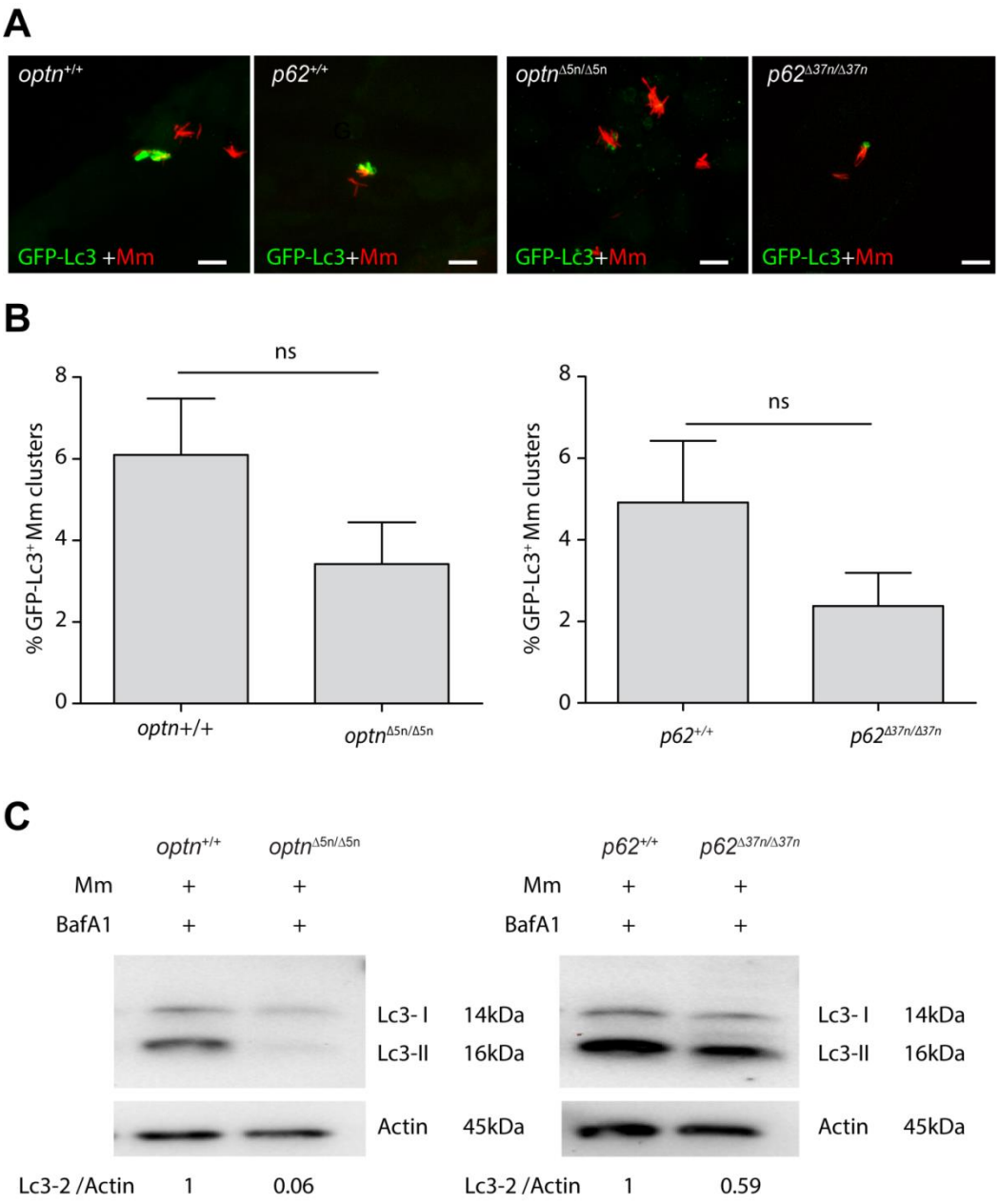

Supplementary figure 4: Optineurin or p62 mutation reduces autophagosome formation during Mm infection

A. Representative confocal micrographs of GFP-Lc3 co-localization with Mm clusters in *optn*$^{+/+}$, *optn*$^{\Delta 5n/\Delta 5n}$, *p62*$^{+/+}$ and *p62*$^{\Delta 37n/\Delta 37n}$ infected embryos at 1 dpi. The arrowheads indicate the overlap between GFP-Lc3 and Mm clusters. Scale bars, 10 µm.

B. Quantification of the percentage of Mm co-localizing with GFP-Lc3 in infected embryos at 1dpi (>6 embryo/group). ns, non-significant, *p<0.05,**P<0.01,***p<0.001.

C. Autophagy activity in Mm infected embryos. Protein samples were obtained from 3 dpi *optn*$^{+/+}$, *optn*$^{\Delta 5n/\Delta 5n}$, *p62*$^{+/+}$ and *p62*$^{\Delta 37n/\Delta 37n}$ infected larvae with Baf A1 12 h treatment (>10 larvae/sample). The blots were probed with antibodies against Lc3 and Actin.

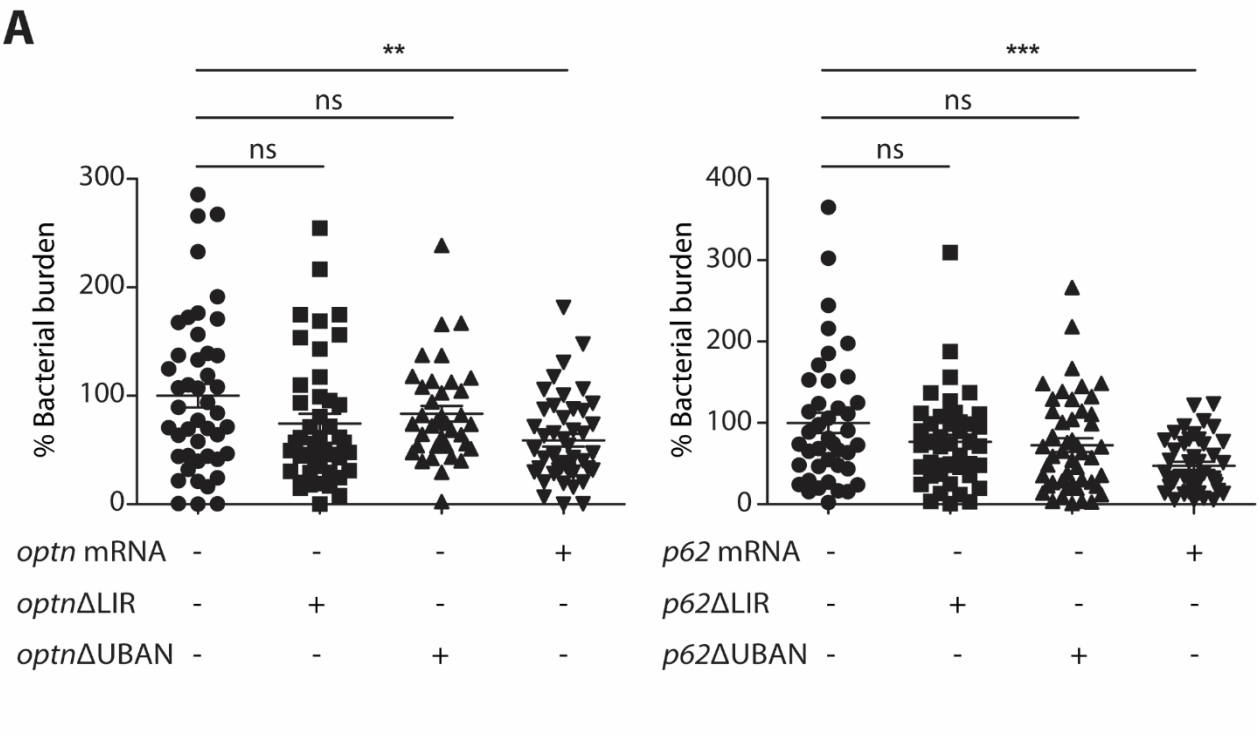

Supplementary figure 5: Transient overexpression of *optn* or *p62* mRNA reduces the susceptibility to Mm

A. Quantification of Mm infection burden in mRNA-injected embryos at 2 dpi. Data are accumulated data from two independent infection experiments. ns, non-significant,*p<0.05,**P<0.01,***p<0.001.

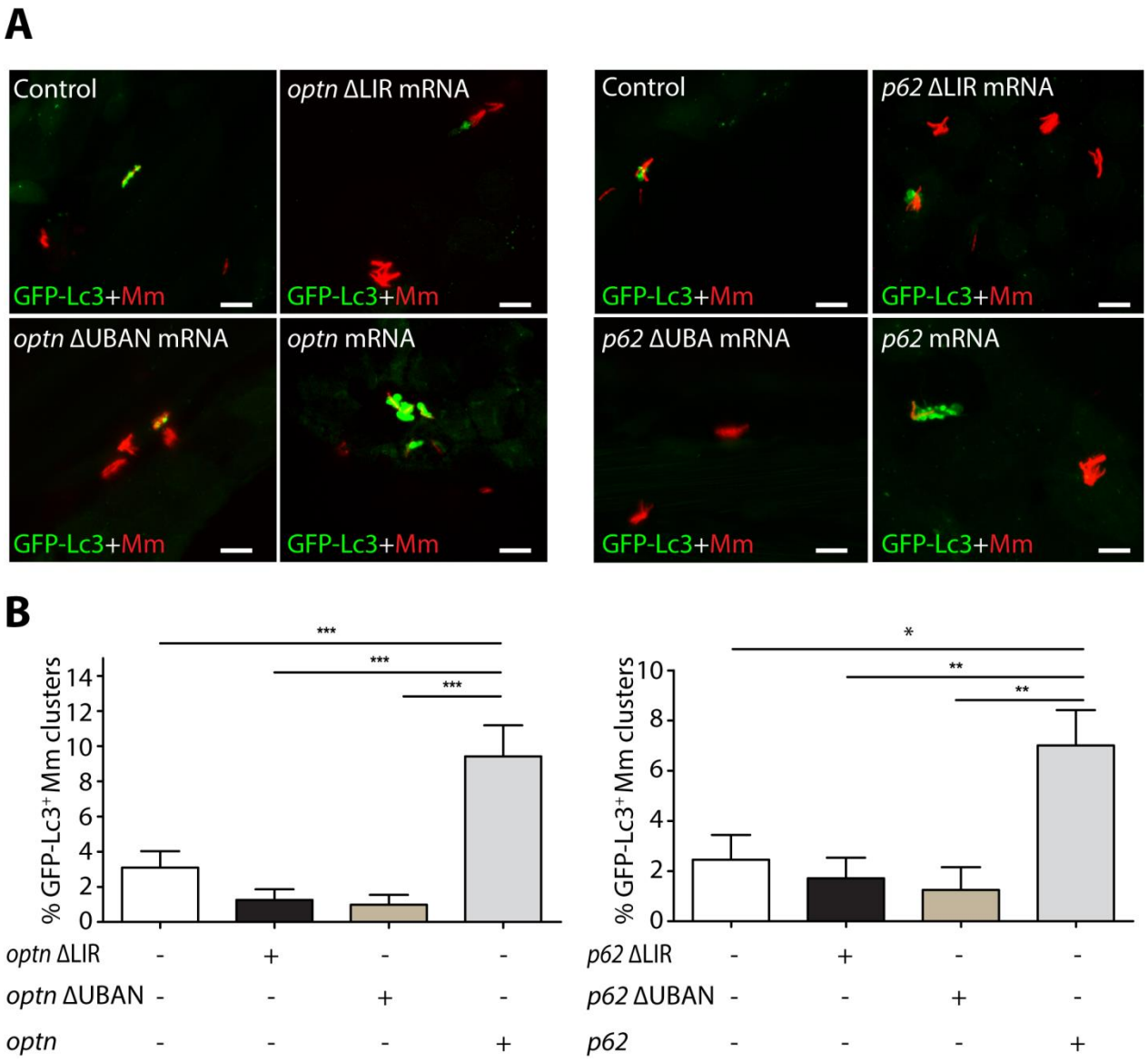

Supplementary figure 6: Transient overexpression of *optn* or *p62* mRNA results in increased recruitment of GFP-Lc3 to Mm clusters at 1 dpi.

A. Representative confocal micrographs of GFP-Lc3 co-localization with Mm clusters in mRNA-injected larvae at 1 dpi. The arrowheads indicate the overlap between GFP-Lc3 and Mm clusters. Scale bars, 10 µm.

C. Quantification of the percentage of Mm clusters positive for GFP-Lc3 vesicles. ns, non-significant,*p<0.05,**P<0.01, *** p<0.001. Data are accumulated from two independent experiments (>15embryo/group). ns, non-significant,*p<0.05,**P<0.01,***p<0.001

Supplementary table 1: Zebrafish lines used

Name	Description	Reference
AB/*TL*	Wild type strain	21
Tg(*CMV*:*GFP-Lc3*)	GFP reporter transgenic zebrafish for Lc3	30
optn$^{+/+}$/GFP-Lc3	Siblings of *optn*$^{\Delta 5n/\Delta 5n}$ /GFP-Lc3 carrying a transgenic GFP-Lc3 reporter	In this study
optn$^{\Delta 5n/\Delta 5n}$/GFP-Lc3	*optn* mutant line carrying a transgenic GFP-Lc3 reporter	In this study
p62$^{+/+}$/GFP-Lc3	Siblings of carrying a transgenic GFP-Lc3 reporter	In this study
p62$^{\Delta 37n/\Delta 37n}$/GFP-Lc3	*p62* mutant line carrying a transgenic GFP-Lc3 reporter	In this study
optn$^{\Delta 5n/\Delta 5n}$	optineurin mutant line	In this study
p62$^{\Delta 37n/\Delta 37n}$	*p62* mutant line	In this study

Supplementary table 2:Target sites for CRISPR/Cas 9 systems

Gene	Name	Target location	Sequence(5'-3')
optn	*optn* target site	Exon 2	GCTGGAAAAAAGTGGAGCTG
p62	*p62* target site	Exon 3	GGACCAGGAGGGCTAAAGTG

Supplementary table 3: Primers for complementation and amplification of sgRNA

Name	Forward (5'-3')	Reverse (5'-3')
optn sgRNA template	GCG**TAATACGACTCACTATAG**GCTGGAAAAAAGTGGAGCTGGTTTTAGAGCTAGAAATAGCAAGTTAAAATAAGGCTAGTC	GATCCGCACCGACTCGGTGCCACTTTTTCAAGTTGATAACGGACTAGCCTTATTTTAACTTGCTATTTCTAGCTCTAAAAC
p62 sgRNA template	GCG**TAATACGACTCACTATAG**GGACCAGGAGGGCTAAAGTGGTTTTAGAGCTAGAAATAGCAAGTTAAAATAAGGCTAGTC	
sg RNA amplify	GCGTAATACGACTCACTATAG	GATCCGCACCGACTCGGT

T7 promoter: **TAATACGACTCACTATAG**. The underlined sequence indicates the target sites for gRNAs designed to mutated *optn* or *p62*

Supplementary table 4: Morpholino sequences

Gene	Name	Target location	Sequence(5'-3')
optn	*optn* MO	Intron2>Exon 2	AGAGCCTCTGTGGGATGCATATAAT
p62	*p62* MO	Intron1>Exon 2	CTTCATCTAGAGACAAAGTTCAGGA

Supplementary table 5: Primers used in this study

Gene	Type	Species	Accession	Forward (5'-3')	Reverse (5'-3')
optn	PCR-cDNA	ZF	ENSDART00000014036.10	ATCAGGAAGAGCAGCATTTCCC	TTAATCTGAAACCCTCCAGACT
p62	PCR-cDNA	ZF	ENSDART00000140061.2	GTCGGCTGAAGTAGGAAACG	ACCCTCCAGGTTTATGCTTG
optn	RT-PCR	ZF	ENSDART00000014036.10	GGACATTAGTCACCCACGT	TTGGAGTTCAGAGTTCATCGCA
p62	RT-PCR	ZF	ENSDART00000140061.2	ATTTGCAGCGAAAAGTGCTC	AGTGAACGGAAACCCAGGAA
optn	Q-PCR	ZF	ENSDART00000014036.10	GACTGAACACTATGGCGTGGA	GAATGCGAATCTGACCTCT
p62	Q-PCR	ZF	ENSDART00000140061.2	GTCATATGGGTCCATCTCCAAT	AGGTGGGGCACAAGTCATAA
PPaib	Q-PCR	ZF	AY391451	ACACTGAAACACGGAGGCAAAG	CATCCACAACCTTCCCGAACAC
optn ΔLIR 1	PCR	ZF	ENSDART00000014036.10	GGAATTCGGATCAGGAAGAGCAGCATTTC	GGAGTTGCTAGGTGAACC TTGA
optn ΔLIR 2	PCR	ZF	ENSDART00000014036.10	AGAATAGCTGATGATGACTTAAAAGTG	AAGGCCTTTTAATCTGAAACCCTCCAGACTGAT
optn	PCR-genotyping	ZF	ENSDART00000014036.10	AGTTTAGAGGAGACCCTCCAGC	AGAGGTCAGATTCTTCGCATTC
p62	PCR-genotyping	ZF	ENSDART00000140061.2	CATCTTGGATTCATCATTACGTA	TCATATGGGGGGTCCTCCT

Supplementary table 6: Accession numbers of selective autophagy receptors

Species \ Proteins	Accession number				
	Optineurin	P62	Calcoco2	TAXBP1	NBR1
Homo sapiens (*H.s*)	ENSG00000123240	ENSG00000161011	ENSG00000136436	ENSG00000106052	ENSG00000188554
Pan troglodytes (*P.t*)	ENSPTRG00000002298	ENSPTRG00000017626	ENSPTRG00000009363	ENSPTRG00000019025	ENSPTRG00000009241
Mus musculus (*M.m*)	ENSMUSG00000026672	ENSMUSG00000015837	ENSMUSG00000006056	ENSMUSG00000004535	ENSMUSG00000017119
Xenopus tropicalis (*X.t*)	ENSGALG00000013738	ENSGALG00000035804	ENSGALG00000001525	ENSGALG00000042822	ENSPTRG00000009241
Gallus gallus (*G.g*)	ENSXETG00000009111	ENSXETG00000015913	ENSXETG00000022806	ENSXETG00000000752	ENSXETG00000014883
Danio rerio (*D.r*)	ENSDARG00000002663	ENSDARG00000075014	ENSDARG00000052515	ENSDARG00000098288 ENSDARG00000056856	ENSDARG00000077297 ENSDARG00000078772
Takifugu rubripes (*T.r*)	ENSTRUG00000010419	ENSTRUG00000017345	ENSTRUG00000011902	ENSTRUG00000018222 ENSTRUG00000015394	ENSDARG00000078772 ENSDARG00000078772

Chapter 5

Summary and discussion

The effective treatment of tuberculosis (TB) remains a significant challenge. Drug-resistant Mycobacterium tuberculosis (Mtb) strains and co-infection with HIV increase the problem of controlling TB. Thus, under the current situation, it is essential to develop effective treatment strategies for Mtb infections. A bottleneck in TB treatment is the long-term residence of bacteria inside organized structures of immune cells, called granulomas [1]. The traditional antibiotics cannot sufficiently penetrate into granulomas and therefore lengthly antibiotic treatment regimes are required to eradicate the infection. Poor patient compliance with such antibiotic therapy results in a rise of multidrug-resistant Mtb strains. Host-directed therapies can help to overcome the limitations of direct anti-bacterial therapies. However, the development of host-directed therapies requires a complete understanding of the interaction between the host and invading pathogens to identify host processes that can be targeted. A useful tool for such studies is the zebrafish model for TB. Zebrafish can be infected with *Mycobacterium marinum* (Mm), which is closely related to Mtb and causes similar disease characteristics. Importantly, the early life stages of the zebrafish (embryos and larvae) provide access to the earliest steps in the host-pathogen interaction that lead to the initiation of granulomas [2, 3].

Mtb is an intracellular pathogen which mainly resides inside immune cells, predominantly macrophages. Thus, increasing the cell's capability to kill Mtb is a valid approach to restrict TB disease progression. Autophagy is a lysosomal degradation process and substantial experimental evidence has demonstrated that autophagy is an important host immune defense mechanism against mycobacterial infection [4-6]. Work in our laboratory has shown that the autophagy modulator Dram1 is activated downstream of mycobacterial recognition by the TLR/MyD88/NFkB pathway to activate autophagy and restrict mycobacterial infection [5]. Overexpression of zebrafish *dram1* increased autophagic targeting of mycobacteria and resulted in lower bacterial burdens. The autophagic control of infection by Dram1 required the selective autophagy receptor p62 and the cytosolic DNA sensor STING. In this thesis, we further explore the function of Dram1 in zebrafish host defense against mycobacterial infection. Furthermore, we study the role of the selective autophagy receptors p62 and Optineurin in this defense mechanism.

DRAM1 has been identified and characterized as a lysosomal membrane protein by Crighton et al. in 2006. Expression of *DRAM1* is induced by DNA damage and its expression is regulated by tumour suppressor factor p53 [7]. It has been reported that DRAM1 functions as a regulator of autophagy and apoptosis in the context of diverse cellular processes, such as immunity, and cellular differentiation [8]. In addition to its link with TB [5], DRAM 1 has also been implicated in several other diseases, including HIV and several forms of cancer [9-11]. Until now, 5 DRAM family members have been identified and partially characterized. They are DRAM1, DRAM2/TMEM77, DRAM3/TMEM150B, DRAM4/TMEM150C and DRAM5/TMEM150A. DRAM2 is most closely related to DRAM1 among the DRAM family members. Like DRAM1, DRAM2 is also involved in cell death and autophagy in response to cellular stress factors. Furthermore, DRAM2 has also been implicated in TB and cancer [12, 13]. The expression of *DRAM3* has been detected in a broad range of normal tissues and tumour cells. It has been demonstrated that DRAM3 regulates autophagic flux and cell survival in response to starvation [14]. DRAM4 and DRAM5 have been identified as DRAM family members in an *in silico* study. DRAM4 could be detected at the plasma membrane but is primarily localized at lysosomes [15]. DRAM5 can form a complex with PI 4-kinase type IIIα (PI4KIIIα) at the plasma membrane to control the production of phosphatidylinositol 4,5-biphosphate $PI(4,5)P_2$ [15]. A potential role for DRAM4 and DRAM5 in regulation of autophagy or cell death has not been investigated yet. Thus, the function of these two DRAM family members requires further elucidation. In summary, DRAM family members play an important role in regulating cellular process in response to diverse stress factors and they are highly conserved from zebrafish, to mouse to human. We speculate that other DRAM family members, besides DRAM1 and DRAM2, could also be involved in host defense mechanisms (Chapter 1). Among all Dram family members in zebrafish, *dram1* is one that is most abundantly expressed in the immune cells of larvae and its expression is strongly induced by infection. Furthermore, our previous work had shown that increasing Dram1 activity can protect zebrafish larvae against Mm infection, based on which we proposed DRAM1 as a potential target for host-directed TB therapy [5]. Therefore, the studies in this thesis were focused on further elucidating the role of dram1 in the zebrafish model for TB.

Dram1 is required to restrict mycobacterial infection in lysosomal compartments and to prevent lytic cell death of infected macrophages

Using CRISPR/Cas9 technology we generated loss-of-function mutant alleles of zebrafish *dram1* to study its function during host defense against mycobacterial infection. Based on confocal image analysis we concluded that macrophages in *dram1* mutants fail to restrict Mm inside lysosomal compartments, which eventually results in cell death of the infected macrophages and excessive growth of extracellular mycobacteria. Furthermore, we demonstrated that the macrophage cell death in *dram1* mutants occurs in a Caspase 1 dependent manner (**Chapter 2**).

The lysosomal protein Dram1 promotes the maturation of autophagosomes by facilitating their fusion with lysosomes [5, 16]. In absence of Dram1, this process is affected, which can explain the reduced acidification of Mm-containing vesicles (**Chapter 2**). On a molecular level, DRAM2 has been reported to interact with the Beclin1-VPS34-UVRAG complex to facilitate the displacement of Rubicon in order to promote the maturation of autophagosomes [12]. Given the large degree of similarity in protein structure between DRAM1 and DRAM2 [17, 18], we speculate that Dram1 might utilize a similar mechanism as DRAM2 in mediating autophagosome maturation.

Mycobacteria-infected macrophages can undergo at least three general types of cell death: apoptosis, necrosis/necroptosis and pyroptosis [19]. Apoptosis is a non-lytic form of cell death, which avoids activation of an inflammatory response. This means that intracellular mycobacteria are encapsulated within the apoptotic envelope until the remains of the apoptotic cell are phagocytIosed by newly recruited macrophages [20-22]. Since uncontrolled extracellular growth of the bacteria is avoided during apoptosis of infected macrophages, this type of cell death is generally considered as host beneficial. Necrosis and pyroptosis, on the other hand, are lytic forms of cell death, meaning that the bacterial content of dying infected macrophages ends up in the extracellular environment. While necrosis is an 'accidental' form of cell death, this type of cell death can also occur as a regulated process, referred to as necroptosis. Pyroptosis is another regulated form of lytic cell death that is characterized by the formation of gasdermin pores in the cell membrane [23]. Pyroptosis is usually dependent

on caspase 1 activation and triggers an inflammatory response [24]. In this study, we found that Dram1 deficiency leads to impaired maturation of mycobacteria-containing vesicles, ultimately resulting in caspase 1 dependent cell death and extracellular overgrowth of bacteria. An important remaining question is how the reduced acidification of mycobacteria-containing vesicles in *dram1* mutants is related to the initiation of pyroptotic cell death in mycobacteria-containing macrophages. This question will need to be addressed in future studies. Other follow up studies regarding the molecular function of Dram1 in host defense should focus on identifying the interaction partners of Dram1/DRAM1 during homeostasis and infection. Collectively, with the analysis of *dram1* mutants presented in this thesis we have provided new evidence for the function for Dram1 in maturation of mycobacteria-containing vesicles, and have uncovered a link between this process and the control of cell survival versus the initiation of programmed cell death (Fig1).

Figure 1: Schematic representation of a macrophage restricting mycobacterial infection via autophagic defense in Wild type and Dram1 deficient larvae (Figure on next page)

1. The invading mycobacteria are phagocytosed by macrophages and detected by pattern recognition receptors, such as Toll-like receptors (TLRs). During phagocytosis, mycobacteria are captured in phagosomes.

2. Whether the mycobacteria-containing phagosome matures into a bactericidal phagolysosome is a crucial factor in the outcome of infection. a) The phagosome fuses with a lysosome to degrade mycobacteria. b) However, mycobacteria have evolved diverse mechanisms to prevent fusion between phagosomes and lysosomes, such as the ESX-1 secretion system that facilitates mycobacterial escape from phagosomes. In the absence of the lysosomal protein Dram1, fusion between phagosomes and lysosomes is impaired, which contributes to mycobacterial escape from phagosomes

3. A proportion of mycobacteria have escaped from the phagosome into the cytosol. Their presence in the cytosol can be sensed and results in ubiquitination of mycobacteria. The DNA damage regulated autophagy modulator 1 (Dram1) activates selective autophagy against ubiquitinated mycobacteria. During this process, the ubiquitin receptors p62 and Optineurin are involved in the delivery of ubiquitinated mycobacteria to autophagosomes. The sequestered mycobacteria will be degraded in autophagolysosomes. However, the targeting of mycobacteria by autophagy is affected in the absence of Dram1 and the formation of autophagolysosomes is impaired.

4. Mycobacterial infection is temporarily restricted inside macrophages to avoid the dissemination of the infection. However, the mycobacteria are not effectively restricted by macrophages in Dram1-deficient larvae, which leads to pyroptotic cell death and extracellular overgrowth of mycobacteria.

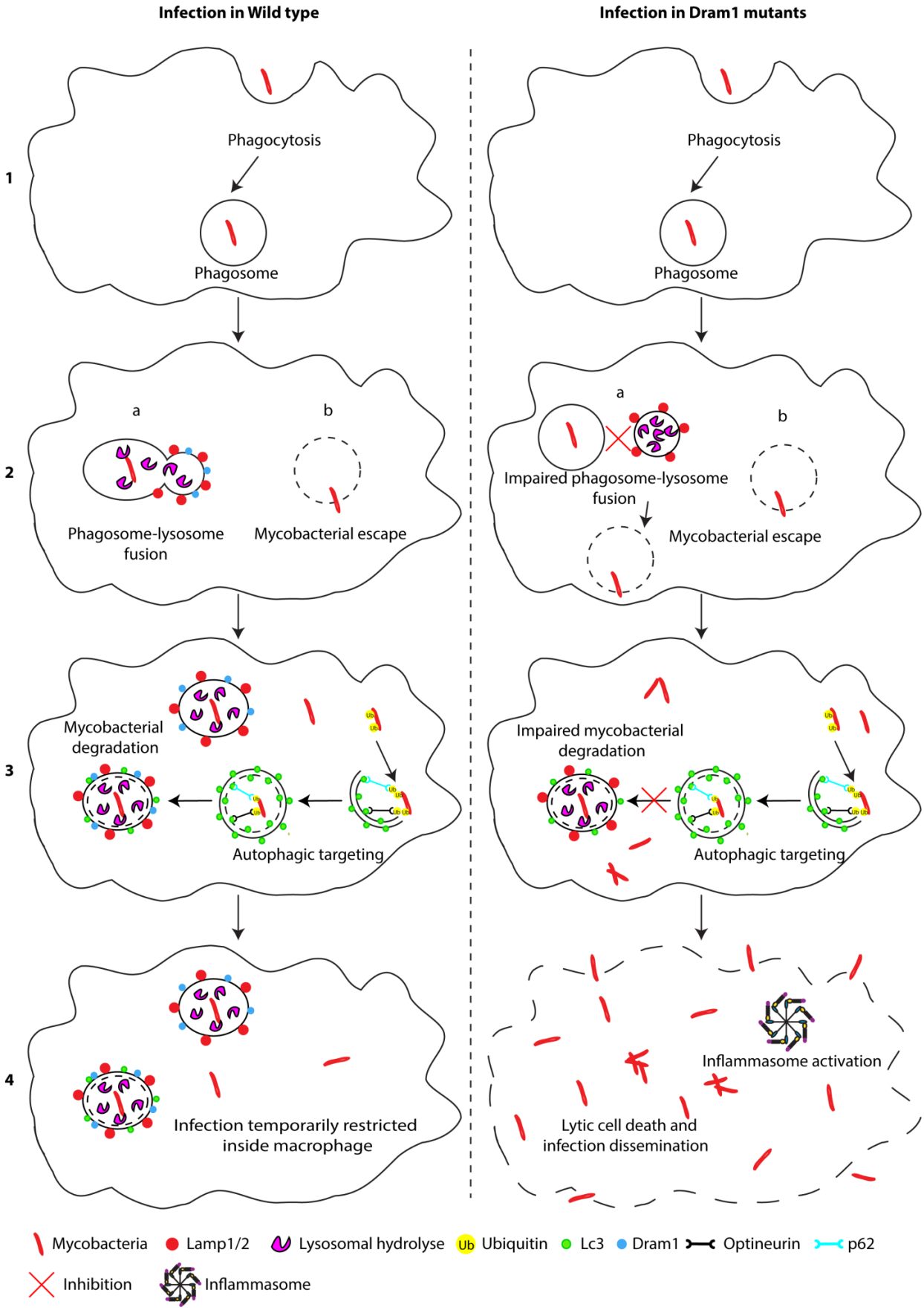
Infection in Wild type
Infection in Dram1 mutants
1
Phagocytosis
Phagosome
2
a
b
Phagosome-lysosome fusion
Mycobacterial escape
Impaired phagosome-lysosome fusion
3
Mycobacterial degradation
Autophagic targeting
Impaired mycobacterial degradation
4
Infection temporarily restricted inside macrophage
Inflammasome activation
Lytic cell death and infection dissemination
Mycobacteria
Lamp1/2
Lysosomal hydrolyse
Ubiquitin
Lc3
Dram1
Optineurin
p62
Inhibition
Inflammasome

Dram1 deficiency affects gene expression of metabolic signaling pathways

In **chapter 2** of this thesis, we described that Dram1 deficiency did not significantly affect autophagy activity and cell death under basal, uninfected conditions. To better understand the function of Dram1 during homeostasis and mycobacterial infection, we performed RNA deep sequencing to analyse the transcriptomes of infected and uninfected *dram1* mutants and wild type sibling (**Chapter 3**). Under uninfected conditions, we found that the proteasome, ribosome, mitochondria, and polymerase pathways were affected to a relatively minor extent due to the absence of Dram1. This suggests that *dram1* mutants have deficiencies or alterations in these metabolic pathways. However, these metabolic alterations did not have a detectable impact on embryo and larval development. Furthermore, we found that Dram1 deficiency does not affect survival or fertility in adult zebrafish (**Chapter** 2). Taken together, we propose that the main function of Dram1/DRAM1 lies in facilitating an appropriate response to certain cellular stress factors, while its functions are somewhat redundant under homeostatic conditions (**Chapter 2** and **Chapter 3**).

Indeed, during mycobacterial infection various gene expression pathways were significantly changed in Dram1-deficient larvae compared with wild type individuals. Specifically, we found that gene expression of regulators of necroptotic and pyroptotic cell death (*hsp90* and *caspa*) was significantly altered in *dram1* mutants compared to wild type larvae infected with the same dose of mycobacteria. In contrast, while expression of *caspase 8* and *caspase 9* was slightly altered, we detected no differences in regulation of apoptosis effector genes in response to infection between infected *dram1*$^{+/+}$ and *dram1*$^{\Delta 19n/\Delta 19n}$ larvae. The analysis of the transcriptomics data confirmed our previous results that macrophages of Dram1-deficient larvae are more likely to undergo pyroptotic cell death when infected with mycobacteria (**Chapter 2**). While we have not addressed this experimentally yet, the results suggest that Dram1-deficient macrophages are more likely to undergo necroptosis in response to mycobacterial infection as well. Previously, it has been shown that DRAM1 mediates cell death of HIV-infected T-cells via lysosomal membrane permeabilization [9], and it would be interesting to investigate whether this is also the case in mycobacteria-infected macrophages. This could

potentially present a direct link between the reduced acidification of mycobacteria-containing vesicles and initiation of lytic cell death in infected Dram1-deficient macrophages.

We found that the gene expression of TLRs was also significantly altered in infected *dram1* mutant larvae compared to infected wild types. The expression of the plasma membrane receptor *tlr2* was reduced in the absence of Dram1, while the expression of the endosomal receptors *tlr*3 and *tlr*9 was significantly increased in Dram1 deficient larvae during mycobacterial infection [25, 26]. This differential expression of pattern recognition receptors might reflect the increased extracellular localization of mycobacteria in the absence of Dram1, which potentially results in adjustments in the expression of plasma membrane and endosomal TLRs. For instance, we speculate that Tlr2 molecules on the plasma membrane are continuously recognizing extracellular mycobacteria, which can result in down regulation of *tlr2* itself as a negative feedback loop. Collectively, we have demonstrated that Dram1 affects transcriptional regulation of metabolic processes; promotes maturation of mycobacteriacontaining vesicles; is required to prevent lytic cell death of macrophages in response to mycobacterial infection; and affects Toll-like receptor recognition of mycobacteria (**Chapters 2 and 3**).

The selective autophagy receptors Optineurin and p62 are required for autophagic targeting of mycobacteria

Recently, the relevance of autophagic defense mechanisms in host immune responses against Mtb infection has been challenged [27, 28]. These reports propose that Mtb utilises virulence mechanisms to suppress autophagic defense mechanisms and that a potential host beneficial function of autophagy factors depends on their role in other processes. Furthermore, mutation of the selective autophagy receptor p62 in mice did not affect the outcome of Mtb infection in this work [27]. In contrast, other studies in mice and zebrafish demonstrated that p62 is required for autophagic targeting of mycobacteria *in vitro* and *in vivo* [4, 5]. Here, we made zebrafish CRISPR/Cas9 loss-of-function mutants of p62 and another selective autophagy receptor, Optineurin, which, like p62, shows induced gene expression during Mm infection in our model. We found that both p62 and Optineurin restrict mycobacterial growth by sequestering

ubiquitinated bacteria to Lc3-positive vesicles (**Chapter 4**). Our findings provide *in vivo* confirmation of the importance of selective autophagy as an innate immune defense mechanism against intracellular mycobacterial pathogens. To the best of our knowledge, this is also the first time that a host protective function for Optineurin has been shown in defense against mycobacterial infection (**Chapter 4**).

Since a combined silencing of p62 and Optineurin did not have an additive effect on the mycobacterial burden compared to single mutation of p62 or Optineurin, we suspect that these receptors are part of the same defense pathway and are mutually dependent in promoting autophagic targeting of ubiquitinated cytosolic mycobacteria. Overexpression of either p62 or Optineurin increased host resistance to mycobacterial infection. To further investigate a potential mutual dependent relationship for these ubiquitin-binding receptors, it will be interesting to overexpress p62 in the Optineurin knock out situation and *vice versa*. If the two receptors truly depend on each other for their host protective effect, overexpression of one of the two will not have a beneficial effect in the absence of the other.

Optineurin and p62 have also been linked to the regulation of cell death [29, 30]. Another important question stemming from our studies is whether Optineurin or p62 are involved in cell death processes during mycobacterial infection. And if so, is this part of the same process of cell death modulation as Dram1? Collectively, this study provided *in vivo* evidence that p62 is involved in autophagic defense against mycobacteria during the critical early steps in the infection process when macrophages are parasitized and granuloma formation is initiated. During this phase, host defense relies on the function of the innate immune system. A similar situation occurs in patients with a compromised adaptive immune system and therefore these patients might benefit from stimulating the autophagic host defense mechanisms. In addition to consolidating the function of p62 in anti-mycobacterial host defense, our study provides the first evidence for a similar role for Optineurin in ubiquitin-dependent autophagic targeting of mycobacteria.

Conclusion

The proper control of cell death during mycobacterial infection is a critical factor in the battle between the host immune system and these pathogens [32]. Despite recent controversies, the current view remains that autophagy is an important host defense mechanism to restrict replication of mycobacteria inside immune cells [4, 6, 27]. Dying infected macrophages release a large number of mycobacteria which are disseminated into other tissues by newly recruited macrophages [3]. Since mycobacterial proliferation predominantly occurs inside immune cells, modulation of the cell-mediated immune response is a promosing potential target for host-directed therapy to control TB or other mycobacterial infections [33]. Based on our studies we propose that the defense pathway mediated by Dram1 is a promising target for host-directed therapy against TB by stimulating autophagic defense and preventing lytic cell death of infected immune macrophages (Chapter 2 and Chapter 3). The current bottleneck is to figure out how to pharmacologically stimulate Dram1/DRAM1 in animal models or human patients. A possible approach would be to directly inject DRAM1 recombinant protein into TB patients to artificially elevate DRAM1 protein levels. DRAM1 protein might directly participate in defense against Mtb. However, it remains unsure whether DRAM1 can be delivered to the appropriate membrane location in infected cells to exert its function. Thus, the more practical approach is to study mechanisms of DRAM1 activation in *in vivo* and *in vitro* models for TB (and other members of the DRAM family), to screen for endogenous modulators or upstream partners that can be used as drugable targets to activate the host defense pathway mediated by DRAM1.

The zebrafish *dram1* knockout mutants generated and characterized here (**Chapter 2)** revealed that deficiency in Dram1 results in uncontrolled mycobacterial infection not only due to impaired maturation of mycobacteria containing vesicles and defects in autophagic targeting, but also due to increased pyroptotic cell death of infected macrophages. In **Chapter 3**, we provide a fundamental characterization of the effect of Dram1 deficiency on the gene expression profiles in health and during mycobacterial infection, which revealed effects on metabolic pathways, lytic cell death, and Toll-like receptor signaling. Finally, in **Chapter 4** we demonstrate that the selective autophagy receptors Optineurin and p62 function in innate host

defense against mycobacterial infection by targeting ubiquitinated bacteria to autophagic compartments. Overall, this thesis presents new *in vivo* evidence for the important function of selective autophagy to inhibit mycobacterial proliferation inside macrophages. Furthermore, the results support that stimulating the innate host defense processes that are dependent on Dram1, p62 and Optineurin could be a useful strategy to explore for adjunctive treatment of TB patients.

References

1. Flynn JL, Chan J. IMMUNOLOGY OF TUBERCULOSIS. Annu Rev Immunol 2001; 19:93-129.
2. Meijer AH. Protection and pathology in TB: learning from the zebrafish model. Semin Immunopathol 2016; 38:261-73.
3. Davis JM, Ramakrishnan L. The role of the granuloma in expansion and dissemination of early tuberculous infection. Cell 2009; 136:37-49.
4. Watson RO, Manzanillo PS, Cox JS. Extracellular M. tuberculosis DNA targets bacteria for autophagy by activating the host DNA-sensing pathway. Cell 2012; 150:803-15.
5. van der Vaart M, Korbee CJ, Lamers GE, Tengeler AC, Hosseini R, Haks MC, et al. The DNA damage-regulated autophagy modulator DRAM1 links mycobacterial recognition via TLR-MYD88 to autophagic defense [corrected]. Cell Host Microbe 2014; 15:753-67.
6. Deretic V. Autophagy in leukocytes and other cells: mechanisms, subsystem organization, selectivity, and links to innate immunity. J Leukoc Biol 2016; 100:969-78.
7. Crighton D, Wilkinson S, O'Prey J, Syed N, Smith P, Harrison PR, et al. DRAM, a p53-induced modulator of autophagy, is critical for apoptosis. Cell 2006; 126:121-34.
8. Mrschtik M, Ryan KM. Another DRAM involved in autophagy and cell death. Autophagy 2016; 12:603-5.
9. Laforge M, Limou S, Harper F, Casartelli N, Rodrigues V, Silvestre R, et al. DRAM triggers lysosomal membrane permeabilization and cell death in CD4(+) T cells infected with HIV. PLoS Pathog 2013; 9:e1003328.
10. Galavotti S, Bartesaghi S, Faccenda D, Shaked-Rabi M, Sanzone S, McEvoy A, et al. The autophagy-associated factors DRAM1 and p62 regulate cell migration and invasion in glioblastoma stem cells. Oncogene 2013; 32:699-712.
11. Humbert M, Mueller C, Fey MF, Tschan MP. Inhibition of damage-regulated autophagy modulator-1 (DRAM-1) impairs neutrophil differentiation of NB4 APL cells. Leuk Res 2012; 36:1552-6.
12. Kim JK, Lee HM, Park KS, Shin DM, Kim TS, Kim YS, et al. MIR144* inhibits antimicrobial responses against Mycobacterium tuberculosis in human monocytes and macrophages by targeting the autophagy protein DRAM2. Autophagy 2017; 13:423-41.

13. Bai S, Tian B, Li A, Yao Q, Zhang G, Li F. MicroRNA-125b promotes tumor growth and suppresses apoptosis by targeting DRAM2 in retinoblastoma. Eye (Lond) 2016; 30:1630-8.

14. Mrschtik M, O'Prey J, Lao LY, Long JS, Beaumatin F, Strachan D, et al. DRAM-3 modulates autophagy and promotes cell survival in the absence of glucose. Cell Death Differ 2015; 22:1714-26.

15. Chung J, Nakatsu F, Baskin JM, De Camilli P. Plasticity of PI4KIIIalpha interactions at the plasma membrane. EMBO Rep 2015; 16:312-20.

16. Zhang XD, Qi L, Wu JC, Qin ZH. DRAM1 regulates autophagy flux through lysosomes. PLoS One 2013; 8:e63245.

17. O'Prey J, Skommer J, Wilkinson S, Ryan KM. Analysis of DRAM-related proteins reveals evolutionarily conserved and divergent roles in the control of autophagy. Cell Cycle 2009; 8:2260-5.

18. Park SM, Kim K, Lee EJ, Kim BK, Lee TJ, Seo T, et al. Reduced expression of DRAM2/TMEM77 in tumor cells interferes with cell death. Biochem Biophys Res Commun 2009; 390:1340-4.

19. Srinivasan L, Ahlbrand S, Briken V. Interaction of Mycobacterium tuberculosis with host cell death pathways. Cold Spring Harb Perspect Med 2014; 4.

20. Martin CJ, Booty MG, Rosebrock TR, Nunes-Alves C, Desjardins DM, Keren I, et al. Efferocytosis is an innate antibacterial mechanism. Cell Host Microbe 2012; 12:289-300.

21. Behar SM, Martin CJ, Booty MG, Nishimura T, Zhao X, Gan HX, et al. Apoptosis is an innate defense function of macrophages against Mycobacterium tuberculosis. Mucosal Immunol 2011; 4:279-87.

22. Stutz MD, Clark MP, Doerflinger M, Pellegrini M. Mycobacterium tuberculosis: Rewiring host cell signaling to promote infection. J Leukoc Biol 2018; 103:259-68.

23. Galluzzi L, Vitale I, Aaronson SA, Abrams JM, Adam D, Agostinis P, et al. Molecular mechanisms of cell death: recommendations of the Nomenclature Committee on Cell Death 2018. Cell Death Differ 2018; 25:486-541.

24. Wallach D, Kang TB, Dillon CP, Green DR. Programmed necrosis in inflammation: Toward identification of the effector molecules. Science 2016; 352:aaf2154.

25. Nishiya T, DeFranco AL. Ligand-regulated chimeric receptor approach reveals distinctive subcellular localization and signaling properties of the Toll-like receptors. J Biol Chem 2004; 279:19008-17.

26. Means TK, Jones BW, Schromm AB, Shurtleff BA, Smith JA, Keane J, et al. Differential Effects of a Toll-Like Receptor Antagonist on Mycobacterium tuberculosis-Induced Macrophage Responses. The Journal of Immunology 2001; 166:4074-82.

27. Kimmey JM, Huynh JP, Weiss LA, Park S, Kambal A, Debnath J, et al. Unique role for ATG5 in neutrophil-mediated immunopathology during M. tuberculosis infection. Nature 2015; 528:565-9.

28. Behar SM, Baehrecke EH. Autophagy is not the answer. NATURE 2015; 528:482-3.

29. Fan L, Yin S, Zhang E, Hu H. Role of p62 in the regulation of cell death induction. Apoptosis 2018; 23:187-93.

30. Slowicka K, van Loo G. Optineurin Functions for Optimal Immunity. Front Immunol 2018; 9:769.

31. Shaid S, Brandts CH, Serve H, Dikic I. Ubiquitination and selective autophagy. Cell Death Differ 2013; 20:21-30.

32. Mahamed D, Boulle M, Ganga Y, Mc Arthur C, Skroch S, Oom L, et al. Intracellular growth of Mycobacterium tuberculosis after macrophage cell death leads to serial killing of host cells. Elife 2017; 6.

33. Kolloli A, Subbian S. Host-Directed Therapeutic Strategies for Tuberculosis. Front Med (Lausanne) 2017; 4:171.

Nederlandse samenvatting

Een effectieve behandeling van tuberculose (tbc) blijft een grote uitdaging. Een toename van antibioticumresistente stammen van *Mycobacterium tuberculosis* (Mtb) en co-infecties met hiv dragen sterk bij aan dit probleem. Het is daarom van essentieel belang om effectieve behandelstrategieën te ontwikkelen voor tbc. Een knelpunt bij de behandeling van tbc is dat de bacteriën gedurende lange tijd in compacte conglomeraten van immuuncellen verblijven, zogenaamde granulomen. De traditionele antibiotica kunnen slechts met moeite doordringen in deze granulomen, waardoor langdurige behandeling noodzakelijk is om de bacteriën volledig uit te schakelen. Deze langdurige behandelingen met een cocktail van antibiotica worden niet altijd volledig afgerond door patiënten, met een sterke toename in het aantal antibioticumresistente Mtb-stammen als gevolg. Medicatie gericht op de gastheer, bijvoorbeeld om de immuunreactie te versterken, kan mogelijk oplossingen bieden voor de beperkingen van de huidige therapieën met antibiotica. Echter, de ontwikkeling van zulke gastheergerichte therapieën vereist een verregaand begrip van de interacties tussen de gastheer en de ziekteverwekker. Door meer inzicht in die interacties te verkrijgen hopen wij aanknopingspunten te vinden voor de ontdekking van medicijnen die aangrijpen op gastheerprocessen die belangrijk zijn voor de afweer tegen tbc. De zebravis is een veelgebruikt onderzoeksmodel voor tbc en is uitermate geschikt voor onderzoek naar interacties tussen gastheer en ziekteverwekker. Zebravisembryo's en -larven kunnen geïnfecteerd worden met *Mycobacterium marinum* (Mm), een bacterie die nauw verwant is aan Mtb en die een infectie met tbc-gerelateerde symptomen veroorzaakt in vissen. Met behulp van zebravisembryo's en -larven is het mogelijk om interacties tussen immuuncellen en Mm-bacteriën te bestuderen tijdens de vroegste stadia van de ontwikkeling van de karakteristieke tbc-granulomen.

Mycobacteriële ziekteverwekkers kunnen overleven en zich vermeerderen in cellen van het immuunsysteem, de macrofagen. Als reactie hierop initiëren macrofagen diverse afweermechanismen in een poging om de intracellulaire bacteriën op te ruimen en verdere verspreiding van de infectie te voorkomen. Er zijn veel factoren – zowel aan de gastheerkant als aan de bacteriële kant – die samen het lot van een geïnfecteerde macrofaag bepalen: ruimt de

macrofaag de bacteriën op, of gaat de cel ten onder aan de infectie? DRAM1, een regulator van autofagie en celdood, is in tijdens eerder onderzoek in verband gebracht met anti-mycobacteriële afweermechanismen die gebruik maken van de autofagiemachinerie. In dit proefschrift hebben we een mutatie in het *dram1*-gen van de zebravis geïntroduceerd met behulp van de CRISPR/Cas9-methode. In deze mutant zagen wij geen verlaging van de activiteit van autofagie in de afwezigheid van infectie. Echter, tijdens Mm-infectie zorgt mutatie van *dram1* voor een verminderde co-lokalisatie tussen bacteriën en autofagiestructuren en voor een verminderde afweer tegen mycobacteriële infecties. Bovendien hebben we aangetoond dat Dram1, een voornamelijk lysosomaal eiwit, noodzakelijk is voor de verzuring van de organellen waarin Mm verblijft. Door middel van intravitale microscopie konden we observeren dat macrofagen zonder Dram1 niet in staat zijn om een mycobacteriële infectie te beteugelen tijdens de vroege stadia van tbc. Uitschakelen van de functionele zebravishomoloog van Caspase 1 zorgde ervoor dat infectieniveaus in *dram1*-mutanten verlaagd werden. Voortbordurend op de eerder beschreven rol van Dram1 bij verzuring van Mm-bevattende organellen, wijzen deze nieuwe resultaten erop dat de aanwezigheid van Dram1 pyroptotische celdood van geïnfecteerde macrofagen voorkomt en op die manier bijdraagt aan de weerstand van de gastheer tegen een mycobacteriële infectie.

Om de functie van Dram1 nader te onderzoeken hebben we door middel van sequentieanalyse van het RNA de volledige genexpressiepatronen in kaart gebracht van ongeïnfecteerde en Mm-geïnfecteerde zebravislarven van de *dram1*-mutant en van wild-type zebravislarven als controlegroep. Deze zogenoemde transcriptoomanalyse liet zien dat in de gezonde situatie het netwerk van genexpressie slechts in geringe mate werd beïnvloed door afwezigheid van Dram1, met detecteerbare verschillen in proteolytische en metabole processen. De transcriptoomreactie op mycobacteriële infectie was echter sterk afwijkend in *dram1*-mutanten, wat suggereert dat de afweerreactie van de gastheer veranderd is in afwezigheid van Dram1. Bovendien vonden we dat de metabole reactie op mycobacteriële infectie die plaatsvindt in wild-type larven afwezig was in *dram1*-mutanten, wat nogmaals wijst op een rol voor Dram1 in metabole processen. Tenslotte is het noemenswaardig dat het verlies van Dram1 celdoodprocessen en herkenning van bacteriën via zogenaamde Toll-receptoren beïnvloedde.

Onze analyse suggereert dat Dram1 betrokken is bij de regulatie van celdoodprocessen die geactiveerd worden tijdens een mycobacteriële infectie, terwijl de herkenning van Mm op een andere manier plaats lijkt te vinden in afwezigheid van Dram1. Samenvattend onthult onze transcriptoomanalyse een rol voor Dram1 in metabole processen onder zowel gezonde omstandigheden als tijdens de cellulaire stress die veroorzaakt wordt door infectie. Bovendien benadrukt onze analyse het belang van autofagiemechanismen in de verdediging van de gastheer tegen mycobacteriële infecties.

In vitro studies hebben aangetoond dat mycobacteriën die ontsnappen vanuit fagosomen naar het cytosol gemarkeerd worden met een afbraaksignaal, ubiquitine, en vervolgens herkend worden door selectieve autofagiereceptoren. Daarentegen is er tot op heden geen *in vivo* bewijs voor een rol van selectieve autofagiereceptoren in de verdediging van de gastheer tegen mycobacteriële infecties en het belang van dit proces is controversieel. In dit proefschrift hebben we het zebravismodel voor tbc gebruikt om de rol van twee selectieve autofagiereceptoren, Optineurin (*optn*) en SQSTM1 (*p62*), in de verdediging van de gastheer tegen mycobacteriële ziekteverwekkers. Hiertoe zijn mutanten van *optn* en *p62* gegenereerd met de CRISPR/Cas9-methode in een transgene GFP-Lc3-zebravislijn die gebruikt kan worden om de autofagiereactie tegen Mm te visualiseren. We vonden dat mutaties in *optn* of *p62* resulteerde in een verminderde autofagiereactie tegen Mm en een verhoogde vatbaarheid voor Mm-infectie. We konden deze resultaten reproduceren door de genen tijdelijk uit te schakelen. Bovendien resulteerde verhoogde genexpressie van *optn* of *p62* door middel van mRNA-injectie in een verhoogde associatie tussen GFP-Lc3 en Mm en een verlaagde infectiegraad. Samenvattend kunnen we op grond van de resultaten van deze *in vivo* studie naar de rol van selectieve autofagiereceptoren concluderen dat zowel Optineurin als p62 noodzakelijk zijn voor autofagie-gerelateerde verdedigingsmechanismen tegen mycobacteriële infecties in de zebravis.

De zebravis *dram1*-mutanten beschreven en gekarakteriseerd in **hoofdstuk 2** van dit proefschrift laten zien dat afwezigheid van Dram1 resulteert in ongecontroleerde Mm-infecties door gebrekkige maturatie van organellen die Mm bevatten, verminderde verdedigingsmechanismen gebaseerd op autofagie en een verhoging van het aantal cellen dat pyroptotische celdood ondergaat. In **hoofdstuk 3** hebben we laten zien dat de afwezigheid van

Dram1 invloed heeft op genexpressienetwerken in zowel ongeïnfecteerde als Mm-geïnfecteerde zebravislarven, met name metabole processen, lytische celdood en signaalroutes van Toll-receptoren. Tenslotte hebben we in **hoofdstuk 4** van dit proefschrift laten zien dat de selectieve autofagiereceptoren Optineurin en p62 een belangrijke rol spelen in de immuunverdediging van de gastheer tijdens mycobacteriële infecties door geubiquitineerde bacteriën te herkennen en aan te vallen door middel van autofagie. Samenvattend levert dit proefschrift nieuw bewijs voor de belangrijke rol van selectieve autofagie in het verhinderen van mycobacteriële proliferatie binnen macrofagen van de gastheer. Bovendien levert dit proefschrift verdere ondersteuning voor de notie dat het stimuleren van de aangeboren immuunprocessen die gebaseerd zijn op de functies van Dram1, p62 en Optineurin, een waardevolle strategie is om nieuwe behandelmethoden voor tbc te ontwikkelen.

Curriculum vitae

Rui Zhang was born on the 7th of June 1987 in Hohhot, Inner Mongolia, China. He completed his high school education at the Hohhot 9 high school in June 2006. In September of this year, he started his BSc study in animal medicine at the Inner Mongolia University for the Nationalities. In June 2010, he obtained his BSc degree. In September of the same year, he started his MSc study at the Hua Zhong Agriculture University with a major in preventive veterinary medicine under supervision of Prof. dr. Aizhen Guo. During his MSc study, he performed research on the selection of attenuated vaccine candidates for control of *Mycoplasma bovis* infection. He also investigated the epidemic of *Mycobacterium bovis* infection in cattle and deer in China. In May, 2013, he obtained a China Scholarship Council-Leiden University Joint Scholarship for carrying out a PhD research project in the Netherlands. After acquiring his MSc degree in June 2013**,** he worked from September 2013 to June 2018 as a PhD student in the group of Prof. dr. Annemarie H. Meijer in the Animal Sciences & Health department at the Institute of Biology of Leiden University. During his PhD study, supervised by Dr. Monica Varela, Dr. Michiel van der Vaart and Prof. dr. Annemarie H. Meijer, he used zebrafish embryos as tuberculosis model and investigated the function of selective autophagy in host defense against mycobacterial infection, resulting in the work presented in this thesis. Following his return to China, he obtained a lecturer position at the HuBei University of Technology, where he will continue to perform research in the area of zebrafish disease models.

List of publications

Zhang, R., Varela, M., Vallentgoed, W., Forn-Cuní, G., van der Vaart, M and Meijer, A.H. The selective autophagy receptors Optineurin and p62 are both required for innate host defense against mycobacterial infection. *Submitted*

Zhang, R., Varela M., Torraca, V., van der Vaart, M and Meijer, A.H. Dram1 deficiency leads to increased susceptibility of zebrafish to mycobacterial infection due to activation of pyroptotic cell death in infected macrophages. *Manuscript in preparation*

Zhang, R., Varela, M., Forn-Cuní, G., van der Vaart, M and Meijer, A.H. Deficiency of the autophagy modulator Dram1 affects the transcriptional regulation of metabolic and immune response pathways during mycobacterial infection. *Manuscript in preparation*

Zhang, R., Han, X, Chen, Y., Mustafa, R., Qi, J, Chen, X., Hu, C., Chen, H., Guo, A. Attenuated *Mycoplasma bovis* strains provide protection against virulent infection in calves. Vaccine 32 (2014) 3107–3114